IDENTIFICATION, SYNTHESIS & DESIGN OF SELECTIVE RABGGTASE INHIBITORS

Zur Erlangung des akademischen Grades eines
Doktors der Naturwissenschaften
(Dr. rer. nat.)
von der Fakultät für Chemie
der Universität Dortmund
angenommene

Dissertation

von
Elisabeth Anouk Stigter, MSc
aus Heerhugowaard, Niederlande

Dekan:	Prof. Dr. Heinz Rehage
1. Gutachter:	Prof. Dr. Herbert Waldmann
2. Gutachter:	Prof. Dr. Roger Goody

Tag der mündlichen Prüfung: 10. Juni 2011

Die vorliegende Arbeit wurde unter Anleitung von Prof. Dr. Herbert Waldmann am Fachbereich Chemie der Universität Dortmund und am Max-Planck-Institut für molekulare Physiologie, Dortmund in der Zeit von Oktober 2007 bis Mai 2011 angefertigt.

Dedicated to my parents: Fred and Emmy

Abstract

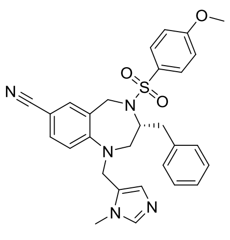

BMS3
IC_{50} (RabGGTase): 74 nM
IC_{50} (FTase): 5 nM

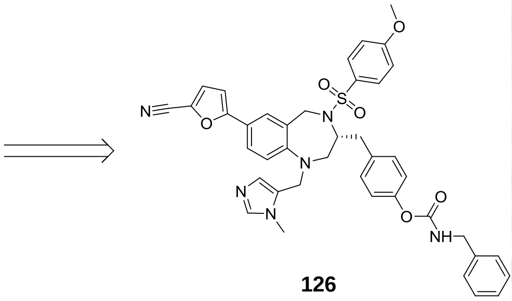

126
IC_{50} (RabGGTase): 49 nM
Selective over FTase & GGTase I

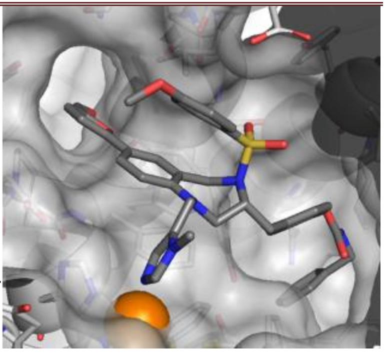

Rab GTPases are the main regulators of eukaryotic intracellular trafficking events. In the last decade, many Rab GTPases and their related proteins have been linked to cancer. In this research, attempts have been made to develop small molecules that interfere with Rab GTPase function by selective inhibition of the essential post-translationally modifying enzyme, RabGGTase. These inhibitors are used as tools to verify RabGGTase as a potential anti-cancer target and could be used in a chemical biology approach to further study Rab-mediated processes.

RabGGTase and its related enzymes FTase and GGTase I together represent the human prenyltransferases, involved in prenylation of the superfamily of small Ras GTPases. The most potent RabGGTase inhibitor known, **BMS3**, was originally designed as FTase inhibitor. Since **BMS3** lacks selectivity with respect to FTase, both *in vitro* and in cells, its pro-apoptotic effect could only be attributed to RabGGTase inhibition indirectly. In order to study the effects of selective RabGGTase inhibition on cancer cell proliferation and, more generally, Rab-mediated cellular processes, the main challenge was the design and synthesis of potent and selective RabGGTase inhibitors with cellular activity. Several approaches have been used in order to obtain such inhibitors. Using a structure-guided design, the scaffold of **BMS3** was decorated with additional groups to gain selectivity for RabGGTase. Going through iterative cycles of design, synthesis and biochemical and biological evaluation, several selective RabGGTase inhibitors were obtained, the most potent being inhibitor **126**. Other strategies to obtain selective RabGGTase inhibitors were evaluated with mixed success. The *in vitro* screening based on a fluorometric RabGGTase assay led mainly to identification of false positives, whereas a scaffold hopping approach resulted in a quick generation of a few prenyl transferase inhibitors with mixed activity toward RabGGTase, FTase or GGTase I.

In order to verify the potential of selective RabGGTase inhibitors and to inspire drug discovery, several cancer cell lines were treated with **126**. It could be shown that **126** selectively inhibited cancer cell line proliferation without being generally cytotoxic to PBMC cells, thereby verifying RabGGTase as potential anti-cancer target.

The iterative effort of design, X-ray structure determination, synthesis and biological evaluation successfully allowed to convert a non-selective inhibitor into a potent, selective, not generally cytotoxic inhibitor. Selective RabGGTase inhibitors may be used as valuable chemical biology tools for further research on Rab mediated processes.

Zusammenfassung

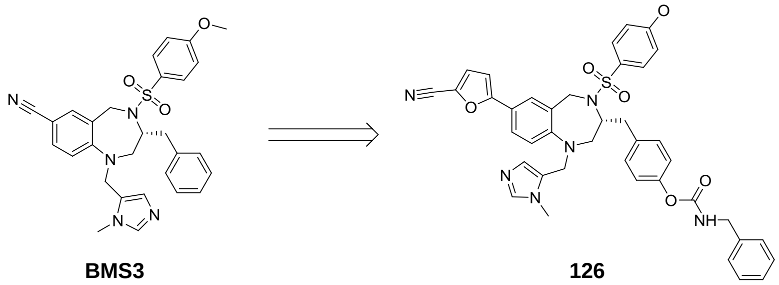

BMS3
IC_{50} (RabGGTase): 74 nM
IC_{50} (FTase): 5 nM

126
IC_{50} (RabGGTase): 49 nM
Inaktiv für FTase & GGTase I

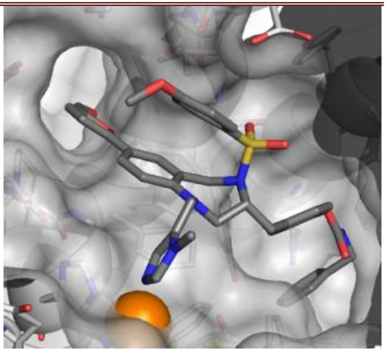

Rab-GTPasen sind die Hauptregulatoren intrazellulärer Transportvorgänge in eukaryotischen Zellen. Im Laufe des letzten Jahrzehnts wurden zahlreiche Rab-GTPasen und mit ihnen verwandte Proteine mit der Entstehung von Krebs in Verbindung gebracht. In der vorliegenden Arbeit wurden selektive Inhibitoren für die RabGGTase entwickelt, ein Enzym das für die korrekte Funktion von Rab-GTPasen unabdingbar ist. Diese Inhibitoren wurden benutzt, um die RabGGTase als krebsrelevantes Protein zu bestätigen und könnten als Werkzeuge für die Untersuchung Rab-vermittelter Prozesse im Sinne eines chemische biologischen Ansatzes eingesetzt werden. RabGGTase und die verwandten Enzyme FTase und GGTase I stellen die humanen Prenyltransferasen dar, die an der Prenylierung der Ras-GTPase-Superfamilie beteiligt sind. Der bisher wirksamste literaturbekannte RabGGTase Inhibitor **BMS3** wurde ursprünglich als Inhibitor für die FTase entwickelt. Da **BMS3** weder *in vitro* noch *in vivo* Selektivität für FTase besitzt, konnte sein proapoptotischer Effekt nur indirekt der Inhibition der RabGGTase zugeordnet werden. Um den Effekt selektiver RabGGTase-Inhibition auf die Proliferaton von Krebszellen und allgemein auf Rab-vermittelte zelluläre Prozesse zu untersuchen, lag der Hauptfokus der vorliegenden Arbeit auf dem Design und der Synthese hochaffiner, selektiver RabGGTase-Inhibitoren mit zellulärerAktivität. Mehrere Herangehensweisen zurEntwicklung derartiger Inhibitoren wurden verwendet. In einem strukturgeleitetem Ansatz wurde **BMS3** mit zusätzlichen funktionellen Gruppen versehen, um die Selektivität für RabGGTasen zu erhöhen. Nach wiederholten Zyklen von Design, Synthese und biochemischensowie biologischen Tests wurden einige selektive RabGGTase Inhibitoren erhalten, von denen **126** der stärkste Inhibitor war. Andere Strategien zur Entwicklung selektiver Inhibitoren führten zu unterschiedlichem Erfolg. Ein fluorometrischer *in vitro* RabGGTase Aktivitätsassay führte hauptsächlich zu falsch-positiven Ergebnissen. Ein Ansatz nach dem Prinzip des “scaffold hopping“

führte zu Inhibitoren mit wechselnder Selektivität gegenüber RabGGTase, FTase oder GGTase I.

Um das Potential selektiver RabGGTase Inhibitoren als Startpunkte für die Wirkstoffentwicklung zu bestätigen, wurden Krebszelllinien mit **126** behandelt. Es konnte gezeigt werden, dass **126** selektiv die Proliferation von Krebszellen hemmt, ohne generell toxisch für PBMC-Zellen zu sein. Diese Ergebnisse unterstreichen die Bedeutung der RabGGTase als vielversprechendes Zielprotein in der Bekämpfung von Krebs.

Wiederholte Zyklen von Design, Kristallographie, Synthese und biologischer Evaluierung ermöglichten es einen unselektiven Inhibitor in einen hochaktiven, selektiven nicht generell toxischen Inhibitor umzuwandeln. Die hergestellten Inhibitoren stellen wichtige Werkzeugefür die chemisch-biologische zukünftige Erforschung von durch Rab vermittelte Prozesse dar.

Contents

Abstract ... vii

Zusammenfassung ... xi

Contents ... xv

Chapter 1: Introduction ... 1

§ 1.1 Ras Superfamily of Small GTPases ... 3
- Ras GTPases ... 3
- Rho GTPases ... 4
- Rab GTPase ... 4
- Ran GTPase ... 4
- Arf GTPases ... 4

§ 1.2 Rab GTPase life cycle ... 5
- § 1.2.1 General structural features of Rab GTPase ... 7

§ 1.3 Stage I: Prenylation &Machinery of small GTPases ... 8
- Prenylation occurs in a step wise manner ... 9
- Structural Biology of FTase, GGTase I and RabGGTase ... 11

§ 1.4 Stage II: The tightly regulated molecular switch ... 14
- § 1.4.1 The Ras family serves as a molecular switch ... 15
- § 1.4.2 GEFs and GAPs ... 15
  - GEFs ... 16
  - GAPs ... 19
- § 1.4.3 Effectors ... 20
- § 1.4.4 Chaperon proteins ... 22

§ 1.5 The role of Rab GTPases in vesicle trafficking ... 23
- § 1.5.1 Rab GTPases as coordinators of vesicle traffic ... 23
  - The Exocytic and Endocytic pathway ... 23
  - I. Vesicle Sorting ... 25
  - II. Vesicle Uncoating ... 26
  - III. Vesicle Motility ... 26
  - IV. Vesicle Tethering ... 27
  - V. Vesicle Fusion ... 27
  - Rab Cascades ... 28
- § 1.5.2 Rab GTPases in disease ... 28
  - Rabs and cancer ... 29
  - Rabs and neurological disease ... 30

Rabs and infectious disease 30

§ 1.6 The Prenylation machinery as drug target........ 31

§ 1.7 RabGGTase as biological target 33

§ 1.7.1 Increasing efforts toward RabGGTase inhibitors 33

Phosphonocarboxylates: Selective inhibitors of RabGGTase 33

Substrate mimic: GGTI-2Z 35

Pyrrolidine-based inhibitors........ 36

Peptides and peptide analogs........ 38

Dual Inhibitors: Tetrahydrobenzodiazepines (THBs) 41

§ 1.8 General drug development strategies 42

§ 1.8.1 From hit… 43

§ 1.8.2 …to lead........ 45

§ 1.8.3 Toward selective RabGGTase inhibitors........ 45

Chapter 2: Aim of the project 47

Chapter 3: Method & tool development for identification of selective RabGGTase Inhibitors........ 51

§ 3.1 Fluorometric RabGGTase assay........ 51

§ 3.2 Fluorometric FTase & GGTase I assay........ 52

§ 3.3 X-ray crystallography 53

RabGGTase 53

FTase 53

§ 3.4 Molecular Modeling........ 54

§ 3.4.1 Preparation of a virtual library........ 54

§ 3.4.2 Preparation of the crystal structures 54

§ 3.4.3 Virtual Screening 54

§ 3.4.4 Analysis of the results........ 55

§ 3.5 Synthesis of tool compounds 56

§ 3.5.1 Synthesis of fluorescent prenyl pyrophosphate (PPP) analogs........ 56

Synthesis of NBD-FPP........ 56

General route toward the synthesis of PPP analogs 57

§ 3.5.2 Synthesis of phosphonocarboxylate RabGGTase inhibitors 60

Chapter 4: Synthesis & Design of selective tetrahydro-benzodiazepine based RabGGTase inhibitors........ 65

§ 4.1 BMS3, a dual inhibitor........ 65

§ 4.2 Virtual Screening......68

§ 4.3 Retrosynthetic analysis......69

§ 4.4 Synthesis of General Building Blocks......70
  § 4.4.1 Optimization of specific N-sulfonylation......71
  § 4.4.2 Optimization of reductive amination......72
  § 4.4.3 Determination of the enantioselectivity......73

§ 4.5 Synthesis & Screening of 1st generation RabGGTase inhibitors......74

§ 4.6 Synthesis & Screening of 2nd generation RabGGTase inhibitors......77

§ 4.7 Crystallization and Overlay studies of 1st and 2nd generation of inhibitors......79

§ 4.8 Design and Synthesis of 3rd generation of inhibitors......82
  § 4.8.1 Virtual screening based on conformational constraints......82
  § 4.8.2 Synthesis& Screening of 3rd generation of inhibitors......83

Chapter 5: Intermezzo – RabGGTase Counterscreens......89

Chapter 6: Toward highly potent selective RabGGTase inhibitors......97

§ 6.1 Computer-aided design of cooperative RabGGTase inhibitors......97

§ 6.2 Synthesis and Screening of 4th generation of inhibitors......99

Chapter 7: Cellular studies of the RabGGTase inhibitors......107

Chapter 8: High Throughput Fluorescent Screening: Leads or Misleads?......113

§ 8.1 Initial hits of the NBD-FPP RabGGTase assay......113

§ 8.2 Furfurylamine based library......114

§ 8.3 Evaluation of benzoxazolone based RabGGTase inhibitors......116

§ 8.4 Evaluation of fluorescent NBD-FPP assay......116

Chapter 9: De novo design of RabGGTase inhibitors......119

§ 9.1 Back to the FTase inhibitors......119
    Synthesis of ABT-FTase inhibitor......120

§ 9.2 General strategy to identify prenyl transferase inhibitors......122

§ 9.3 First example of successful scaffold hopping......125

§ 9.4 Scaffold Hopping Future Prospective......126

Chapter 10: Concluding Remarks......129

Experimental Section......135

§ 10.1 Virtual screening procedure for RabGGTase and FTase 135
§ 10.1.1 General procedure for virtual screening 135
§ 10.1.2 Specific binding constraints in RabGGTase VHS: 136

§ 10.2 Assay procedures 137
§ 10.2.1 Solution based fluorometric biochemical RabGGTase assay procedure for IC_{50} determination of THBs. 137
§ 10.2.2 Solution-based fluorometric FTase assay. 137
§ 10.2.3 Solution-based fluorometric GGTase I assay. 138
§ 10.2.4 Cell culture 138
§ 10.2.5 Reprenylation assay 138
§ 10.2.6 Alamar Blue Assay 139

§ 10.3 Synthetic procedures 140
§ 10.3.1 General Information 140
§ 10.3.2 Synthesis of Tool compounds 141
§ 10.3.3 Synthesis of General Building Blocks 74a&b 146
§ 10.3.4 Synthesis of 1stGeneration THBs 152
General Procedure I for O-methylation of THBs: 152
General Procedure II for O-aminoacylation of THBs: 155
General Procedure III for O-triflation of THBs 158
General Procedure IVa for Suzuki couplings of THBs and arylboronic acids: 159
General Procedure IVb for Suzuki couplings of THBs and arylboronic acids: 160
§ 10.3.5 Synthesis of 2nd Generation THBs 161
§ 10.3.6 Synthesis of 3rdGeneration THBs 168
§ 10.3.7 Synthesis of 4th Generation THBs 171
§ 10.3.8 Synthesis of 5th Generation THBs 177
§ 10.3.9 Synthesis of furfuranyl analogs 191
General Procedure V for oxidation of furan 191
General Procedure VI for hydrogenation 191
§ 10.3.10 Synthesis of benzoxazolone 195
§ 10.3.11 Synthesis of de novo compounds 197
General Procedure VII for synthesis of tetrahydroquinazolinones 200

List of Abbreviations 203

References 207

Supplementary Data .... a

Virtual Screening Input data .... b

Cellular data of all tested compounds and cell lines .... *c*

Assignment by analogy, NMR example of compound 91 .... *d*

1H NMR .... d

COSY .... e

APT .... f

HSQC .... g

HMBC .... h

Acknowledgement .... **k**

Declaration/Eidesstattliche Erklärung .... **o**

Chapter 1: Introduction

Around 13% of all deaths worldwide are caused by cancer[1]. In 2008, 12.7 million cancer cases and 7.6 million cancer deaths were registered worldwide. Related to the increasing life expectation, it is estimated that one out of three people in the developed world will develop cancer during their life[1].

Therefore, it is not surprising that great efforts are undertaken, mainly within the pharmaceutical industry, to develop anti-cancer agents. Cancer, though, covers a wide variety of diseases with different characteristics but a common effect: unrestricted proliferation of tumor cells[2].

Several strategies have been adopted to develop anti-cancer agents over the last century. Cisplatin, a major anti-cancer drug, covalently links to guanine DNA bases, obscuring DNA repair and hence causing cell death[3]. Another way to inhibit cellular proliferation is the inhibition of microtubule dynamics. Natural products such as vinblastine and paclitaxel (taxol) regulate cell division by destabilization or stabilization of microtubules, and represents potent anti-cancer drugs as well[4]. Since the aforementioned strategies involve many cellular processes these treatments are generally accompanied by various, often severe, side effects[2]. To bypass these severe side effects, target specific anti-cancer drugs are desirable. Historically, the best known examples are anti-estrogen and anti-androgen agents for breast and prostate cancer, respectively[5, 6].

Recently other drug specific tumor targets have been uncovered and introduced into the clinic. Kinase inhibitors represent one such class of compounds (although most kinase inhibitors inhibit a range of different kinases)[7]. The most successful kinase targeting oncogenic drug is the Abl kinase inhibitor imatinib (Gleevec)[8] and is especially effective in the treatment of chronic myelogenous leukemia (CML). In CML the Abl gene is fused to a breakpoint cluster (BCR) gene, resulting in a highly expressed constitutively active chimeric BCR–Abl oncoprotein[8].

Transmembrane tyrosine kinase receptors represent another attractive target, since they are often essential for tumor growth[9]. Besides small molecule inhibitors, humanized antibodies against these receptors have been developed[10, 11]. The top-selling anti-cancer drug of 2010,a monoclonal antibody of Roche named Avastin targets the transmembrane tyrosine kinase vascular endothelial growth factor receptor (VEGFR). Antibodies represent some distinct characteristic compared to small molecule drugs; they possess larger half-lives and target the extracellular part of the receptor, compared to the intracellular portion targeted by small molecules[2]. However, the FDA has recently questioned the beneficial effect of Avastin in metastatic breast cancer. Together with the associated high costs, the use of antibodies as anti-cancer drugs is under debate at the moment[12].

Small GTPases represent another group anti-cancer drug targets[13]. The Ras GTPases control many signaling cascades, including the MAP-kinase pathway that controls cell growth, differentiation and survival. Many tumors contain mutated forms of Ras GTPases, which are constitutively active[14]. Therefore, inhibition of Ras GTPase represents an alternative attractive anti-cancer strategy. Since Ras GTPases require post-translational modification with a lipid to exert their functions, efforts have been undertaken to inhibit the responsible post-translational modification by the enzymes farnesyl transferase (FTase) and geranylgeranyl transferase I (GGTase I)[15]. So far, farnesyl transferase inhibitors (FTIs) were tested in various tumors with poor success, which was related to cross-prenylation of Ras GTPases by GGTase I[16]. (Will be described in more detail in § 1.6.)

The observation that some FTIs were effective in tumor cell lines with no mutations in Ras, led to the finding that an additional small GTPase family member, Rab, could represent a new anti-cancer drug target. The related prenyl transferase Rab geranylgeranyl transferase (RabGGTase) was inhibited by some FTIs. In addition, chemical genetics studies with interfering RNA confirmed that the inhibition of RabGGTase led to p53 independent apoptosis[17]. In contrast to Ras GTPases, Rab GTPases are mainly responsible for vesicular trafficking, and an obvious link with proliferation is lacking. The role of Rab GTPases in receptor internalization and hence signal transduction and receptor recycling is the most cited reason for their role in cancer[18].

To clarify the role of Rab GTPases in biological processes in general and in cancer in particular, a chemical biology approach would be advantageous. Chemical biology represents a growing field of research in which bioactive small molecules are used as tools to investigate and manipulate biological systems[19, 20]. A selective inhibitor of RabGGTase would be an effective agent to manipulate Rab GTPase controlled biological processes and would give access to an in depth analysis of the role of Rab GTPases in cancer and other diseases.

In this thesis, efforts to obtain a selective inhibitor of RabGGTase with cellular activity will be described. Before the design, synthesis and evaluation of these small RabGGTase inhibitors with promising cellular activity will be discussed, an overview of the current stage of research will be given. After a short introduction of the Ras GTPase superfamily, the general mode of action of Rab GTPases will be discussed, followed by their implications in disease as well as first efforts described in the literature to obtain RabGGTase inhibitors.

§ 1.1 Ras Superfamily of Small GTPases

The Ras superfamily of small guanosine triphosphatases (small GTPases) belongs to the class of Guanine nucleotide-binding proteins (G Proteins)[21]. In general, G proteins transduce extracellular signals into intracellular changes through second-messenger cascades[22]. Of the small G proteins, the Ras superfamily with more than 150 human members is the most studied[23, 24]. Based on sequence and functional similarity, the Ras superfamily can be roughly divided into five major classes: Ras, Rho, Rab, Ran and Arf small GTPases (Figure 1.1). Due to variations in structure, post-translational modification and effector and regulator proteins, the Ras superfamily of Ras GTPases function as sophisticated modulators of a complex and diverse range of cellular processes.

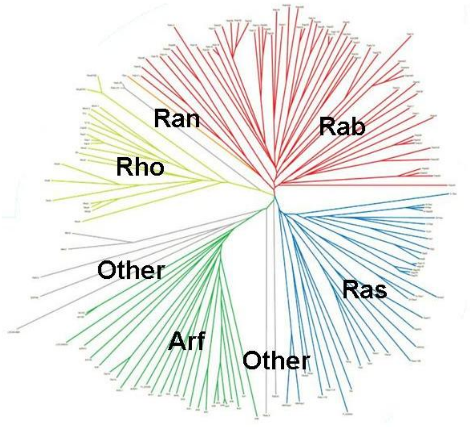

	Human Genes /Isoforms	Function
Rab	61/63	Intracellular vesicle trafficking
Ras	36/39	transmembrane signal transduction, gene expression
Arf	27/39	Intracellular vesicle trafficking
Rho	20/22	cytoskeletal reorganization gene expression
Ran	1/1	microtubule organization nucleocytoplasmic transport
Other	9/10	-

Figure 1.1: Ras Superfamily of GTPases, adapted from Wennerberg *et. al*[25].

Ras GTPases

The Rat sarcoma (Ras) proteins are involved in signaling events. They serve as signaling nodes, which are activated by extracellular stimuli. Activated Ras interacts with a large array of downstream effectors, ultimately involved in gene expression and regulation of cell proliferation, differentiation and survival[25]. The best characterized Ras signaling pathway is activation of Ras by the epidermal growth factor receptor tyrosine kinase[26]. Mutations in the Ras family proto-oncogenes (NRas, HRas and KRas) are found in thirty percent of all human cancers, therefore, multiple approaches are undertaken to develop tumor therapies targeting Ras pathways[27, 28].

Rho GTPases

Ras homologous (Rho) proteins are key regulators of signal transduction networks that regulate actin organization, cell cycle progression and gene expression[29]. Like Ras, the activation of these signaling events is mediated by extracellular stimuli. Rho GTPases have been implicated in the regulation of cell polarity, cell movement and cell-matrix interactions as well as in regulation of endocytosis and exocytosis[30]. This diversity of cellular processes is reflected by the variation of Rho-effector and -regulator proteins[25, 31-33]

Rab GTPase

Ras-like proteins in brain (Rab) proteins represent with more than 60human members the largest branch of the superfamily[34]. Rab GTPases regulate intracellular vesicular transport and trafficking of proteins in the endocytic and secretory pathways[35]. They are responsible for a wide range of trafficking events, involving vesicle formation, budding and transport, and vesicle fusion and vesicle-content-release. Therefore, they localize to specific intracellular compartments uniform with their function in distinct vesicular transport processes. For example, Rab1 is involved in the Golgi network, whereas Rab5 is located in the early endosomes[25, 35].

Ran GTPase

Ras-like nuclear (Ran) protein is the most abundant small GTPase in the cell and is involved in nucleocytoplasmic transport of RNA and proteins[36]. Ran GTPase, mainly situated at the nucleus, interacts with importin to promote cargo release and its GDP/GTP cycling also regulates mitotic spindle assembly, DNA replication and nuclear envelope assembly[25, 37].

Arf GTPases

ADP-ribosylation factor (Arf) proteins are involved in regulation of vesicular transport, similar to Rab GTPases. Arf1 regulates formation of vesicle coats in the exocytic and endocytic pathways. Arf proteins can function in multiple steps. Arf6, for example, can regulate actin organization as well as endocytosis[25].

Clearly, the superfamily of Ras GTPase regulates a diverse spectrum of biological processes. However, they show many similarities in sequence classification, mechanisms of activation and effector associations. Furthermore, after being synthesized in the cytosol, all Ras GTPases undergo crucial post-translation modifications, mostly by the addition of lipids to facilitate their membrane association.

The common themes will be described in the following sections mainly guided by our protein class of interest: Rab GTPases.

§ 1.2 Rab GTPase life cycle

Before going into detail about the regulatory mechanisms behind function of the Ras GTPase superfamily in general, and Rab GTPases in particular, a typical Rab GTPase life cycle will be shortly described here.

The reversible association of Rab GTPases with intracellular membranes and other proteins is essential for their function. In order to establish these interactions for Rab GTPase, a post-translational modification involving the attachment of a geranylgeranyl group to Rab's C-terminal cysteine(s) is necessary. This geranylgeranylation takes place directly after the synthesis of Rab GTPase in the cytosol. This so called prenylation is carried out in a ternary complex of RabGGTase and Rab Escort Protein (REP) (Figure 1.2, stage I)[38]. This process will be discussed in more detail in § 1.3.

After prenylation and delivery to the membrane, Rab GTPase enter its next stage (Figure 1.2, stage II). Membrane bound Rab GTPase can be activated by the exchange of GDP for GTP by guanine nucleotide exchange factor (GEF) and deactivated by the hydrolysis of GTP to GDP by a GTPase activating protein (GAP). Upon activation, Rabs can interact with numerous effector proteins to exert their function. After being switched off by GAP, Rab is recruited from the membrane by guanosine nucleotide dissociation inhibitor (GDI). GDI solubilizes Rabs and transports them back to their donor membrane, in order to start a 2nd stage II life cycle[39]. This process will be discussed in more detail in § 1.4.

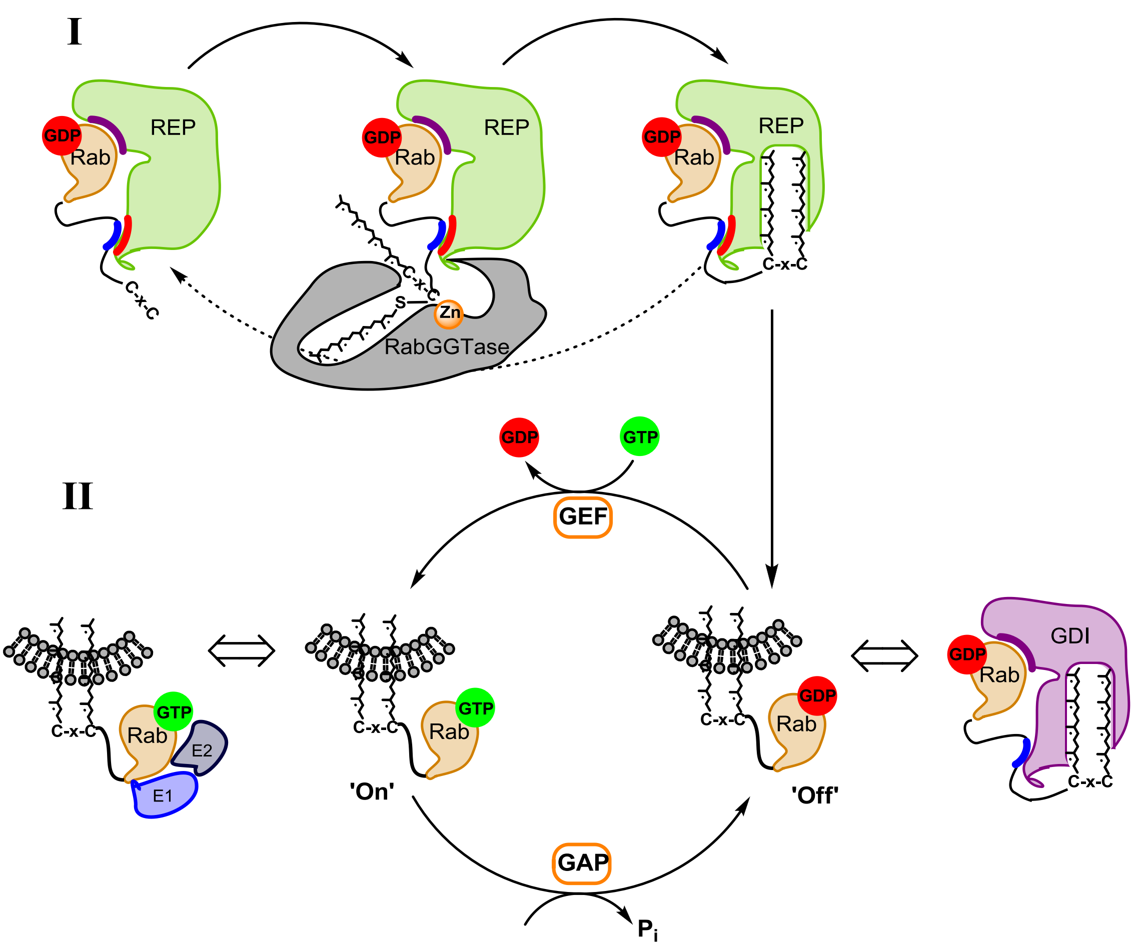

Figure 1.2: The life cycle of Rab GTPases, I: Geranylgeranylation of Rab proteins is essential for membrane binding and proper function. II: Once properly decorated, Rab proteins cycle between a GDP-bound off and GTP-bound on state, mediated by GEFs and GAPs.

In order to study the relevance of Rab mediated processes, these processes can be perturbed on several levels. For example, in the second stage small molecules can be developed to selectively disrupt protein-protein interaction between Rab and a specific effector, GEF, GAP or GDI. However, a more general strategy, to disturb all Rab mediated processes would be targeting the post-translational prenylation. This strategy will be pursued in this thesis, describing the efforts to develop potent, selective small molecule inhibitors of RabGGTase. Since RabGGTase is related to the other prenyl transferase FTase and GGTase I, these enzymes need to be considered as potential anti-targets during selective inhibitor development.

Before going into the inhibitor design, Rab GTPase mode of actions and biological functions, as well as the several delicate levels of regulation will be discussed in the following paragraphs.

§ 1.2.1 General structural features of Rab GTPase

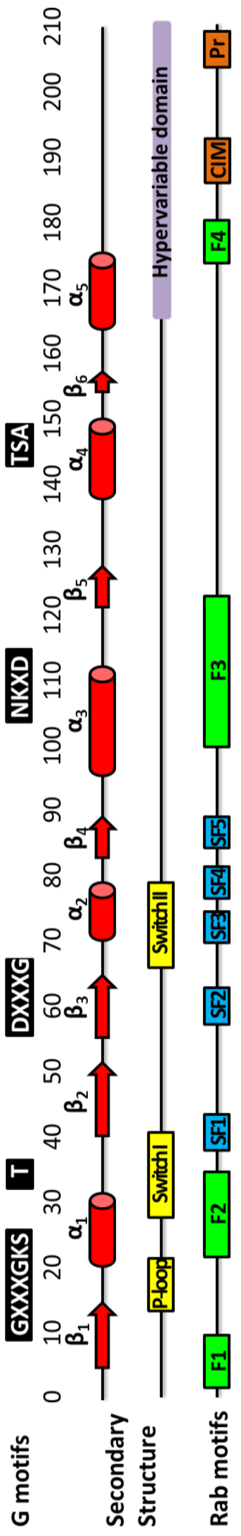
G motifs
Secondary Structure
Rab motifs
0
10
20
30
40
50
60
70
80
90
100
110
120
130
140
150
160
170
180
190
200
210
GXXXGKS
T
DXXXG
NKXD
TSA
β_1
α_1
β_2
β_3
α_2
β_4
α_3
β_5
α_4
β_6
α_5
P-loop
SwitchI
SwitchII
Hypervariable domain
F1
F2
SF1
SF2
SF3
SF4
SF5
F3
F4
CIM
Pr

Figure 1.3: Common Ras GTPase G motifs, Rab Family (RabF) and Rab subfamily motifs (RabSF), and prenylation motif (Pr).

The tight regulation of Rab GTPases is reflected by several structural motifs involved in interaction with the associated proteins. The Rab proteins share a fold that is common to all small GTPases of the Ras superfamily, consisting of a six-stranded β sheet (5 parallel and 1 antiparallel) surrounded by five α helices (Figure 1.3). All small GTPases contain a set of five conserved G box sequences, motifs that are directly involved in guanine nucleotide binding, Mg^{2+} binding and GTP hydrolysis [40, 41]. The G1 box, also known as a P-loop or Walker A motif, is a purine nucleotide binding signature. The G2 box is located in one of the sequences that reorient as a function of GDP or GTP binding and provide major components of effector binding surface. Only the threonine residue in this switch region is conserved over all subfamilies. The G3 box is involved in binding a nucleotide-associated Mg^{2+} ion and is well conserved among superfamily members. To confer specificity to GTP over ATP, residues in G4 are involved in hydrogen bond interaction with the guanine. In addition, they provide stabilizing interaction with G1 box residues. The G5 box primarily makes indirect associations with the guanine nucleotide and is less well conserved among the supergroup members[24]. In addition, all the small GTPases contain so called switch regions, which are crucial for the small GTPases to interact with their GAPs, GEFs and certain effectors. These two switch regions overlap to some extend with the G box motifs.

Sequence analysis by Pereira-Leal *et al.* indicated five amino-acid stretches that are characteristic for all Rab GTPases[42]. These RabF regions cluster in and around the switch regions and are claimed to provide criteria for identifying Rab proteins. In addition, the authors identified four regions that can be used to define the subfamilies of Rab GTPases. Since these RabSF domains are on two distinct surfaces of the GTPase, it has been suggested that these domains are at least partially responsible for discrimination of specific down-stream effectors. Indeed, it could be shown in the crystal structure of Rab3a and its effector rabphillin-3A that both the switch regions and some Rab subfamily specific motifs contributed to the interactions[43].

In addition to these RabF and RabSF regions, another conserved motif necessary for binding to REP via their hydrophobic C-terminal binding region (CBR) is characteristic for all Rab GTPase. This CBR interacting motif (CIM) consists of two apolar residues flanking a polar amino acid near the C-terminus and is crucial for the association to GDI and REP and hence prenylation[44-46].

§ 1.3 Stage I: Prenylation & Machinery of small GTPases

Lipid posttranslational modifications are a common requirement for proper function for most Ras GTPases family members. These lipid modifications involve the attachment of fatty acids such as myristoyl (Arf) and palmitoyl (Ras, Rho) as well as the attachment of isoprenoids (Ras, Rho and Rab)[25].

The incorporation of isoprenoids, known as prenylation, is crucial for membrane association and proper function of small GTPases Rab, Ras and Rho. Prenylation involves the covalent attachment of a prenyl moiety to a C-terminal cysteine. In general, a prenylpyrophosphate (PPP) serves as the prenyl donor whereas a prenyl transferase (PTase) enzyme catalyzes the attachment. All eukaryotes possess three PTases: FTase, GGTase I and RabGGTase[47-49]. FTase carries out a farnesylation, whereas GGTase I and RabGGTase carry out a geranylgeranylation or digeranylgeranylation respectively. The lipid substrates, farnesylpyrophosphate (FPP) and geranylgeranylpyrophosphate (GGPP) are both products from the mevalonate or deoxyxylulose-5-phosphate isoprenoids biosynthesis pathways (Figure 1.4)[50].

The Rab family displays a set of one or two cysteine containing C-terminal motifs (CC, CXC, CCX, CCXX, CCXXX, CXXX), which are (di)geranylgeranylated by RabGGTase. This is done in a ternary complex of Rab GTPase, RabGGTase and REP, in which REP recognizes unprenylated Rab GTPases and presents them to RabGGTase. Rab GTPases then interact with the plasma membrane with their prenyl group(s)[51]. There are two REP proteins found in mammals, REP1 and REP2[52].

Ras and Rho GTPase family member possess a C-terminal CAAX box (C=Cys, A=aliphatic, X=any amino acid)[53], which represents a recognition sequence for FTase and GGTase I, thus in this case, no ternary complex is required. Therefore, FTase and GGTase I are also known as CAAX transferases. Roughly, geranylgeranylation occurs when the CAAX sequence ends in leucine or phenylalanine, whereas farnesylation takes place in all other cases[54]. However, it has been shown that this subdivision is not that strict; GGTase I for example, can cross prenylated FTase' substrates if FTase function is inhibited[55].

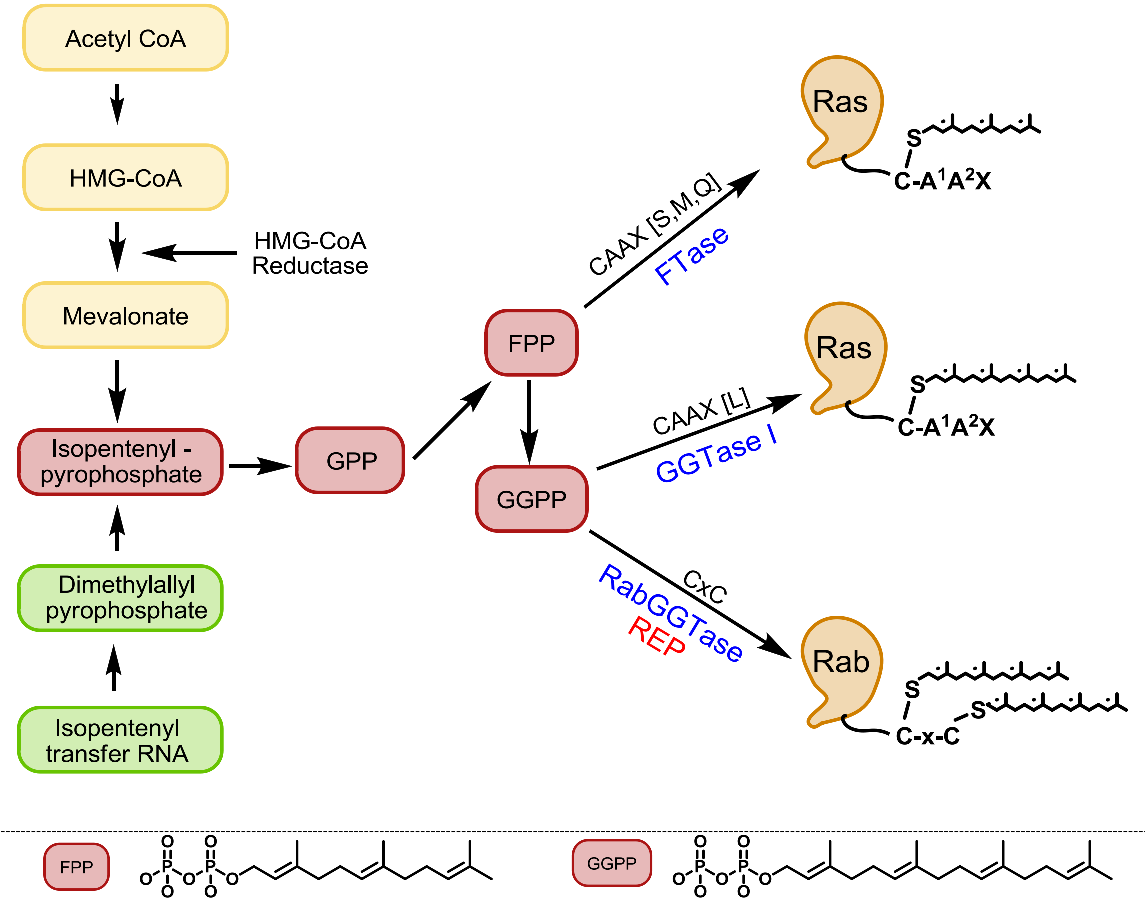
Acetyl CoA
HMG-CoA
HMG-CoA Reductase
Mevalonate
Isopentenyl - pyrophosphate
Dimethylallyl pyrophosphate
Isopentenyl transfer RNA
GPP
FPP
GGPP
CAAX [S,M,Q]
FTase
CAAX [L]
GGTase I
CxC
RabGGTase
REP
Ras
S
C-A^{1}A^{2}X
Ras
S
C-A^{1}A^{2}X
Rab
S
S
C-x-C
FPP
GGPP
O
P
O

Figure 1.4: Isoprenoid synthesis pathway and related prenyl transferases

Prenylation occurs in a step wise manner

Kinetic studies for the CAAX transferases suggest an ordered prenylation sequence (Figure 1.5). First, PPP binds to the apo enzyme, followed by the CAAX substrate. In the active site of PTase, the cysteine coordinates to a conserved Zn^{2+} ion, thereby activating its thiol for nucleophilic attack [56-58]. During the prenylation reaction, the pyrophosphate barring a negative charge is released. This negative charge is stabilized by Mg^{2+} or a conserved leucine in FTase and GGTase I, respectively [59, 60]. After prenylation, the substrate is released either by rebinding of PPP or unprenylated protein. The release of prenylated substrate is shown to be the rate limiting step under saturated reaction conditions, whereas the chemical reaction itself seems to be rate limiting under subsaturated conditions [61-64].

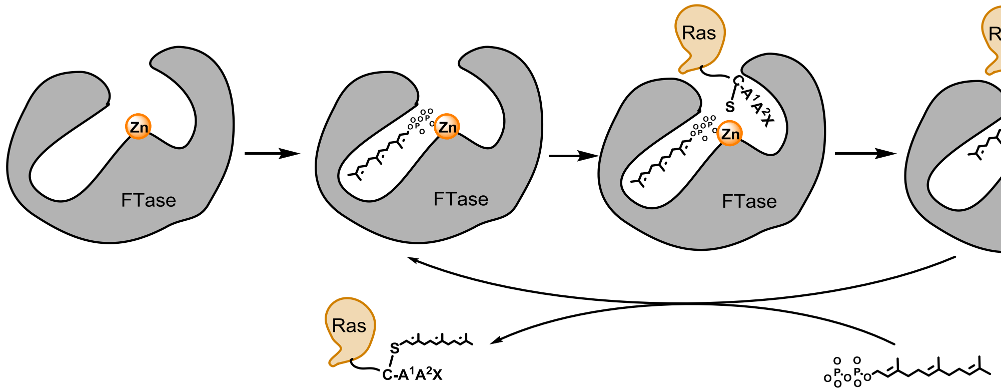

Figure 1.5: Mechanistic model of FTase-mediated protein prenylation.

The prenylation sequence of RabGGTase is presented by a more complicated picture and has been studied by a combination of classical biochemical and spectroscopic methods complemented by crystallization studies toward the ternary Rab:REP:RabGGTase structure[65-70]. Although this structure has not been solved to date, molecular modeling studies on binary complexes Rab7:REP and Rab7:RabGGTase resulted in a model structure that matched the biochemical data (Figure 1.7c) [46, 70]. In this model, the three important specificity domains have been included. The switch I and II regions of Rab GTPase interacts with the Rab binding platform (RBP). Furthermore, Rab interacts with a hydrophobic patch (C-terminal binding region, CBR) of REP, with its CBR binding motif (CIM). The CIM consists of two large hydrophobic residues adjacent to a polar residue. Results from molecular modeling suggested that Rab associates with REPs RBP into a low affinity complex[46], upon association of CBR with CIM the complex affinity increases by an order of magnitude. This complex then associates with GGPP bound RabGGTase. Since the cysteines only participate in weak interaction with RabGGTase, two sequential prenylation can be carried out in a single arrangement. The dissociation of prenylated Rab GTPases involves two steps, first GGPP displaces the geranylgeranylated product, second the geranylgeranyl moieties bind to REP and GGPP bound RabGGTase is released (Figure 1.6)[70-72].

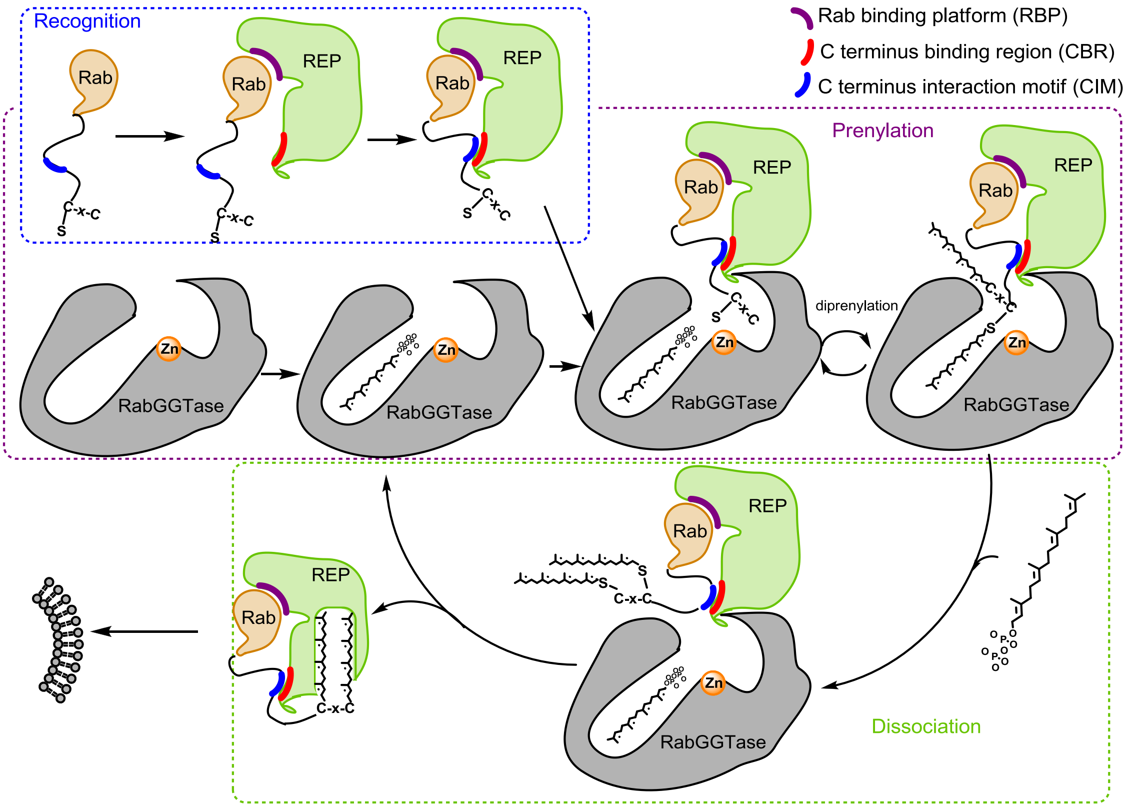
Recognition
Rab binding platform (RBP)
C terminus binding region (CBR)
C terminus interaction motif (CIM)
Rab
REP
C-x-C
S
Prenylation
diprenylation
Zn
RabGGTase
Dissociation

Figure 1.6: Mechanistic model of RabGGTase-mediated protein prenylation.

Structural Biology of FTase, GGTase I and RabGGTase

FTase, GGTase I and RabGGTase all exist as αβ heterodimers(Figure 1.7). They are zinc metalloenzymes binding one Zn^{2+} ion per protein dimer. This Zn^{2+} ion is essential for the catalytic activity of the enzymes by means of activating the thiol toward nucleophilic attack[54].

FTase and GGTase I share identical α units, with an almost identical structure. The β subunit of FTase and GGTase I share only 25% sequence identity but have very similar structures as well. RabGGTase presents 30% homology with the CAAX transferases and has four distinct structural domains. The α-subunit, opposed to FTase and GGTase I, is composed of three domains: a helical domain, an Ig-like domain formed by an eight-stranded β-sandwich and a leucine-rich repeat (LRR) domain. Despite the 22% sequence identity, the helical domain is structurally very similar to the α subunit of FTase. The role of the additional LRR and Ig like domains, both absent in lower eukaryotic versions of RabGGTase, remains unknown[73].

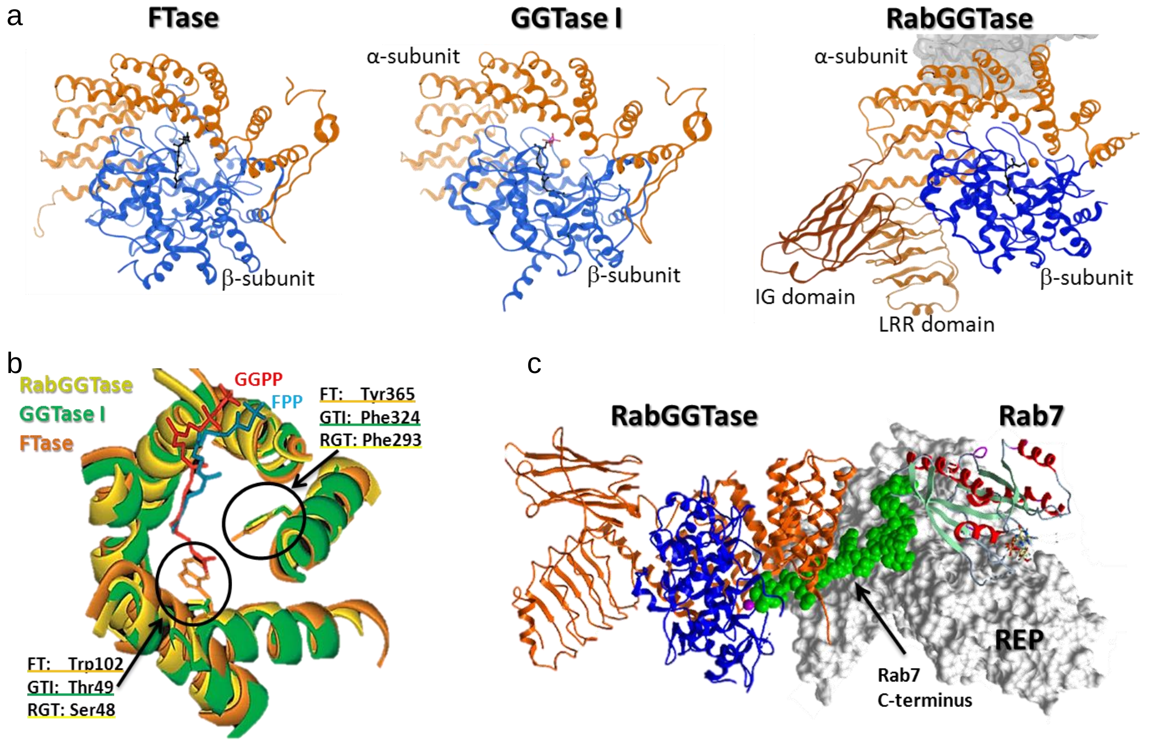
a
FTase
GGTase I
RabGGTase
α-subunit
α-subunit
β-subunit
β-subunit
IG domain
LRR domain
β-subunit
b
RabGGTase
GGTase I
FTase
GGPP
FPP
FT: Tyr365
GTI: Phe324
RGT: Phe293
FT: Trp102
GTI: Thr49
RGT: Ser48
c
RabGGTase
Rab7
REP
Rab7
C-terminus

Figure 1.7:(a) Crystal structures of FTase (1D8E), GGTase I (1N4P) and RabGGTase (1LTX). (b) an overlay of their β-unit active sites[51], Trp102 of FTase would clash with the last isoprene unit of GGPP. (c) the modeled ternary Rab7:REP:RabGGTase complex[46].

The β subunit is arranged in a similar fashion for all PTases, the twelve helices form an α-α barrel. One end of this barrel is closed whereas the opposite end is open creating a deep, funnel-shaped cavity in the center. This cavity is mostly hydrophobic in nature and lined with conserved aromatic residues and comprises the lipid binding site. A positively charged cluster is located near the opening of the cavity to interact with the diphosphate moiety[54].

Substrate specificity for GGPP or FPP seems to be determined by a single residue in the bottom of the hydrophobic binding site. In GGTase I and RabGGTase this residue is a small amino acid such as threonine or serine allowing GGPP to bind. In FTase this residue is replaced by a tryptophan constricting the length of the isoprenoids in favor of FPP[51, 54] (Figure 1.7b, Figure 1.8). Some implication for CAAX-box specificity can be deduced from differences in the β-subunit of FTase and GGTase I[54]. Two anchor points within the recognition motif (cysteine and C-terminus) makes specific interactions with the enzyme discriminating against peptides with wrong length or without cysteine. The A^1 residue is solvent exposed, whereas the A^2 and X residues are buried in the active site. Consequently A^2 and X contribute largely to peptide selectivity. At A^2 various amino acids can be accommodated. The respective FTase

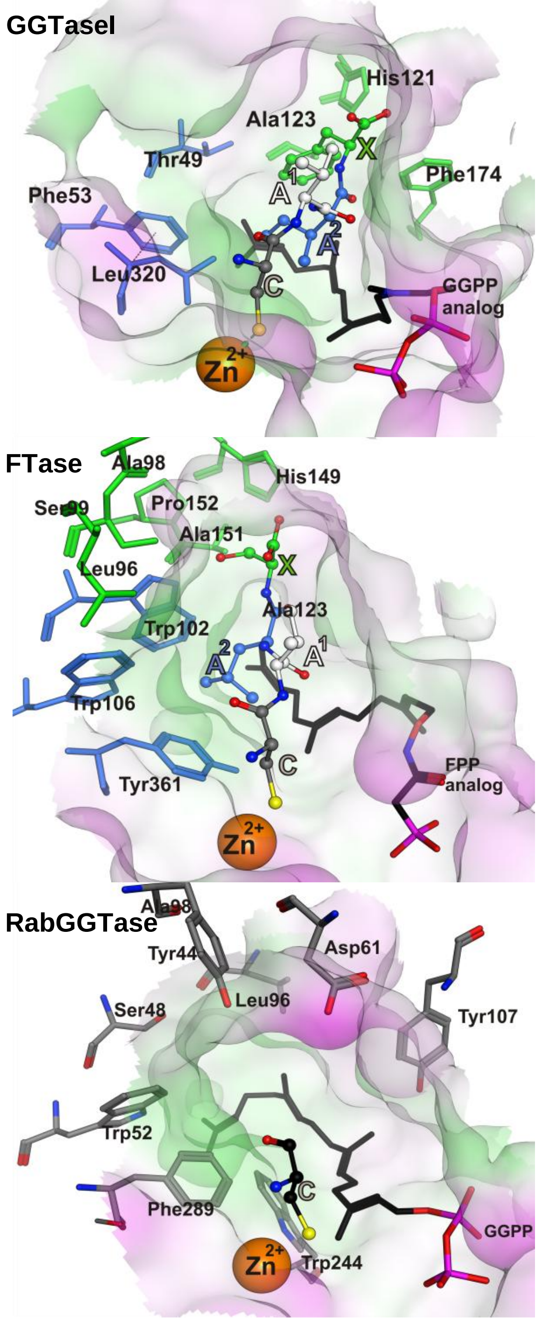
GGTaseI
His121
Ala123
Thr49
X
Phe174
Phe53
A1
A2
Leu320
C
GGPP analog
Zn2+
FTase
Ala98
His149
Ser99
Pro152
Ala151
X
Leu96
Ala123
Trp102
A2
A1
Trp106
C
FPP analog
Tyr361
Zn2+
RabGGTase
Ala98
Tyr44
Asp61
Leu96
Ser48
Tyr107
Trp52
C
Phe289
GGPP
Zn2+
Trp244

Figure 1.8: Detailed comparison of the active site of GGTase I (1TNB), FTase (1TN8) and RabGGTase (overlaid with cysteine, 3DST). A^1 is solvent exposed in both GGTase I and FTase; A^2 interacts with the blue residues whereas X interacts with the green residues. No such particular binding interaction has been found for RabGGTase substrates. The surface representation reflects the lipophilicity of the pocket. Green=lipophilic, purple=hydrophilic, white=neutral.

and GGTase I A^2 binding sites clearly show an increased aromatic character of FTase relative to GGTase I.

Although this has subtle effect on Ras-peptide binding it has a marked effect on inhibitor binding, by providing potential selectivity for either GGTase I or FTase. The X-residue binding site of FTase and GGTase I show distinct electrostatic properties. The FTase pocket is more polar and GGTase I is more hydrophobic. Both pockets will not allow binding of larger residues like tryptophan because of potential steric clashes[54].

As previously mentioned RabGGTase has no specific recognition pattern and enables a digeranylgeranylation process. Since the structure of RabGGTase reveals a large 7.5 Å hydrophobic tunnel nearby the exit groove, it has been suggested that monoprenylated Rab relocates into this tunnel[61]. Recent co-crystallization attempts of RabGGTase in complex with mono- and di-prenylated Rab7 C-termini though, showed no additional electron density in this tunnel[70]. For all peptides the geranylgeranyl moiety was located in the GGPP binding site and for the di-prenylated peptide the second geranylgeranyl product could not be detected. Since the electron densities of all peptide chains were poor, it was suggested that no highly stabilizing interactions are formed with either the active site or the hydrophobic tunnel of RabGGTase. The only strong interaction found was between the prenyl moiety and the GGPP binding site[70].

Comparison of the binding sites of all three prenyl transferase clearly shows structural resemblances and differences. This can be exploited in the design of prenyl transferase inhibitors. Targeting the lipid binding site with GGPP analogues, will most probably lead to dual inhibitors of GGTase I and RabGGTase. One example of such an inhibitor will be discussed in § 1.7.1. CAAX peptidomimetics can generate dual inhibitors of FTase and GGTase I. Inhibitors containing structural features such as zinc binders close to aromatic hydrophobic groups are likely to inhibit both RabGGTase and FTase, as will come forward in this thesis. In order to obtain specific inhibitors for one of the PTases, rational design seems to be crucial.

In this paragraph the post-translational prenylation, crucial for the association to membranes and hence, function of the GTPases Rab, Ras and Rho has been stressed. The prenylation can be carried out by three different prenyl transferases: the CAAX transferases FTase and GGTase I, responsible for the prenylation of Ras and Rho proteins and RabGGTase, responsible for prenylation of Rab proteins.

Now that the Rab GTPases are properly prenylated, they continue in the next ‘life stage’, to function as tightly regulated molecular switches in order to act in diverse biochemical and biological processes.

§ 1.4 Stage II: The tightly regulated molecular switch

Small GTPases show high-affinity binding for GDP and GTP, with a low tendency of GTP hydrolysis and GDP/GTP exchange activity. Consequently, GDP/GTP cycling is controlled by two main classes of regulatory proteins. GEFs promote formation of the active GTP-bound form, whereas GAPs accelerate the intrinsic GTPase activity to promote formation of the inactive GDP-bound form. Both shared and distinct GEFs and GAPs are utilized within GTPase family members, whereas GTPases in different branches exhibit structurally distinct but mechanistically similar GAPs and GEFs[74]. The two nucleotide-bound states have similar conformation but pronounced differences corresponding to the switch regions (Figure 1.3, Figure 1.9). It has been found that the GTP-bound conformation possesses a high affinity for regulator proteins and effectors, which are informed by these conformational changes[26, 75]. Effector molecules are those that interact with GTP-bound small GTPases, and hence, this state is regarded as the active form of all Ras superfamily GTPases. However, for Rab, Arf and Ran GTPases the cycling between the GDP-bound and GTP-bound states are also critical for their activities, since distinct functions are associated with each nucleotide-bound form[25].

§ 1.4.1 The Ras family serves as a molecular switch

Ras GTPases, thus, cycle between an ‘on’ GTP-bound and an ‘off’ GDP-bound state, thereby controlling processes ranging from cell growth to vesicular transport. The difference in structure of GDP- and GTP- bound Ras family proteins are subtle and are mainly limited to the so called ‘switch regions’. These regions are identified to show an increased flexibility both in NMR and electron paramagnetic resonance studies as well as in X-ray crystal structures[76, 77]. Interesting to note is the large variation in structural details of GDP-bound forms compared to GTP-bound forms[78, 79]. The trigger for this conformational change seems to be universal and has been described as a ‘loaded spring mechanism’[80]. In the triphosphate bound form two hydrogen bonds are formed between the phosphate oxygen to the main chain NH groups of Thr and Gly residues in switch I and switch II respectively. Upon release of the γ-phosphate the hydrogen bonds are broken and the switch regions can relax in the GDP-specific conformation (Figure 1.9). The extent of this conformational switch is different among the GTPases; most Rab family members show only minor changes involving the switch regions[80].

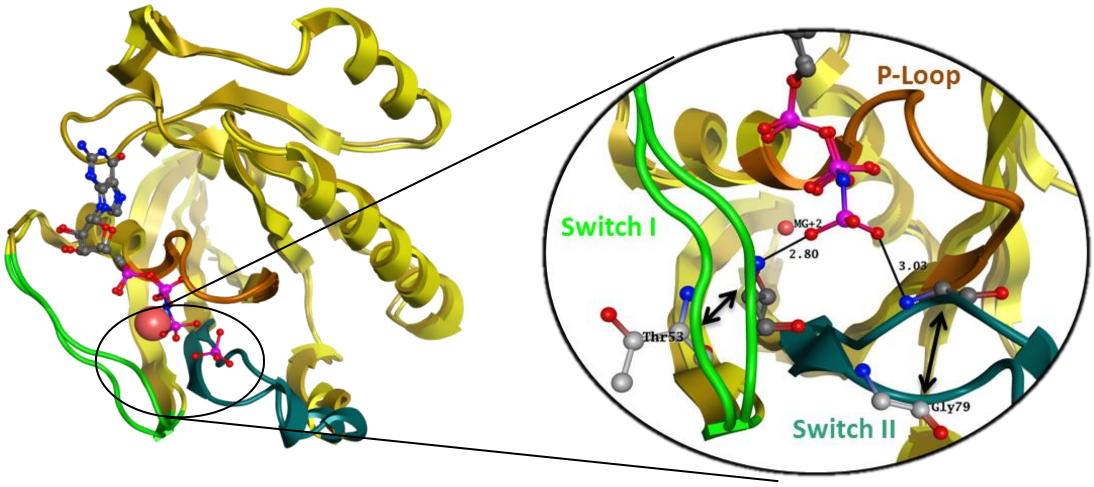

Figure 1.9: Universal Switch Mechanisms of Ras GTPases, depicted for Rab5c (pdb 1Z07, 1Z0D). The hydrogen bonds between Thr53 and Gly79 break upon release of the γ-phosphate leading to a conformational change in the switch regions.

§ 1.4.2 GEFs and GAPs

As mentioned before, the intrinsic exchange of GDP to GTP is slow, as well as the hydrolysis of GTP back to GDP. To control the initiation and duration of Ras activation, specific regulators known as GEFs and GAPs are necessary.

GEFs

GEFs accelerate the exchange from GDP to GTP in a competitive manner. GEF binds to the GDP-GTPase complex and upon binding, GDP is released. This series of reactions is reversible by rebinding of a nucleotide, predominantly GTP, due to its higher concentration in the cell. These reactions are fast and reversible; GEF acting as a catalyst to increase the rate at which the equilibrium between the two states of the protein is reached[81, 82]. The position of equilibrium is dictated by the relative affinities of the GTPases for GDP and GTP, the intracellular concentrations of the nucleotides and the affinities and concentration of additional proteins[80]. GEFs are normally conserved within a given subfamily, but, in contrast to the GTPases themselves, not structurally related. Some general mechanistic similarities can be extracted though. The GEFs interact with the switch I and switch II regions and insert residues close to or into the P loop and the Mg^{2+} binding site. This results in structural changes that are inhibitory for binding of the phosphates to the metal ion[80]. Since binding studies showed the β-phosphate to be the major component of tight binding of the nucleotide, structural disturbance of the P loop most likely contributes to the drastically decreased affinity[80].

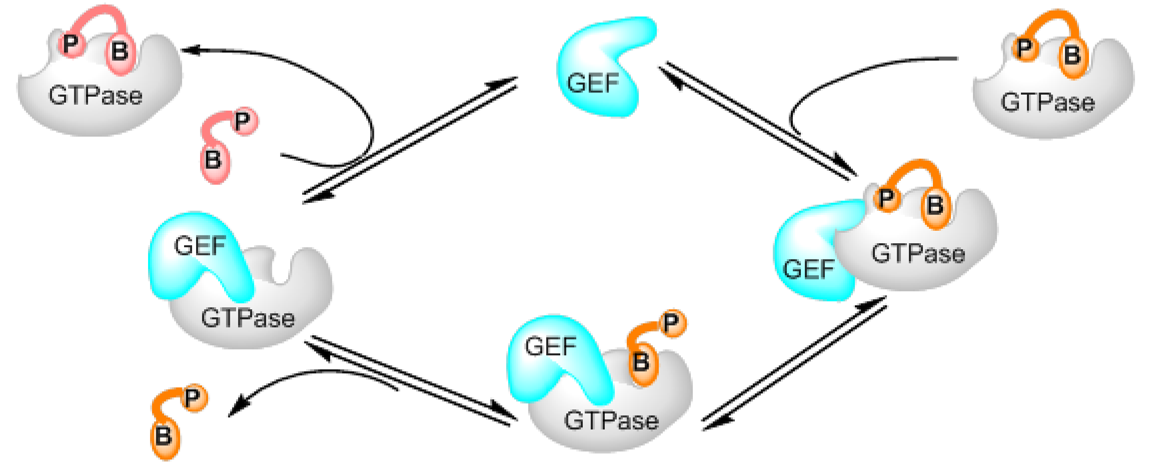

Figure 1.10: Schematic activity of GEF, acting as a catalyst in the nucleotide exchange reaction. The exchange reaction occurs in successive reversible steps. The nucleotide (orange) interacts with the G protein (gray) via its base (B) and its phosphate moieties (P). The GEF (blue) competes with the nucleotide for binding with the G protein and thereby promotes nucleotide exchanges. Inspired by Bos *et al.*[83].

In the last decades, many crystal structures of Ras GTPases in complex with their related GEFs have been determined. The majority of these structures though, are determined without bound nucleotide, giving a rather static picture. For a more complete description of the initial reaction pathway structures of GEF-Ras-GDP are needed. So far, these kind of complexes have only been realized for mutated Arf GTPase and a related plants enzyme of Rho GTPase, Rop GTPase[84, 85].

For Rab GTPases and related yeast proteins (YPTs), so far only nucleotide free GEF complexes have been determined. The five structures published to date are depicted in Figure 1.11[86-90]. In the first place, it is very clear from these complexes that GEFs for Rab GTPases are structurally unrelated. However, also in the GEF-Rab complexes unifying themes in activation can be retrieved. Switch I displacement occurs in all of the GEF-Rab complexes. The broadly conserved phenylalanine/tyrosine that interacts with the guanine ring in nucleotide bound state is displaced by GEF, thereby facilitating nucleotide migration. In addition, the GEFs disturb the Mg^{2+} phosphate site, either through direct occupation or by promoting conformational changes. More insights into the detailed reaction pathway, however, require structures of GEF-Rab-GDP complexes[91].

All Rab related GEFs have a clearly defined mechanism for recruitment to a defined membrane compartment, which is crucial to promote Rab activation in a specific tethering or organelle identity pathway[91]. Rabex-5, for example, acts as a GEF on Rab5 at the early endosome, where it is crucial for controlling the dynamics of membrane fusion. Rabex-5 itself is recruited to endosomes by interaction with ubiquitinated cargo molecules and the Rab-effector protein Rabaptin-5[92-94]. These interactions provide a means to restrict its GEF activity to the early endocytic pathway where Rab5 is required. The Vsp9-domain GEF protein family, to which Rabex-5 belongs, are thought to be specific for Rab5 subfamily proteins; specific Vsp9 domain proteins might associate with different parts of the early endocytic pathway and target different members of groups within the Rab5 subfamily to control unique trafficking pathways[91]. Specific GEFs, thus, contributes to the specificity of the cellular trafficking pathways of the small Rab GTPases.

A remark needs to be placed by at least two of these crystal structures. Mss4, which exact function remains unknown, recently has been shown to only interact with secretory Rab proteins, and in addition shows rather low inefficient GEF activity. Therefore Wixler *et al.* proposed that Mss4 is rather a chaperone for exocytic Rab GTPases than a GEF[95]. SidM, also known as DrrA is not a native GEF, but is an element of *legionella pneumophilia* that hijacks the Rab 1 trafficking pathway[90, 96].

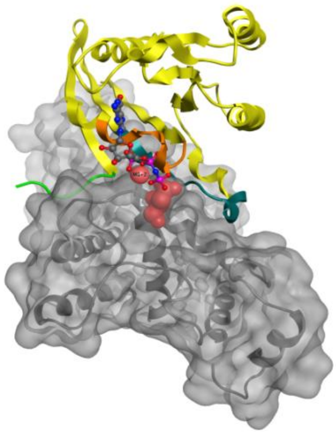

2OT3: Rabex-5, Rab 21, Asp Finger

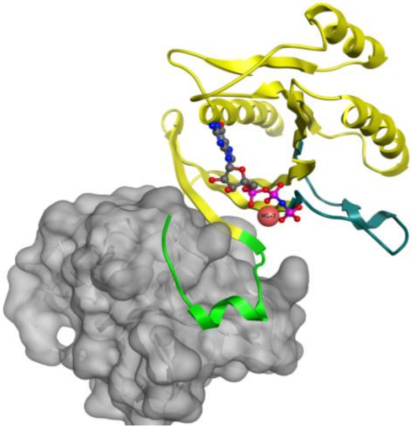

2FU5: Mss4, Rab 8

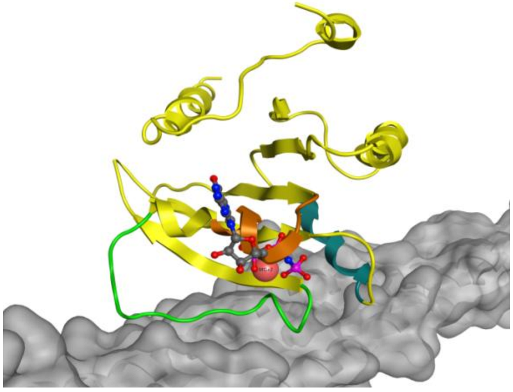

2OCY: Sec 2, Sec 4

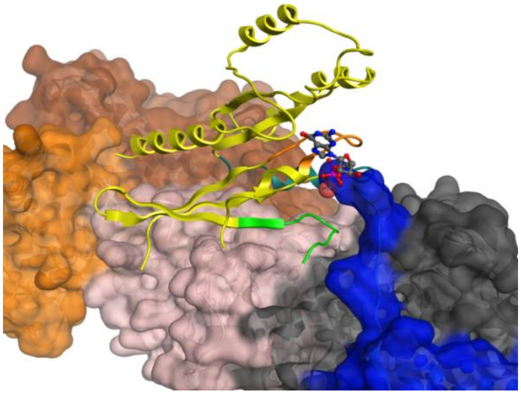

3CUE: **Trapp** (Trs31, Bet3cD, Trs23, Bet5, Bet3cE)Ypt1

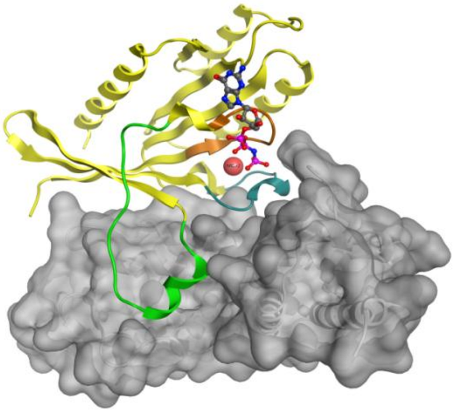

3JZA: SidM/DrrA, Rab 1

Switch 1
Switch II
P-loop
Mg^{2+}
GTP

Figure 1.11: Different Rabs and its GEFs (nucleotide GTP and Mg^{2+} are extracted from Rab5c after superposition) The Rabex-5 accelerates nucleotide exchange by supplying an aspartate finger, destabilizing Mg^{2+} and GDP binding and stabilizing the nucleotide free intermediate[86]. Mss4 induces unfolding of switch I, thereby promoting nucleotide release[87]. Sec2 stabilizes switch I of Sec4 in a conformation that conflicts with nucleotide binding[88]. TRAPP 1 complex uses the C-terminus of Bet3p Chain E (Bet3cE) by occupation of the Mg^{2+} phosphate region and trapping switch I of YPT1 in open conformation[89] SidM/DrrA disrupts the Mg2+/phosphate region by interaction with the switch regions, inducing a displacement of switch I form the nucleotide side[90].

GAPs

The intrinsic rate of GTP hydrolysis is very slow for the Ras superfamily of GTPases. Therefore, the hydrolysis of GTP to GDP is promoted by GAPs. The first mechanistic insights in GAP activation were derived from Ras:RasGAP[97] and Cdc43:RhoGAP[98] crystal structures and showed the involvement of an essential arginine, interacting with the active site of the GTPase. To hydrolyze GTP into GDP, a water molecule needs to attack. The RasGAP stabilizes the position of Gln61 in Ras, which in turn coordinates this attacking water. In addition an arginine inserts in the phosphate binding site and stabilizes the transition state by neutralizing the negative charge of the γ-phosphate. Interestingly, mutation in Gln61 frequently occurs in human tumors and stops GAP induced hydrolysis[97]. A similar mechanism was found for the RhoGAP complex. The general mechanism is depicted in Figure 1.12a

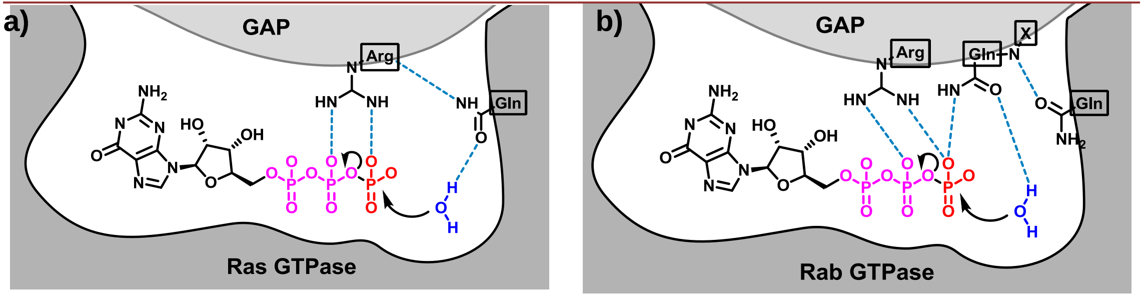

Figure 1.12: General mechanism of GAP promoted GTP hydrolysis for (a) Ras GTPases and (b) Rab GTPases. Specific GAP and GTPase residues are involved in promoting catalysis by coordinating the water molecule for nucleophilic attack and stabilizing the transition state by neutralizing negative charge at the γ-phosphate.

The same catalytic glutamine is also conserved in Rab and the arginine finger is observed in many RabGAPs. Surprisingly, upon structural determination of a Rab:RabGAP complex between the conserved TBC (Trec2/Cdc16/Bub2) domain of Gyp1p, Rab33, GDP and AlF_3 a different transition state was found[99]. Since it is not possible to observe a real transition state, $AlF_3$is used as a transition mimic. The interaction still seems to be stabilized by an arginine finger; however the Rab-glutamine is not interacting with the attacking water. Instead, it binds to the GAP, which in turn positions a Gyp1p-glutamine to interact with the pyrophosphate and attacking water (Figure 1.12b, Figure 1.13). These observations suggest that TBC domains act as dual finger GAPs, supplying an arginine and glutamine finger to enhance GTP hydrolysis [94].

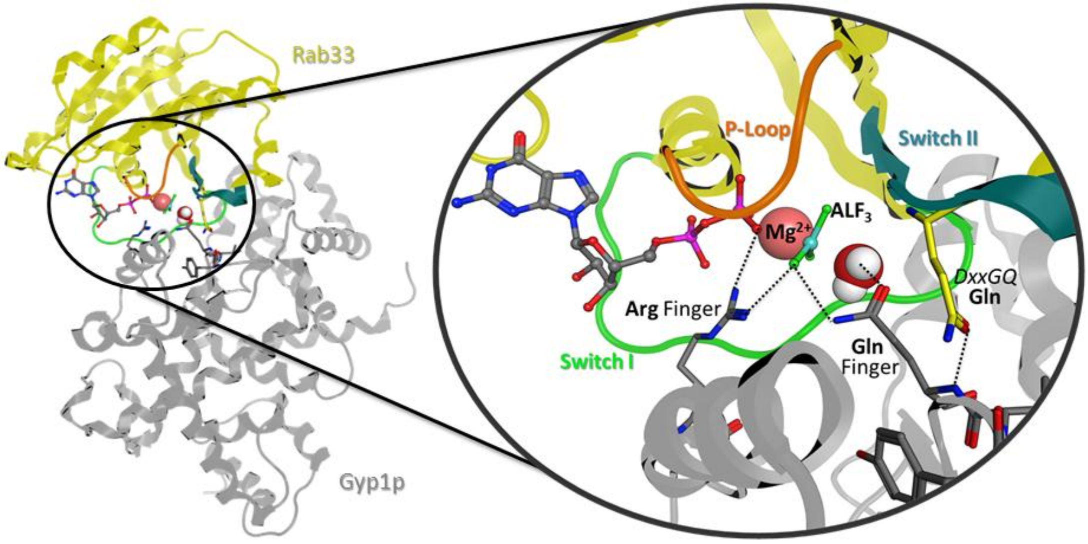

Figure 1.13: Crystal structure of Rab33 in complex with Gyp1p. AlF_3 is used as phosphate transition state mimic (2G77).

In general, Rab GAPs attenuate Rab activity, either temporally or spatially and to decrease Rab activation to prevent accumulation in undesirable locations. Because of these requirement multiple GAPs may act on a single Rab to refine its site of action[91].

§ 1.4.3 Effectors

Effectors for GTPases by definition interact more tightly with the GTP-bound than with the GDP-bound form. Indeed, it has been supported by structural analysis that effector binding involves binding to the switch regions of GTPases[80].

Rab GTPases interact with diverse effectors in their active state to facilitate cargo sorting, to establish long range tethering linkages preceding SNARE-mediated fusion and to couple vesicles or organelles to motor proteins in order to facilitate transport. [94] Except for small families of homologous Rab-binding domains (RBDs), various Rab effectors share little sequence identity. Several effector RBDs in complex with Rab GTPases have been solved and illustrate the similarity and divergence at the structural level (Figure 1.14).

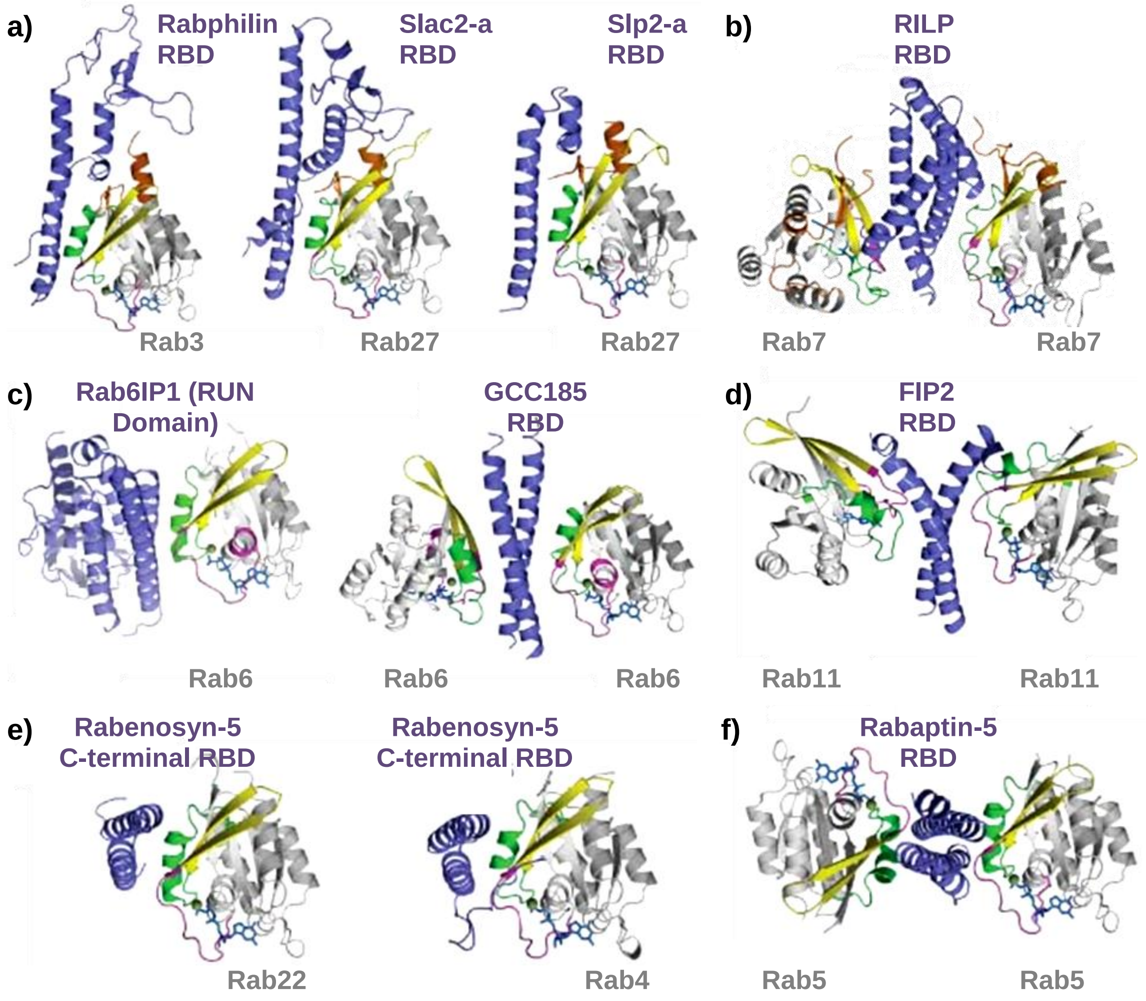
a)
Rabphilin RBD
Slac2-a RBD
Slp2-a RBD
b)
RILP RBD
Rab3
Rab27
Rab27
Rab7
Rab7
c)
Rab6IP1 (RUN Domain)
GCC185 RBD
d)
FIP2 RBD
Rab6
Rab6
Rab6
Rab11
Rab11
e)
Rabenosyn-5 C-terminal RBD
Rabenosyn-5 C-terminal RBD
f)
Rabaptin-5 RBD
Rab22
Rab4
Rab5
Rab5

Figure 1.14: Rabs and their effectors. (a) Structural related RBDs of Rabphilin[43], Slac2-a[100] and Slp2-a[101] with Rab3 and Rab27. (b) RILP:Rab7[102] complex. (c) Rab6IP1[103] and GCC185[103] in complex with Rab6 (d) FIP3:Rab11[104] complex (e), Rabenosyn-5[105] in complex with Rab22 and Rab4 and (f) Rabaptin-5:Rab5[106] complex. Adapted from Lee *et al.*[94].

In general, all known Rab-effector complexes involve interaction of one[43] (Rabphilin:Rab3, Figure 1.14a) or two α-helices of the effector with the GTPase binding site of Rab GTPase, involving switch I, switch II and interswitch regions. These two helices can come from homodimeric coiled coil structures (Rabaptin-5:Rab5[106], Figure 1.14f) or from helix-turn-helix motifs from different regions of the effector molecule (Figure 1.14e). In the Rab6:Rab6IP1[103] complex, the helices are part of a so called helical bundle RUN (RPIP8, UNC-14, NESCA) domain.

Another common feature of all Rab-effector interactions involves the hydrophobic triad, consisting of a phenylaniline and a tryptophan in the interswitch region and a tyrosine near the end of switch II. The phenylalanine residue is part of a conserved IGIDF motif (RabF1), which occurs in most Rab proteins but not in other GTPases. Since this motif undergoes major structural changes upon GTP hydrolysis, it seems to play a significant role in providing specific recognition pattern for the GTP bound Rab GTPases[107]. The specificity of an effector for a particular Rab protein is most likely defined by a combination of interactions with this hydrophobic triad together with additional interaction both inside and outside the switch region.

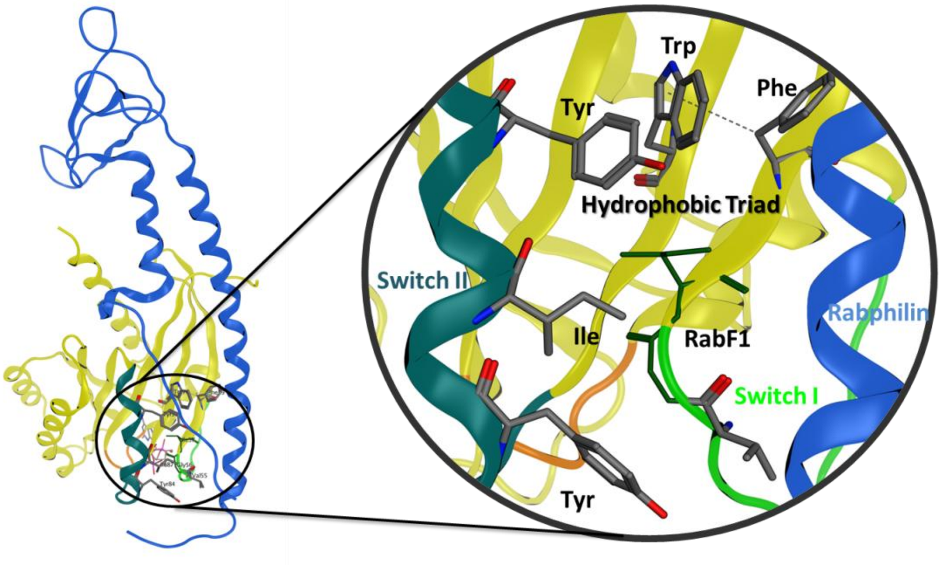

Figure 1.15: Hydrophobic triad interacting with effector. Switch I, Switch II and RabF1 domain, common contributors of effector interactions. (Depicted for Rab3/Rabphilin-3a, pdb:1ZPB[43])

§ 1.4.4 Chaperon proteins

The posttranslational lipid modifications create a lipidated hydrophobic domain that is necessary for attachment to specific proteins as well as anchoring to the membranes. This last process is dynamic, and involves association and dissociation from the compartment membranes. For Rab and Rho protein subfamily members the dissociation into the cytosol is energetically unfavorable. Therefore, guanosine nucleotide dissociation inhibitor (GDI) proteins function as chaperones, rendering the geranylgeranylated proteins soluble. Although these GDIs have no sequence or structural relationship, they share some biological features. GDIs bind with high affinity to the isoprenyl moiety; they can interact with many subfamily members and they slow down the dissociation of the nucleotide. As a consequence GDI serves as a cytosolic reservoir for their corresponding GTPases[108]. In addition to GDI the subfamily of Rab GTPases requires another chaperone protein REP, previously discussed in § 1.3. During the post-translational prenylation, REP is responsible for the specific recognition of Rab proteins and for presenting them to RabGGTase. After geranylgeranylation, REP keeps the geranylgeranyl modified Rab soluble and presents it to the membrane. REP and RabGDI show some striking resemblance in structure but a co-crystal structure of REP:RabGGTase clearly indicates some important side chain interactions which are not present in RabGDI. This explains the fact that RabGGTase is able to interact with REP but not with RabGDI.[107]

In this paragraph, it has been shown that the Ras superfamily of GTPases is able to act on diverse biological processes via a general, highly regulated, mode of action. GTPases act as molecular switches going from the GDP-bound off state into the GTP-bound on state. The ‘switching lever’, is regulated by GAPs and GEFs, since both intrinsic hydrolysis and dissociation of respectively GTP and GDP are too slow for these GTPases. In the active state, the GTPases can interact with their effectors leading to a diverse array of signaling and trafficking events in the cell. Rab and Rho proteins have additional chaperone proteins, GDIs to keep them soluble within the cytosol, representing a 3rd level of regulation of these GTPases. In the next paragraph, the role of the tightly regulated Rab GTPases in vesicle trafficking will be discussed.

§ 1.5 The role of Rab GTPases in vesicle trafficking

§ 1.5.1 Rab GTPases as coordinators of vesicle traffic

In all eukaryotic organisms there is the need to transfer content between distinct membrane-enclosed organelles in a specific and regulated manner. Such transport requires several stages such as vesicle budding, specific transportation, docking/tethering and fusion with their target compartments. Rab GTPases are the key regulators of all these processes on both the exo- and endocytic pathways through their indirect interactions with coat components, motors and SNAREs. These Rab proteins, containing more than 60 family members, are localized to distinct intracellular membranes, thereby controlling diverse crucial trafficking processes (Figure 1.16).

The Exocytic and Endocytic pathway

Trafficking follows two main pathways, the exocytic and endocytic pathways. The exocytic pathway represents the movement of cargo from the endoplasmic reticulum (ER) through the trans Golgi to the plasma membrane (PM). Newly synthesized proteins enter the ER during their translation via a translocon pore. In order to exit the ER; vesicles form at the so-called ER exit sites and move to the cis Golgi. The vesicular transport between the Golgi cisternae is poorly understood. It has been proposed that vesicles move cargo forward and resident proteins backward between the Golgi cisternae[109].

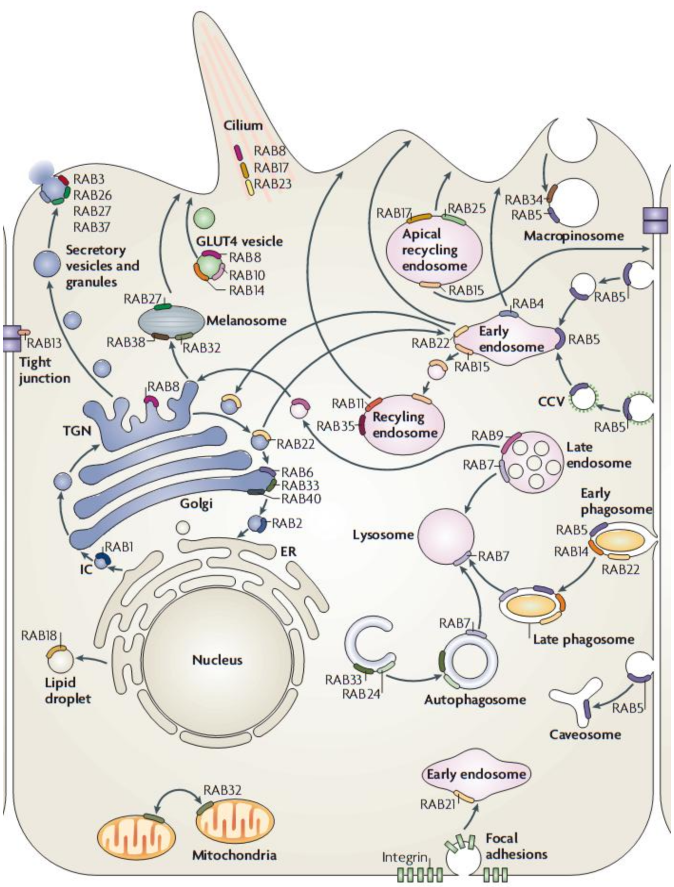
Cilium
RAB8
RAB17
RAB23
RAB3
RAB26
RAB27
RAB37
Secretory vesicles and granules
GLUT4 vesicle
RAB8
RAB10
RAB14
RAB27
Melanosome
RAB13
Tight junction
RAB38
RAB32
RAB8
TGN
Golgi
RAB1
IC
RAB18
Lipid droplet
Nucleus
ER
RAB22
RAB6
RAB33
RAB40
RAB2
RAB17
RAB25
Apical recycling endosome
RAB15
RAB34
RAB5
Macropinosome
RAB5
RAB4
RAB22
Early endosome
RAB5
RAB15
CCV
RAB5
RAB11
RAB35
Recyling endosome
RAB9
RAB7
Late endosome
Early phagosome
Lysosome
RAB7
RAB5
RAB14
RAB22
Late phagosome
RAB7
RAB33
RAB24
Autophagosome
RAB5
Caveosome
Early endosome
RAB21
Integrin
Focal adhesions
RAB32
Mitochondria

Figure 1.16: Localization and function of selected Rab GTPases. Rab1 mediates ER-Golgi trafficking. Rab2 regulates Golgi-ER trafficking. Rab4 regulates fast endocytic recycling. Rab5, localized at early endosomes, phagosomes, caveosomes and plasma membrane controls endocytosis and endosome fusion of clathrin-coated vesicles (CVVs). Rab6 is involved in intra-Golgi trafficking. Rab7 mediates maturation of late endosomes and phagosomes, as well as their fusion with lysosomes. Rab9 mediates trafficking from late endosomes to the trans-Golgi network (TGN). Rab11 mediates slow endocytic recycling. Rab27 acts in various types of regulated exocytic events as well as in translocation of melanosomes to the cell periphery. (Adopted from Stenmark)[18].

During the last step of the exocytic pathway, exocytosis, secretory vesicles are formed at the trans-Golgi and fuse with the PM to deliver their protein and lipid cargo. As a direct consequence of this pathway, resident proteins as well as excess lipids have to be retrieved back to their 'home compartments'. Therefore, every forward transport step is complemented by a retrograde transport step. Major intersections are the IC (intermediate compartment) in between the ER and Golgi as well as recycling endosomes, which recycle proteins back to the PM or Golgi[109].

The endocytic pathway represents the internalization of cargo from the cell milieu. This internalization can happen via a variety of routes, for example through dynamin-dependent routes such as clathrin-coated vesicles (CCVs), caveolar endocytosis or raft-dependent internalization, where dynamin is essential for vesicle scission and dynamin-independent uptake. The best studied endocytic pathway starts after CCVs formation. After vesicle uncoating, the vesicles fuse to form early endosomes. These early endosomes sort cargo into a variety of different pathways and have a characteristic tubular/vesicular morphology. The tubules splice off while carrying membrane proteins into the recycling pathway, whereas the vesicular portion matures into a late endosome. Parts of the late endosome are internalized as vesicles and fused with the lysosome, where internalized material and membrane proteins are degraded[109].

The exocytic pathway and endocytic pathway are interconnected on several stages. For example, newly synthesized endosomal and lysosomal proteins and lipids are shuttled from the trans Golgi to the early endosomes. These proteins, labeled with mannose-6-phosphate, are sorted by M6P receptors (M6PRs) into vesicles and targeted to endocytic compartments. These M6PRs then travel from early endosomes to late endosomes, upon which they are retrograde transported to the Golgi[109].

Rab proteins are highly involved in both the endo- and exocytic pathway and crosstalk. They are involved in all steps of vesicular transport; sorting/budding, uncoating, motility and tethering/fusion (Figure 1.17). All these transport steps requires binding of Rab effectors to active Rab proteins.

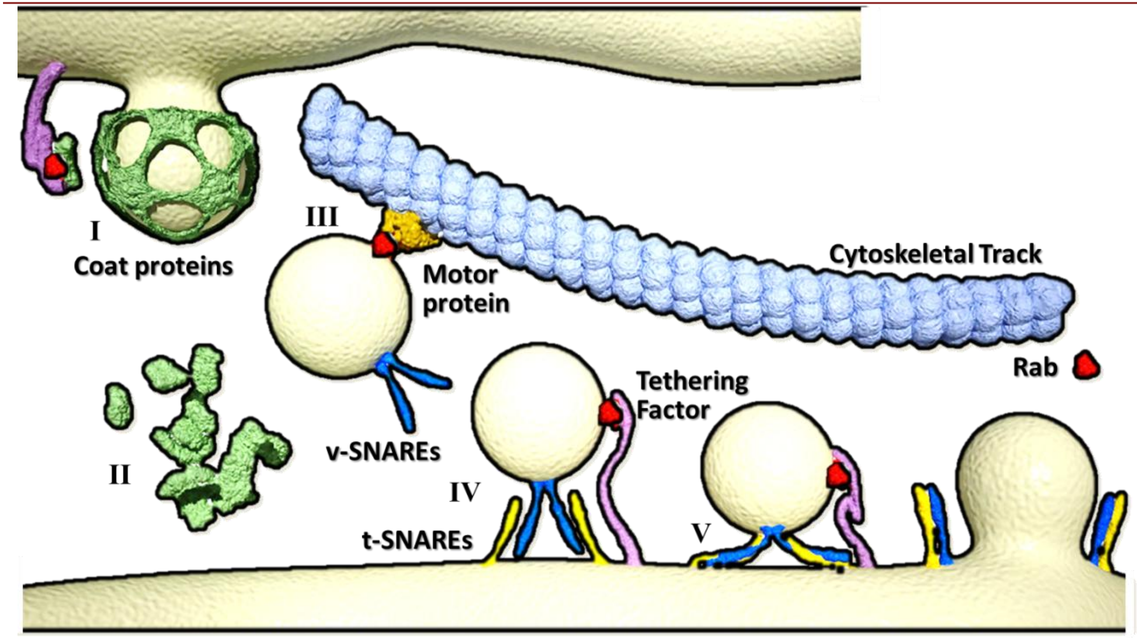

Figure 1.17: Sequential steps of vesicle trafficking, I) sorting, II) uncoating, III) Motility, IV) docking, V) fusion, adapted from Vazques-Martinez et al[110]. The independent steps are described in the text.

I. Vesicle Sorting

Cargo selection into specific coated transport vesicles is a fundamental mechanism in intracellular trafficking. There are three main types of coated vesicles, CCVs, and vesicles coated with coat protein complex I (COPI) or coat protein complex II (COPII). Small GTPases Arf (CCV/COPI) and Sar1(COPII) regulate coat assembly and disassembly[111]. The formation of such a coat is cargo-specific. This specificity is partially due to recognition of structural features of the cargo, but ensured further by membrane curvature, lipid composition and Rab GTPases[112].

For example, the retrograde transport of M6PRs from late endosomes to the trans Golgi network has been linked to late endosomal Rab9. TIP47 is a sorting adaptor that recognizes the cytosolic tail of M6PRs and is also an effector of Rab9[113]. The interaction with GTP-boundRab9 causes the recruitment of TIP47 to the late endosomes and increases the affinity of TIP47 for its cargo. Thereby, Rab9 mediates the M6PR sorting into late endosomal recycling buds.

Rab5 is another Rab GTPase identified in cargo sequestration. McLauchlan*et al.* showed that Rab5-GDI recruitment is necessary to ensure ligand sequestration in the formation of clathrin-coated pits[114]. Upon recruitment of the coat proteins into the membrane, matrices are formed. These matrices however are only capable of ligand sequestration after additional recruitment of Rab5-GDI. Interestingly, Rab5 is also involved in the next step of vesicle trafficking: vesicle uncoating.

II. Vesicle Uncoating

The vesicle coat, necessary for sorting and budding, interferes with membrane fusion and therefore needs to be disassembled prior to engagement with the target membrane[18]. It has been shown that Rab5 and its GEF GAPVD1 (GTPase-activating protein and VPS9 domain-containing protein 1, containing an N-terminal GAP domain and a C-terminal GEF domain) can coordinate uncoating of endocytic vesicles consistent of clathrin coat and cargo adaptor protein complex AP2[115]. The AP2 derived vesicles are stabilized by phosphoinositide (PI) and enhanced by phosphorylation of an AP2 subunit by AP2-associated kinase 1 (AAK1). Uncoating is promoted by a direct displacement of AAK1 by GAPVD1 as well as a Rab5 mediated increased turnover of the PI. The Rab GTPase and its GEF thus displays a synergistic effect on vesicle uncoating.

III. Vesicle Motility

Vesicle delivery is mediated by actin filaments and microtubules, which facilitate local and long-range vesicle transport, respectively[116]. Motor proteins are capable of guiding directional vesicle transport along these molecular cables. Actin-mediated transport occurs via members of the myosin family[117]. Two families of motor proteins are involved in microtubule transport. In general, kinesin motors transport cargo toward the plus end of the microtubules located in the cell periphery, whereas dynein motors mediates cargo transport toward the microtubule organizing center (MTOC)[118, 119].

Several Rab GTPases have been identified to interact with motor proteins. Rab6, for example can interact with Rabkinesin-6 and leads from the Golgi toward the plus end of the microtubule[120]. Interestingly Rab6 can also interact with the dynactin subunit p150^{Glued}, hence traveling in the opposite direction[121]. Thus, active Rab GTPases can both regulate plus-end and minus-end transport of Golgi compartments. Other Rabs that interact with motor proteins, either direct or indirect, are Rab4, Rab5, Rab7, Rab8, Rab11 and Rab27a. The major involvement of Rab GTPases in vesicle motility most likely reflects the important role of Rab GTPases in connecting the transport vesicle to its designated motor[116].

IV. Vesicle Tethering

Once an organelle is close to its target membrane, tethers mediate the initial recognition of the vesicle. These tethering factors, which interact with Rab GTPases, can be roughly divided into two categories; long range tethers and short range, multisubunit complexes[122, 123]. For example, Sec4, a yeast Rab GTPase recruits Sec15, a subunit of the octameric exocyst tethering complex involved in the targeting of post-Golgi vesicles to the plasma membrane[124]. Besides the Rab binding domain, the exocyst complex bears subunits that bind to Rho GTPases located on the plasma membrane. Therefore, binding of Rab to the exocyst leads to proximity of the vesicle to the Rho GTPase containing plasma membrane[125]. Other examples of Rab GTPases involved in tethering are Rab1, by binding to p115[126] and Rab5, by the binding tethering factor early endosome antigen 1 (EEA1)[127] or rabenosyn 5[128].

V. Vesicle Fusion

Once the vesicle is docked to its acceptor membrane, fusion has to take place. The actual fusion process is mediated by SNARE (soluble NSF attachment protein receptor where NSF stands for N-ethyl-maleimide-sensitive fusion protein) proteins. SNAREs are classically divided in vesicle snares (*v*-SNAREs) and target snares (*t*-SNAREs). The *v*-SNARE is incorporated in the vesicle and interacts with the *t*-SNARE on the target membrane. They contain a SNARE motif of 60-70 amino acids arranged in heptad repeats, which can undergo coiled-coil formation. Upon pairing of a single *v*-snare with three *t*-snares a stable intertwined helix is formed between the different membranes known as a *trans*-SNARE complex. The *trans*-SNARE complex is ‘zipped up’ from the N-terminal ends toward the C-terminal membrane anchors, pulling the membranes together, opening up a fusion pore and finally vesicle fusion. NSF then uses ATP to unravel the coiled-coil interaction and parts the SNARE for reuse[129].Ohya *et al.* showed that Rab5 and SNARE proteins synergistically drive endosomal fusion by interaction with several accessory proteins. Rab5 effector rabenosyn-5 interacts with SNARE accessory factor vacuolar protein sorting-associated protein 45(VPS45), whereas linker protein prenylated Rab acceptor 1(PRA1) binds to both Rabs and SNAREs[130]. Thereby, Rab GTPases have been implicated to participate in driving the fusion process[131].

After membrane fusion, the associated Rab GTPase is converted to its inactive GDP bound form, extracted by GDI and transported to the donor membrane. It has been proposed that a GDI displacement factor (GDF) promotes the reinsertion of Rab GTPase into the donor membrane[132]. However, it has been suggested recently that GEF activity alone, by exchanging GDP into GTP, can be sufficient to extract Rab from GDI into the target membrane as well[90].

Rab Cascades

Different Rab-defined compartments are addressed while a vesicle transits from one organelle to another. Interestingly, it has been shown for some Rabs that specific population exists; Rab4, Rab5 and Rab11 domains, although dynamic, do not significantly mix over time. The same pattern is observed in the late endosomes, comprising distinct membrane domains for Rab7 and Rab9. It is proposed that the mechanism for this behavior relates to a Rab GEF and GAP cascade. Upstream Rabs are responsible for recruiting GEF for their downstream Rabs, whereas the downstream Rabs in turn recruits a GAP for their upstream Rabs. These countercurrent cascades ensure that appropriate downstream Rab is recruited and upstream Rab is inactivated in parallel[133]. Several modes of cross talk have been described in addition (Figure 1.18), thereby presenting a regulation mechanism at the meta-level of Rab trafficking in addition to the tight regulation of Rab activity already regulated by its GEFs and GAPs[18].

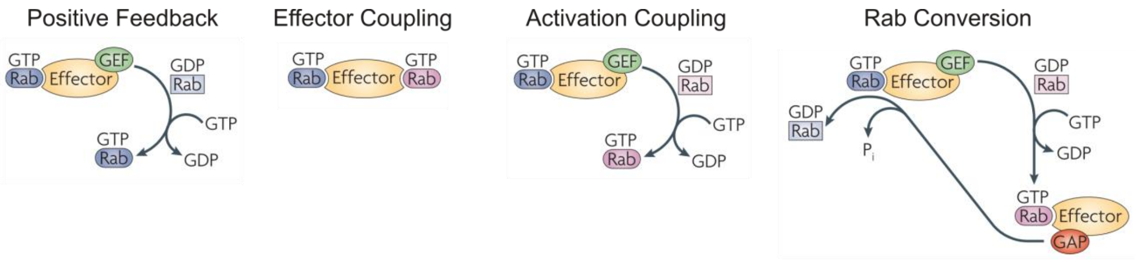
Positive Feedback
GTP
GEF
Rab
Effector
GDP
Rab
GTP
GTP
Rab
GDP
Effector Coupling
GTP
GTP
Rab
Effector
Rab
Activation Coupling
GTP
GEF
Rab
Effector
GDP
Rab
GTP
GTP
Rab
GDP
Rab Conversion
GTP
GEF
Rab
Effector
GDP
Rab
GDP
Rab
P_i
GTP
GDP
GTP
Rab
Effector
GAP

Figure 1.18: Coordination of Rab Functions. a) Positive feedback loop: a Rab effector complex contains GEF for the same Rab. b) Effector coupling: the effector has binding sites for two Rabs, thereby coordinating microdomains in the same membrane. c) Activation coupling: a GEF for the downstream Rab is part of the effector complex. d) The effector of downstream Rab contains a GAP for its upstream Rab. (Adapted from Stenmark[18])

§ 1.5.2 *Rab GTPases in disease*

The central role of Rab GTPases in membrane trafficking and thereby its overall physiological importance is reflected by many diseases, either associated with Rabs themselves, their regulators or their effectors. Infectious, neurological and endocrinological diseases result from pathogen-induced or inherited dysfunction of Rab pathways, signifying the crucial role of membrane trafficking in immunity and exocytosis**[18]**. Some examples of diseases due to inherited dysfunction in Rab GTPases and related enzymes are given in Figure 1.19

Whereas mutations in Ras and related subfamily Rho were well known for their oncogenic roles, the involvement of Rab GTPases in human cancer has only recently been acknowledged. Several Rab family members as well as effectors and regulator genes have been implicated in tumorigenesis[134].

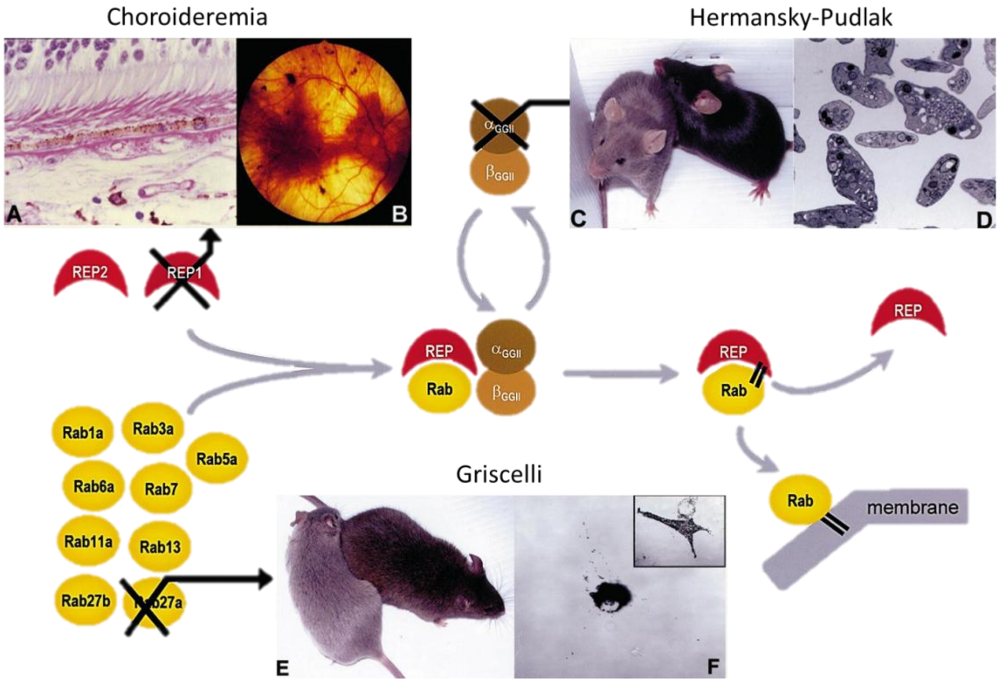
Choroideremia
Hermansky-Pudlak
A
B
C
D
α_{GGII}
β_{GGII}
REP2
REP1
REP
Rab
α_{GGII}
β_{GGII}
REP
Rab
REP
Rab1a
Rab3a
Rab5a
Rab6a
Rab7
Rab11a
Rab13
Rab27b
Rab27a
Griscelli
Rab
membrane
E
F

Figure 1.19: Disease due to impaired function of Rab GTPase or related enzymes. Choroideremia is caused by mutation in REP1. Mutation in the α-subunit of RabGGTase leads to hypopigmentation in the Hermansky-Pudlak syndrome. Mutation in Rab27a is involved in Griscelli syndrome type 2, causing partial albinism with immunodeficiency. Adapted from Pereira-Leal*et al.*[52].

Rabs and cancer

There is a tight regulation between receptor signaling and membrane trafficking[135]. Therefore, the involvement of Rab GTPases in cell signaling is also reflected by the association of cancer with Rab dysfunction[18]. In particular, Rabs have been implicated in the progression of multiple cancers[134] due to the significant role of membrane traffic in metastatic transformation of tumor cells[136]. The best characterized example of Rab implicated in cancer is Rab25. Rab25 is frequently overexpressed in breast and ovarian cancer and is associated with decreased survival[137]. Since Rab25 is involved in trafficking through recycling endosomes[138], it is speculated that the effect of Rab25 on proliferation and apoptosis are caused by aberrant recycling of signaling receptors[18]. Recent studies showed that Rab25 interacts directly with the transmembrane proteinβ_1 integrin. By directing the localization of integrin-recycling vesicles Rab25 contributes to tumor progression and facilitates invasive cell migration of the tumor cells[139]. In total at least 21 different Rab genes have been implicated in tumorigenesis, as well as related proteins like RabGDI RabGGTase α-subunit and Rabaptin-5[140].

Rabs and neurological disease

Rabs have also been implicated in neurological diseases. Specialized functions of Rabs are important for neurite growth and remodeling (*e.g.* Rab11, Rab13), synaptic functions (Rab3) and general nervous system development (Rab23)[141]. Parkinson's disease has been connected to Rab activity as well. α-Synuclein (αsyn), a protein with unknown function that can aggregate into insoluble fibrils, represents a main component of Lewy Bodies once mutated or overexpressed. Lewy Bodies are the typical aggregates of proteins inside nerve cells observed in Parkinson's disease and Alzheimer's disease[142]. Interestingly, mutated αsyn(point mutation A30P) was found to interact with Rab3a, Rab5 and Rab8, whereas no interaction was observed for wild-type αsyn[143]. In addition, it was found that the phenotype of overexpressed αsyn disrupting ER-to-Golgi transport, could be rescued by overexpression of Rab1[144], thus reducing the toxic effect. Also Rab3 and Rab8 have been associated with αsyn, indicating that αsyn may affect several membrane trafficking pathways[145]. Other neurological diseases that are associated with Rab include Huntington's disease (Rab8 and Rab11), carpenter syndrome (mutated Rab23), non-specific X-linked mental retardation (mutated GDI1) and Charcot-Marie-Tooth disease (mutated Rab7)[18, 133].

Rabs and infectious disease

Pathogens can use the endocytic pathway in order to enter cells. Therefore, some infectious microorganisms hijack Rab-dependent pathways to ensure their own uptake. For example, *Salmonella enterica* and *Salmonella typhimurium* reside in *Salmonella* containing vesicles (SCV) in cells that transition from Rab5 to Rab7[146]. Rab7 is then positioned close to the Golgi by its effectors[147]. Acidification releases specific factors that block the compartment from fusing with the lysosome and anchors the SCV to the Golgi, an association necessary for intracellular bacterial replication[148]. Interestingly, the SCV accumulates a variety of Rab proteins, but not those which are responsible of phagosome maturation into lysosomes, thereby bypassing this process[149]. *Chlamydia*, once inside the cell, uses a similar mechanism and avoids being directed to the lysosomes. It releases effector proteins that prevent recruitment of Rab5, Rab7 and Rab9 and recruits exocytic and Golgi-bound Rabs like Rab4, Rab11 and Rab1[150]. Pathogen hijacking of vesicles can also occur between the ER and IC. *Legionella pneumophilia* secretes proteins that target the GTP cycle of Rab1. DrrA act as both a GEF and GDF for Rab1, whereas another protein known as LepB act as a Rab1 GAP[151]. Consequently, *Legionella*-containing vacuoles recruit Rab1 and behave functionally as ER or IC like-membranes, thereby evading destruction in lysosomes.

§ 1.6 The Prenylation machinery as drug target

Mutations in the superfamily of Ras GTPases leading to cancer are mostly associated with a constitutively active GTP-bound conformation[152]. Therefore, strategies have been developed in order to reduce activity of the GTPases. Since Ras GTPases require posttranslational isoprenylation for correct membrane association and function, the lipidation step has been targeted for drug discovery[153]. Several strategies (summarized in Figure 1.20) can be adopted to inhibit the prenylation reaction. One option is the depletion of substrates for the prenylation reaction, either farnesylpyrophosphate (FPP) or geranylgeranylpyrophosphate (GGPP). These substrates are both products of the mevalonate or the deoxyxylulose-5-phosphate isoprenoid biosynthesis pathways.[50] Small molecule intervention, using statins to inhibit HMG-CoA reductase or employing bisphosphonates to inhibit FPP synthase, result in depletion of the prenyldonor and hence in inhibition of posttranslational prenylation. Such a strategy, however, leads to the inhibition of all prenylation reactions as well as to blockage of formation of other secondary products of the mevalonate pathway such as terpenoids and hormones.[154]

A more attractive strategy would be the selective inhibition of the PTases.

Especially FTase has been an attractive target for anti-cancer drug development due to its ability to farnesylate oncogenic HRAS, NRAS and KRAS, which are often overexpressed in human cancers. Several developed FTase inhibitors (FTIs) have reached clinical trials (Figure 1.21). Preclinically, they showed inhibition of FTase in the low nM range for HRAS and KRAS and were found to be active in a large panel of cancer cell lines. The observed preclinical potency of these agents, however, was not reflected in the clinical trials[15]. Only tipifarnib (**1**) and lonafarnib (**2**) were tested in Phase III clinical trials, whereas BMS-214662 (**3**) did not succeed into Phase II due to dose-limiting toxicity without clear effect. Phase III trials were unsuccessful for both tipifarnib and lonafarnib, due to absence of clear anti-tumor activity[153, 155]. FTIs in general did not show the anticipated activity in solid tumor cells as single agents[16].

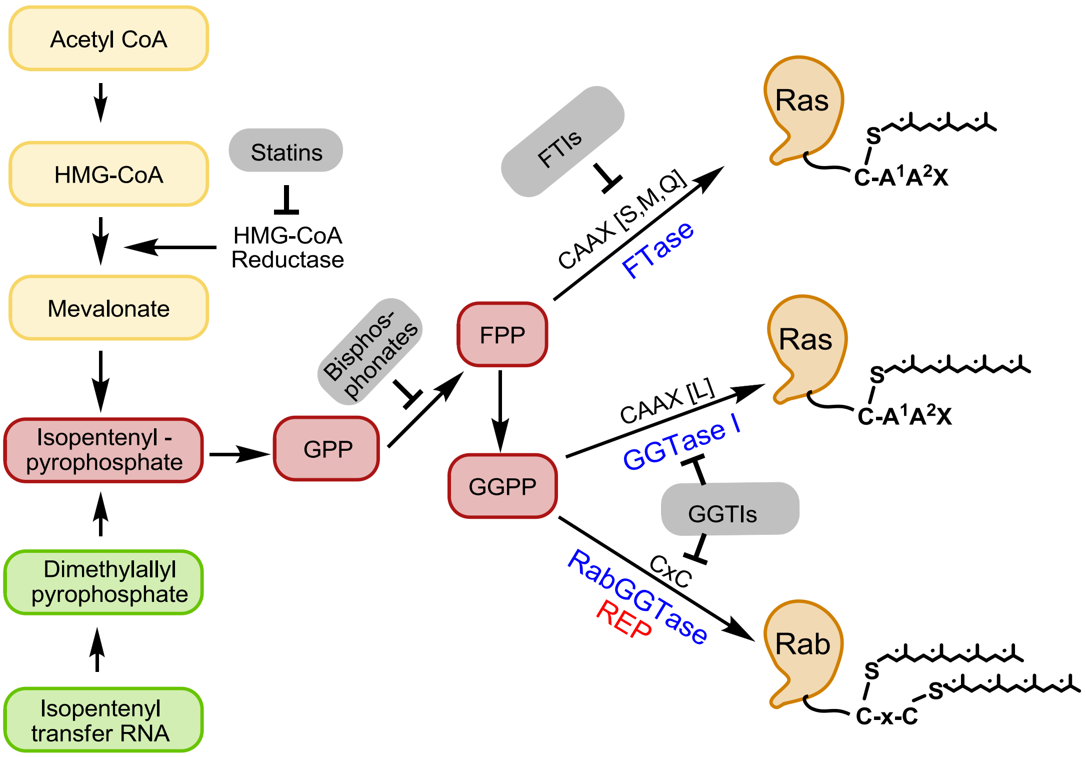
Acetyl CoA
HMG-CoA
Statins
HMG-CoA Reductase
Mevalonate
Isopentenyl - pyrophosphate
Dimethylallyl pyrophosphate
Isopentenyl transfer RNA
GPP
Bisphos- phonates
FPP
GGPP
FTIs
CAAX [S,M,Q]
FTase
CAAX [L]
GGTase I
GGTIs
CxC
RabGGTase
REP
Ras
Ras
Rab
S
C-A1A2X
S
C-A1A2X
S
S
C-x-C

Figure 1.20: Isoprenoid synthesis pathway and potential therapeutic interventions.

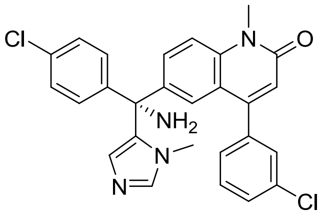

Tipifarnib (**1**)

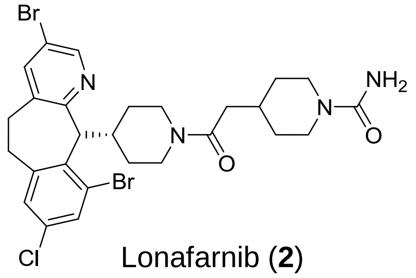

Lonafarnib (**2**)

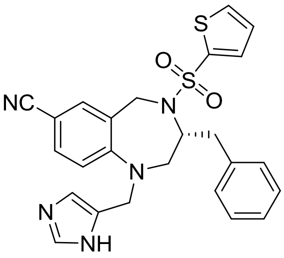

BMS-214662 (**3**)

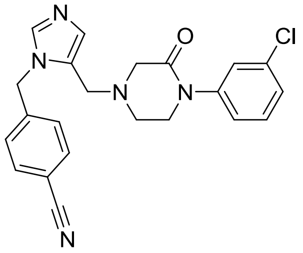

L778123 (**4**)

Figure 1.21: FTIs that reached clinical trials.

The alternative prenylation of KRAS and NRAS by GGTase I has been cited as the main reason for the lack of activity of FTase inhibitors in these clinical trials[16]. Therefore, inhibitors that simultaneously alter FTase and GGTase I have been developed. FTI L778,123 (**4**), a dual inhibitor of FTase and GGTase I was well tolerated in phase I and phase II clinical trials and was shown to inhibit Rap1A and HDJ2 but not KRAS. However, QT prolongation which is associated with lethal arrhythmias was observed in at least one of the patients and further development was aborted[156]. The proof-of-concept that inhibition of the RAS protein function by inhibition of the prenyl transferases is of clinical use still remains inconclusive.

Interestingly, Lackner *et al.* showed that compounds related to BMS-214662 were also potent inhibitors of RabGGTase. In addition, they found the apoptotic effect in *C. elegans* related to RabGGTase and not FTase inhibition by using RNA*i*[17]. Therefore, RabGGTase could also be a potential anti-cancer target.

§ 1.7 RabGGTase as biological target

§ 1.7.1 Increasing efforts toward RabGGTase inhibitors

The increasing association of Rab GTPase with cancer, as well as the findings that RabGGTase could be the actual target of some FTIs, shows a clear need for the development of small molecule tools to inhibit RabGGTase selectively.

During the course of the last decade, limited efforts have been made toward the development of RabGGTase inhibitors. The type of inhibitors includes GGPP mimics, phosphonocarboxylates, peptide-based inhibitors and small molecule inhibitors. However, the inhibitors developed so far suffer from various drawbacks, such as lack of clear structure-activity-relationships (SAR) or absence of cellular activity. In this paragraph, the developed inhibitors and their properties will be discussed.

Phosphonocarboxylates: Selective inhibitors of RabGGTase

The first reported inhibitor of RabGGTase was a phosphonocarboxylate derivative of risedronate, a bisphosphonate drug which inhibits FPP synthase and thereby the function of bone-resorbing osteoplasts. The phosphonocarboxylate derivative, named 3-PEHPC, was shown to inhibit bone resorption as well, albeit by a different mechanism (5, Figure 1.22). It was shown that 3-PEHPC specifically inhibited RabGGTase, thereby being the first selective inhibitor of RabGGTase reported.[157] 5 inhibited Rab prenylation in J774 macrophage cells in a dose-dependent manner with a cellular IC_{50} of 560 µM. A similar IC_{50} of 600 µM was determined using a radioactive *in vitro* assay with RabGGTase, Rab1a, REP1 and [^{3}H]GGPP. The specific effect of 3-PEHPC on RabGGTase was further demonstrated employing different prenylation substrates, HRas, Rap1 and Rab6, which are prenylated by FTase, GGTase I and RabGGTase respectively. Prenylation of Rab6 was completely inhibited by 5, without affecting the prenylation of HRas and Rap1. Therefore, it was suggested by the authors that 3-PEHPC was a selective inhibitor of RabGGTase and consequently, an inhibitor of bone resorption.

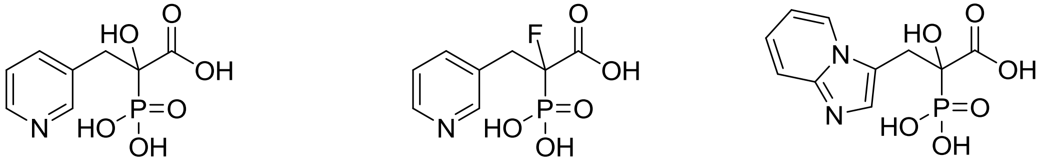

5 3-PEHPC[157] — IC_{50}=24.1 µM[158]-600 µM[157]

6 F-3-PEHPC[158] — IC_{50}=16.3 µM

7 (+)-3-IPEHPC[159] — IC_{50}=1.3 µM

Figure 1.22: Phosphonocarboxylate inhibitors of RabGGTase.

Some inhibitors based on 3-PEHPC were developed to address the moderate activity of 3-PEHPC. In order to assess the role of the α-OH group in binding and bone mineral affinity, Marma *et al.* synthesized halogenated derivatives of 3-PEHPC[158]. It could be shown that the α-OH group was essential for bone mineral affinity, but played no major effect in RabGGTase affinity. This suggests that RabGGTase is not the important target for the cellular effect. Halogenated analogs all were active in a similar range (1-1.5 times as potent as 3-PEHPC, 6, Figure 1.22), indicating a lack of interactions between the α-OH and the RabGGTase active site.

The most active phosphonocarboxylate-based RabGGTase inhibitor 7 was reported by Baron *et al.* and possessed in contrast to the pyridine ring in 3-PEHPC an imidazo[1,2-a]pyridine core, based on another bisphosphonic acid: minodronic acid[159, 160]. Interestingly, a mixed inhibition mode was found both regarding the substrate (GGPP) and the protein (Rab1). Upon further experimentation, it was found that these phosphonocarboxylate based inhibitors only effectively inhibited the 2nd prenylation of RabGGTase. Whereas Rab proteins containing a double cysteine prenylation motif such as Rab1a, Rab5a, Rab6a and Rab27a were all inhibited by 7, no inhibition was observed for single cysteine prenylation motif containing proteins like Rab13, Rab18 and Rab23. Furthermore, it was found that the inhibitor did not compete for the RabGGTase-bound GGPP both in Rab free and Rab bound state. It appeared that 7 somehow locked the GGPP in the RabGGTase binding site, therefore, it was suggested that the inhibition may reflect the inability of a binding transition, not allowing the monoprenylated Rab to move to a second binding site to undergo its 2nd prenylation. Considering all these observations, it was proposed that phosphonocarboxylates most probably bind into a putative binding site, which is occupied upon migration of the monoprenylated Rab preparing for the 2nd prenylation.

Although compound 7 seems to be a promising tool compound, there are some drawbacks. Obviously, the compound only inhibits the 2nd prenylation and therefore cannot be used to study prenylation of Rabs which undergo monoprenylation. Further, it was subsequently shown that 7 also inhibited geranylgeranylpyrophosphate synthase (GGPPS)[159, 160]. Therefore, its effect in cells cannot be contributed to RabGGTase inhibition alone.

Substrate mimic: GGTI-2Z

Recently, a non-peptidomimetic dual inhibitor of GGTase I / RabGGTase has been reported by Sane *et al*.[12]. The compound, named GGTI-2Z (8) in combination with Lovastatin (9), a HMG-CoA reductase inhibitor, was shown to inhibit GGTase I and RabGGTase without affecting farnesylation. This combination therapy of inhibitors targets the prenylation pathway at two distinct steps; depletion of the cellular prenylpyrophosphates (PPP) pools via statin treatment, as well as inhibition of the prenyltransferases. Cumulatively, a competitive prenyl transferase inhibitor (PTI) will be more effective at the lower level of PPP induced by the statin[16]. It was found that the combination therapy of 8 & 9 resulted in an increase in unprenylated Rap1 and Rab5, respectively indicating inhibition of GGTase I and RabGGTase (Figure 1.23). Since these enzymes show a close homology, it is not surprising that this substrate mimic inhibits both enzymes. It was found that the combination therapy synergistically inhibits proliferation and induces cell cycle arrest of STS-26T MPNST, directly associated with induction of autophagy. A similar inhibition of proliferation was shown in 1c1c7 murine hepatoma cells and MCF10.DCIS cells, models for human breast ductal carcinoma, whereas no toxicity in normal immortalized Schwann cells was found. It remains an open question though, to which extents these effects are regulated by inhibition of GGTase I, RabGGTase or a combination of these enzymes.

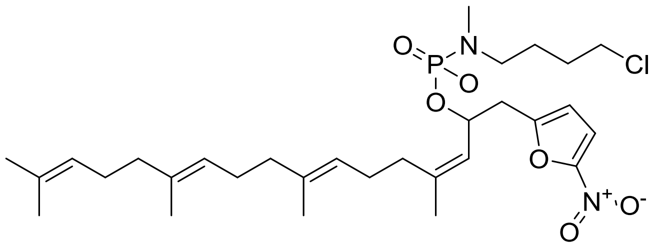
O
P
N
O
Cl
O
O
N+
O-
O

8GGTI-2Z[12]

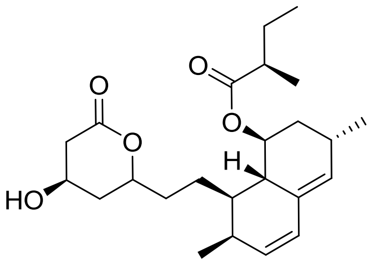

9 Lovastatin

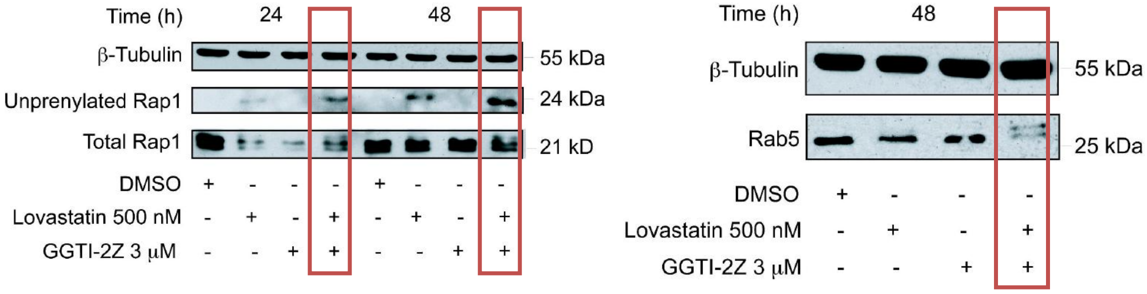
Time (h)
24
48
β-Tubulin
Unprenylated Rap1
Total Rap1
55 kDa
24 kDa
21 kD
DMSO + - - - + - - -
Lovastatin 500 nM - + - + - + - +
GGTI-2Z 3 μM - - + + - - + +
Time (h)
48
β-Tubulin
Rab5
55 kDa
25 kDa
DMSO + - - -
Lovastatin 500 nM - + - +
GGTI-2Z 3 μM - - + +

Figure 1.23: Inhibition of prenylation in STS-26T cells by GGTI-2Z/lovastatin combination treatment. a) Inhibition of Rap1 prenylation. b) Detection of Rab5. Unprenylated GTPases migrate more slowly on SDS-PAGE gels**[12]**.

Pyrrolidine-based inhibitors

Using a split-and-pool combinatorial synthesis strategy, Watanabe *et al.* developed a geranylgeranyl transferase inhibitor (GGTI) enriched library of pyrrolidine-based inhibitors[161]. Initially the library was screened to identify GGTase I inhibitors (Table 1.1, compound **10**). Some potent GGTase I inhibitors displayed inhibition of proliferation of several cancer cell lines such as breast cancer cell line MCF-7 and leukemic cell line Jurkat via inhibition of cell cycle progression. It was found that some GGTase I inhibitors (compounds **11, 12**) in addition showed moderate RabGGTase inhibition. Further screening of the library identified more RabGGTase inhibitors. These inhibitors all possessed a characteristic aliphatic R^3 tail. Further, it seemed that a bromide as R^2-substituent was an important feature to obtain selectivity for RabGGTase over GGTase I.

Table 1.1: Pyrrolidine-based GGTase I and RabGGTase inhibitors.

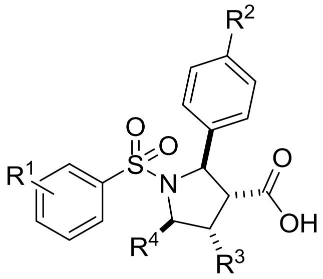

Entry	Compound	R1	R2	R3	R4	*In vitro* IC50 [µM] GGTase I	 RabGGTase	 FTase
1	**10**	2-Me	Cl	H	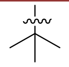	0.5	>10	>100
2	**11**	-	Cl	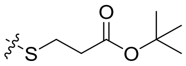	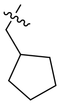	2.4	3.1	>100
3	**12**	4-Cl	Cl	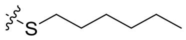	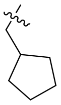	8.9	7.0	>100
4	**13**	4-Me	Br	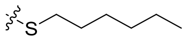	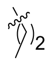	>50	2.1	>100
5	**14**	4-Me	Br	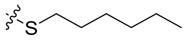	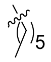	>50	2.2	>100

During competition experiments, it was shown that the inhibitors were competitive with regard to Rab GTPases and uncompetitive regarding the GGPP substrate. A K_i of 1.36 ± 0.38 µM was determined for **13**. Inhibition of Rab geranylgeranylation in cells was examined by identifying the amount of unprenylated Rab5b protein in NIH3T3 cells. Upon treatment with 10 - 20 µM **13**, Western blotting showed a clear unprenylated band of Rab5b protein. In addition, after ultracentrifugation, a larger amount of Rab5b was found in the soluble fraction upon treatment with **13**. In this subcellular fractionation study, the supernatant represents the soluble fraction and the pellet the membrane fraction. Thus, treatment of cells with **13** results in more Rab5b protein in the cytosol. Additional experimentation by Nguyen *et al.* using a different prenylation assay showed that this result was most probably not a consequence of cellular RabGGTase inhibition[162]. After cellular prenylation of Rab in COS7 cells in the presence of a pyrrolidine compound, followed by *in vitro* reprenylation with the affinity labeled GGPP analog biotin-GPP, the amount of affinity labeled Rab-biotin-geranyl conjugate was analyzed. Analysis of cells treated with either **13** or **14** did not show any presence of biotin-geranyl conjugate, which corresponds to no inhibition of cellular prenylation, even up to concentrations of 50 µM. Therefore, the effect and mechanism of these small molecules related to RabGGTase inhibition remains unclear.

Peptides and peptide analogs

A peptide based library of RabGGTase inhibitors was reported by Guo *et al.* [163] and Tan *et al.,*[164] loosely based on the FTase inhibitor Pepticinnamin E (**15**). This library containing 469 peptides was screened using an *in vitro* fluorometric Rab prenylation assay[69]. In this assay, a fluorescent analogue of GGPP, named NBD-FPP, is employed as the prenyl substrate. Upon prenylation in the presence of RabGGTase, Rab, REP and NBD-FPP, an increase of fluorescence is observed due to the relocalization of the NBD fluorophore into the hydrophobic pocket of REP. Consequently, inhibition of RabGGTase results in less fluorescence and this can be conveniently monitored. In total, 33 peptides based on Pepticinnamin E were found to inhibit RabGGTase at a low micromolar range. Inhibition of Rab prenylation with these compounds could also be shown in a cellular system using a biotin-containing analog of GGPP, Biotin-GPP[163]. Additionally, selectivity of the inhibitors was further studied using an *in vitro* prenylation assay with the three prenyl transferases. Some of them showed similar inhibitory activities for all the PTases (**18**, **19**), but some selective RabGGTase inhibitors such as peptide **20** were also identified (Table 1.2).

Cellular activity of these compounds was investigated in COS-7 cells by quantifying the prenylation of an overexpressed EYFP-Rab7 fusion protein in cell lysates using Biotin-GPP as a substrate, followed by subsequent detection with streptavidin-coupled horseradish peroxidase in a Western blot. Indeed, compound **17** inhibited completely the prenylation at a concentration of 100 µM, the same effect seen with compactin, a known inhibitor of the mevalonate pathway used as a positive control. Selective inhibitor **20** showed a 70% inhibition of the compactin effect. No cytotoxicity was observed for all compounds up to 100 µM.[66]

To get insight into the binding mode of these peptides, attempts to co-crystallize the inhibitors with RabGGTase were undertaken. The first described co-crystal structure of an inhibitor-RabGGTase construct was obtained for **16**.[163] The inhibitor was shown to bind in the active center at the interface of the α and β subunits of RabGGTase (Figure 1.24a). The peptide adopts an extended conformation with the C terminus pointing outwards. Except for hydrogen-bonding with some residues of the β subunit, between the carbamate and Arg144, the imidazole and Tyr97, and the carboxylic acid and Tyr241, the interactions between the peptide and enzyme are mainly hydrophobic. The analysis of the structure revealed additional sites near the catalytic center that could represent anchor points for inhibitors to increase the activity and specificity for RabGGTase (Figure 1.24a).

Table 1.2: Examples of peptide based inhibitors of RabGGTase

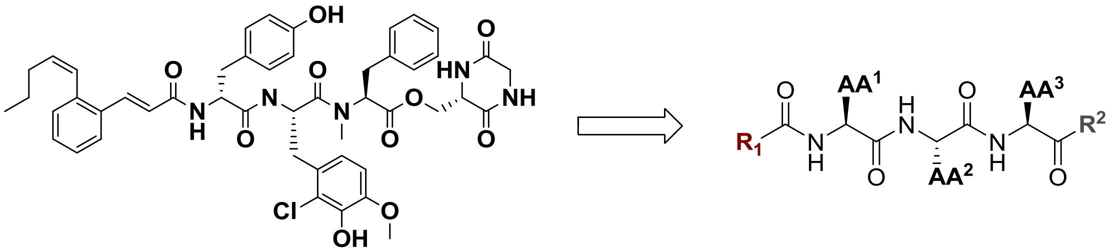

Pepticinnamin E(**15**)

Entry	Cmpd	R^1	AA^1	AA^2	AA^3	R^2	In vitro RabGGTase IC$_{50}$[µM]	Cellular Reprenylation IC$_{50}$[nM]		
								RabGGTase	FTase	GGTase I
1	**16**	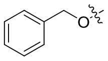	L-His	L-(Me)Phe	L-Tyr	OH	22.7±1.7	nd	nd	nd
2	**17**	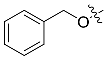	L-His	L-(Me)Phe	L-Tyr	NH-OH	9.0±1.0	nd	nd	nd
3	**18**	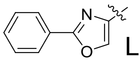	L-His	Gly	L-His(Trt)	OH	8.1±1.0	14±1.3	13±1.0	6.9±2.3
4	**19**	$C_{10}H_{21}$	L-His	L-His	L-Tyr	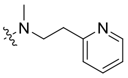	11.0±2.1	10±0.9	35±5.8	60±5.3
5	**20**	$C_{10}H_{21}$	L-His	L-Phe	L-Tyr	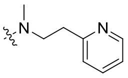	4.7±0.1	2.8±0.1	>100	>100

nd=not determined

Site 1, composed of residues Asp287, Pro288, and Phe289 and located on the tip of helix 12 ends at the active site, could contribute to potential hydrophobic interaction. Site 2, represented by the Zn^{2+} ion could be targeted by typical zinc binding moieties such as hydroxamic acids. Site 3, built of Arg232 and Lys235, is positively charged to anchor GGPP's phosphate groups.

Indeed, the presence of a hydroxamic acid moiety improved the potency 2-3 fold (**17**). However, after solving the co-crystal structure of **17** it was found that this improvement was not due to zinc coordination as expected (not shown). Alternatively, inhibitor **17** flipped by 180° and, as a consequence, the hydroxamic acid group was located at the bottom of the GGPP binding pocket. Instead, histidyl AA^{1}coordinated to the zinc ion, indicating that it was possible to target the reactive center of the active site.

In order to increase the affinity even more, the *N*-terminus was decorated with alkylaryl or lipid chain moieties to establish more interactions with the lipid binding site (LBS), which accommodates the GGPP. In addition, nitrogen-containing heterocycles or amines were introduced to increase the chance of coordinating to the zinc ion at the *C*-terminus (**20**). This strategy led indeed to several low micromolar inhibitors. However, the co-crystal structures of selective RabGGTase inhibitor **20** revealed that the binding mode differed again. The histidine coordinated to the zinc, whereas R^2 deeply binds into the LBS, stabilized by edge to face T-stacking with Trp244 and a water-mediated hydrogen bond. A further hydrogen bond interaction was observed between the AA^2tyrosine residue of **20** and Tyr97.

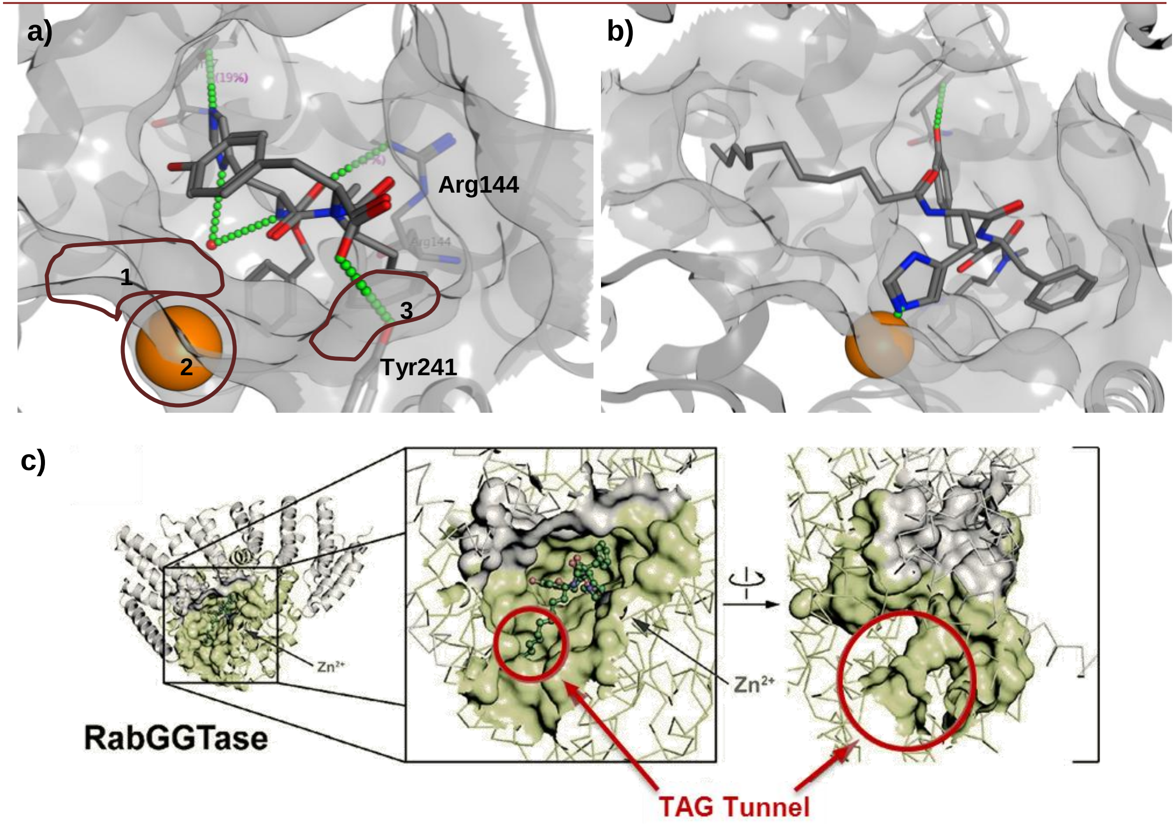

Figure 1.24: RabGGTase in complex with **16**. a) Surface and stick representation of **16** in the binding site. Green dashed lines represent hydrogen bonding. Highlighted areas (dark red) represents sites that can be used for further lead optimization. b) Surface and stick representation of **20** in the binding site. Green dashed lines represent hydrogen bonding. c) Active sites and exit grooves of RabGGTase (3HXE), showing the RabGGTase selective TAG tunnel. Adapted from Tan *et al*.[164]

Most interestingly, the lipid chain of **20** extends into a tunnel adjacent to the GGPP binding site, referred to as the “TAG tunnel”. Since the TAG tunnel is absent in FTase and GGTase I, this RabGGTase unique feature probably contributes to the selectivity of **20** and could aid further design of selective RabGGTase inhibitors.

In conclusion, the solid phase synthesis of a large amount of peptides led to a diverse set of RabGGTase inhibitors with moderate inhibition of prenylation in cells. These results show that the flexible peptide backbone is probably not suitable for a structure-guided inhibitor approach or SAR analysis due to different binding modes adopted by the peptides. However, the structural insights obtained from the inhibitor-RabGGTase co-crystal structures provide crucial information that can be used for the development of other potent and specific RabGGTase inhibitor.

Dual Inhibitors: Tetrahydrobenzodiazepines (THBs)

The most active RabGGTase inhibitor reported so far was developed as a FTI inhibitor. Bristol-Myers Squibb developed imidazole-containing tetrahydrobenzodiazepines (THB) as FTIs. BMS-214662 (**3**), which entered clinical trials, was shown to be a highly potent inducer of apoptosis and an efficacious suppressor of a variety of human tumors. However, the proapoptotic activity of these THB based compounds did not correlate with their potency against FTase[165], therefore it was suggested that these FTIs might have another target. Using an RNA*i* knockdown screen in *C. elegans*, Lackner *et al.* identified several genes associated with Rab GTPases as strong inducers of apoptosis: genes encoding for the HOPS complex in yeast which interacts with GTPase Rab7 and genes encoding for Rab7 and Rab5[17]. In addition, RNA*i* directed against GDI1 and GDI2 as well as RabGGTase-α and RabGGTase-β subunit was effective at inducing germline apoptosis. Next, the authors studied whether BMS1 (**21**) had a synergistic effect with RabGGTase-α RNA*i*. Due to the suppression of RabGGTase enzyme expression, the effect of a potential RabGGTase inhibitor should be potentiated. Indeed, it was shown that **21** increased the level of apoptosis on this RabGGTase depleted system. To investigate if these FTIs indeed inhibited RabGGTase some of the FTIs were tested in a radioactive based *in vitro* screen for RabGGTase activity. The results of this screen are summarized in Table 1.3.

Table 1.3: Activity of compounds in enzyme inhibition and cellular assays.

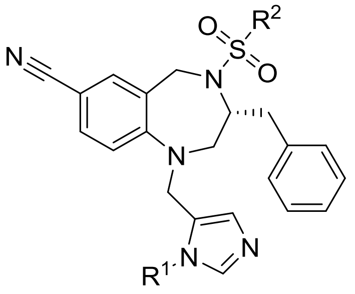

Core 1

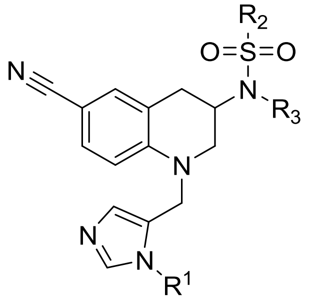

Core 2

Entry	Cmpd	Core	R^1	R^2	R^3	*In Vitro* IC_{50} [nM] *FTase*	 *RabGGTase*	HCT116 EC_{50} [μM]	*C. elegans* apoptosis
1	BMS1 (**21**)	1	H	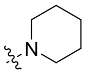	-	7.8	21	0.4	++
2	BMS2 (**22**)	1	H	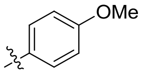	-	2.4	36	3.3	+
3	**BMS3** (**23**)	1	Me	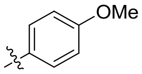	-	1.4	16	0.04	+
4	BMS4 (**24**)	2	Me	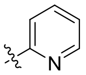	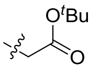	1.5	540	30	-
5	BMS5 (**25**)	2	Me	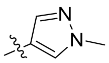	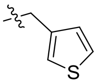	1.4	25	3.3	*nd*
6	BMS-214662 (**3**)	1	H	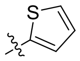	-	1.3	*nd*	0.03	*nd*

In comparison to another FTI (BMS4), which shows similar inhibition of FTase but significantly lower inhibition of RabGGTase, the reported activity for RabGGTase correlated with the apoptotic effect, whereas no such relation existed for FTase. Therefore, it seems that the proapoptotic effect of these FTIs is related to RabGGTase. Together with the discovery of this highly potent RabGGTase inhibitor class, the experiments by Lackner *et al.* thus, implicated an important role for RabGGTase in cancer and apoptosis.[17]

§ 1.8 General drug development strategies

As mentioned in the last paragraph, several successful efforts have been made toward selective RabGGTase inhibitors. However, they all display moderate or no cellular activity. Further, there is a lack of structural information about the mode of inhibition of these compounds. In order to obtain a clear structure-activity-relationship as well as an effective inhibitor for chemical biology studies, more efforts to obtain selective RabGGTase inhibitors are necessary. There are several general approaches to obtain small molecule inhibitors; a brief description will be given in the next paragraph.

§ 1.8.1 From hit…

In general, the development of a lead is described as a ‘hit to lead’ process[166].

The hit normally represents the primary active compound. This hit needs to be validated in order to verify its identity, purity and activity. Once the hit is synthesized and the activity has been confirmed this ‘validated hit’ can be optimized[167].

In order to identify a hit series, several approaches are possible. These methods can be divided into those that require very detailed target and ligand information and those that are generally serendipity-based[167]. High-throughput screening (HTS) is the most widely used technology for hit discovery and falls in the serendipity-based category. HTS normally involves the screening of a large chemical library, compiled of natural products and synthetic libraries, in a target based or phenotypic screen[168, 169]. In a target based *in vitro* HTS-screen the library is screened for a specific target. A threshold is normally set for a certain degree of inhibition, in order to find a sufficient number of initial hits. These hits can be optimized to obtain a lead series with clear structure-activity-relationship for its specific target, going through iterative cycles of synthesis, screening and design. Such a target based approach is also pursued in this thesis, in order to develop selective RabGGTase inhibitors. A phenotypic screen on the contrary is normally a cell-based assay, where chemical entities are screened for their phenotypic effect. In this case, the direct target of the hit is unknown. The target (s) can be identified by pull down experiments and can lead to potentially new targets involved in a certain phenotypic behavior[168].

The HTS approach historically relied on libraries compiled of natural products and synthetic compound libraries. Combinatorial chemistry represents synthesis technologies to generate compound libraries rather than single products, for example using solid-phase chemistry, automated (robotic) synthesis and high-throughput purification equipment. However, these chemical libraries frequently lack structural diversity. Consequently, information rich biological read outs often could not be obtained using this type of ultra-high-throughput synthesis. Therefore, pharmaceutical companies are focusing on improving and diversifying compound collections and making them globally available for HTS campaigns[167]. Besides the more serendipity based-approaches like HTS, more knowledge based-approaches are also pursued in order to obtain hits. These strategies can be based on structural information, obtained from X-ray crystallography or NMR as well as on information derived from endogenous ligands or non-natural small molecules reported in the literature and patents[167]. This type of information can be used for *de novo* ligand design[170]. Structural data of the target can be used to design chemical libraries.

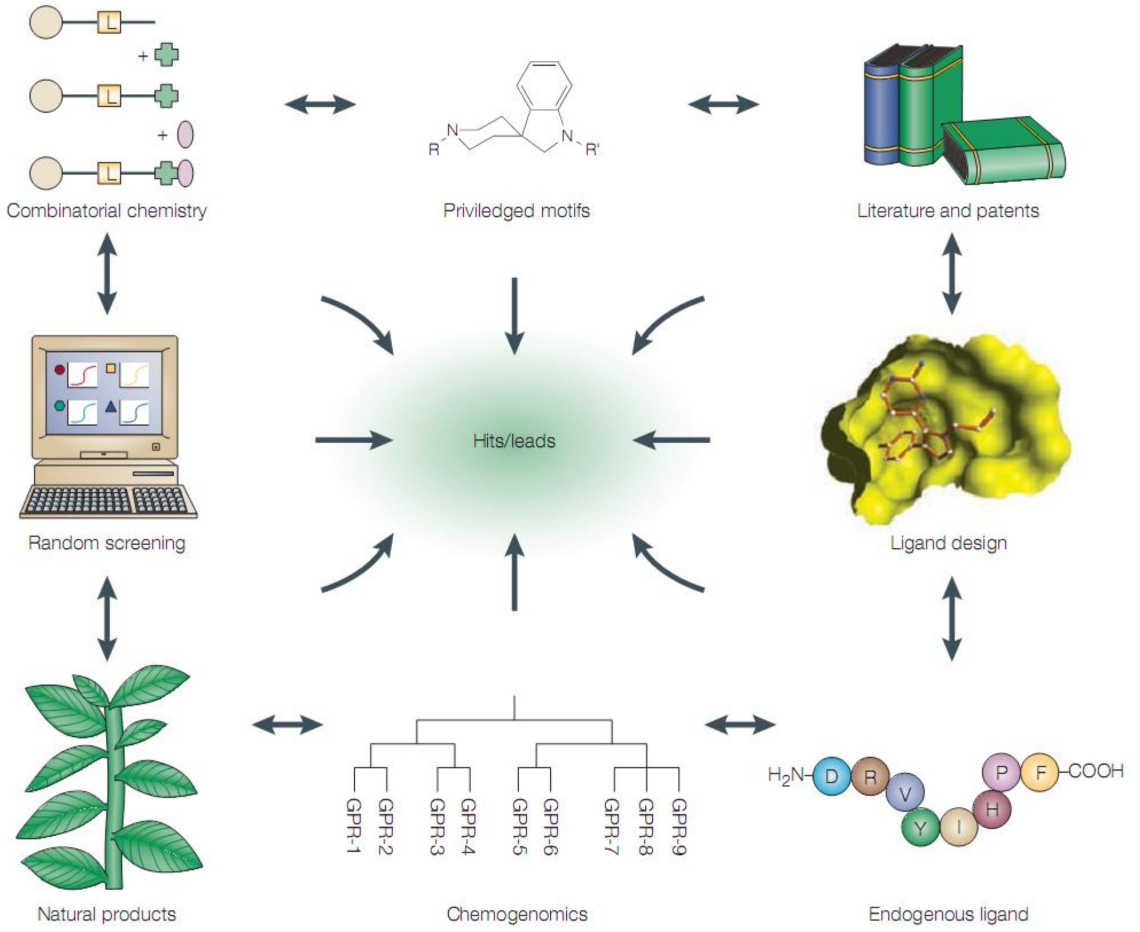
Combinatorial chemistry
Priviledged motifs
Literature and patents
Random screening
Hits/leads
Ligand design
Natural products
Chemogenomics
Endogenous ligand
L
N
R
R'
GPR-1
GPR-2
GPR-3
GPR-4
GPR-5
GPR-6
GPR-7
GPR-8
GPR-9
H2N
D
R
V
Y
I
H
P
F
COOH

Figure 1.25: Hit identification strategies involve both knowledge-based and serendipity-based approaches[167].

An understanding of the mechanism of action can aid in the development of transition-state mimics as inhibitors, whereas ‘4 dimensional’ virtual screening processes can be applied in order to evaluate a large library of compounds in order to prioritize chemical entities[167, 171]. Although these computational methods are very promising, they can only be regarded as prediction tools. Analysis of known endogenous ligands or small molecules from literature can be used to generate libraries containing a privileged structure[172]. Such a privileged structure represents a specific core or scaffold that conveys activity toward a protein family or limited set of its members independently of additional substituents attached to this core[167].

A more integrated approach of serendipity and knowledge based discovery is presented by targeted libraries and chemogenomics. Chemogenomics involves the investigation of classes of compounds against families of related proteins[173]. Once a target protein is identified to correspond to a particular family cluster, compound libraries biased for this family cluster should obtain hits for the specific target protein as well.

§ 1.8.2 ...to lead

Once a hit has been identified, this hit is normally developed into a lead, going through iterative cycles of design, synthesis and biological evaluation. A lead is a chemical structure or series of structures that demonstrate activity and selectivity in a series of relevant screens, such as pharmacological-, biochemical- and *in vivo* studies. This forms the basis for a focused medicinal chemistry effort for lead optimization in order to identify a clinical candidate that presents a patentable, unique core structure[167]. Besides displaying a good potency for the target protein, which is inherent of a lead, several other conditions have to be considered. In order for a lead to successfully progress into clinical trials it should possess good ADME (absorption, distribution, metabolism, and excretion) properties. Dose-limiting solubility, poor absorption, cytochrome P_{450} interactions and metabolic instability are all hampering factors in order to progress a lead into the clinic and should be considered in the early stages of drug discovery[174].

The latter properties necessary for a lead to become a potential drug are not necessarily considered in the design of chemical biology tool compounds. Such tool compounds are generally applied to cells or microorganisms and therefore ADME properties are less relevant. In this case, optimization of target selectivity and (cellular) potency is the main objective of the ‘lead’.

§ 1.8.3 Toward selective RabGGTase inhibitors

Several general approaches mentioned above could be used as a starting point for the development of selective RabGGTase inhibitors as chemical biology leads. Following the knowledge based approach, it was hypothesized that **BMS3** (**23**), the dual FTase/RabGGTase inhibitor, could be an excellent starting point for a structure-based design of selective RabGGTase inhibitors. In this thesis the efforts toward the design and synthesis of selective RabGGTase inhibitors, going through iterative cycles of co-crystallization, virtual screening, docking, synthesis and biological evaluation will be described.

Besides the ‘design for selectivity’ of **BMS3** based analogs, the ‘serendipity-based’ HTS approach to obtain RabGGTase inhibitors has been applied to identify potential new RabGGTase inhibitors. Finally, a more mixed approach has been pursued. The identification of a privileged scaffold led to the development of a small, targeted library following a *de novo* approach.

Chapter 2: Aim of the project

A selective RabGGTase inhibitor would be a valuable tool compound to study the effect of selective RabGGTase inhibition on cancer cell proliferation and, more generally, Rab-mediated cellular processes. The aim of the research described in this thesis was to develop selective RabGGTase inhibitors that potently and selectively inhibit (cellular) Rab geranylgeranylation. In order to obtain these inhibitors three different hit identification strategies were used:

1) Increasing selectivity of the known dual inhibitor **BMS3**
2) High-throughput screening and lead optimization
3) *de novo* design

In order to obtain these potent and selective inhibitors, an iterative cycle of synthesis, screening, crystallography and design was pursued. The three different approaches represent different starting points (hit discovery) in this iterative cycle and give all unique potential ways to obtain RabGGTase inhibitors. The process is depicted in Figure 2.1. The process is presented in a 3D spiral; every cycle in the right direction will lead to a better inhibitor. The hit, in the several scenarios is represented by **BMS3** in the dual inhibitor approach (1), by a new inhibitor identified with the HTS approach (2) or a virtual designed inhibitor in the *de novo* design approach (3).

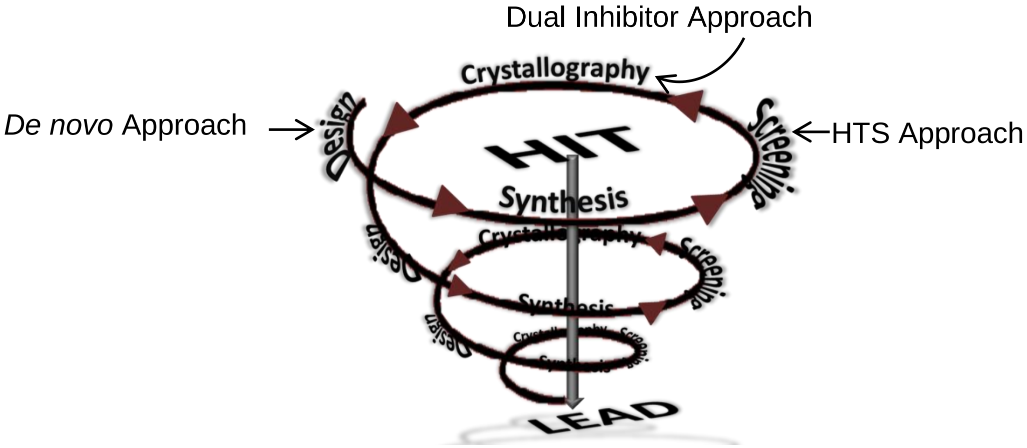
Dual Inhibitor Approach
De novo Approach
HTS Approach
Crystallography
Design
Screening
HIT
Synthesis
Crystallography
Design
Screening
Synthesis
Design
Crystallography
Screening
Synthesis
LEAD

Figure 2.1: A typical structure-based inhibitor design cycle, shown in a 3D perspective

The developed inhibitors with low nM activity will be assessed on their capacity to inhibit prenylation in cells and will be tested on their ability to inhibit proliferation in cancer cell lines.

All aspects of the project will be described in the following chapters. To provide an overview of the complete project, input of the following colleagues and collaborators is also included:

Dr. Robin Bon (synthesis of ***BMS3*** *and L778,123, synthesis of some THB-analogs) Dr. Zhong Guo (crystallization studies) Dr. Axel Choidas, Dr. Sascha Menninger, Dr. Alexander Wolf (LDC, assays)*

Chapter 3: Method & tool development for identification of selective RabGGTase Inhibitors

As described in the previous chapter, the aim of the project is to develop selective RabGGTase inhibitors following a typical iterative cycle of design, synthesis, screening and crystallography. Some prerequisites are necessary for such an inhibitor-development program. In order to identify or evaluate new hits an assay system is needed. To analyze the selectivity, counterscreens for GGTase I and FTase need to be carried out. For these assays many tool compounds are needed, either as substrates or control compounds in the respective assays. In order to increase the selectivity of dual inhibitor **BMS3** or to carry out *de novo* design, co-crystal structures should ideally be available. In this chapter the methods and tools that are necessary to obtain selective RabGGTase inhibitors and their preparation are discussed.

§ 3.1 Fluorometric RabGGTase assay

In order to screen a large library of compounds for RabGGTase assay using a fluorometric approach, R.S. Goody and co-workers developed an assay employing a fluorescent analog of GGPP[66]that was adapted to a continuous fluorometric assay for RabGGTase[69]. In this assay, 3,7,11-trimethyl-12-(7-nitrobenzo[1,2,5] oxadiazo-4-ylamino)dodeca-2,6,10-trienyl pyrophosphate (NBD-FPP, **27**) serves as the lipid substrate.

GGPP (**26**):

NBD-FPP(**27**):

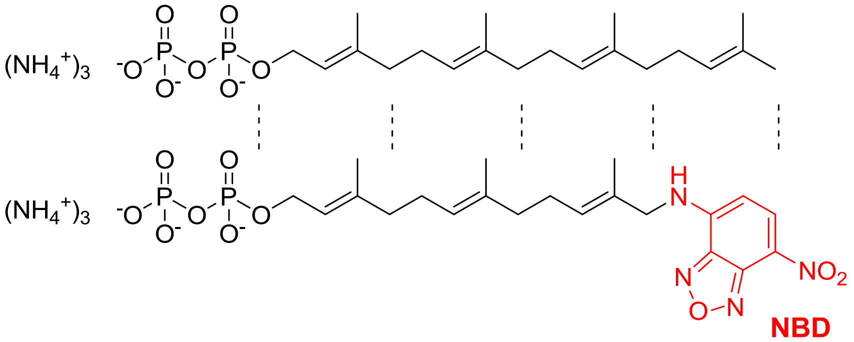

Figure 3.1: NBD-FPP as fluorescent analog of GGPP.

The principle of the assay is based on the increase of fluorescence upon binding of NBD in a hydrophobic area. Upon reaction in the presence of REP, RabGGTase, Rab7 and NBD-FPP an increase in fluorescence is detected. At the emission maximum an increase of 23-fold was detected, which was found to be related to relocation of NBD into a hydrophobic pocket of REP[69].

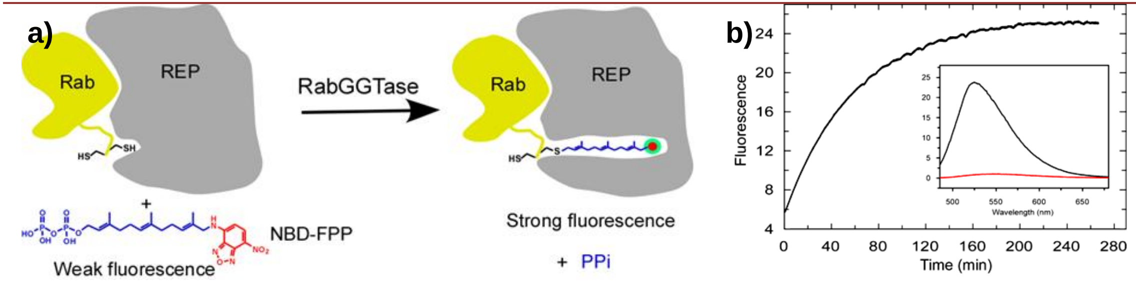

Figure 3.2: a) schematic principle of the assay, b) fluorescence increase over time of the prenylation reaction, as followed by a fluorescent spectrophotometer. Adapted from Wu *et al*.[69]

Upon efforts to optimize this assay in a high-throughput format to screen the complete CGC compound library (ca. 30.000 members) and to minimize the amounts for RabGGTase, Rab7 and REP needed for the assay, it was found that NBD-FPP bleached severely over time. High amounts of proteins were needed in order to obtain good statistical parameters with this bleached NBD-FPP. Therefore a new batch of NBD-FPP was synthesized (the synthesis is described in § 3.5.1). With the fresh batch of NBD-FPP the proteins could be used in much lower concentration. In addition, it was possible to measure at a concentration of just 50 nM RabGGTase, which was important for the analysis of highly active RabGGTase inhibitors.

§ 3.2 Fluorometric FTase & GGTase I assay

In order to verify if the identified RabGGTase inhibitors are indeed selective, the inhibitors needed to be screened for closely related prenylation enzymes FTase and GGTase I. Both assays were adopted from literature procedures[175-177]and mainly performed by collaborators at the Lead Discovery Center (LDC). The principle of the assays is depicted in Figure 3.3.

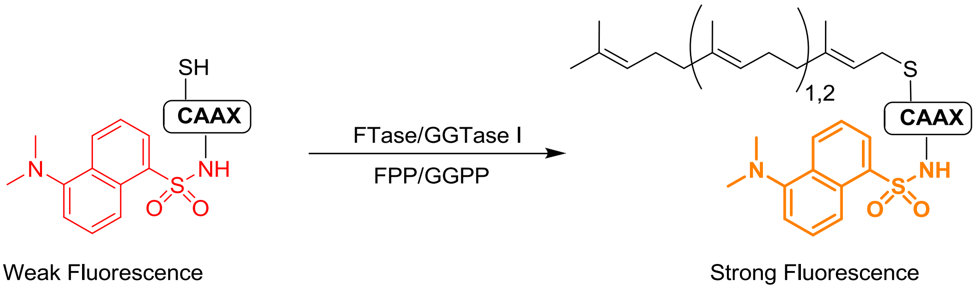

Figure 3.3: Schematic principle of the fluorometric FTase and GGTase I assay.

In general, a short CAAX peptide fused to a dansyl group was farnesylated or geranylgeranylated by FTase or GGTase I, respectively. Prenylation results in an increase in fluorescence of the dansyl group, related to the hydrophobic environment created by the attached prenyl, over time. Inhibition of this process, thus, resulted in less enhancement of fluorescence.

§ 3.3 X-ray crystallography

The crystal structures obtained during this project have been determined by Dr. Zhong Guo. In this paragraph, the design of the crystal structures constructs of RabGGTase and FTase is shortly discussed. A detailed description of the procedures can be found in his PhD thesis[178].

RabGGTase

In order to obtain insight in the molecular basis of activity and selectivity, co-crystal structures of the inhibitors were desirable. Therefore, a crystalline RabGGTase construct was needed. As mentioned in § 1.3, RabGGTase bares two additional structural domains, Ig and LRR, compared to FTase and GGTase I. Since both FTase and GGTase I gave crystalline constructs, it was suggested that a RabGGTase mutant lacking these domains should be more amenable to crystallization[70]. The RabGGTaseΔIgΔLRR mutant indeed crystallized and its apo structure could be determined at 1.8 Å resolution. This same construct was used in order to obtain co-crystal structures of inhibitor/RabGGTase complexes by soaking.

FTase

Rat FTase, expressed in *E. coli.*, gives readily crystalline constructs. However, in its native form the active site is occupied with the last amino acids of the β unit C-terminal, which interact mainly through hydrogen bonds and hydrophobic interactions. Therefore, a truncated mutant of FTase has been engineered in order to obtain good resolution crystals with an open active site. The removal of the last 10 amino acids of the C-terminus of the β unit successfully gave construct FTase_α_β_CΔ10, which yielded decent crystals that diffracts to a high resolution shell. The apo structure could be determined at 2.8 Å resolution. This same construct was used in order to obtain co-crystal structures of inhibitor/FTase complexes by soaking.

§ 3.4 Molecular Modeling

Molecular modeling represents a powerful method in order to optimize inhibitors, predict binding modes and for design of *de novo* inhibitors. Several software packages are available to virtually screen a large set of potential inhibitors. In this thesis, GOLD has been used in order to identify promising selective RabGGTase inhibitor-candidates. Before docking, the library and the enzymes have to be prepared for screening; these processes will be described in the following sections. The total workflow is summarized in Figure 3.4

§ 3.4.1 Preparation of a virtual library

The virtual library was assembled by the combination of a core scaffold with a large number of substituents. The core scaffold and substituents were prepared in ChemDraw (see Supporting Information for the input file). The library was subsequently prepared in Pipeline Pilot; the structures were assembled and stereoisomers and tautomers were enumerated. To convert each 2D drawing obtained from Pipeline Pilot into a 3D structure -required for virtual screening- the database was subsequently minimized in MOE (version 2009.10)[179] using database minimize, with MMFF94x forcefield and an RMS gradient of 0.1. The database was used as such for the following docking procedures.

§ 3.4.2 Preparation of the crystal structures

The crystal structures of RabGGTase and FTase were prepared for docking by removal of co-crystallized ligands (*e.g.* inhibitor or prenyl pyrophosphate), followed by the addition of hydrogens using the Protonate3D function in MOE.

§ 3.4.3 Virtual Screening

Ligands were docked into the proteins using GOLD (version 4.1.1)[180, 181]. Since the imidazole is known to bind to the zinc atom, a binding constraint was set by defining an imidazole substructure with defined distance to the zinc atom (min 1.5 Å, max 3.5 Å, spring constant = 5). The binding site was defined by a sphere of radius 15 Å around a residue in the binding site (Tyr361 in FTase and Phe289 in RabGGTase). The ChemScore scoring function was used in combination with most accurate automatic genetic algorithm settings (autoscale = 1). Ten solutions were generated for all inhibitors.

§ 3.4.4 Analysis of the results

The scores for RabGGTase and FTase were compared for each compound, assuming that a compound with a high score for RabGGTase and a low score for FTase would be most selective. The compounds that satisfied these conditions and showed a preserved binding mode in RabGGTase were further evaluated for their synthetic feasibility and synthesized.

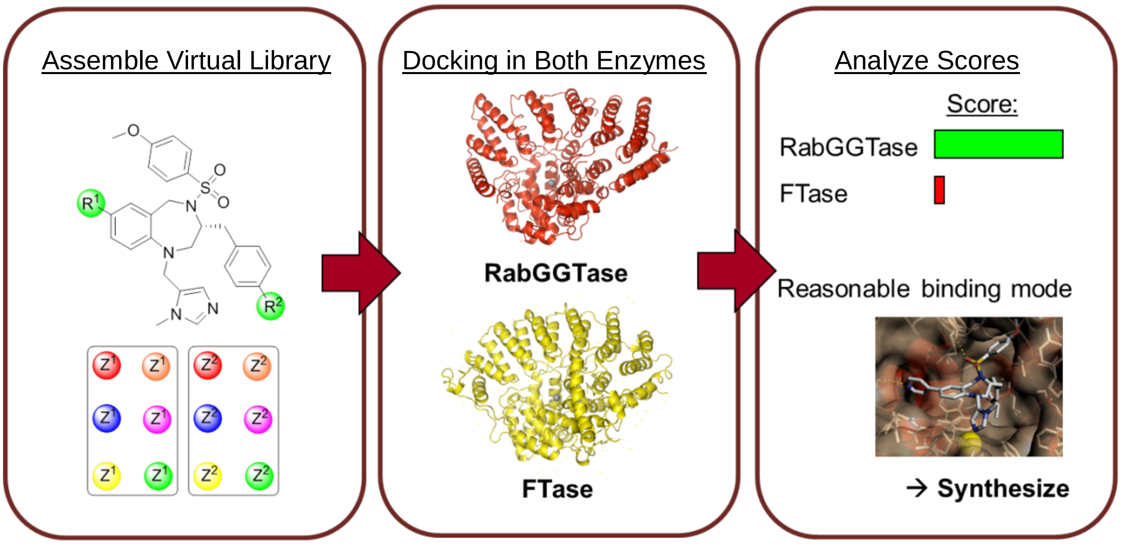
Assemble Virtual Library
O
S
O
O
N
R1
N
N
N
R2
Z1
Z2
Docking in Both Enzymes
RabGGTase
FTase
Analyze Scores
Score:
RabGGTase
FTase
Reasonable binding mode
→ Synthesize

Figure 3.4: Molecular Modeling workflow. 1) The virtual library was created by assembly of a core structure with various substituents. The compounds in the library were minimized to obtain their local-minimum 3D-conformations, which were used as input for the virtual screening. The enzymes were prepared for docking. 2) All members in the virtual libraries are docked in both RabGGTase and FTase (10 times) every solution is scored. 3) The best solutions in RabGGTase and FTase of every member were compared. Compounds which scored high for RabGGTase and low for FTase were expected to represent selective RabGGTase inhibitors and prioritized for synthesis.

§ 3.5 Synthesis of tool compounds

§ 3.5.1 Synthesis of fluorescent prenyl pyrophosphate (PPP) analogs

Synthesis of NBD-FPP

Since the NBD-FPP batch had severely bleached over time, a new batch was synthesized. The synthesis of NBD-FPP has been reported in the literature several times and is a lengthy procedure with two crucial but low-yielding transformations[66, 182, 183]. The synthesis is outlined in Scheme 3.1.

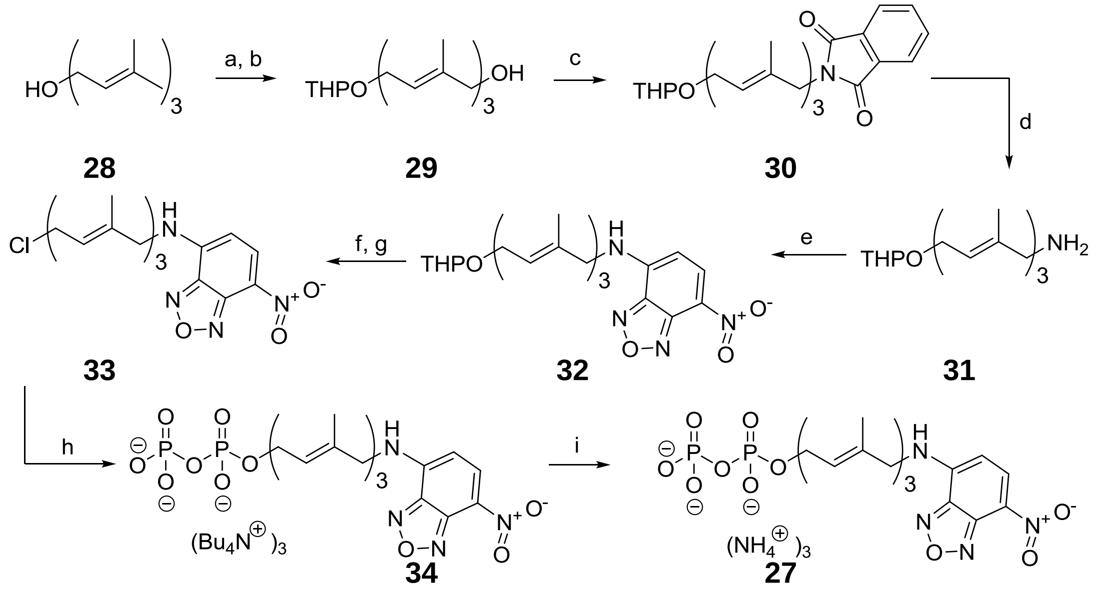

Reagents and Conditions (a) DHP, PPTS, DCM, 99% (b) 70% t-BuOOH, $H_2Se_2O_3$, salicylic acid, DCM, 25% (c) phthalimide, PPh_3, DIAD, THF, 62% (d) hydrazine, EtOH, 85% (e) NBD-Cl, $NaHCO_3$, MeCN, 52% (f) PPTS, EtOH, Δ, 99% (g) NCS, Me_2S, DCM, -40°C, 99% (h) TTBAP, MeCN (i) dowex cation exchange (NH_4^+), 20% (2 steps)

Scheme 3.1: Synthesis of NBD-FPP.

First, farnesol (**28**) was protected with THP in quantitative yield. Then an allylic oxidation was carried out employing $H_2Se_2O_3$/t-BuOOH/salicylic acid to give **29** in 25% yield. The low yield was due to substantial side product, mostly related to the overoxidation of the alcohol to the aldehyde. Therefore, it was important to carefully monitor the reaction. Using Mitsunobu conditions, the alcohol was allowed to react with phthalimide to give **30** in 62% yield, which was reduced with hydrazine to the allylic amine **31** in 85%. This approach is similar to the Gabriel synthesis[184]. The amine was subsequently treated with NBD-Cl to give **32**. Then, the protective group was removed and the alcohol was subsequently subjected to a chlorination reaction with dimethylsulfide and NCS in DCM giving **33** with 100% conversion. Without purification due to the relative instability of **33**, the chloride was converted into the pyrophosphate

34, using tris tetrabutylammonium pyrophosphate (TTBAP). The tetrabutylammonium counterion was exchanged for ammonium by ion-exchange chromatography. Purification using a short C_{18} column gave **2** in 20% yield over 2 steps.

General route toward the synthesis of PPP analogs

NBD-FPP is just one of many substrates that has been used as stand-in for GGPP to analyze prenylation reactions. Another analog that is used to analyze geranylgeranylation reactions is for example biotin-GPP. Shorter analogs are interesting as well, for example to study the effect of farnesylation[73]. Therefore, it would be desirable to have a more straightforward procedure to obtain these inhibitors. Dr. Debapatrim Das has investigated a new approach to synthesize these PPP analogs. Instead of incorporating the desired tag in the middle of the PPP synthesis, a photolabile protective group was incorporated, which could be removed at the final stages of the synthesis. The free amine can then be treated with various N-hydroxysuccinimide esters (NHS esters) to introduce fluorescent or affinity-probe tags. The general synthesis route is summarized in Scheme 3.2.

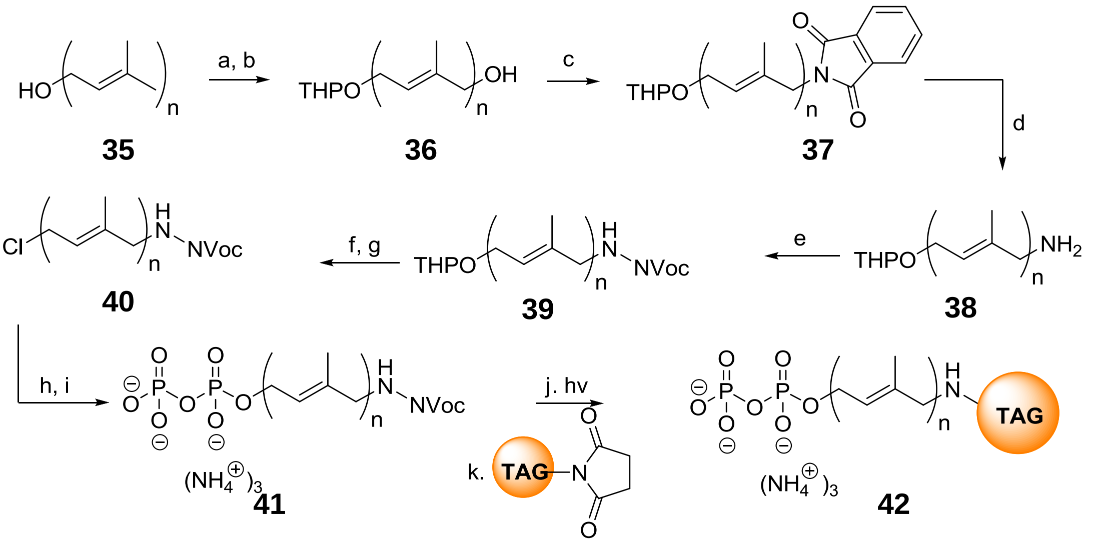

Reagents and Conditions (a) DHP, PPTS, DCM (b) 70% t-BuOOH, H_2SeO_3, salicylic acid, DCM (c) phthalimide, PPh_3, DIAD, THF (d) hydrazine, EtOH,(e) NVocCl, DIPEA, DCM (f) PPTS, EtOH, Δ (g) NCS, Me_2S, DCM, -40°C (h) TTBAP, MeCN (i) dowex cation exchange (NH_4^+), (i)hv 350 nM, (k) TAG-NHS, Et_3N, DCM/DMF

Scheme 3.2: general synthesis route to PPP analogs, 10 step sequence.

Intermediate **38** was obtained via a similar route as described for NBD-FPP of protection, allylic oxidation and introduction of the allylic amine. The free amine was then protected with nitroveratryloxycarbonyl (NVoc), a photolabile group. The subsequent four steps, comprising THP-deprotection, chlorination, introduction of pyrophosphate and ion exchange, were carried similar to the NBD-FPP synthesis. The obtained pyrophosphate prenyl analogues were deprotected by UV irradiation to obtain a free amine which was allowed to react with various NHS-esters such as biotin-NHS or rhodamine-NHS esters.

Although this synthetic route offers a more divergent approach toward PPP analogs, there are still some drawbacks. The allylic oxidation suffers from incomplete conversion and is low yielding (typically around 20%). In addition, a substantial amount of overoxidized aldehyde is formed as a byproduct. Furthermore, the total reaction sequence involved 10 steps.

It was envisioned that the overoxidation of the alcohol into the aldehyde could also be used to our advantage. This aldehyde would allow the introduction of the amine by reductive amination. First, an attempt was made to introduce the NBD group directly. Therefore, NBD-Cl was converted to NBD-NH_2 which was subsequently allowed to react with **43**. Unfortunately, the reductive amination was unsuccessful, which was probably related to the electrodeficient character of the aniline-like NBD. This approach thus, was unsuccessful to incorporate a fluorescent group in the beginning of the synthesis.

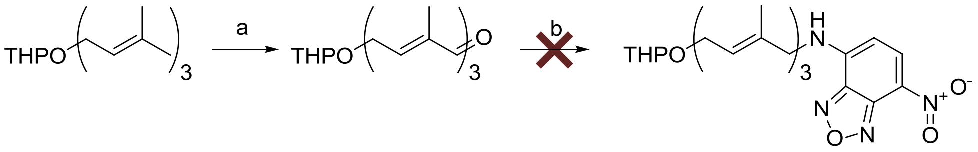

28 **43** **44**

Reagents and Conditions (a) 70% t-BuOOH, H_2SeO_3, salicylic acid, DCM, 22% (b) NBD-NH_2, $NaBH(OAc)_3$, TFA, THF, failed

Scheme 3.3: Attempts to introduce the fluorophore via the aldehyde.

However, the aldehyde functionality could still be of interest in the general PPP analog route (Scheme 3.4). It was envisioned that the aldehyde could react with allylamine, which would introduce the amine functionality as well as the protective group at once. This could be followed by direct conversion of the THP-protected alcohol into a bromide using triphenylphosphine dibromide. This bromide can then be converted into the pyrophosphate in one pot[185]. This synthetic route would reduce the sequence with four steps. A critical step would be the deprotection of the allylamine in the presence of a pyrophosphate.

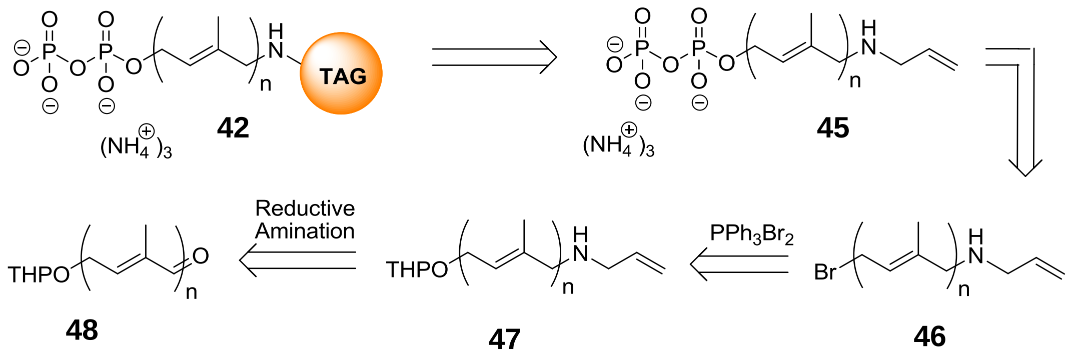

Scheme 3.4: Retrosynthesis of PPP analogs, 7 step synthesis.

In order to verify the potential of this route, first attempts to follow this synthetic route have been carried out on the shortest, dimethylallyl analog. The synthesis is outlined in Scheme 3.5

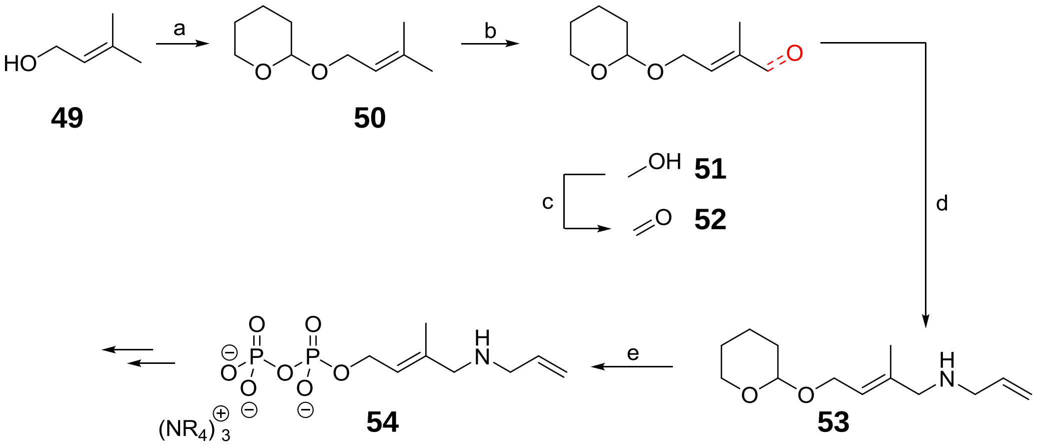

Reagents and Conditions (a) DHP, PPTS, DCM, 99% (b) 100% *t*-BuOOH, SeO_2, tetrazole, DCM, (c) MnO_2, Na_2CO_3(77%, 2 steps), (d) allylamine, NaBH$(OAc)_3$, AcOH, THF, 60%, (e) PPh_3Br_2, TBAPP, DCM, MeCN

Scheme 3.5: Synthesis of PPP analogs via the aldehyde functionality.

After introduction of the THP group, **50** was subjected to the allylic oxidation conditions. In order to promote the conversion into the aldehyde, a slightly modified procedure was used. Using 100% *t*BuOOH, SeO_2, and tetrazole as a co-catalyst, the conversion could be improved to 80%, however still in favor of the alcohol. After work-up, the mixture was treated directly with MnO_2 to convert the alcohol into the aldehyde quantitatively providing 77% of **52**. Reductive amination employing allylamine in the presence of 1 equiv. of acetic acid and sodium triacetoxyborohydride as the reducing agent gave **53** in 60% yield. This was subsequently converted into the pyrophosphate **54**, performing the deprotection and introduction of the pyrophosphate moiety in one pot. At first, it was envisioned to carry out the deprotection with the tetrabutylammonium counterions, since this enhances the solubility of the pyrophosphates. This however, gave major complications in the characterization of the compounds by NMR. Next, after ion exchange, the ammonium form of **54** was subjected to deprotection methods, however no conversion could be observed due to insolubility problems. Therefore, the deprotection of the allylamine in tetrabutylammonium counterion state requires further investigation.

§ 3.5.2 Synthesis of phosphonocarboxylate RabGGTase inhibitors

In order to get an insight in the difference between monogeranylgeranylation and digeranylgeranylation, it would be interesting to be able to compare the effect of the phosphonocarboxylate inhibitors that only inhibit the 1st prenylation with RabGGTase inhibitors that inhibit both prenylation steps. Therefore 3-PEHPC (5) and (+)-3-IPEHPC (**7**) were synthesized.

Independent synthesis steps of 3-PEHPC were described in patent[186, 187] and public literature[188] but appeared to be low yielding or unreliable. First nicotinaldehyde **55** was allowed to react with N,N-dimethylglycine ethyl ester **56** using *in situ* generated sodium ethoxide as a base. Acidic work up resulted in the hydrolysis of the dimethylamine, giving **57** in reasonable yield[186]. Attempts to obtain **58**, employing dimethylphosphite in analogy to patent literature were unsuccessful [187] (Scheme 3.6). Therefore, other methods to obtain the phosphonocarboxylate were investigated. Soroka *et al*. described the transformation of aldehydes and ketones into their corresponding α-hydroxyalkylphosphonates analogs using trialkylphosphites under anhydrous acidic conditions[189]. Although there was no precedence for our particular system; the conditions worked smoothly giving access to **59** in good yield. Deprotection of the esters resulted in known RabGGTase inhibitor 3-PEHPC 5 (Scheme 3.7).

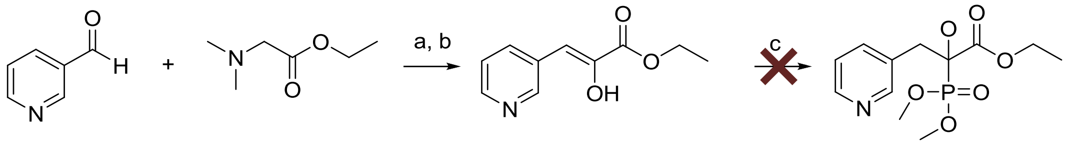

55 **56** **57** **58**

Reagents and Conditions (a) NaH, EtOH, Et_2O (b) 1N HCl, 65% (2 steps) (c) $(MeO)_2P(O)H$

Scheme 3.6: Synthetic attempts toward phosphonocarboxylate inhibitor 3-PEHPC.

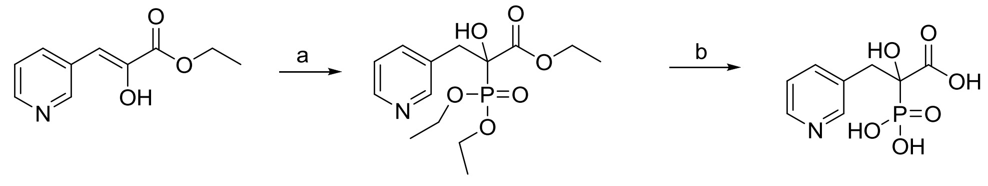

57 **59** 5

Reagents and Conditions (a) $P(OEt)_3$, HCl, DCM, 75% (b) HCl, EtOH, 80%

Scheme 3.7: New efficient route in order to obtain phosphonocarboxylate inhibitor 3-PEHPC.

During the course of the project, a low µM based phosphonocarboxylate inhibitor 3-IPEHPC was reported in the literature [159, 160]. This inhibitor was synthesized analogous to the approach used to obtain 3-PEHPC (Scheme 3.8). Using Vilsmeier-Haack conditions, imidazo[1,2-a]pyridine was converted into its corresponding aldehyde[190]. With the aldehyde in hand, the same procedures were followed as described for 3-PEHPC, leading to racemic 3-IPEHPC 7 in a good overall yield.

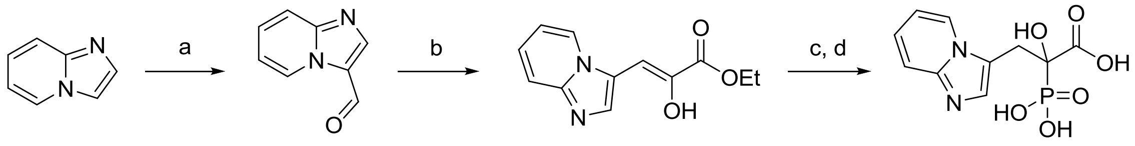

60 **61** **62** **7**

Reagents and Conditions (a) $POCl_3$, DMF, 30% (b) i. $P(OEt)_3$, HCl, DCM, ii. HCl, EtOH, 99% (c) $P(OEt)_3$, HCl, DCM (d) HCl, EtOH, 67% (2 steps)

Scheme 3.8: Synthesis of 3-IPEHPC.

Interestingly the authors of 3-IPEHPC reported similar problems in reproducing the patent literature and therefore chose another strategy. Their synthesis route is outlined in Scheme 3.9. Instead of condensing aldehyde **61** with N,N-dimethylglycine ethyl ester, ethylazidoacetate was used to obtain intermediate **63** in moderate yield. Subsequent reduction of the azide into the amine and hydrolysis then led to **62**. Under prolonged heating with a large excess of diethylphosphite **65** was obtained, which was hydrolyzed immediately.

Comparing the literature procedures with the newly developed synthesis, the general synthesis outlined here (Scheme 3.8) smoothly converts aromatic aldehydes in three steps into phosphonocarboxylates analogs. This opens up a valid and quick alternative to synthesizing phosphonocarboxylate libraries, potentially leading to more potent inhibitors of the 2nd geranylgeranylation step.

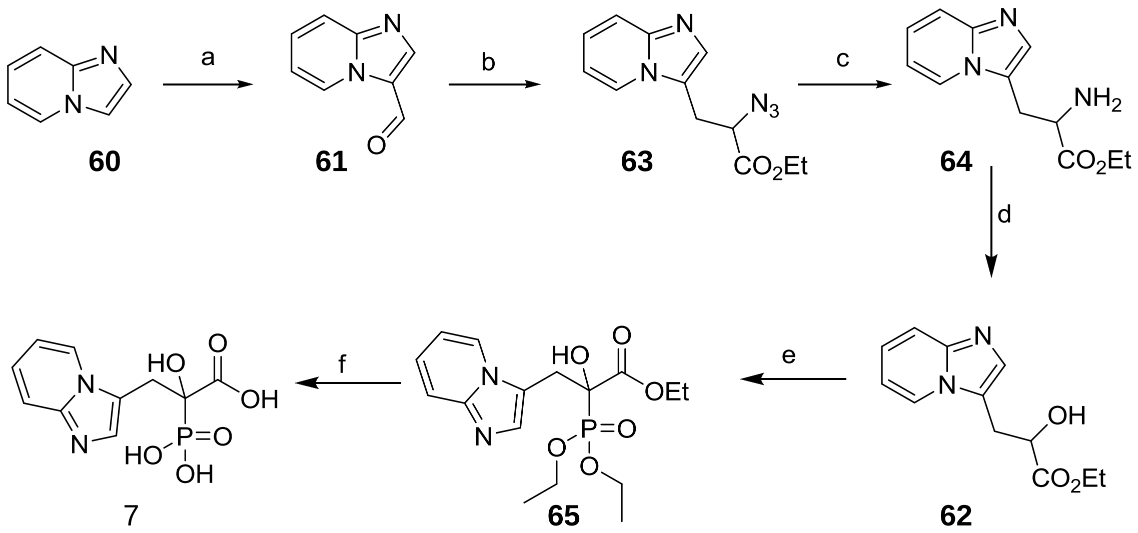
60
a
61
b
63
c
64
d
62
e
65
f
7
N
N
O
N3
CO2Et
NH2
OH
HO
OEt
OH
P=O
HO
O

Reagents and conditions: (a) Vilsmeier reagent, from 2-140 °C, 31%; (b) $N_3CH_2CO_2Et$, EtONa/EtOH, from -30 °C to rt, 4 h, 55%; (c) H_2, 10%Pd/C, MeOH, 2.5 h, rt, 100%; (d) $AcOH/H_2O$ (7/1, v/v), 1.5 h, 0 °C, 59%; (e) $(EtO)_2P(O)H$, 70 °C, 21 h; (f) 6 N HCl, 6 h, reflux, 60% over 2 steps

Scheme 3.9: Procedure toward 3-IPEHPC as reported in the literature[160].

Chapter 4: Synthesis & Design of selective tetrahydro-benzodiazepine based RabGGTase inhibitors

§ 4.1 BMS3, a dual inhibitor

The best RabGGTase inhibitor known so far, **BMS3** (**23**), was designed as an FTase inhibitor. In order to increase selectivity toward RabGGTase, structure-based design was applied. Herefore, **BMS3** needed to be synthesized and co-crystallized with a crystallizable RabGGTase construct as developed by Guo *et al.*[163]

BMS3 was synthesized by Dr. Robin Bon according to literature procedures[191, 192] and soaked into both RabGGTase and FTase, which resulted in the binary RabGGTase:**BMS3**, the ternary RabGGTase:**BMS3**:GGPP and the ternary FTase:**BMS3**:FPP co-crystal structures

The binding modes and conformations of **BMS3** in these structures are highly similar. In both enzymes the imidazole coordinates to the catalytic zinc ion, whilst the phenyl ring of the tetrahydrobenzodiazepine (THB) core π-stacks with the Tyr361 or the Phe289 residue of FTase and RabGGTase, respectively. The phenylmethyl moiety extends toward the lipid binding sites in both enzymes and is involved in extensive T-stacking with hydrophobic residues of the enzymes (Figure 4.1). These common interaction patterns result in the twisted form of the central THB-phenylmethyl unit observed in both enzymes. The anisylsulfonyl group adopts a pseudo-axial position and is involved in internal π-stacking interactions. In RabGGTase an additional hydrogen bond interaction is formed between the sulfonyl moiety and Tyr44, whereas this group is mostly solvent exposed in FTase. In RabGGTase:**BMS3**:GGPP, the nitrile group of **BMS3** is close to the TAG-tunnel, whereas this group is close to the protein surface in Ftase:**BMS3**:FPP merely showing dipolar interactions to hydrophobic residues. The shared binding interactions are reflected in the reported *in vitro* and cellular data of **BMS3** in the literature, giving an IC_{50} of 1.4 nM and K_i of 7 nM for FTase and a IC_{50} of 16 nM and K_i of 50 nM for RabGGTase[17, 162]. This proves **BMS3** a potent inhibitor for both FTase and RabGGTase.

BMS3

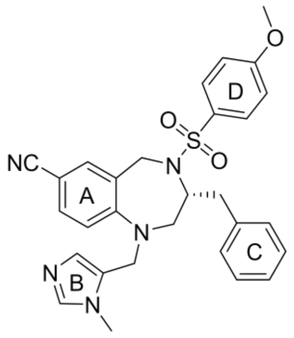

FTase IC_{50} = 16 nM

RabGGTase IC_{50}= 1.4 nM

HCT116 EC_{50}= 40 nM

C. Elegans apoptosis inducer

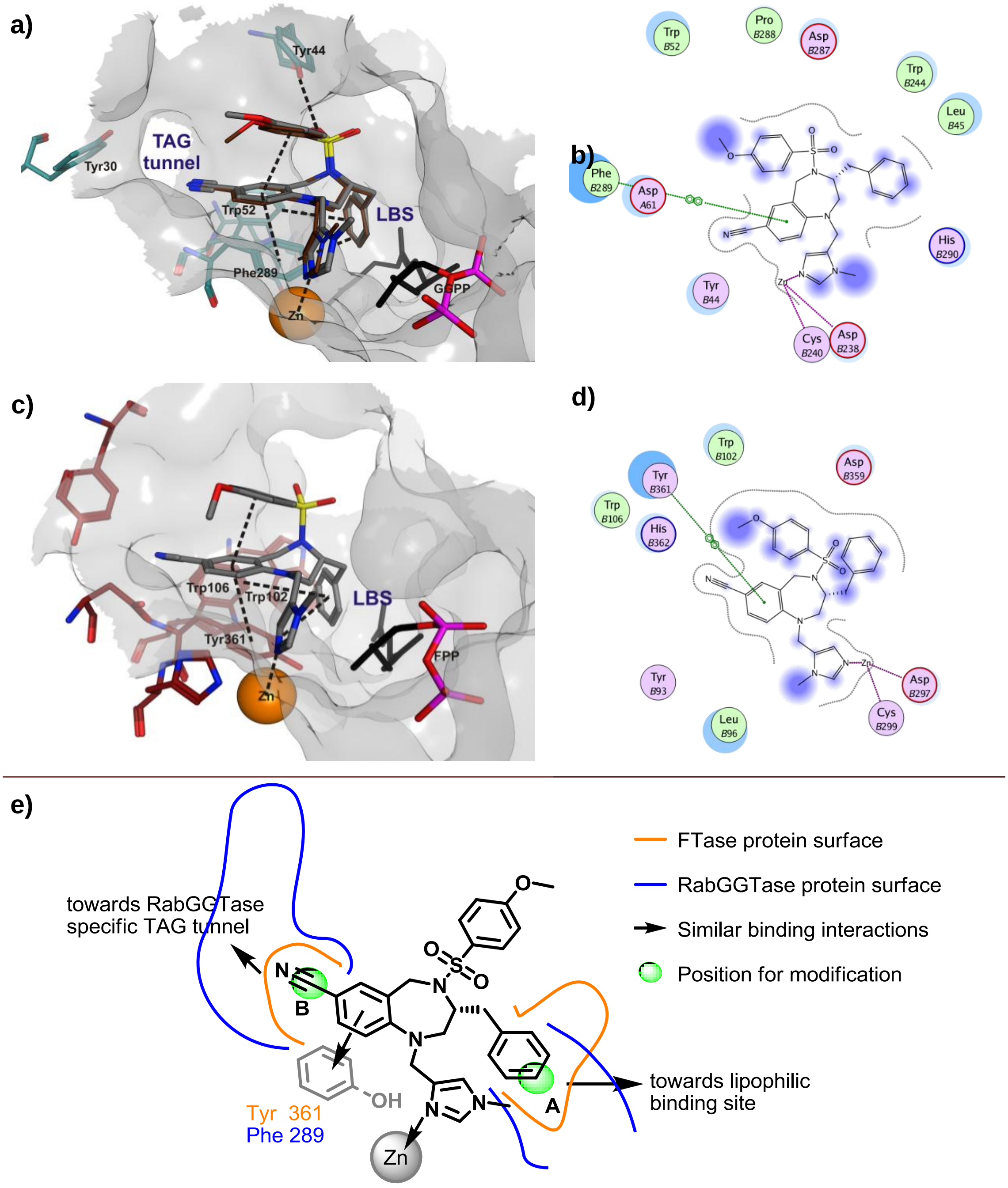
a)
Tyr44
Tyr30
TAG tunnel
Trp52
LBS
Phe289
GGPP
Zn
b)
Trp B52
Pro B288
Asp B287
Trp B244
Leu B45
Phe B289
Asp A61
His B290
Tyr B44
Cys B240
Asp B238
c)
Trp106
Trp102
Tyr361
LBS
FPP
Zn
d)
Trp B102
Tyr B361
Asp B359
Trp B106
His B362
Tyr B93
Leu B96
Asp B297
Cys B299
e)
towards RabGGTase specific TAG tunnel
FTase protein surface
RabGGTase protein surface
Similar binding interactions
Position for modification
B
A
Tyr 361
Phe 289
Zn
towards lipophilic binding site

Figure 4.1: Co-crystal structures of **BMS3**: a, b) Surface representation of active site of **BMS3**:RabGGTase:GGPP complex (PDB access code 3PZ2). The imidazole coordinates to the zinc ion, whereas the sulfonamide forms hydrogen bonds with Tyr44. The 3-benzyl moiety interacts with Trp52 and Phe289 by edge-face stacking, whereas the tetrahydrobenzodiazepine (THB) moiety stacks face-face with Phe289. The conformation is further stabilized by internal π-stacking of the THB with the anisylsulfonyl group. The nitrile points toward the TAG tunnel. The orientation of **BMS3** in the binary complex **BMS3**:RabGGTase is depicted in brown lines (PDB access code 3PZ1). The black dashed lines indicate interactions between ligand and enzyme. c, d) Surface representation of the active site of **BMS3**:FTase:FPP complex (PDB access code 3PZ4); the imidazole coordinates to the zinc ion. The 3-benzyl moiety interacts with Trp102 and Trp106 by edge-face stacking. The THB interacts with Tyr361 and is further involved in internal π-stacking with the anisylsulfonyl group, which is mainly solvent exposed. The black dashed lines indicate interactions between ligand and enzyme. e) Schematic representation of the common binding modes of **BMS3**.

In order to reach selectivity toward RabGGTase, possible modifications of **BMS3** were considered guided by the co-crystal structures. It was decided to keep the anisylsulfonyl group and imidazole constant. The imidazole was kept since it represents the crucial zinc binding moiety. The anisylsulfonyl moiety was already shown to be highly variable in FTase without leading to significant changes in activity[192], whereas this group is involved in hydrogen bonding within RabGGTase. Therefore no significant selectivity gain for RabGGTase by varying this group was expected and it was decided to keep the anisylsulfonyl group constant to ensure the positive internal π-stacking.

Since the TAG tunnel is a unique feature of RabGGTase, introduction of larger moieties at position **B** instead of the nitrile were expected to accommodate in the RabGGTase TAG tunnel while they would clash with the FTase surface.

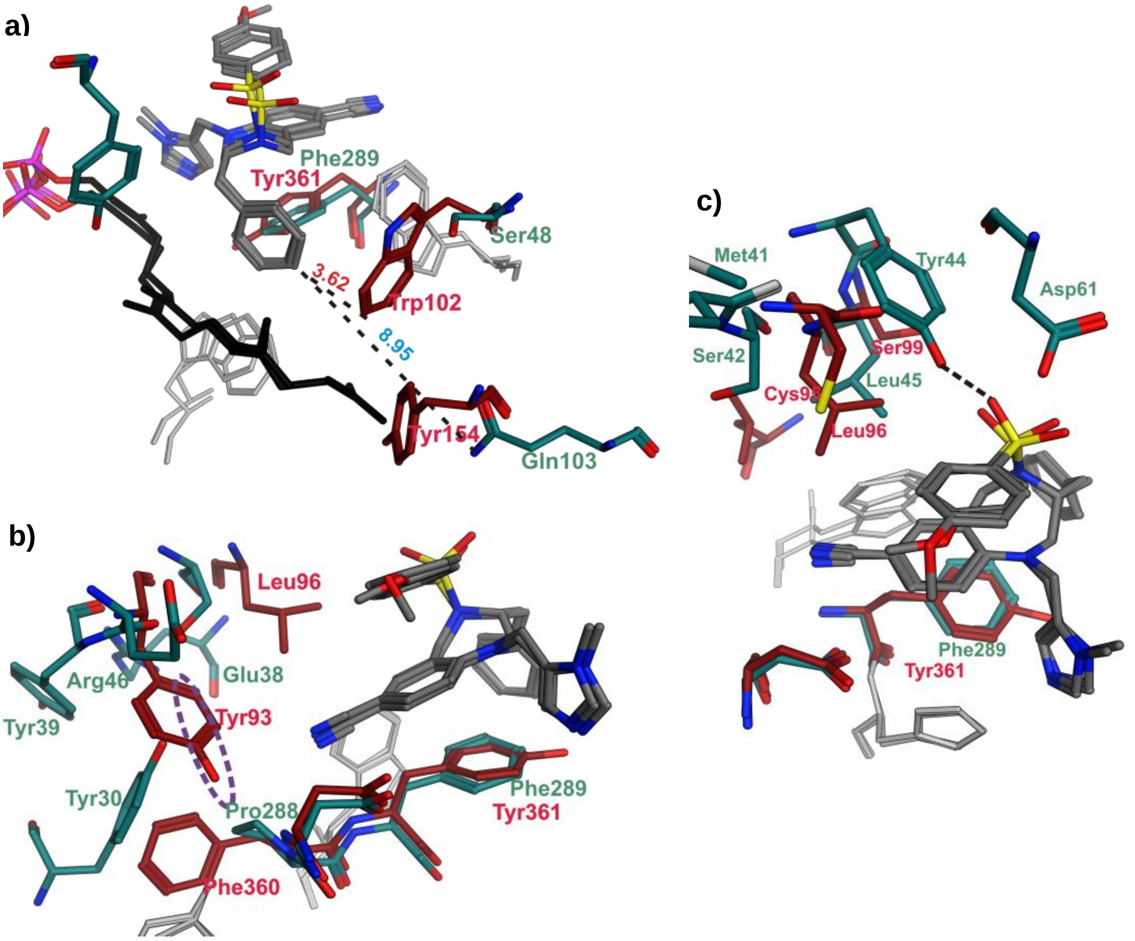
a)
Phe289
Tyr361
Ser48
3.62
Trp102
8.95
Tyr154
Gln103
b)
Leu96
Glu38
Arg46
Tyr39
Tyr93
Tyr30
Pro288
Phe289
Tyr361
Phe360
c)
Met41
Tyr44
Asp61
Ser42
Ser99
Cys98
Leu45
Leu96
Phe289
Tyr361

Figure 4.2: Overlay of **BMS3** in FTase and RabGGTase. Residues of FTase are highlighted in red, residues of RabGGTase in green. a) The 3-benzyl group of THB T-stacks with Trp102 in FTase, whereas Ser48 in RabGGTase opens up a large space for modifications. b) The nitrile group in FTase is close to the surface, within RabGGTase it points to the TAG tunnel (indicated in purple dotted line). Possible interactions with the nearby Tyr30 could be explored by incorporation of hydrogen bond acceptors. c) The anisylsulfonyl group interacts with Tyr44 in RabGGTase, no clear interactions are observed in FTase.

Furthermore, it was envisioned that the introduction of hydrogen bond acceptors could lead to interactions with the nearby Tyr30.

The phenylmethyl of **BMS3** approaches the lipid binding sites (LBSs) of both enzymes. In FTase, the bulky Trp102, which ensures the selectivity for FPP over GGPP, is close to the phenylmethyl moiety and is involved in π-stacking interactions. In RabGGTase, this tryptophan is replaced by a small serine and therefore leaves room for a larger binding cavity. It was expected that the introduction of larger groups at position **A** (Figure 4.1e) would result in selectivity for RabGGTase over FTase due to the expected steric clash with Trp102. The described differences of the binding site of FTase and RabGGTase are depicted in Figure 4.2.

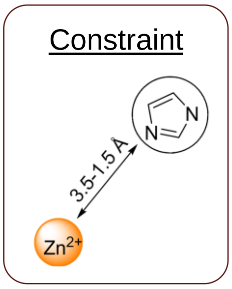

To obtain selective inhibitors a synthetic route had to be designed to, preferably, manipulate these groups in the last steps of the synthesis. To identify successful moieties to attach at these positions, a virtual screening had to be carried out. In this chapter, the synthesis of several generations of RabGGTase inhibitors will be described, following the typical iterative cycle of a structure-based project of design, synthesis and biological evaluation.

§ 4.2 Virtual Screening

To select a reasonable set of THB based inhibitors a virtual screening was carried out. A large set of virtual molecules was assembled and energy minimized. The co-crystal structures of FTase and RabGGTase were prepared for virtual screening by adding hydrogens and deleting the original ligand, **BMS3**, from its binding site. Then the set of virtual molecules was screened against both FTase and RabGGTase using GOLD. For the screening, a constraint was set between the imidazole and zinc ion in the binding site to assure realistic screening results. The scores for the individual virtual molecules were calculated by subtracting the screening scores for FTase from the screening scores for RabGGTase. The higher the total score, the more likely this molecule would be a selective inhibitor for RabGGTase. The top molecules of the screens were evaluated by their binding pose and their synthetic accessibility. Some of the top result binders from the first virtual screening are depicted in Figure 4.3. To indicate that the figures are related to docked structures instead of crystal structures, the surface of the protein is colored beige instead of grey.

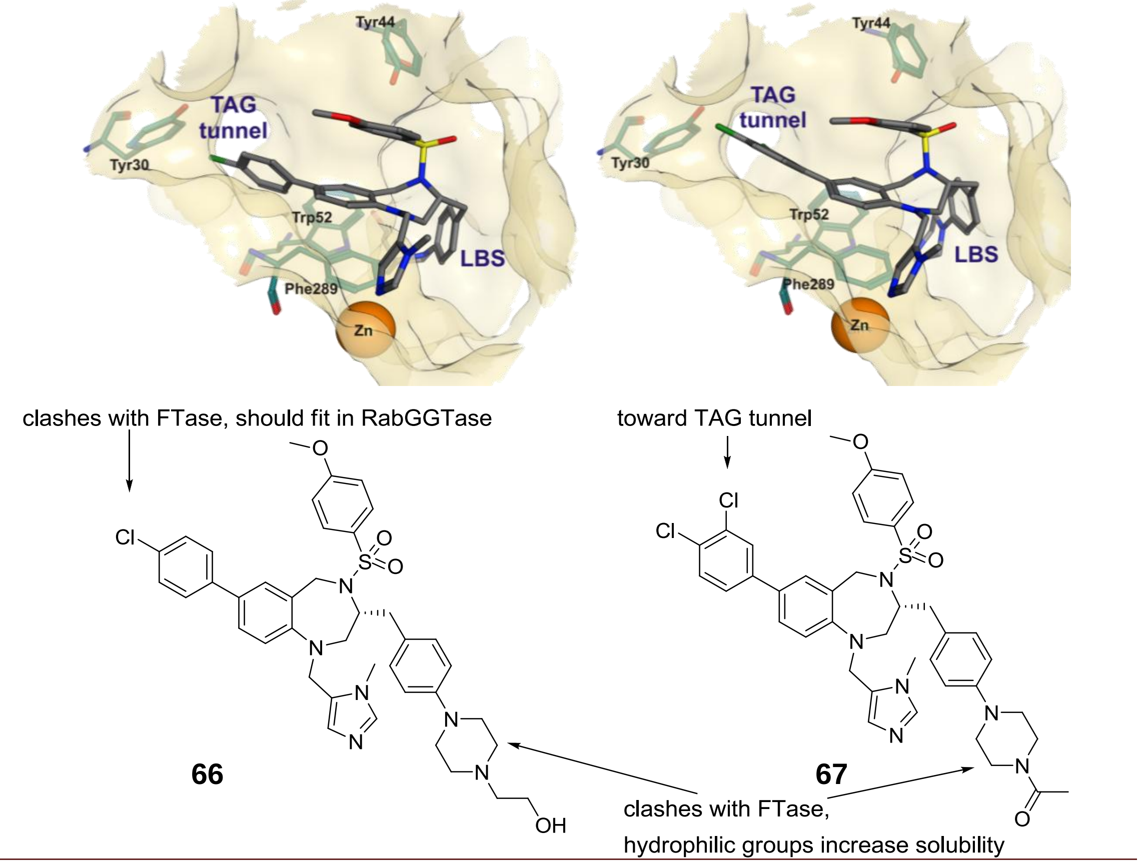
Tyr44
TAG tunnel
Tyr30
Trp52
LBS
Phe289
Zn
Tyr44
TAG tunnel
Tyr30
Trp52
LBS
Phe289
Zn
clashes with FTase, should fit in RabGGTase
toward TAG tunnel
66
67
clashes with FTase,
hydrophilic groups increase solubility

Figure 4.3: Selection of top results of first virtual screening. a) Docking solution of **66** in RabGGTase, the surface of the protein is depicted in beige. b) Docking solution of **67** in RabGGTase. c) 2D representation of the 2 ligands: the design principles are indicated with black arrows.

It was expected that the introduction of a para-chloro-substituted aromatic ring would result in a clash with the surface of FTase, whereas it would fit in RabGGTase. The meta-chloro substituent was designed to approach the RabGGTase TAG tunnel. The introduction of hydrophilic groups, approaching the lipid binding site, was predicted to result in both selectivity as well as an increase in solubility.

§ 4.3 Retrosynthetic analysis

In order to obtain the inhibitors that approach the TAG tunnel and lipid binding site, a versatile route toward the derivatization at $R^1$and R^2 of the general THB scaffold **68** needed to be developed to modify the THBs ideally in the last steps.

Retrosynthetically, it was envisioned that THB **69** would be an excellent starting point for modification. **69** could be obtained from building block **70**, which could be constructed from 5-bromoisatoic anhydride **71** and the methylester of D-tyrosine **72**. Further modification by sulfonylation and reductive amination would lead to the target structure **69**, in analogy to the synthetic route of Bristol-Myers Squibb [191, 192].

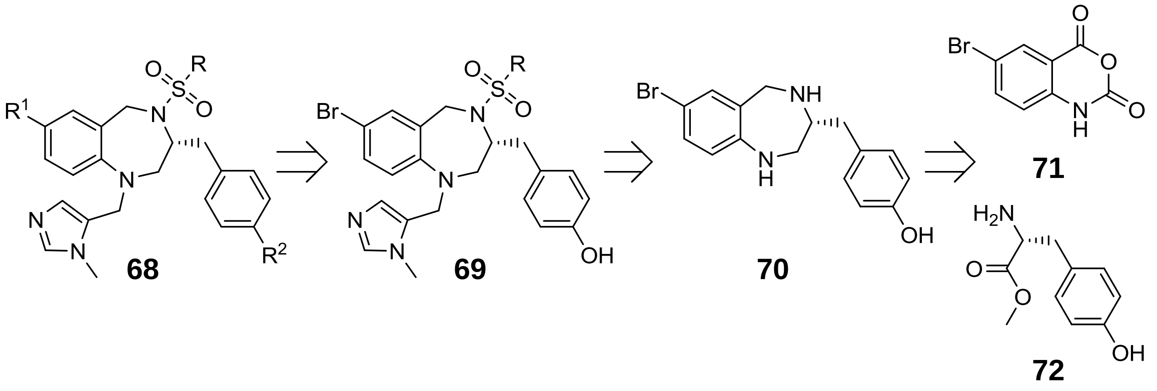

Scheme 4.1: Retrosynthetic analysis toward THB **69.**

§ 4.4 Synthesis of General Building Blocks

Condensation of D-tyrosine-methyl-ester **72** with 5-bromoisatoic anhydride **71** under reflux conditions in pyridine led to 1,4-benzodiazepine-2,5-dione, which was reduced to its corresponding tetrahydrobenzodiazepine (THB) **70** using borane in THF in an overall yield of 62%. Subsequent copper catalyzed cyanation led to the formation of **70**b. Due to easy deprotonation of the phenolic hydroxyl group in combination with easy protonation of the basic nitrogens, special care needed to be taken during work-up. Most problems could be circumvented by using weak aqueous base like sodium bicarbonate.

The last two steps toward the general building block involved selective N-sulfonylation followed by reductive amination and needed some optimization. This will be described in the next paragraphs (§ 4.4.1 and § 4.4.2). The synthesis of the general building blocks is summarized in Scheme 4.2. Building block **74b**, containing the nitrile, can serve as precursor for the first generation of THB analogs targeting the LBS. Building block **74a**, containing the bromide, serves as precursor for the later generation of analogs, targeting the TAG tunnel and LBS. The synthesis of THB-based RabGGTase inhibitors was conducted together with Dr. Robin Bon.

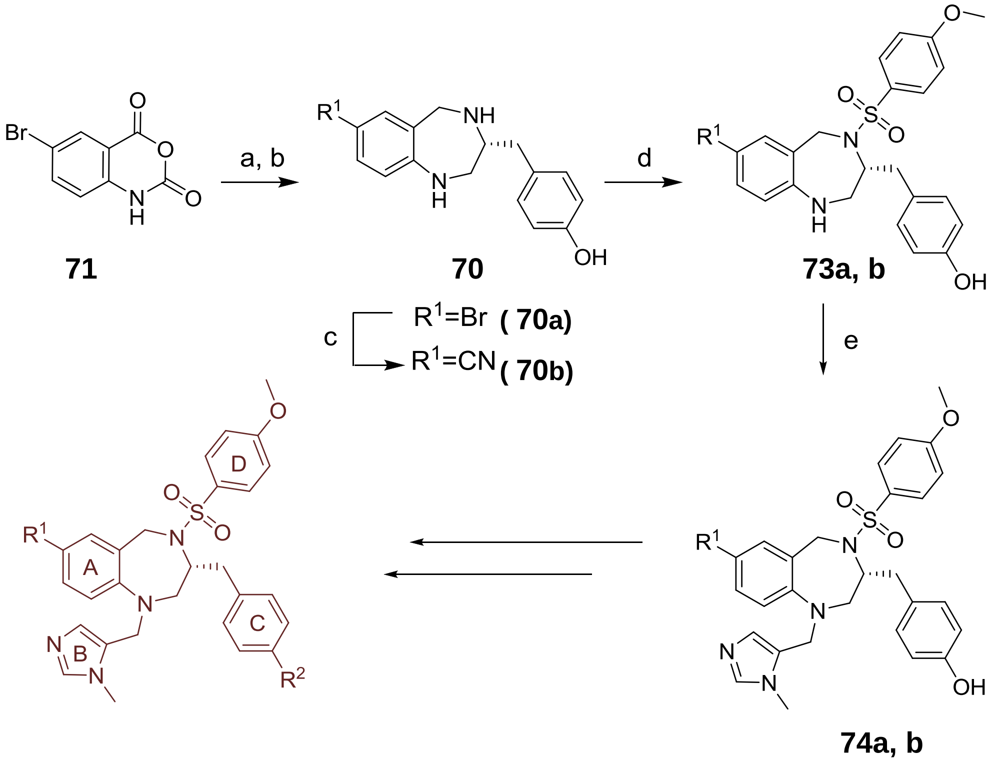
Br
O
O
N
H
O
71
a, b
R1
NH
N
H
OH
70
d
O
O
S
O
N
R1
N
H
OH
73a, b
c
R1=Br (70a)
R1=CN (70b)
e
O
D
O
S
O
R1
N
A
N
N
B
N
C
R2
O
O
S
O
R1
N
N
N
N
OH
74a, b

Reagents and Conditions (a) D-Tyr-OMe*HCl (**72**), DMAP, pyridine, 3 days, reflux (b) BH_3 in THF, 16h, reflux, 62% (2 steps) (c) CuCN, DMF, 0.5h, µw 210°C, 67% (d) 4-methoxybenzenesulfonylchloride**75**, pyridine, 16h, rt, 61%-71% (d) N-methylimidazole 5-carboxaldehyde **76**, TFA, TFAA, Et_3SiH, DCM, 16h, rt 80-83%

Scheme 4.2: Synthesis of general building blocks **74a** & **b.**

§ 4.4.1 Optimization of specific N-sulfonylation

In order to introduce the anisylsulfonyl moiety at the amine in the presence of the phenolic hydroxyl group selectively, different conditions were screened on THB **70**b (Table 4.1).

Table 4.1: Condition screening for sulfonylation.

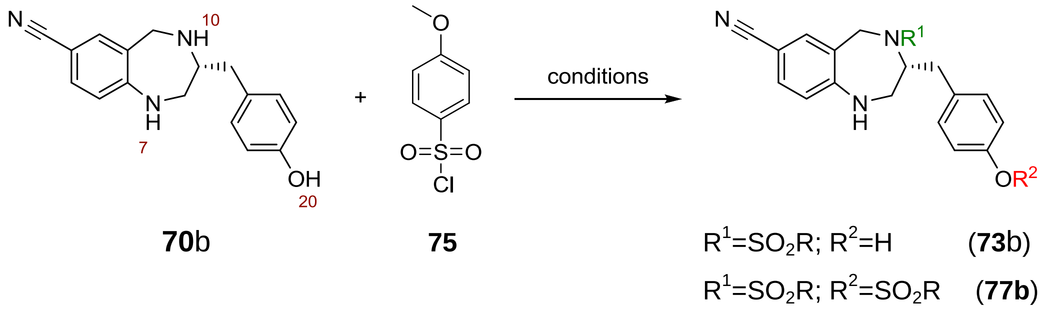
N
10
NH
N
H
7
OH
20
70b
+
O
O=S=O
Cl
75
conditions
N
NR1
N
H
OR2
R1=SO2R; R2=H (73b)
R1=SO2R; R2=SO2R (77b)

entry	Base	Solvent	yield **73**b	yield **77**b
a	Pyridine (5 equiv) DMAP (0.1 equiv)	THF	33 %	12 %
b	DIPEA (3 equiv)	THF	55 %	26 %

c	Pyridine	Pyridine	71 %	1 %

It was expected that activation of the amine for nucleophilic attack by addition of base could subsequently activate the phenol leading to a competition between N- and O-sulfonylation.

The results show that in the presence of a weak base such as pyridine the desired product could be obtained chemoselectively in 71% yield (entry c). The use of stronger bases like DIPEA in THF resulted in both mono-N-sulfonylated product and unwanted di-sulfonylated byproduct in lower yields. Therefore, further scale-up reactions were carried out in pyridine as a solvent and base.

§ 4.4.2 Optimization of reductive amination

The last step involved the reductive amination of N-methylimidazole-5-carboxaldehyde and **73** to obtain final building block **74**. However due to the inactivated secondary amine only low conversions were reached using standard reductive amination conditions. Besides some product, mainly starting material was recovered, which is related to the reversible character of imine formation. (Table 4.2, entry a, b)

The addition of a water scavenger like TFAA, by analogy to patent literature[193] led to complete conversion of **73** into **74** in high yield (entry c). The proposed mechanism is depicted in Figure 4.4.

Table 4.2: Optimized conditions for the reductive amination.

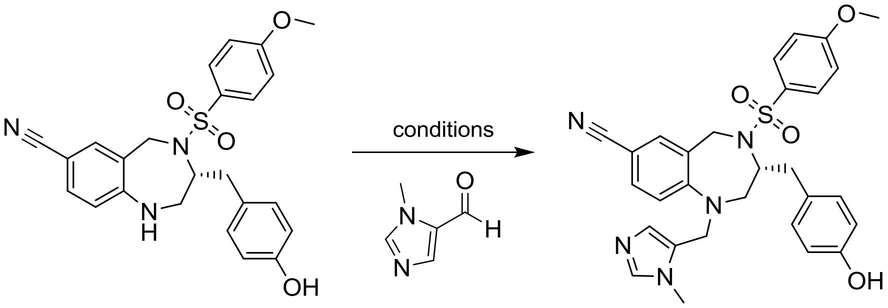

73b **76** **74**b

entry	reducing agent	additives	Solvent	Yield
a	NaBH(OAc)$_3$	AcOH	THF	32%
b	Et$_3$SiH	TFA	DCM	35%
c	Et$_3$SiH	TFA, TFAA	Toluene	85%

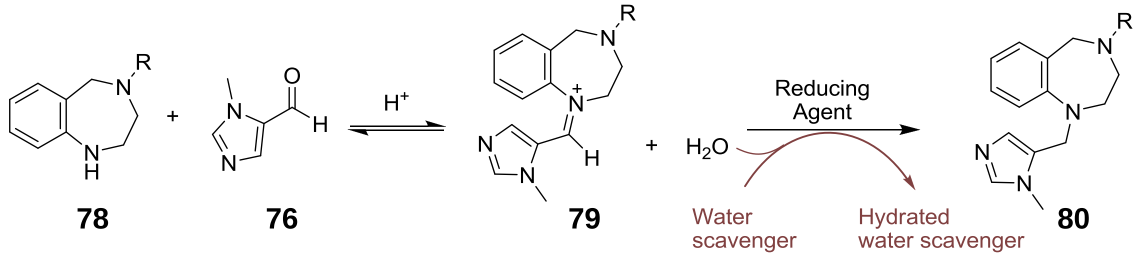

Figure 4.4: Using a water scavenger such as TFAA, the equilibrium is shifted toward product **74b.**

§ 4.4.3 Determination of the enantioselectivity

In order to determine the enantioselectivity of the respective route, the same synthetic steps as described in Scheme 4.2 were carried out starting from L-tyrosine methyl ester in order to obtain the S-enantiomer of **74**a. The two pure enantiomers as well as the mixture were separated by chiral HPLC, which showed that the building block was obtained in high enantiomeric (>98.5%) purity.

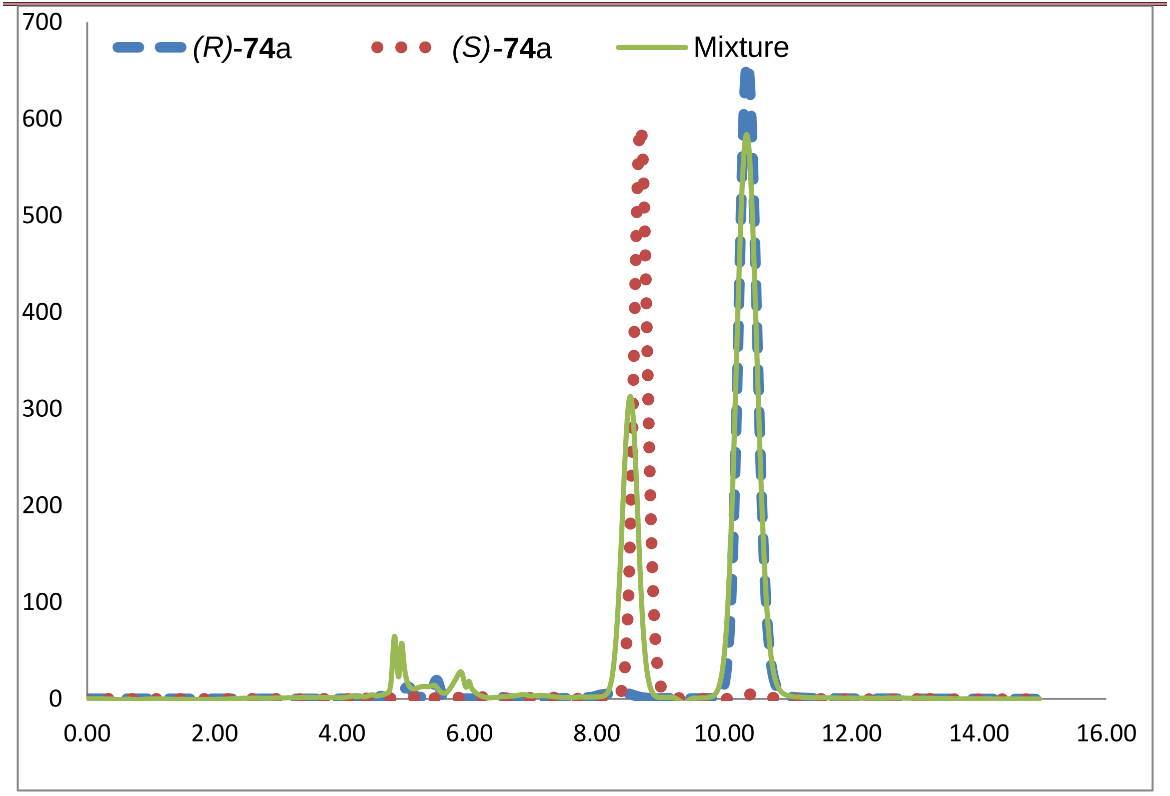

Figure 4.5: chiral HPLC trace of THB-building block **74a.**

§ 4.5 Synthesis & Screening of 1st generation RabGGTase inhibitors

Having building block **74**b in hand, the effect of extending the THBs toward the lipid binding site could be examined. The moieties introduced were inspired by the virtual screening results, as well as by the wide scope of possible chemical transformations on the phenolic hydroxyl group. Transformations envisioned were aminoacylation (**81**) and alkylation (**82**) as well as triflation (**83**) followed by Suzuki-Miyaura coupling (**84**) or Buchwald-Hartwig amination (**85**) and are depicted in Scheme 4.3

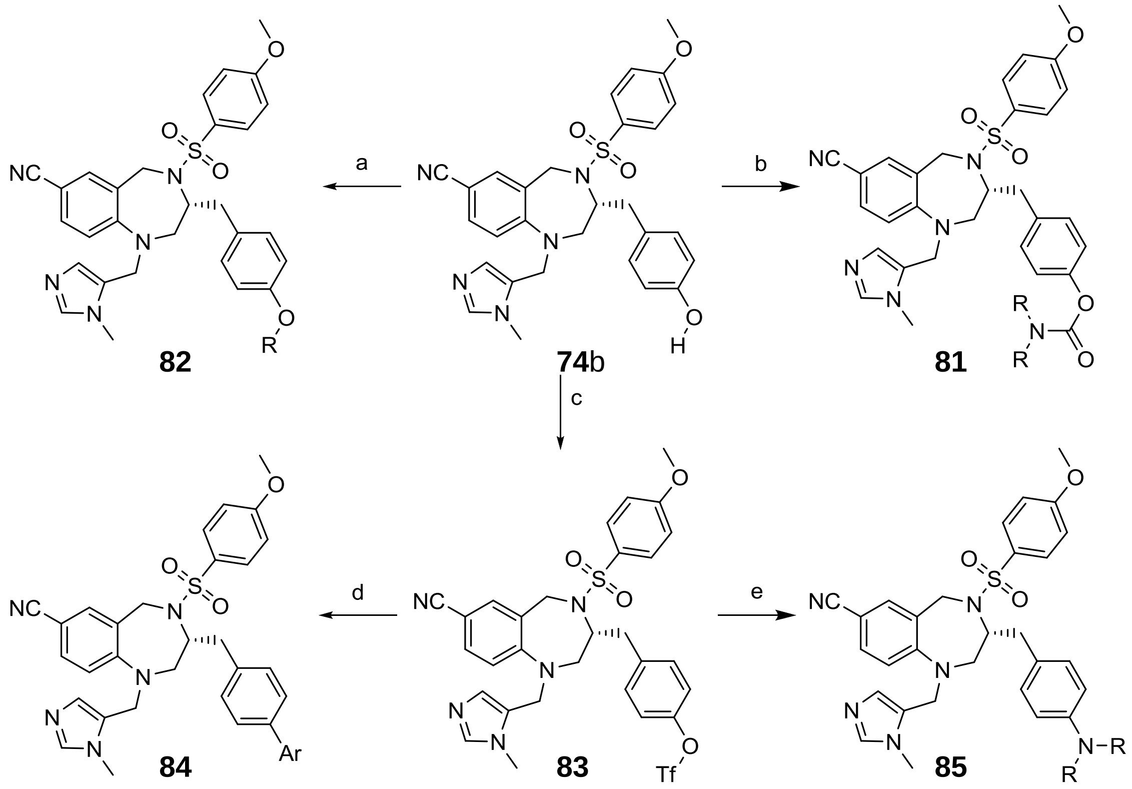

(a) alkylation (b) aminoacylation (c)triflation (d)Suzuki coupling (e)Buchwald-Hartwig

Scheme 4.3: Synthetic modifications leading to the first generations of inhibitors.

Alkylation was achieved in high yields by addition of alkyl, allyl or benzyl bromide with sodium hydride as a base. Aminoacylation was performed by addition of either isocyanates or carbamoyl chloride in the presence of base, leading to the corresponding products in excellent yield. Building block **83** was obtained in high yields using triflating reagent **86**, whereas standard triflate conditions using triflic anhydride gave disappointed yields. These triflates could be manipulated by transition-metal catalyzed reactions, successfully illustrated by the introduction of 3-pyridine-

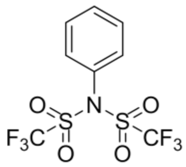

86

boronicacid under standard Suzuki coupling conditions. These modifications resulted in the 1st generation of inhibitors based on **BMS3** and emphasize the phenolic hydroxyl group as a versatile handle for modification.

The collection was screened using fluorometric FTase[175, 176] and RabGGTase assays.[69, 182] (§ 3.1&§ 3.2). These fluorometric assays are continuous and less laborious alternatives to their corresponding radioactivity-based assays. For **BMS3**, we determined an IC_{50} of 724 nM for RabGGTase and an IC_{50} of 6 nM for FTase (Table 4.3)

The pronounced difference in IC_{50} values for these enzymes compared to previously reported values from radiometric assays[194] is related to the use of artificial fluorescent substrates in these assays. Therefore, the improvement factor was introduced to indicate the improvement in selectivity for RabGGTase, compared to the dual inhibitor **BMS3** (*vide supra*):

$$\text{Improvement Factor} = \frac{IC_{50_{RabGGTase}}(BMS3) \quad IC_{50\_RabGGTase}(Inhibitor)}{IC_{50_{FTase}}(BMS3) \quad IC_{50\_FTase}(Inhibitor)}$$

Consequently, an increase in selectivity for RabGGTase compared to dual inhibitor **BMS3** will lead to a factor larger than 1, whereas a decrease in selectivity for RabGGTase will lead to a factor between 0 and 1. **BMS3** will always have an improvement factor of 1 by definition.

In addition IC_{50} values for GGTase I were measured to evaluate the selectivity of our THB-based inhibitors with respect to all three prenyl transferases.

It can be concluded from the table that decorating the 3-phenol results in a general increase for RabGGTase inhibition and a general decrease in FTase inhibition, validating the lipid binding site as a pocket to increase selectivity. However, the extended compounds showed only a minor (1-16 fold) decrease in FTase inhibition, opposed to the large decrease which was expected due to the predicted clash with Trp102. Therefore, it is likely that the inhibitors and/or FTase adopt their binding conformation to the newly introduced moieties. In order to obtain completely selective inhibitors, it seemed that modification at both sides of the scaffold is necessary.

Table 4.3: Synthesis & Screening of 1st generation inhibitors.

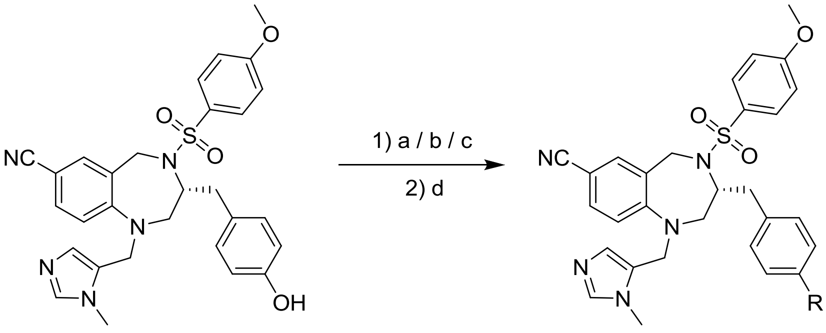

74b **87-94**

Reagents and Conditions: (a) alkylbromide, NaH, DMF (b) isocyanate, Et_3N, DCM (c) TfN(Ph)Tf (**86**), Et_3N, DCM (d) arylboronic acid, $Pd(PPh_3)_4$, K_2CO_3, DCE/H_2O, 80 °C

				In vitro IC_{50} [nM]			
entry	cmpd	R	Yield [§]	RabGGTase	FTase	GGTase I	IF
1	**BMS3**	H	-	724±321	6±3	>99,500	1.0
2	**74**b	OH	-	1,011±465	5.2±0.2	>99,500	0.6
3	**87**	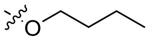	92% [a]	162±10	10±7	>99,500	7.4
4	**88**	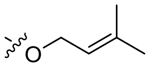	94% [a]	39±10	15±8	>99,500	46.4
5	**89**	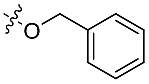	85% [a]	441[#]	99.3±59	>99,500	27.2
6	**90**	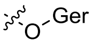	94% [a]	2,072[#]	1,012±688	>99,500	58.9
7	**91**	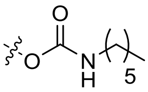	98% [b]	243±20	9.2±4.2	>99,500	4.6
8	**92**	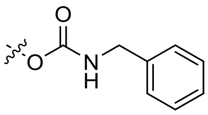	96% [b]	72±2	<5[$]	>99,500	<8.4
9	**93**	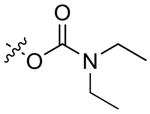	72% [b]	38±7	<5[$]	2,020±384	<15.9
10	**83**	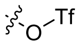	94% [c]	>9,500	10.5±3.9	>99,500	nc
11	**94**	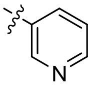	94%* [d]	353±158	4.3±2.2	3,643[#]	1.5

[§]method used, *from triflate **83,** Ger = geranyl, [$]lower detection limit, [#]single point measurement, nc = not calculated, IF = Improvement Factor.

§ 4.6 Synthesis & Screening of 2nd generation RabGGTase inhibitors

Although the selectivity moderately increased for the 1st generation of RabGGTase inhibitors, the hypothesis that extending in both directions would give selectivity toward RabGGTase still needed to be tested. Herefore, a similar synthetic strategy was adopted.

To extend the THB scaffold towards both the TAG tunnel and the LBS, general building block **74**a (Scheme 4.2), containing the bromide was used. The bromide was subjected to Suzuki conditions in order to introduce several moieties meant to approach the TAG tunnel. Coupling of building block **74**a with arylboronic acids in the presence of $Pd(PPh_3)_4$ and Na_2CO_3 as a base gave THBs **97**, **99** and **104** in good yields. Subsequent modifications at the 3-phenol group were carried out to obtain the target compounds (Table 4.4). THBs **103**, **105** and **106** were obtained in good yields, using the methodology described for the 1st generation of inhibitors. Triflate **100** was further exploited using Buchwald-Hartwig and Sonogashira conditions. The Buchwald-Hartwig coupling, using $Pd_2(dba)_3$ as the catalyst, Johnphos **95** as ligand and NaO*t*Bu as a base gave THB **101** in good yield. THB **102** was synthesized in moderate yield using typical Sonogashira conditions. This 2nd generation of THBs particularly resembled the suggestions from *in silico* screening. For example, **102** was among the best scoring compounds from the virtual screening.

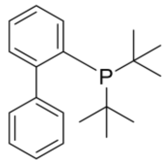

JohnPhos 95

Table 4.4: Synthesis & Screening of the 2nd Generation of THB-based inhibitors.

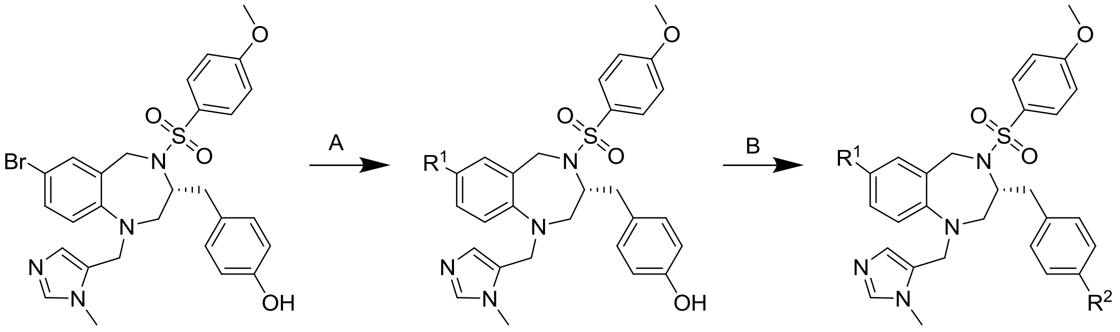

74a **96-106**

A: arylboronic acid, $Pd(PPh_3)_4$, Na_2CO_3, dioxane/H_2O, 80°C. **B**: (a) isocyanate, Et_3N, DCM; (b) alkylbromide, NaH, DMF; (c) TfN(Ph)Tf (**86**), Et_3N, DCM; (d) alkyne, $Pd(PPh_3)_4$, CuI, Et_3N, TBAI, DMF, 70 °C(e) amine, NaOtBu, $Pd_2(dba)_3$, JohnPhos (**95**), THF; (f) arylboronic acid, $Pd(PPh_3)_4$, K_2CO_3, DCE/H_2O, 80 °C;

					In vitro IC_{50} [nM]			
entry	cmpd	R^1	R^2	Yield §	RabGGTase	FTase	GGTase I	IF
1	**BMS3**	CN	H	-	724±321	6±3	>99,500	1
2	**96**	Br	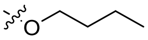	$99\%^{b}$	>9,500	$406^{\#}$	>99,500	6.8
3	**97**	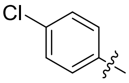	OH	$77\%^{A}$	>9,500	194±78	>99,500	<2
4	**98**	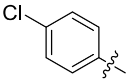	OTf	$72\%^{c1}$	>9,500	>9,700	>99,500	nc
5	**99**	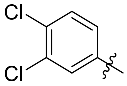	OH	$89\%^{A}$	>9,500	120.5±84.9	>99,500	nc
6	**100**	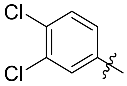	OTf	$82\%^{c1}$	>9,500	>9,700	>99,500	nc
7	**101**	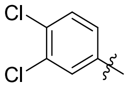	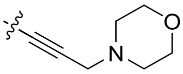	$56\%^{d2}$	>9,500	>9,700	>99,500	nc
8	**102**	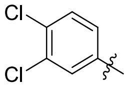	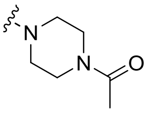	$82\%^{e2}$	>9,500	979±262	>99,500	nc
9	**103**	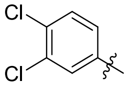	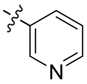	$57\%^{f2}$	>9,500	>9,700	>99,500	nc
10	**104**	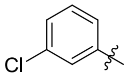	OH	$70\%^{A}$	1,302±478	42±10	>99,500	3.9
11	**105**	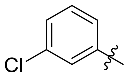	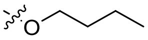	nd ^{b1}	6,515±1,839	>9,700	>99,500	nc
12	**106**	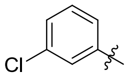	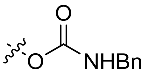	$90\%^{a1}$	2,264±844	123±24	>99,500	6.6

[§]Method used [1]From corresponding arylTHB, [2]From corresponding triflate, [#]single point measurement, nc = not calculated IF = Improvement Factor.

Unfortunately, as clear from the IC_{50} data shown in Table 4.4, the incorporation of these aryl groups did not result in an increase in selectivity; the 2nd generation of THBs showed almost no inhibitory activity for RabGGTase. Only the meta-chloroaryl-substituted THB (**104**) retained potency, although it is three fold less potent compared to **BMS3**.

Thus modification at R^1 alone, extending toward the TAG tunnel, did not result in any selectivity gain. THB **105**, which bears additional groups to approach the TAG tunnel (metachloro aryl) and LBS (butyl), was found to be a weak selective RabGGTase inhibitor. To get a better structural insight into the activity- and selectivity data of the THB library, co-crystallization and docking studies were carried out.

§ 4.7 *Crystallization and Overlay studies of 1st and 2nd generation of inhibitors*

Although the extended THB library did not result in full selectivity for RabGGTase as compared to FTase, some of the compounds showed a high increase in selectivity (over 50 fold). To get a better insight into the effect of the extensions on binding on an atomic level, co-crystallization studies were carried out by Dr. Zhong Guo. Inhibitors **92** and **93** could be successfully soaked into both FTase and RabGGTase, (Figure 4.6 & Figure 4.7). The co-crystal structures revealed that the binding mode of the THB moiety is highly conserved in both enzymes. The π-stacking of ring A with the aromatic enzyme residues and imidazole-zinc binding locks the seven-membered ring connected to the imidazole moiety in an L-shaped fashion. The orientation of the phenolic portion (ring C), either connected to a phenylcarbamate or diethylaminecarbamate, appears to be more flexible; **92** shows a conformational change in this area, while **93** adopts the same conformation as **BMS3**.

In the complex **92**:FTase:FPP (Figure 4.6a, b) this conformational change, which also leads to loss of some hydrophobic interactions, is the main difference between **92** and parent compound **BMS3**. This difference however does not result in a decrease in potency of inhibition. In the complex **92**:RabGGTase (Figure 4.6c, d) an extra hydrogen bond between the sulfonyl group of the ligand and Tyr44 is formed. In addition, there seems to be an extra hydrophobic interaction between the introduced benzylcarbamate and the lipid binding site of the enzyme.

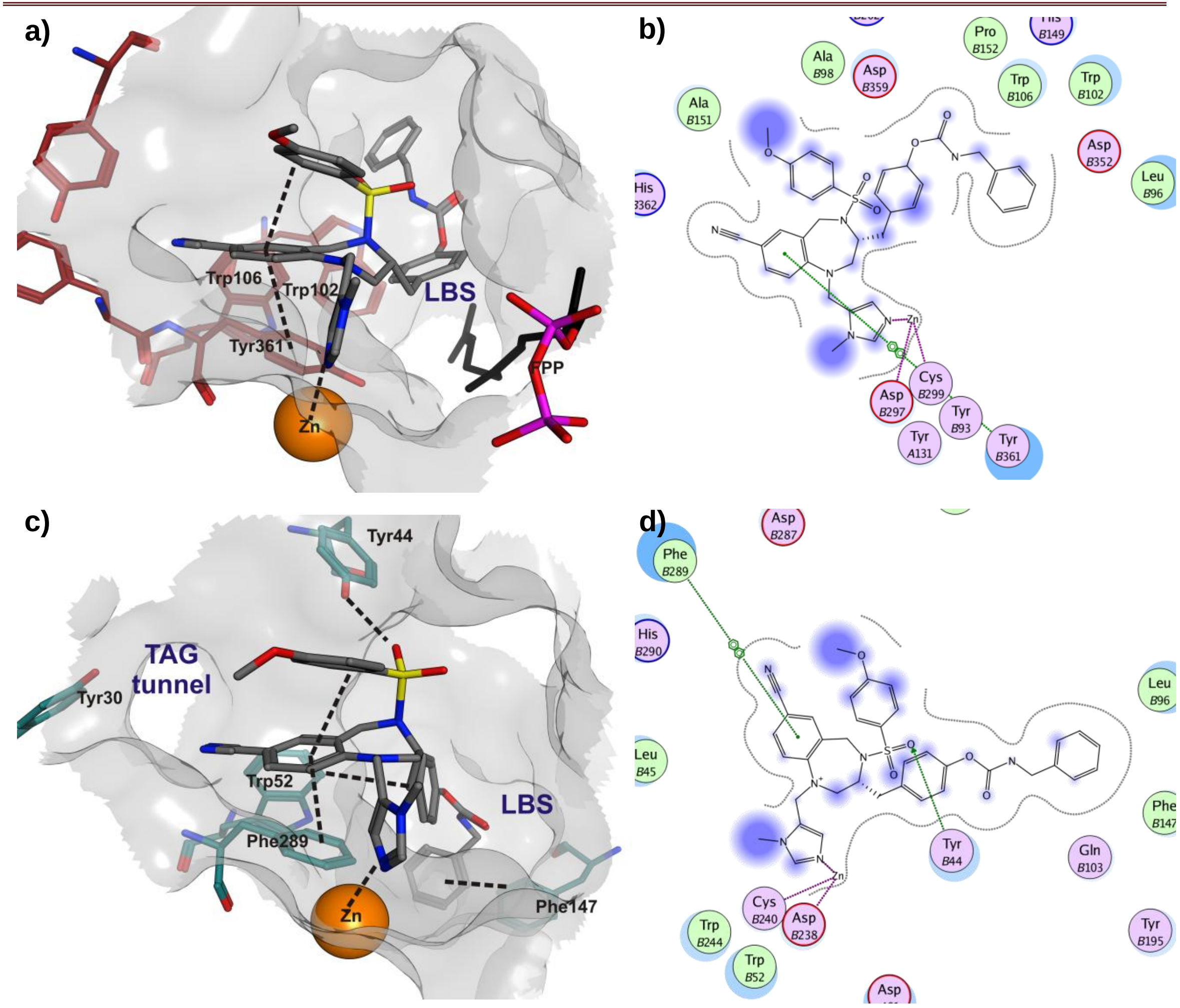
a)
Trp106
Trp102
Tyr361
LBS
FPP
Zn
b)
Ala B98
Asp B359
Pro B152
His B149
Trp B106
Trp B102
Ala B151
Asp B352
Leu B96
His B362
Cys B299
Asp B297
Tyr B93
Tyr A131
Tyr B361
Zn
c)
Tyr44
TAG tunnel
Tyr30
Trp52
Phe289
LBS
Zn
Phe147
d)
Asp B287
Phe B289
His B290
Leu B96
Leu B45
Phe B147
Tyr B44
Gln B103
Cys B240
Asp B238
Trp B244
Trp B52
Tyr B195
Asp
Zn

Figure 4.6: Co-crystal structures of **92**: a) Surface representation of active site of **92**:FTase:FPP complex. Similar to **BMS3**, the imidazole coordinates to the zinc ion. The THB interacts with Tyr361 and is further involved in internal π-stacking with the anisylsulfonyl group. The 3-benzyl moiety extends to the back, disrupting the interactions with Trp102 and Trp106. The black dashed lines indicate interactions between ligand and enzyme. b) schematic representation of **92**:FTase interactions. c)Surface representation of the active site of **92:**RabGGTase complex. Similar to **BMS3**, the imidazole coordinates to the zinc ion, whereas the sulfonamide forms hydrogen bonds with Tyr44. The 3-benzyl moiety interacts with Trp52 and Phe289 by edge-face hydrophobic stacking, whereas the THB moiety stacks face-face with Phe289. The conformation is further stabilized by internal π-stacking of the THB with the anisylsulfonyl group. The additional benzylcarbamate contributes with an edge-face hydrophobic stacking with Phe147. The black dashed lines indicate interactions between ligand and enzyme. d) Schematic representation of **92**:RabGGTase interactions.

The co-crystal structure of **93**:FTase (Figure 4.7a, b)revealed that the Trp102 residue, originally contributing with an edge-face T-stacking interaction, is flipped by 180°. This opens up extra space in the hydrophobic area, allowing the extended THBs to bind. However, an extra hydrogen bond interaction is formed between Trp106 and the diethylcarbamate group. In total these changes sum up to an approximately similar

$IC_{50}$for FTase. In the complex **93**:RabGGTase (Figure 4.7c, d) extra interactions are realized by a cation-π-interaction between Arg144 and the 3-benzyl moiety (ring C)

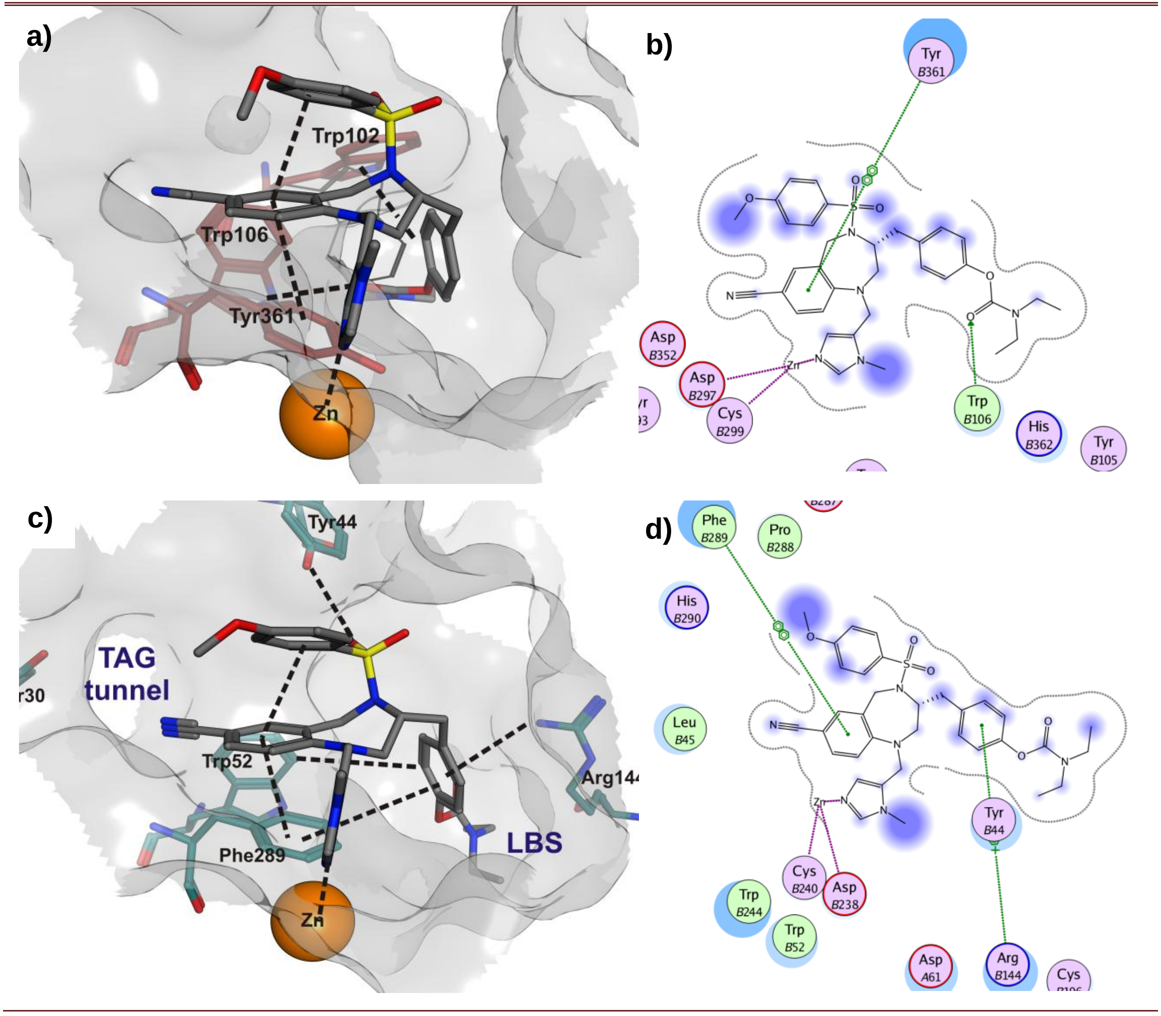
a)
Trp102
Trp106
Tyr361
Zn
b)
Tyr B361
Asp B352
Asp B297
Cys B299
Trp B106
His B362
Tyr B105
c)
Tyr44
TAG tunnel
r30
Trp52
Arg14
Phe289
Zn
LBS
d)
Phe B289
Pro B288
His B290
Leu B45
Tyr B44
Cys B240
Asp B238
Trp B244
Trp B52
Asp A61
Arg B144
Cys

Figure 4.7: Co-crystal structures of **93**: a) Surface representation of active site of **93**:FTase complex. The imidazole coordinates to the zinc ion. The THB interacts with Tyr361 and is further involved in internal π-stacking with the anisylsulfonyl group. The additional diethylcarbamate functionality is adopted via a reorientation of Trp102 by 180° and forms hydrogen bonds with Trp106. The black dashed lines indicate interactions between ligand and enzyme. b) schematic representation of **93**:FTase interactions. c) Surface representation of the active site of **93:**RabGGTase complex. Similar to **BMS3**, the imidazole coordinates to the zinc ion, whereas the sulfonamide forms hydrogen bonds with Tyr44. The 3-benzyl moiety interacts with Trp52 and Phe289 by edge-face hydrophobic stacking, whereas the THB moiety stacks face-face with Phe289. The conformation is further stabilized by internal π-stacking of the THB with the anisylsulfonyl group. The additional diethylcarbamate contributes with cation-π-stacking with Arg144. The black dashed lines indicate interactions between ligand and enzyme. d) Schematic representation of **93**:RabGGTase interactions.

The crystal structure analysis shows that both the inhibitors and the FTase binding site adopt different conformations due to the extensions of the THBs, resulting in selectivity profiles similar to that of **BMS3**. This accentuates the need for extensions in other or additional directions to obtain selective inhibitors.

However, as could be deduced from the second generation of inhibitors, the TAG tunnel only allows specific modifications. Attachment of a bulky aryl group, like para-chloro-aryl, led to complete loss of RabGGTase activity. This was contradictive to the virtual screening results, which indicated **102** as a potentially selective RabGGTase inhibitor.

Retrospectively, the rigid shape of THB found for all co-crystallized inhibitors could account for this observation. Overlay studies of 3,4-dichlorophenyl-substituted THB **99** showed a potential clash with the binding site assuming this rigid binding pose (Figure 4.8). Therefore, it was concluded that it was necessary to incorporate smaller heteroaromatic rings without para-substituents.

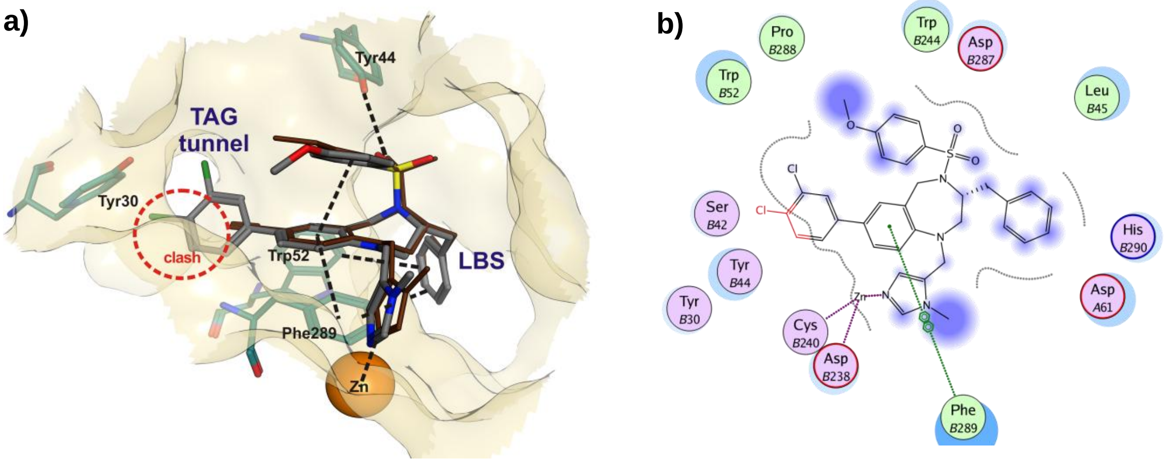
a)
Tyr44
TAG
tunnel
Tyr30
clash
Trp52
LBS
Phe289
Zn
b)
Pro
B288
Trp
B244
Asp
B287
Trp
B52
Leu
B45
O
O
O
Cl
Cl
N
N
Ser
B42
His
B290
Tyr
B44
Asp
A61
Tyr
B30
Zn
N
N
Cys
B240
Asp
B238
Phe
B289

Figure 4.8: Individual docking results of **99**; an overlay with structure of **BMS3**:RabGGTase:GGPP. Assuming a rigid THB-core binding pose, the para-chlorophenyl cannot adjust toward the TAG tunnel, and clashes with the binding pocket.

§ 4.8 Design and Synthesis of 3rd generation of inhibitors

§ 4.8.1 Virtual screening based on conformational constraints

Incorporation of substituted aromatic rings most probably resulted in a clash with the RabGGTase surface, which disrupts the important π-stacking with the THB moiety (ring A) and imidazole-zinc binding. In order to identify additional promising candidates a virtual high-throughput screening (VHTS) with extra conformational constraints was carried out. Herefore, the conformation of the THB was fixed between Phe289 and the zinc ion, in order to mimic the π-stacking and imidazole–zinc interaction, which seems essential for activity. Solutions should be obtained that exactly fit in the RabGGTase binding site. The counter screen for

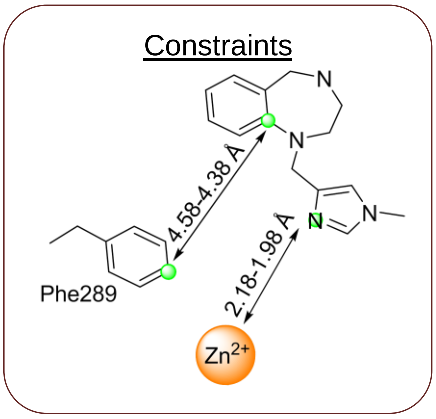
Constraints
N
N
N
N
4.58-4.38 Å
2.18-1.98 Å
Phe289
Zn2+

FTase was carried out like the first time, with just one constraint; the imidazole-zinc binding.

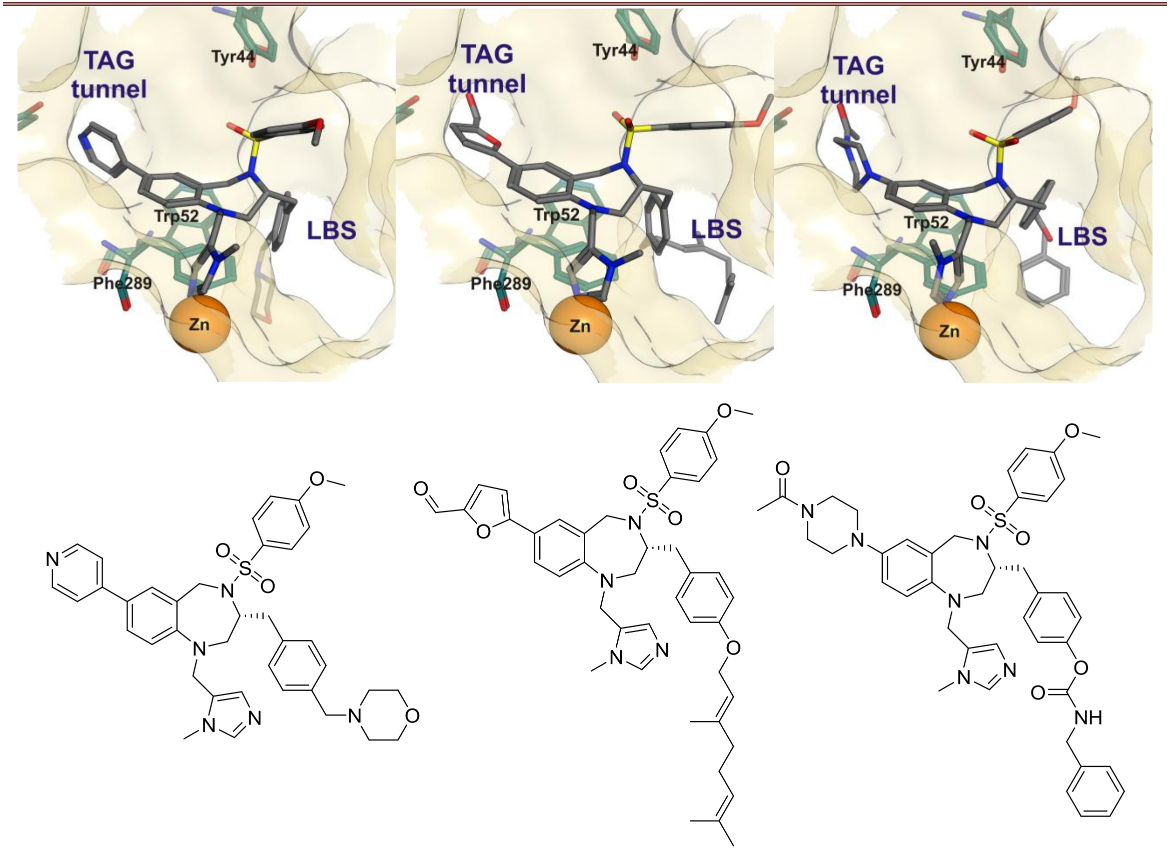

Figure 4.9: Virtual Screening solutions in RabGGTase employing two constraints.

In Figure 4.9 some typical solutions of the docked compound set are displayed. Heteroaromatic groups such as pyridine or furanaldehyde both extend toward the TAG tunnel without distorting the general binding pose. Other suggestions were flexible groups like N-acetylpiperazine, which could adjust toward the TAG tunnel. The latter group would have the additional advantage of increasing the solubility of the compounds.

§ 4.8.2 Synthesis& Screening of 3rd generation of inhibitors

Encouraged by our new hypothesis a five-membered furanaldehyde was attached to the building block using Suzuki coupling conditions. Then the phenolic hydroxyl group was decorated and the compounds were subjected to *in vitro* screening of RabGGTase and FTase.

Table 4.5: Synthesis of 3rd generation of inhibitors

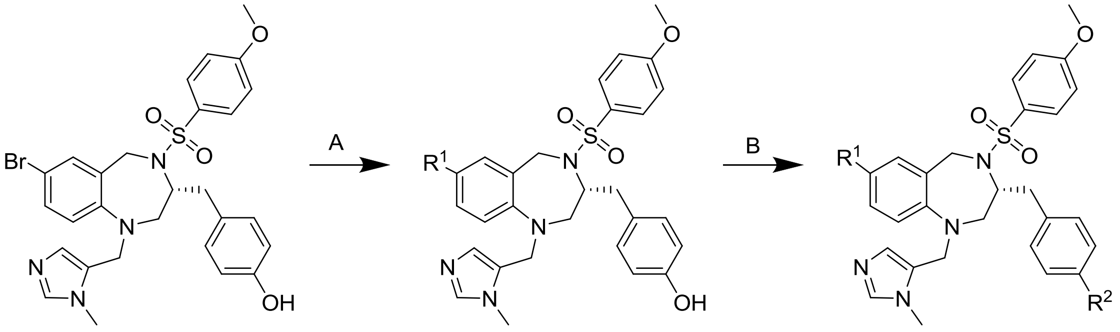

74a **107-109**

A: aryl boronic acid, $Pd(PPh_3)_4$, Na_2CO_3, dioxane/H_2O, 80°C **B**: (a) isocyanate, Et_3N, DCM

					In vitro IC_{50} [nM]			
entry	cmpd	R^1	R^2	Yield §	RabGGTase	FTase	GGTase I	IF
1	**BMS3**	CN	H	-	724±321	6±3	>99,500	1.0
2	**107**	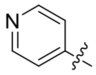	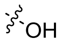	68%^{A}	8,843$^{\#}$	13.6±8.6	>99,500	0.2
3	**108**	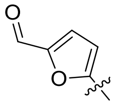	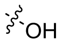	68%^{A}	206±13	7±3	>99,500	4.1
4	**109**	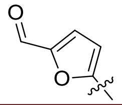	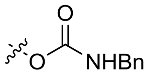	82%^{a1}	141±26	>9,700	>99,500	nc

§Method used [1]From corresponding arylTHB, #single point measurement, nc = not calculated IF = Improvement Factor.

As can been derived from Table 4.5 the introduction of a smaller five-membered ring successfully led to an active RabGGTase inhibitor. The counter screen on our FTase assay showed that the introduction of both groups indeed resulted in complete loss of FTase activity. So, compound **109**, besides providing ‘a proof of concept’, is the first selective low nM inhibitor of RabGGTase. Efforts to crystallize **108** and **109** by Dr. Zhong Guo resulted in co-crystal structures of **108** in both FTase and RabGGTase, as well as a co-crystal structure of **109** in complex with RabGGTase (Figure 4.10)

The co-crystal structure of **108**:FTase:FPP, revealed that the addition of the furanal at R^1 results in a compressed binding mode. The furanal moiety barely fits in the small hydrophobic space and, as expected, orients toward the exit groove of the active site, which seems to result in a conformational change at the other end of the ligand. In order to keep the favorable conformation for π-stacking and zinc binding, the phenolic portion of the molecule turns by 180°, a similar phenomenon as seen for ligand **92**. This causes the loss of favorable hydrophobic interactions with the binding site Trp residues (Figure 4.10a & b).

In complex **108**:RabGGTase, the furanal moiety orients toward the TAG tunnel. Further, the structure closely resembles the **BMS3**:RabGGTase complex, showing the same binding mode and conformation (Figure 4.10c & d).

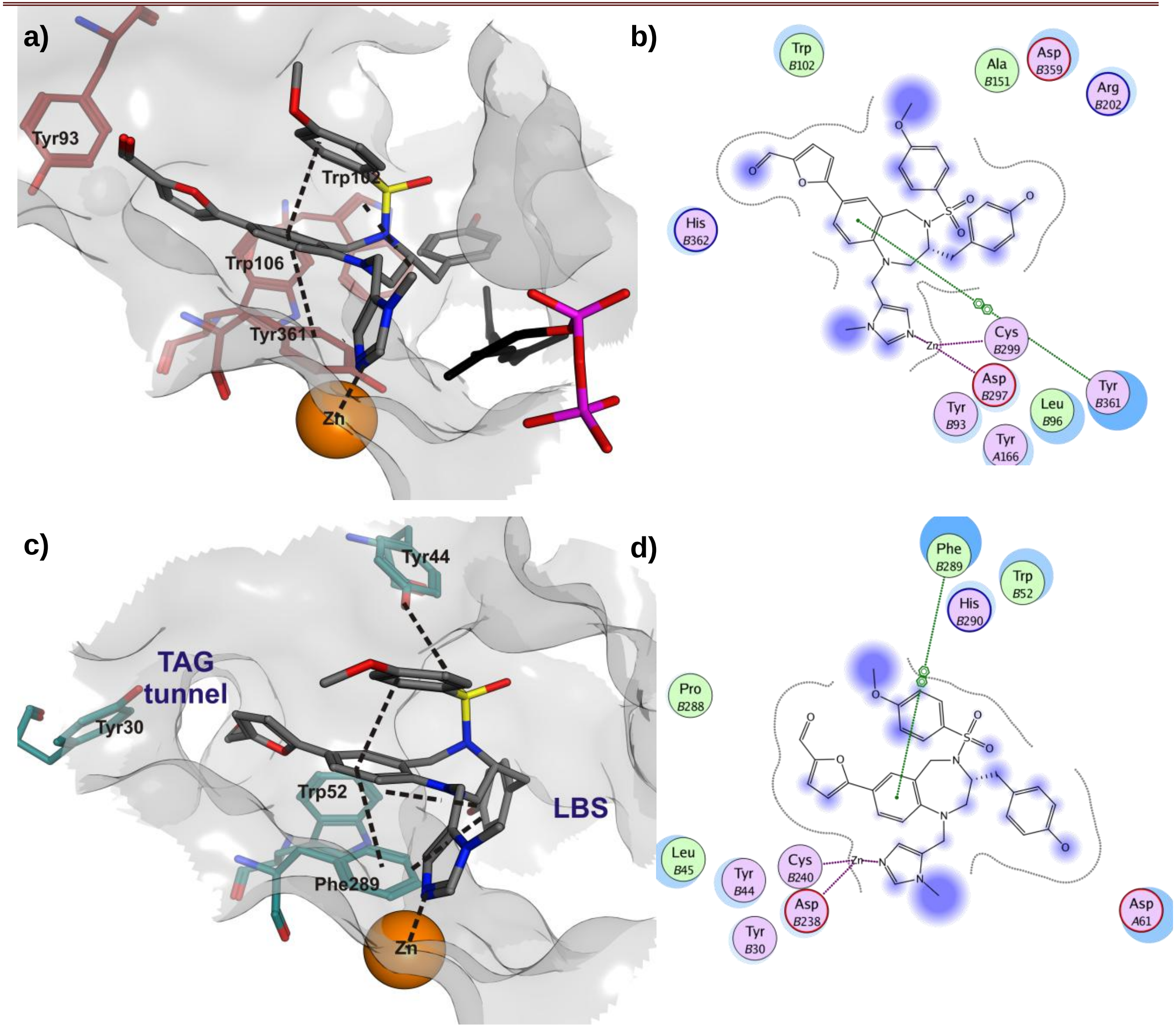
a)
Tyr93
Trp102
Trp106
Tyr361
Zn
b)
Trp B102
Ala B151
Asp B359
Arg B202
His B362
Cys B299
Asp B297
Tyr B361
Leu B96
Tyr B93
Tyr A166
c)
Tyr44
TAG tunnel
Tyr30
Trp52
Phe289
LBS
Zn
d)
Phe B289
Trp B52
His B290
Pro B288
Leu B45
Tyr B44
Cys B240
Asp B238
Tyr B30
Asp A61

Figure 4.10: Co-crystal structures of **108** and **109**: a) Surface representation of active site of **108**:FTase:FPP complex. The imidazole coordinates to the zinc ion. The THB interacts with Tyr361 and is further involved in internal π-stacking with the anisylsulfonyl group. The additional furanal barely fits in the FTase pockets and induces a conformational change of the 3-benzyl moiety, disrupting the favorable hydrophobic interactions with Trp106. The black dashed lines indicate interactions between ligand and enzyme. b) Schematic representation of **108**:FTase interactions. c) Surface representation of the active site of **108**:RabGGTase complex. Similar to **BMS3**, the imidazole coordinates to the zinc ion, whereas the sulfonamide forms hydrogen bonds with Tyr44. The 3-benzyl moiety interacts with Trp52 and Phe289 by edge-face hydrophobic stacking, whereas the THB moiety stacks face-face with Phe289. The conformation is further stabilized by internal π-stacking of the THB with the anisylsulfonyl group. The additional furanal occupies the entrance of the TAG tunnel but the expected hydrogen bond interaction between the aldehyde and Tyr30 cannot be observed. The black dashed lines indicate interactions between ligand and enzyme. d) Schematic representation of **108**:RabGGTase interactions.

The crystal structures of the compounds targeting either the LBS or the TAG tunnel complement the *in vitro* data. Obviously, extension of the THB in only one direction is not sufficient for selectivity. The predicted clashes with the binding site of FTase were circumvented via reorientation of Trp102 in the enzyme or via adoptive behavior of the ligand. Interestingly, in FTase the introduction of the furanal moiety induces a conformational change of the 3-benzyl moiety, which approaches the surface area of FTase composed of residuesAla151, Arg202 and Trp102.

The conformational change of the 3-benzyl moiety (C ring) resulting in a new binding pose could even increase the chance to get selective RabGGTase inhibitors by combining substituents that approach both the TAG tunnel and the LBS and provides a rational explanation for the selectivity profile observed for the first selective RabGGTase inhibitor, **109**.

Figure 4.10a&b shows the first crystal structure of a THB-based selective RabGGTase inhibitor. In this structure, the features of ligands **92** & **108** are combined.

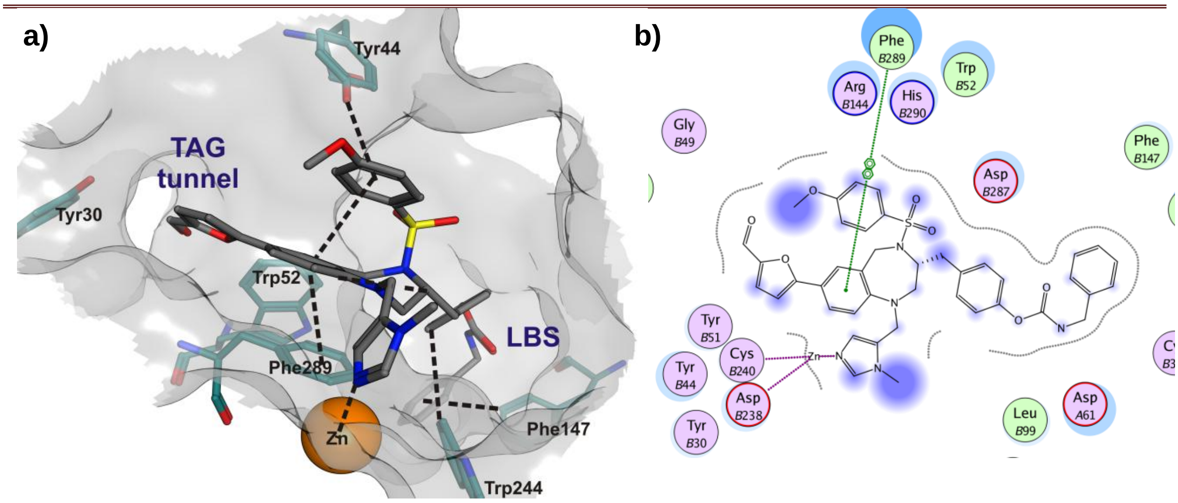

Figure 4.11: a) Surface representation of the active site of **109**:RabGGTase complex. Similar to **BMS3**, **92** & **108** the imidazole coordinates to the zinc ion, whereas the sulfonamide forms hydrogen bonds with Tyr44. The 3-benzyl moiety interacts with Trp52 and Phe289 by edge-face hydrophobic stacking, whereas the THB moiety stacks face-face with Phe289. The conformation is further stabilized by internal π-stacking of the THB with the anisylsulfonyl group. The additional furanal occupies the entrance of the TAG tunnel but the expected hydrogen bond interaction between the aldehyde and Tyr30 cannot be observed. The additional benzylcarbamate contributes with an edge-face hydrophobic stacking with Phe147. The black dashed lines indicate interactions between ligand and enzyme. b) Schematic representation of **109**:RabGGTase interactions.

The RabGGTase: **109** co-crystal structure shows that **109** binds in a mode similar to **BMS3**, with the imidazole coordinating to the catalytic zinc ion and the THB core of **109**, although slightly twisted compared to **BMS3**, π-stacking with Phe289. In agreement with the predictions from docking studies, the benzyl carbamate occupies the lipid binding site of RabGGTase, while the furanal substituent approaches the TAG tunnel. The arrangement of the benzylcarbamate in the LBS results in an extra edge-face π-stacking to Phe147, as well as a conformational change of the 3-benzyl substituent, now π-stacking with Trp244 instead of Phe289 and Trp52. Surprisingly, the aldehyde moiety is not involved in a hydrogen bonding interaction with Tyr30, but is pointing into the TAG tunnel. The observed interactions together add up to a selective RabGGTase inhibitor (IF>8000) with an IC_{50}value of 141 nM for RabGGTase and an IC_{50}value of over 10 µM for FTase.

Chapter 5: Intermezzo – RabGGTase Counterscreens

During the course of the project, our collaborators at the Lead Discovery Center (LDC) developed alternative assay systems. Several different systems were compared; fluorescence based *in vitro* screening with the original system using NBD-FPP, affinity bead assays using biotin-GPP as well as radioactive [^{3}H]-GGPP based and cellular screening assays. The *in vitro* assays are summarized in Figure 5.1.

The NBD-FPP- and biotin-GPP- based assays are both substrate analogs of GGPP, whereas the radioactive [^{3}H]-GGPP assay resembles the native prenylation system the most. All assays require the ternary complex of Rab, REP and RabGGTase. The presence of an effective inhibitor of RabGGTase will, in all cases, lead to a decrease in signal compared to the non-inhibitor condition.

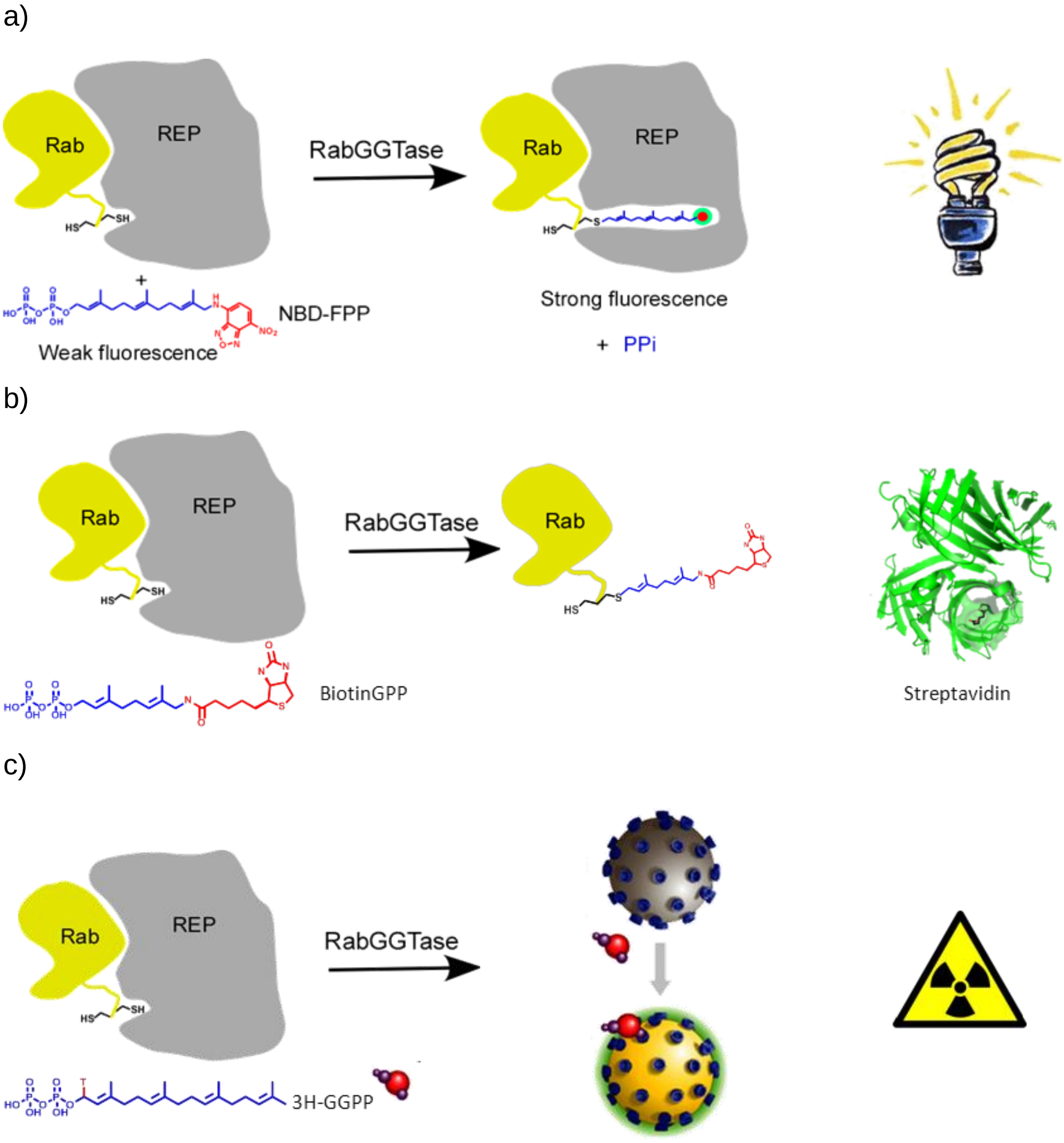
a)
Rab
REP
HS
SH
+
NBD-FPP
Weak fluorescence
RabGGTase
Rab
REP
Strong fluorescence
+ PPi
b)
Rab
REP
RabGGTase
Rab
BiotinGPP
Streptavidin
c)
Rab
REP
RabGGTase
3H-GGPP

Figure 5.1: RabGGTase *in vitro* assays using (a) NBD-FPP, (b) Biotin-GPP, (c) ^{3}H-GGPP.

To study the cellular prenylation, a two-step procedure has been developed and optimized to a 96 well plate, medium throughput format. The general principle of the assay is depicted in Figure 5.2. HeLa cell lines were cultured and treated with an inhibitor. After the treatment with inhibitors, the cells were lysed and subsequently prenylated *in vitro* with biotin-GPP. With Western blotting all Rab-biotin-GPP conjugates were detected. Inhibition led to increased labeling of endogenous Rab proteins, whereas no inhibition resulted in an absence of signal.

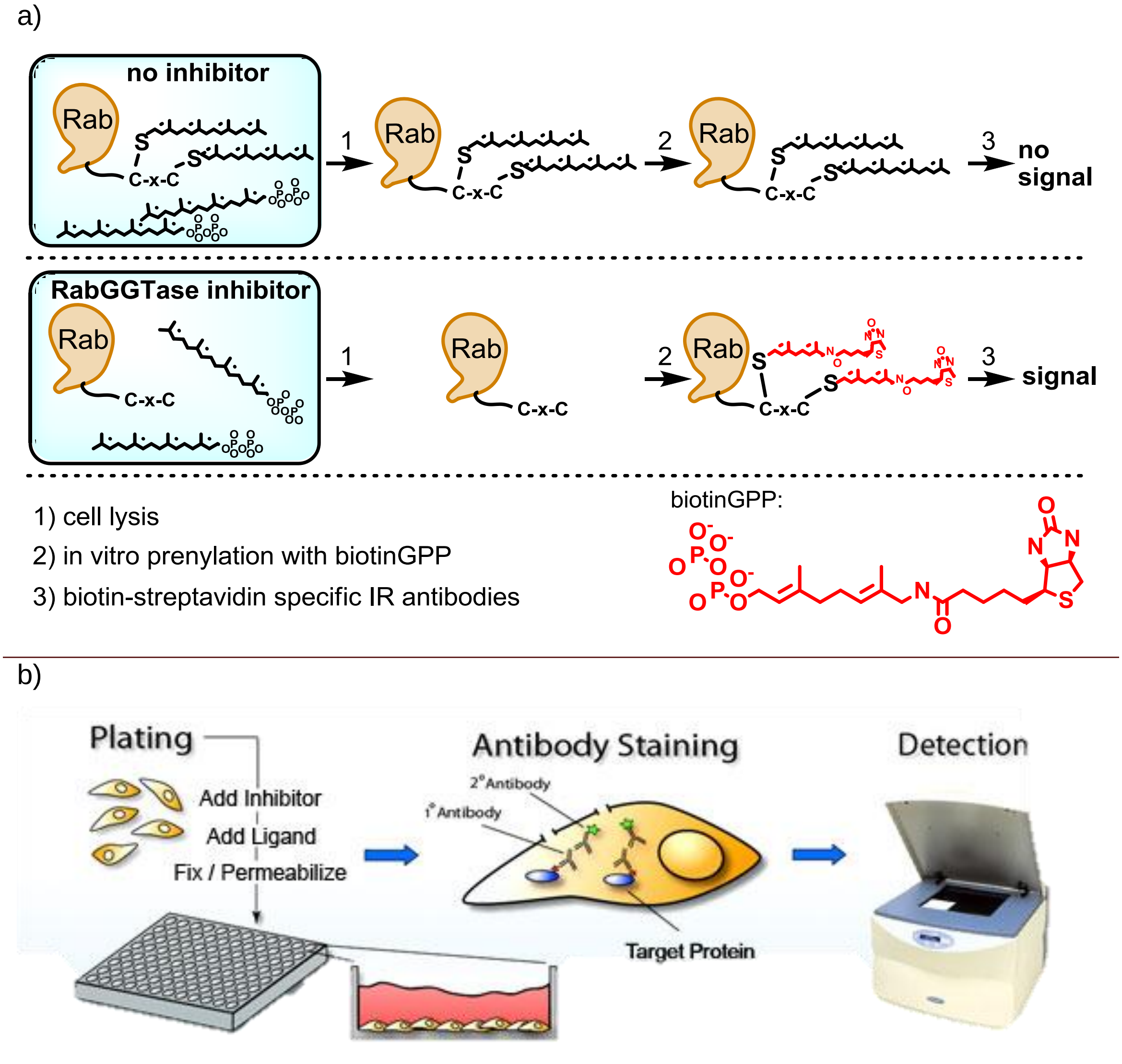
a)
no inhibitor
Rab
S
S
C-x-C
1
2
3
no signal
RabGGTase inhibitor
signal
1) cell lysis
2) in vitro prenylation with biotinGPP
3) biotin-streptavidin specific IR antibodies
biotinGPP:
b)
Plating
Add Inhibitor
Add Ligand
Fix / Permeabilize
Antibody Staining
2° Antibody
1° Antibody
Target Protein
Detection

Figure 5.2: RabGGTase cellular prenylation assay (a) and the detection system (b)[195]

To validate these assays some of the developed THB-based RabGGTase inhibitors were analyzed. The results of the various inhibitors in the different assays are plotted in Figure 5.3.

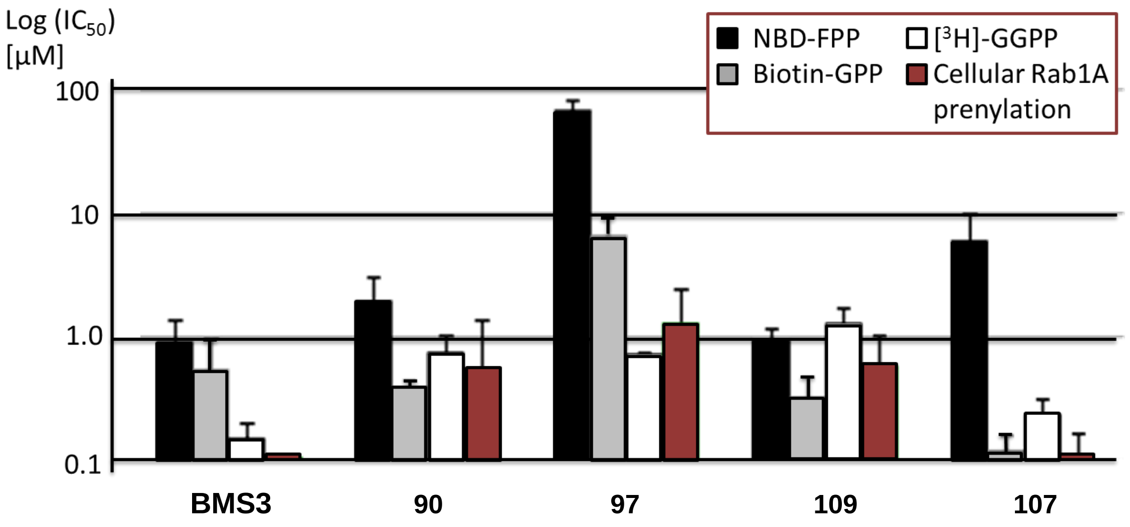

Figure 5.3: Overview of inhibitory activity and binding modes of selected compounds.

Unexpectedly, the data between the different screening assays showed no general correlation. Some of the inhibitors with promising inhibition in the NBD-FPP assays showed low µM inhibition in the radioactivity based GGPP assay (**109**). Other inhibitors which seemed to have low potential in the NBD-FPP assay were highly active in the radioactivity based GGPP assay (**107**). Comparing the different biochemical *in vitro* assays with the initial cellular screen, the radioactive GGPP assay showed the highest correlation.

Unfortunately, in the cellular reprenylation assay as well as in the radioactive assay, selective inhibitor **109** appeared to be 100 fold less active compared to **BMS3**, although it can still be regarded as a moderately active inhibitor with an IC_{50} of 1 µM*in vitro*. The result for inhibitor **107** was more promising; it seemed that the THB with the additional pyridine-group toward the TAG tunnel was just as active in the radioactive and cellular prenylation assay as **BMS3** opposed to the moderate activity observed in the NBD-FPP assay.

Since the results between NBD-FPP and GGPP showed such extensive discrepancies, and the GGPP assay correlated better with the cellular studies, it was decided to base the further development of RabGGTase inhibitors on the radioactive assay. Therefore, most of the compounds were rescreened and the IC_{50} values and new improvement factors are summarized in Table 5.1

Table 5.1: *in vitro* results of the THB based library on the radioactive assay

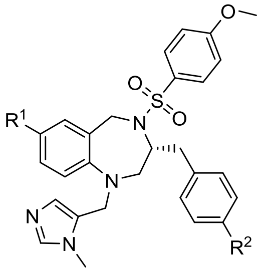

				In vitro IC50 [nM]				
Entry	Cmpd	R^1	R^2	RabGGTase$^{\mathrm{FL}}$	RabGGTase$^{\mathrm{RA}}$	FTase	GGTase I	IF$^{\mathrm{RA}}$
1	**BMS3**	CN	H	724±321	6.4±4.8	6±3	>99,500	1.00
2	**74**b	CN		1,011±465	<4[$]	5.2±0.2	>99,500	1.39
3	**87**	CN	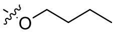	162±10	156±49	10±7	>99,500	0.1
4	**88**	CN	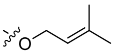	39±10	63±24	15±8	>99,500	0.3
5	**89**	CN	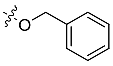	441[#]	181±14	99.3±59	>99,500	0.59
6	**90**	CN	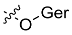	2,072[#]	23.5±4.5	1,012±688	>99,500	45.93
7	**91**	CN	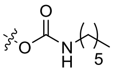	243±20	15.5±1.5	9.2±4.2	>99,500	0.63
8	**92**	CN	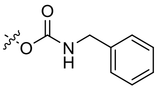	72±2	6±4	<5[$]	>99,500	0.89
9	**93**	CN	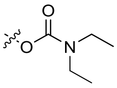	38±7	123±22	<5[$]	2,020±384	0.04
10	**83**	CN	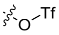	>9,500	1496±100	10.5±3.9	>99,500	0.01
11	**94**	CN	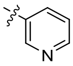	353±158	11±2	4.3±2.2	3,632±15	0.42
12	**97**	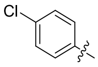		>9,500	706±246	194±78	>99,500	0.29
13	**100**	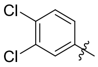	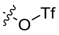	>9,500	>9,500	>10000	>99,500	nc
14	**101**	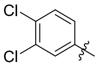	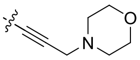	>9,500	>9,500	>10000	>99,500	nc
15	**102**	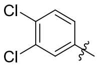	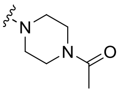	>9,500	2,827±977	979±262	>99,500	0.4
16	**103**	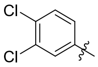	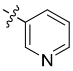	>9,500	8,491±1,510	>10000	>99,500	nc
17	**104**	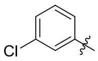		1,302±478	68.7±19.6	42±10	>99,500	0.7
18	**106**	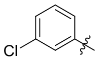	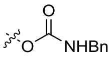	2,264±844	263.3±49.5	123±24	>99,500	0.5
19	**107**	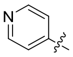		8843[#]	<4[$]	13.6±8.6	>99,500	3.6
20	**108**	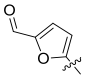		206±13	12.8±8.8	7±3	>99,500	0.6
21	**109**	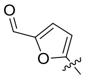	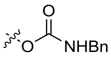	141±26	1547±101	>9,700	>99,500	nc

FL=fluorescent based assay, RA=radioactive based assay, [$]lower detection limit, [#]single point measurement, nc=not calculated, IF=improvement factor.

Two trends were found in the comparison of both assays. In general, some of the aryl-modifications (2nd generation) turned out to be moderately active RabGGTase inhibitors in the radioactive assay, while they showed no inhibition in the NBD-FPP assay (*e.g.* **97**, **104**, **107**). In contrast, a decrease in inhibitory activity was observed for most of the compounds of the first generation, compared to the original NBD-FPP assay.

These results hint in the direction of an effect of the GGPP substrate on binding of the compound, either non-competitive or cooperative. The modifications in the first generation involved an extension toward the lipid binding pocket, which could result in competitive binding. Since the enzyme has a very high affinity for GGPP, this competition could lead to the observed decrease in inhibition. To prove this theory, some competition studies were carried out by Dr. Yaowen Wu (with NBD-FPP). However, only compound **90** was found to be competitive, while **97**, **107** and **109** were all found to be non-competitive, which disproved the hypothesis.

The other option would be that the natural GGPP substrate and the tetrahydrobenzodiazepine moiety have a cooperative mode. This could explain the general increase in inhibitory activity in the radioactivity based assay compared to the fluorescent based assay for the 2nd generation; in the radioactive assay format, this would lead to an extra hydrophobic interaction between the 3-benzyl of the compound and GGPP, which is absent in the NBD-FPP based assay. This can also explain the great variety in the 1st generation. Some of the compounds could obtain a slightly different binding mode, interrupting positive interactions with the GGPP substrate, which results in a decrease of inhibitory activity (*e.g.* **87**, **89**, **93**,) while other substituents will still allow this positive T-stacking interaction (*e.g.* **91**, **92**, **94**,). This hypothesis is graphically depicted in Figure 5.4.

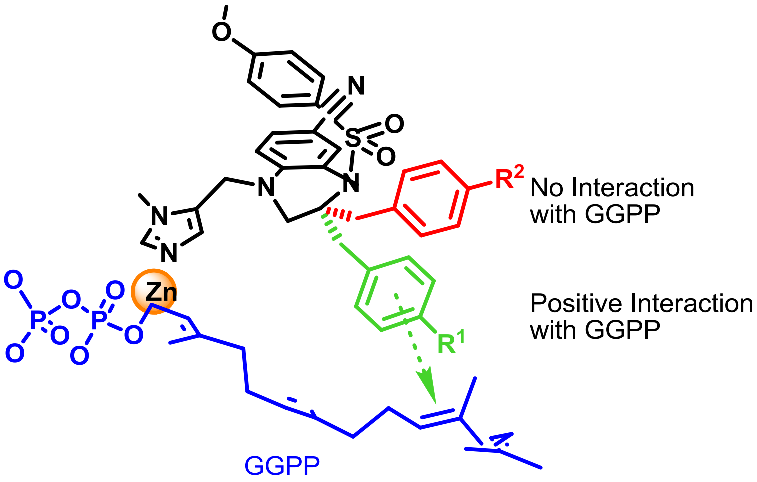

Figure 5.4: Schematic representation of different binding modes relative to GGPP, cooperative and non-competitive. R^{1}substituent is not influencing the conformation, allowing π-interaction, while R^2 substituent disturbs the conformation, breaking the π-interaction.

It could be imagined that such a negative effect can be similar to the effect of **92** in FTase (Figure 4.6a, b)

If this hypothesis would be true, then inhibitors with substituents having a non-competitive or cooperative binding mode toward the natural GGPP ligand should remain active in the RabGGTase radioactive based assay. To identify such substituents an extra virtual screening was carried out for the next generation.

Chapter 6: Toward highly potent selective RabGGTase inhibitors

§ 6.1 Computer-aided design of cooperative RabGGTase inhibitors

Due to the discrepancies of the assays, an extra virtual screening with GGPP present in the binding site was carried out. The constraints between the imidazole and zinc as well as the benzodiazepine core and Phe289 similar to the previous virtual screening, were kept. By including the GGPP substrate in the virtual screening, the new solutions should be compatible and/or interacting with the GGPP substrate. Some of the highest scoring compounds are depicted in Figure 6.1

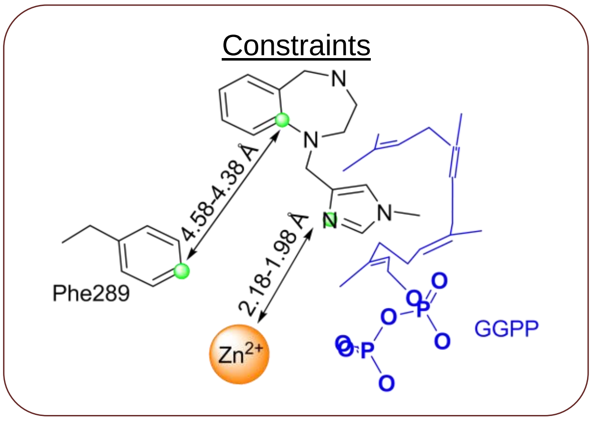

The suggested groups for R^1 mainly encompass small heteroaromatic rings like furan or furan-nitrile and pyridines. The more flexible groups such as N-acetyl-piperazine, which were among the top hits in the virtual screening without GGPP, were not found in the top solutions. For R^2 mainly additional aromatic groups are suggested, which could be involved in favorable π-stacking with the GGPP in the binding site. Especially 3-pyridine and aniline were present in the top100 solutions several times. Although the aniline group is known to be unfavorable concerning metabolism in later stages of drug development, it was decided to incorporate this group as a ‘proof of principle’ for GGPP compatible RabGGTase inhibitors. As an alternative, more stable phenylethers could be incorporated, although they score slightly less in the virtual screening.

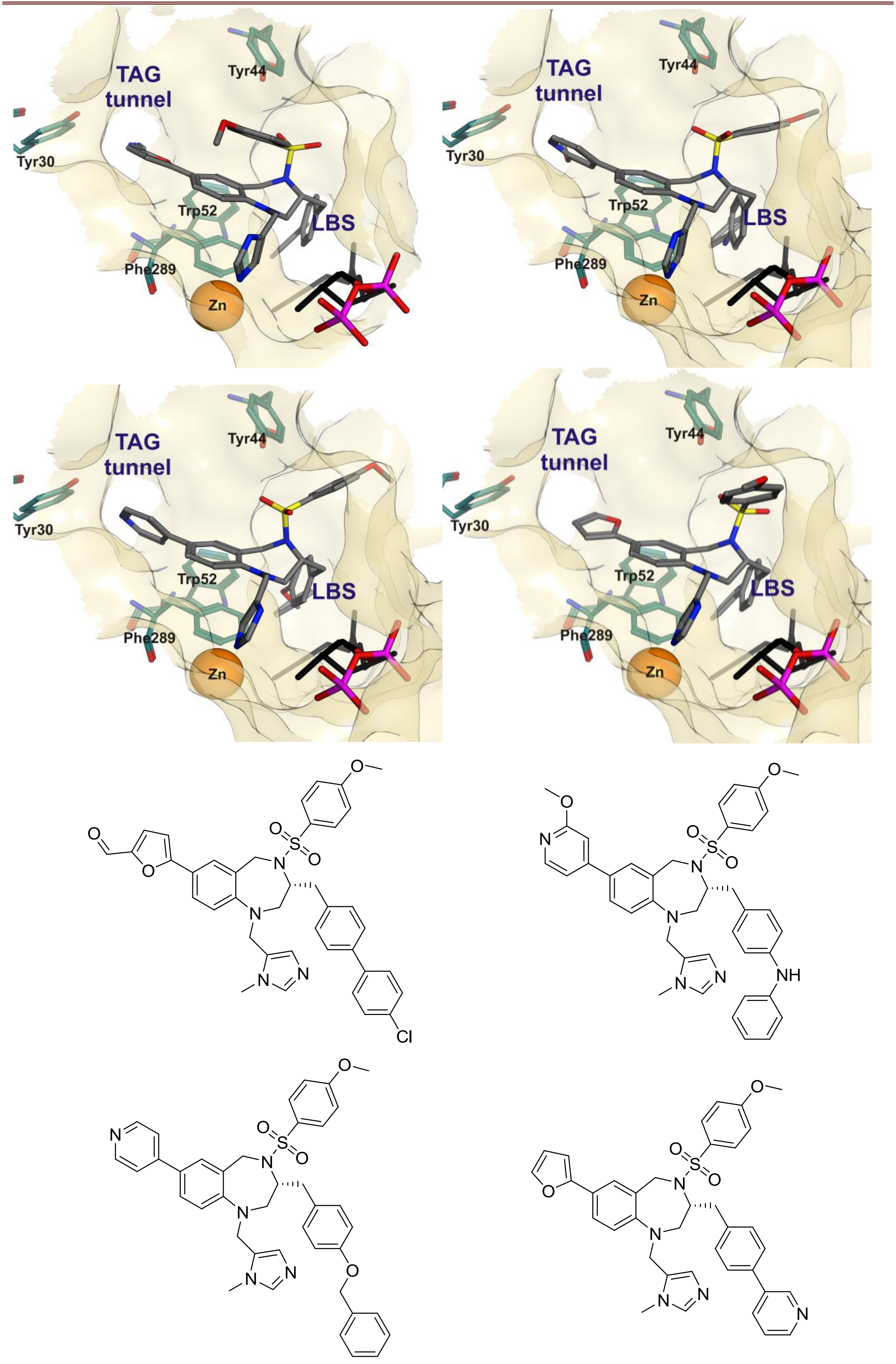
TAG tunnel
Tyr44
Tyr30
Trp52
LBS
Phe289
Zn
TAG tunnel
Tyr44
Tyr30
Trp52
LBS
Phe289
Zn
TAG tunnel
Tyr44
Tyr30
Trp52
LBS
Phe289
Zn
TAG tunnel
Tyr44
Tyr30
Trp52
LBS
Phe289
Zn

Figure 6.1: Docking solutions with GGPP in the binding site

§ 6.2 Synthesis and Screening of 4th generation of inhibitors

Since the radioactive assay also shows a sharp inhibition profile for the modification extending toward the TAG tunnel, it was decided to first introduce some extra (hetero)cyclic aromatic group, small five membered rings and some flexible amide bond linked groups to find the most suitable groups to extend toward this site and to verify the virtual screening. These different groups could be efficiently introduced using transition metal-based cross coupling procedures. The Suzuki-coupling with some heteroaromatic rings resulted in low to moderate yields (*e.g.* **111**), most probably related to the instability of the boronic acid counterpart. Aminocarbonylation using Herrmann's palladacycle **110**, air stable Fu's salt ($[(t\text{-}Bu)_3PH]BF_4$) and molybdenum hexacarbonyl under microwave irradiation afforded **115** and **116** in low, unoptimized yields. Optimization of the procedure would most likely involve adjustment of the reaction time and temperature. Buchwald-Hartwig couplings of **74a** and N-acetylpiperazine or aniline gave THBs **117** and **118**. Irrespective of some of the low, unoptimized yields, a sufficient amount of material could be synthesized for initial screening against RabGGTase and FTase. The results are summarized in Table 6.1

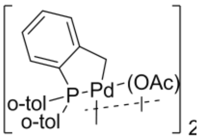

Herrmann's palladacycle
110

Table 6.1: Synthesis and Screening of the 4th generation of THBs: approaching the TAG tunnel

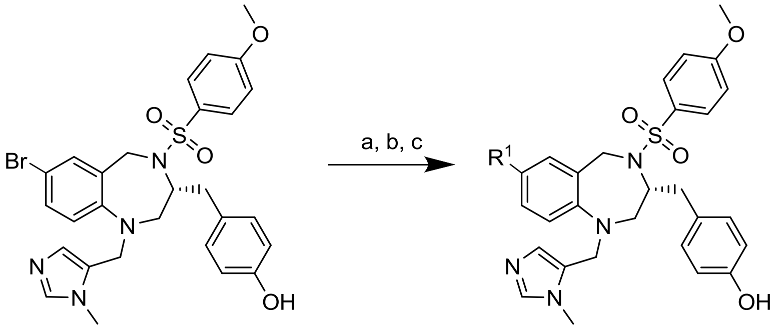

74a **111-118**

(a) arylboronic acid, Pd(PPh$_3$)$_4$, K$_2$CO$_3$, DCE/H$_2$O (b) amine, Mo(CO)$_6$, Fu's salt, Hermann's palladacycle (**110**), DBU, THF; (c). amine, NaOtBu, Pd$_2$(dba)$_3$, JohnPhos (**95**), THF

				In vitro IC$_{50}$ [nM]			
entry	cmpd	R[1]	Yield[$]	RabGGTase	FTase	GGTase I	IF
1	**BMS3**	CN	-	6.4±4.8	6±3	>99,500	1.0
2	**111**	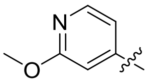	40%[a]	5.5±1.5	18.6±0.6	>99,500	3.6
3	**112**	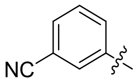	52%[a]	22.5±7.5	34.4±21.2	>99,500	1.6
4	**113**	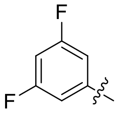	82%[a]	185±8	172±117	>99,500	1.0
5	**114**	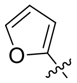	61%[a]	55±10	81.7±70.3	>99,500	1.6
6	**115**	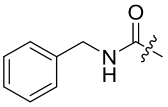	16%[b]	19±2	7±1.6	>99,500	0.4
7	**116**	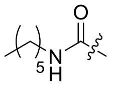	13%[b]	70.5±11.5	20.7±4.6	>99,500	0.3
8	**117**	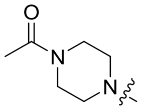	30%[c]	27±6	112±91	>99,500	4.4
9	**118**	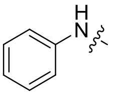	33%[c]	246.5±52.5	454±207	>99,500	2.0

[$]Method used [1]From corresponding arylTHB, [2]From corresponding triflate, IF=Improvement Factor

From Table 4.1 it can be derived that there is one additional group that stands out due to its activity and selectivity: the 2-methoxy-pyridine group. Interestingly, this group occurred several times in the top 10 of the virtual screening.

Another hint from the virtual screening was to introduce a 2-cyanofuran moiety. Herefore, attempts were undertaken to transfer the furanal moiety of **108** into a nitrile. In principle, the aldehyde can be condensed with hydroxylamine to give the corresponding oxime, which can be dehydrated to the nitrile[196]. The reaction and corresponding conditions are summarized in Table 6.2. For the first attempt, entry a, the aim was to convert the furanaldehyde to the nitrile **120** in one step. This resulted in a mixture of four compounds, which consisted of **119**, **120** and very unusually, their counterparts lacking the imidazole. Thus, under these conditions, the imidazoyl methyl group was cleaved. Therefore, the reaction was carried out in a two-step sequence. First, the aldehyde was converted to the oxime employing hydroxylamine in DCM/MeOH. Second the oxime was subjected to dehydration conditions. Reflux in acetic anhydride resulted in the nitrile, but these harsh conditions resulted in degradation and addition of an acetate group to the phenol. Eventually the nitrile was successfully obtained by addition of 6 equivalents of TFAA at room temperature, giving the nitrile in good yield.

Table 6.2: Conditions toward 2-cyanofuran substituted THB.

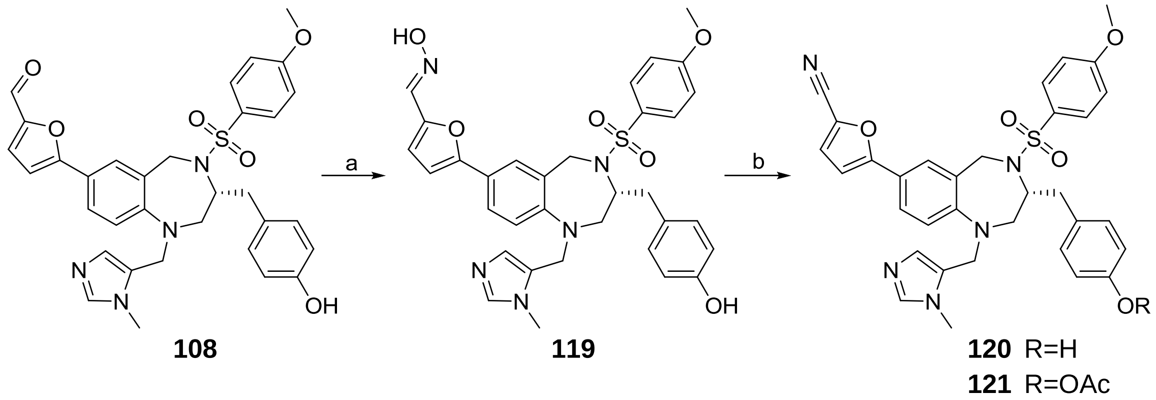

entry	SM	Reagent	Solvent	Temperature	Product	Yield
a	**108**	Et_3N, $NH_2OH.HCl$	NMP	100°C	mixture	Nd
b	**108**	Et_3N, $NH_2OH.HCl$	DCM/MeOH	rt	**119**	80%
c	**119**	Ac_2O	Ac_2O	reflux	**121**	26%
d	**119**	TFAA	DCM	rt	**120**	83%

Due to the limited quantity of 2-methoxypyridine boronic acid available, as well as its instability, another route toward THB **111** was envisioned to improve the yields (Scheme 6.1). Conversion of the THB **74**a into its boronic ester **122** would lead to a general coupling partner, which subsequently could be reacted under Suzuki coupling conditions to obtain 2-choropyridine substituted THB. This 2-chloropyridine, then, could be converted into 2-methoxypyridine. Furthermore, **123** opens up extra possibilities to introduce longer substituents, *e.g.* by condensation with ethanol or butanol.

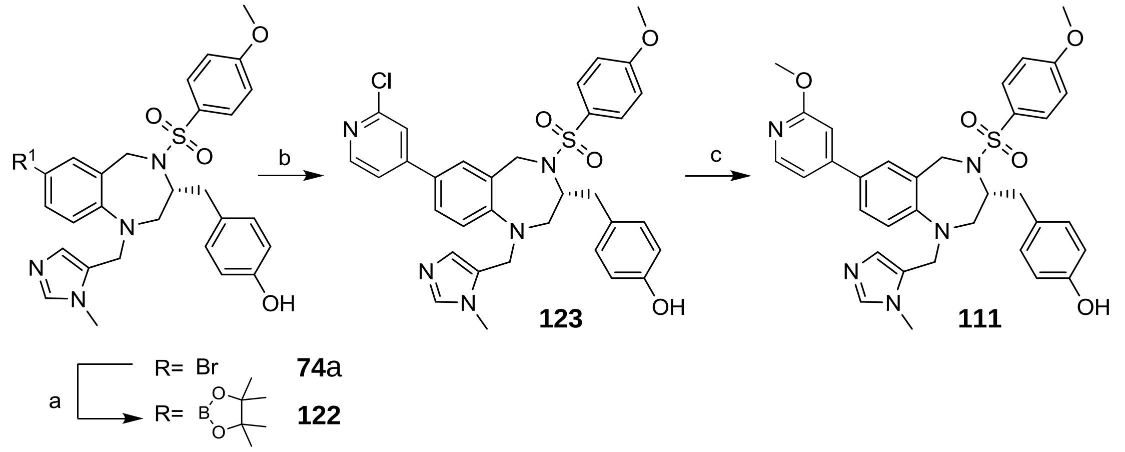

Reagents and Conditions: (a) bis(pinacolato)diboron, Pd(dppf)Cl$_2$, KOAc, DMSO, (b) 4-bromo-2-chloropyridine, K_2CO_3, DME/H_2O, (52%, 2 steps), (c) NaOMe, MeOH, DMSO (71%)

Scheme 6.1: Alternative synthesis route to compound **111**

Unfortunately the overall yield for the conversion of **74a** to **111** was not improved. This route though, opens up more possibilities to diversification, either via coupling reaction of boronate **122** or via nucleophilic aromatic substitution of the 2-chloropyridine.

With the THBs decorated with the most promising R^1 candidates in hand (the 2-cyanofuran and the 2-methoxy-pyridine) the next step was to introduce GGPP compatible groups at the R^2 position. The virtual screening suggested some promising substituents. Top solutions included, among others, benzylamine, aniline and 3-pyridine. The binding poses of these groups suggested stabilizing interactions between the aromatic residues and GGPP substrates, while retaining the binding mode of the THB core. For comparison, the benzylcarbamate substituent was synthesized as well.

The R^2 groups were installed using similar transformations of the phenolic hydroxyl group, described in § 4.5 and § 4.6. Alkylation with benzyl bromide in the presence of sodium hydride resulted in benzyl substituted **127** & **132** in good yields, aminoacylation with benzylisocyanate resulted in compounds **126** & **131**. Triflation (**128** & **133**), followed by Suzuki coupling with 3-pyridineboronic acid gave **129** & **134**. Buchwald-Hartwig modification of the triflate with aniline in the presence of sodium tert-butoxide unfortunately resulted, besides traces of the product, mainly in hydrolysis of the substrates. Changing the base to cesium carbonate resulted in a mixture of hydrolyzed compound and product, providing a sufficient amount of material for screening (**130** & **135**). Although the low nM activity of **BMS3** was not reached by the newly introduced substituents, the inhibitory activity could be reduced from low µM to low nM activity (**109** *versus* **129** & **134**) which shows the potential of the GGPP-compatible design principle. Unfortunately, **129** & **134** both showed potential inhibitory activity on FTase as well. This finding suggests that the introduction of this moiety leads to a similar behavior in FTase as observed with compound **93**. The introduction of an aniline or a parachloro-aryl rendered the THBs practically inactive.

Table 6.3: Synthesis and screening of 5th generation of THB library: GGPP compatible.

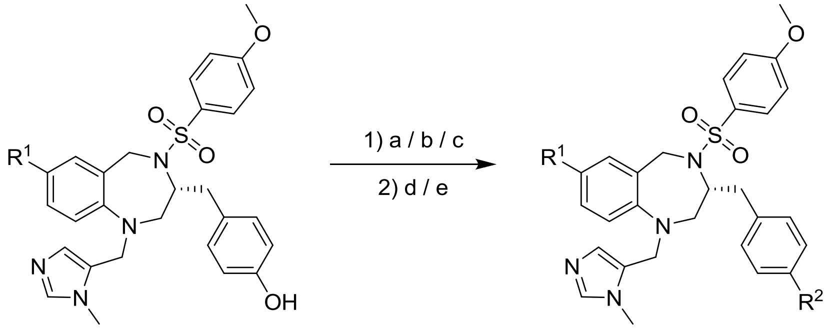

(a) isocyanate, Et$_3$N, DCM; (b) NaH, BrR[2], DMF; (c) **86**, Et$_3$N, DCM; (d) arylboronic acid, Pd(PPh$_3$)$_4$, K$_2$CO$_3$, DCE/H$_2$O, 80 °C; (e) amine, NaOtBu, Pd$_2$(dba)$_3$, JohnPhos(**95**) THF.

					In vitro IC_{50} [nM]			
entry	cmpd	R[1]	R[2]	Yield[$]	RabGGTase	FTase	GGTase I	IF
1	**BMS3**	CN	H	-	6.4±4.8	6±3	>99,500	1.0
2	**108**	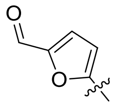	OH	-	12.8±8.8	11.4±10	>99,500	0.95
3	**109**		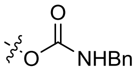	-	1,547±101	>9,700	>99,500	nc
4	**124**		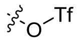	86%[c]	4,292±1,327	>9,700	>99,500	nc
5	**125**		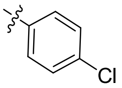	84%[f]	2,240±1,235	>9,700	>99,500	nc
6	**120**	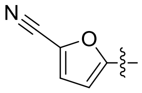	OH	-	<14[$]	26.9±20	>99,500	2.0
7	**126**		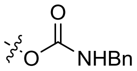	71%[a]	260±18	>9,700	>99,500	nc
8	**127**		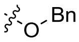	69%[b]	577±282	>9,700	>99,500	nc
9	**128**		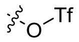	99%[c]	nd	nd	nd	nd
10	**129**		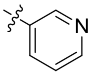	68%[d]	37±21	109.9±41.1	>99,500	3.2
11	**130**		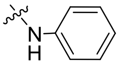	43%[e]	1,056±41	1,212±261	>99,500	1.2
12	**111**	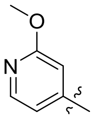	OH	-	5.5±1.5	18.6±0.6	>99,500	3.6
13	**131**		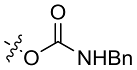	86%[a]	55±11	321±291	>99,500	6.2
14	**132**		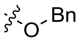	81%[b]	5,245±1,129	2,556±545	>99,500	0.5
15	**133**		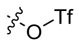	90%[c]	nd	nd	nd	nc
16	**134**		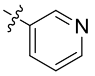	84%[d]	121.3±3.3	79±13.3	>99,500	0.7
17	**135**		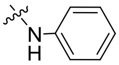	75%[e]	5,719±1,765	2,432±2,182	>99,500	0.5

[§]Method used [1]From corresponding arylTHB, [2]From corresponding triflate, [$]lower detection limit, [#]single point measurement, nc=not calculated, nd=not determined, IF=Improvement Factor.

In order to find an explanation for the observed dual activity of compound **129**, the structure was docked in the FTase surface of **93**:FTase:FPP and compared to the solution obtained for docking in **BMS3**:FTase:FPP. Indeed the docking score observed in **93**:FTase:FPP was significantly higher than the original score in **BMS3**:FTase:FPP (Figure 6.2). This supports the hypothesis that the flexibility of Trp102 leads to more tolerance toward enlarged THBs.

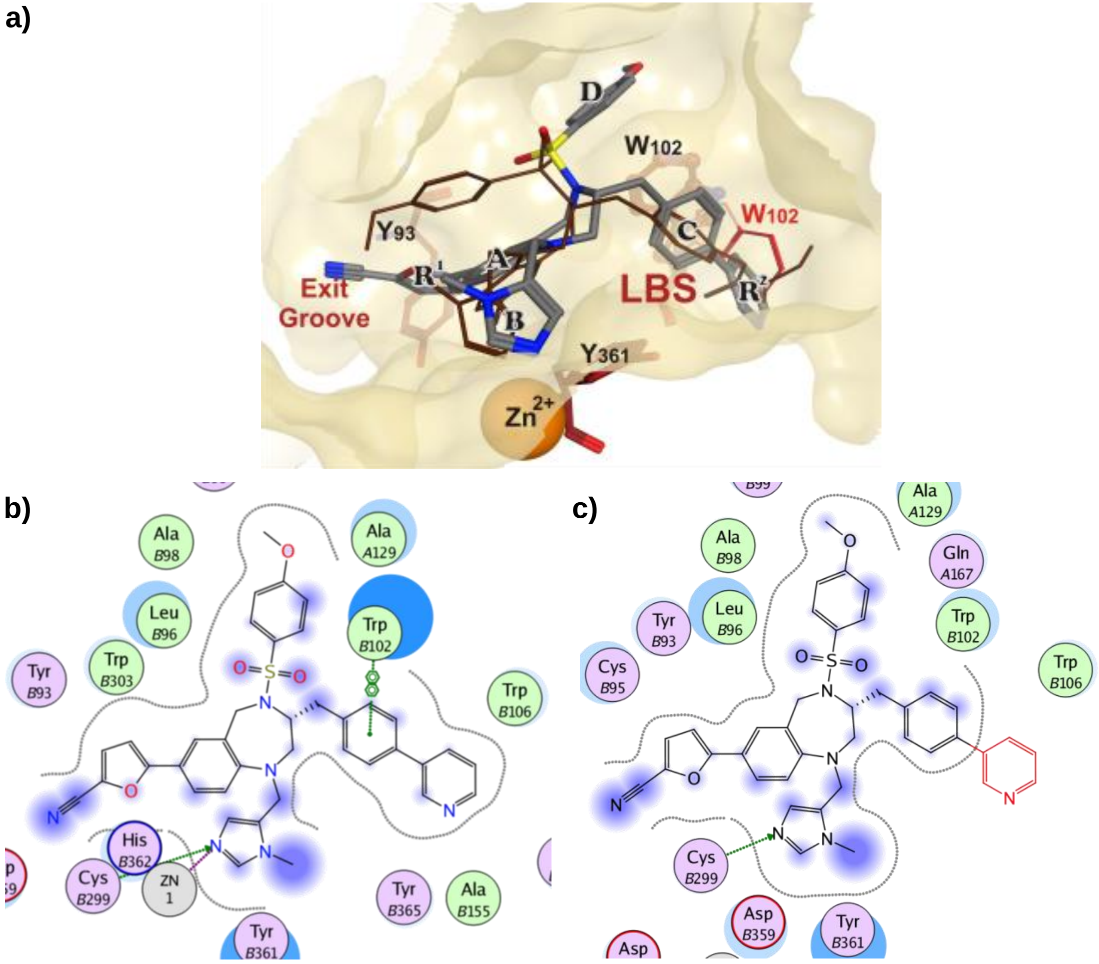
a)
D
W102
Y93
C
W102
A
R1
Exit
Groove
LBS
R2
B
Y361
Zn2+
b)
Ala B98
Ala A129
Leu B96
Trp B102
Tyr B93
Trp B303
Trp B106
O
O=S=O
N
N
O
N
N
N
N
His B362
Cys B299
ZN 1
Tyr B361
Tyr B365
Ala B155
c)
Ala A129
Gln A167
Ala B98
Leu B96
Trp B102
Tyr B93
Cys B95
Trp B106
O
O=S=O
N
N
O
N
N
N
N
Cys B299
Asp B359
Tyr B361
Asp

Figure 6.2: a) Surface representation of the active site of **93**:FTase with **129** docked in the active site. The docking solution shows that R^2 would fit in the enlarged pocket caused by Trp102 rotation. An overlay of the original Trp102 position exemplifies the clash. b) Schematic interaction of docked **129** with the active site of **93**:FTase, allowing binding. c) Schematic interaction of docked **129** overlaid with the active site of **BMS3**:FTase, showing the predicted clash.

Altogether, it can be stated that FTase in general shows a more adaptive behavior toward the extended THBs than expected on basis of the original **BMS3** crystal structures. The crystal structures obtained from FTase, which showed adaptive behavior of Trp102 upon binding of extended THBs gives a reasonable explanation for these observations (see Figure 4.7). Since this tryptophan is known to be responsible for the substrate selectivity[197] and GGPP is known to be an inhibitor of FTase[54] it could be speculated that GGPP induces a similar shift of this tryptophan. This shift, would allow GGPP to bind, but renders the enzyme inactive toward its substrates.

One option to get a narrower selection of potential selective RabGGTase inhibitors would be to carry out a virtual screening for FTase with defined flexible residues in the binding site, opposed to the static docking used in this optimization process.

The radioactive GGPP assay showed potential for increase of potency toward RabGGTase by designing GGPP compatible R-groups (Table 6.3). However, a delicate balance between potency and selectivity was observed. It seems that RabGGTase in general does not tolerate many extensions, contrary to the assumption made from the virtual screening. It was found that the THB core should retain its fixed position, therefore only allowing the introduction of groups that exactly accommodate into the TAG tunnel, such as furan-nitrile. The search for GGPP compatible inhibitors was not as successful as expected, many predicted extensions were found to render the inhibitors inactive against RabGGTase. Although the introduction of 3-pyridine (**129** & **134**) led to a significant gain in RabGGTase activity opposed to the competitive inhibitors they were unselective regarding FTase.

Fortunately, some combination of THB-extensions led successfully to the development of potent and selective RabGGTase inhibitors. The combination of a furanaldehyde with a benzylcarbamate led to a 1.5 µM selective inhibitor of RabGGTase (**109**). The transformation of this furanaldehyde into the 2-cyanofuran led to even higher potency and gave access to two potent and selective RabGGTase inhibitors **126** (260 nM) and **127** (577 nM).

In order to uncover more selectivity prerequisites for RabGGTase, FTase and GGTase I, it would be interesting to explore other scaffolds than the described THBs. However, before we turn to potential new scaffolds as RabGGTase inhibitors, the potential of the new THBs in cancer cell lines will be discussed. With a focus on the selective RabGGTase inhibitors: compounds **109** & **126**.

Chapter 7: Cellular studies of the RabGGTase inhibitors

In order to evaluate if RabGGTase is a relevant anti-cancer target via small molecule intervention, the inhibitors were tested in several cancer cell lines by the LDC. Therefore, the THB-based inhibitors were first tested in the reprenylation assay to observe their activity in a cellular system (assay described in Chapter 5). In Table 7.1 and in the supplementary data, the data of the reprenylation and cell based assay are summarized. It can be derived from the table that the *in vitro* activity roughly correlates with the cellular reprenylation activity of the RabGGTase inhibitors. The discrepancies are most likely related to external factors like cell permeability and solubility. However, most of the active inhibitors *in vitro* show good cellular potency as well.

The compounds listed in Table 7.1 have been selected for their different types of inhibitory activity. **83** is a selective FTase inhibitor, **109** and **126** are selective RabGGTase inhibitors, whereas **101** is inactive. The other compounds listed are all dual inhibitors, with different potencies for RabGGTase and FTase. First, it is important to note that all tested inhibitors are inactive up to 10 µM in the PBMC assay, providing first indications that this compound class is not generally cytotoxic. Second, it could be shown that the selective RabGGTase inhibitors both resulted in inhibition of cancer cell proliferation. Compound **126** (entry 8), a selective inhibitor of RabGGTase with a similar RabGGTase potency as **BMS3**, inhibited all cancer cell lines as potent as dual inhibitor **BMS3**. Interestingly, the selective FTase inhibitor (**83**, entry 4) with a similar FTase potency as **BMS3** only retained its activity on the A2780 cell line. These results indicate that inhibition of RabGGTase alone is sufficient to inhibit cancer cell proliferation.

Comparison of inhibitor **126** with **129** shows that the GGPP compatible design is not as crucial for inhibition of cellular prenylation as has been observed in the *in vitro* assays. One explanation could be that the GGPP concentration in the cells is different from the GGPP concentration in the radiometric assay, and hence, has less impact on the inhibition. The concentration of GGPP in NIH/3T3 cells has been determined at 0.145 pmol/10^6 cells,[198] which would correspond to approximately 65 nM GGPP, 30 fold less compared to the amount of GGPP used in the *in vitro* assay.

Upon close inspection of the data, some other trends could be observed. Dual inhibitor **93**, which showed potent FTase and moderate RabGGTase activity, effectively inhibited proliferation of the HCT116 and A2780 cells, but showed a clear drop in activity for the HeLa cells.

Table 7.1: Cellular results of the THB based library

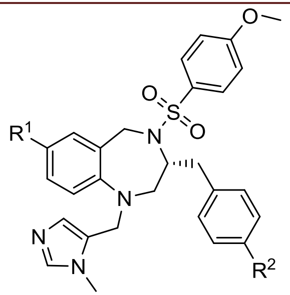

				In vitro IC$_{50}$ [nM]		Cellular IC$_{50}$ [nM]	Cellular viability IC$_{50}$ [nM]				
entry	cmpd	R^1	R^2	FTase	RabGGTase	RabGGTase Reprenylation	HCT116	HeLa	A2780	PBMC	IF^{RP}
1	**BMS3**	CN	-	4.9±0	6.4±4.8	74±34	63±8	101±2	43±0	>10000	1
2	**92**	CN	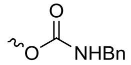	13.2±14.1	6±4	81±32	231±0	151±0	130±0	>10000	2.5
3	**93**	CN	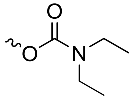	5.2±0.3	122.7±21.7	343±29	75±10	745±303	43±9	3836±0	0.2
4	**83**	CN	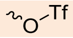	**10.5±3.9**	1495.5±99.5	>10000	1049±0	1960±0	92±0	>10000	0.02
5	**101**	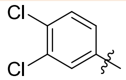	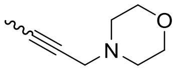	>9,700	>10000	>10000	4974±0	9308±0	3261±0	>10000	nd
6	**109**	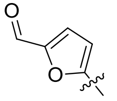	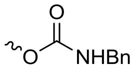	>9,700	1547±101	**311±193**	443±173	797±330	589±199	>10000	485
7	**120**	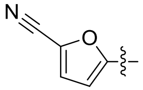	OH	*26.9±20*	*<14*	*11±5*	*2±1*	*21±4*	*18±1*	*>10000*	*37*
8	**126**	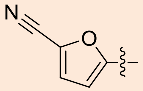	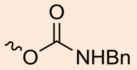	>9,700	260±18	**49±32**	35±1	101±11	115±3	>10000	3082
9	**129**	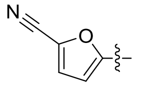	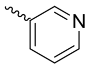	109.9±41.1	37±21	54	71±10	130±11	222±1	>10000	42

This data was complemented by the activity profile of dual inhibitor **92**, showing potent RabGGTase and moderate FTase inhibitory activity. In this case, the inhibition of proliferation of HeLa cells was retained whereas the activity for HCT116 and A2780 slightly dropped. These data combined suggest that HCT116 and A2780 cells are more sensitive to FTase inhibition than HeLa cells.

Furthermore, it can be seen that inactive THB **101** (entry 5) shows no inhibition of cancer cell line proliferation, as expected. Inhibitor **120**, which shows a remarkable cellular reprenylation inhibitory activity for RabGGTase and a moderate *in vitro* activity for FTase, shows a significant effect on cancer cell line proliferation, giving IC_{50} values in the range of 2-21 nM. This shows the potential of low nM inhibitors of RabGGTase to inhibit cancer cell proliferation. The shown inhibition of cancer cell proliferation (both Ras-transformed and non-Ras-transformed) by the highly selective RabGGTase inhibitors **126** and **109** is in accordance with the finding that RabGGTase siRNA, but not FTase siRNA, induces increased apoptosis in *C. elegans* and in A549 cells[17].

Altogether, diversification of the THB scaffold by an iterative cycle of synthesis, screening and design, guided by crystal structure determination led to the conversion of a dual FTase/RabGGTase inhibitor into potent, selective, not generally cytotoxic inhibitors. Selective inhibitor **126** (49 nM, cellular IC_{50}), inhibits cancer cell proliferation as potent as dual inhibitor **BMS3** and shows the potential of selective RabGGTase inhibitors as a plausible anti-cancer strategy; it emphasizes that RabGGTase should be considered as an anti-cancer target.

Additional studies to confirm the therapeutic relevance of RabGGTase will give extra insight in the effect of RabGGTase and hence, Rab GTPase disturbance. It could be interesting to determine if the inhibitors actually induce apoptosis, compared to the measured toxicity in the proliferation assays. Furthermore, it would be interesting to test the selective inhibitors in a wide panel of different cancer cell lines in order to establish the generality of RabGGTase inhibitors as anti-cancer therapy.

In addition, side effects should also be taken into account, since Rab GTPases and related effector and modulator proteins have been associated with neurological diseases as well as infectious diseases. For example, overexpression of Rab1 was shown to reduce the toxic effect of αsyn, an inducer of Alzheimer's disease. In such a context RabGGTase inhibition is probably undesirable.

Besides the therapeutic relevance, the selective RabGGTase inhibitors will be valuable tool compounds as well. The exact role of Rab GTPase in vesicular trafficking could be studied more closely using a chemical biology approach. Since there are so many players in the vesicular trafficking pathways in both the endocytic and exocytic pathway it would be interesting to study to which extent Rab GTPase function is essential for correct trafficking. To which extent would processes like vesicle budding, vesicle uncoating, vesicle motility, vesicle tethering and vesicle fusion be impaired by inhibition of RabGGTase? Which downstream processes will be affected? Is there a link with signaling pathways leading to cancer cell proliferation? Such studies would enlarge the understanding of the complicated trafficking pathway in general, and the role of Rab GTPases in particular.

Chapter 8: High Throughput Fluorescent Screening: Leads or Misleads?

§ 8.1 Initial hits of the NBD-FPP RabGGTase assay

High throughput screening (HTS) is a powerful tool to identify potential inhibitors with new chemical entities. Therefore we set out to screen the in house CGC library to identify potential new inhibitors.

In Chapter 5 the different RabGGTase assay formats have been described and it became clear that the activity profile of the inhibitors differed between the fluorescent and radioactive based assay. In order to enable the optimization of the cellular activity, the substances were evaluated using the radioactive based assay.

However, to identify new chemical entities as potential inhibitors of RabGGTase by HTS, the NBD-FPP fluorometric assay seemed to represent a continuous and less laborious alternative for the radioactive assay.

As shortly mentioned in Chapter 3, it was found that the NBD-FPP, the fluorescent analog of GGPP had bleached severely over time. Therefore, a new batch was synthesized which was used for the HTS of the CGC library of *circa* 30 000 substances. With the new batch NBD-FPP the substrates, protein and enzyme could be used in lower concentrations. Since Rab and REP are both very precious enzymes, this adjustment was necessary to allow the screening of the full library.

In total three different compound classes were identified as low µM inhibitors of RabGGTase: psoromic acid (**136**, a natural product), furfurylamine **137** and benzoxazolone **138**. (Table 8.1).

Psoromic acid analogs have been synthesized by Dr. Celine Deraeve. Most analogs made, however, were inactive. Especially the aldehyde moiety of psoromic acid was essential for activity. Psoromic acid seems to inhibit RabGGTase by an unusual auto-inhibition mechanism and the exact mode of inhibition is currently under investigation.

Table 8.1: RabGGTase inhibitors identified by fluorescent HTS.

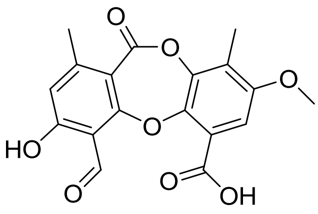	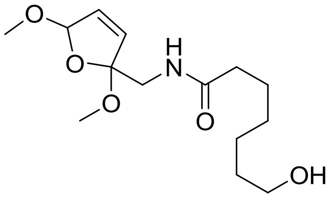	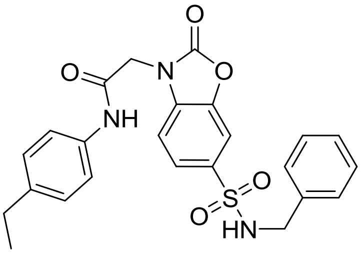
136	**137**	**138**
IC_{50} = 2.1±0.3 µM	IC_{50} = 32.7±3.0 µM	IC_{50} = 7.8±1.1 µM

§ 8.2 Furfurylamine based library

In order to check the integrity of the hits and to obtain a synthetic route to derivatives, a small library of compounds based on **137** was synthesized. The synthesis of the derivatives is outlined in Table 8.2. Starting from furfurylamine three different R^1 groups were introduced. Reaction of furfurylamine with an excess of 6-caprolactone gave **139** in quantitative yield, whereas the octane moiety (**141**) was installed using octanoyl chloride and Et_3N as a base. Employing standard peptide coupling conditions, geranic acid and furfurylamine gave **144** in good yield. The next step involved the oxidation of the furan moiety into scaffold **B**. Therefore, a solution of bromine in methanol was slowly added to a cooled mixture of substituted furfurylamine in diethylether. This method successfully furnished substrates **137** and **142**. Both products were found to be extremely acid labile, in order to obtain the substances sufficiently pure, it was necessary to employ Et_3N during chromatography and to use neutralized chloroform for NMR measurements. Unfortunately, it was impossible to convert **144** into scaffold B. Using the described reaction conditions a complicated mixture of substrates was obtained. All attempts to selectively oxidize the furan, for example with chloramine B, were unsuccessful. Therefore, no further derivatives were made for this compound class.

Substances **137** and **142** were subsequently hydrogenated into scaffold **C**. The first attempts to obtain this scaffold by treating the substrate with 10% Pd/C in methanol under hydrogen atmosphere were unsuccessful, which was most probably due to inactivation of the catalyst. It was found that prestirring the mixture with activated coal, followed by filtration and addition of the catalyst, was necessary in order to get full conversion. By this procedure, **140** and **143** could be obtained in moderate yields after removal of the catalyst by filtration.

Table 8.2: Synthesis of a library of furfurylamines

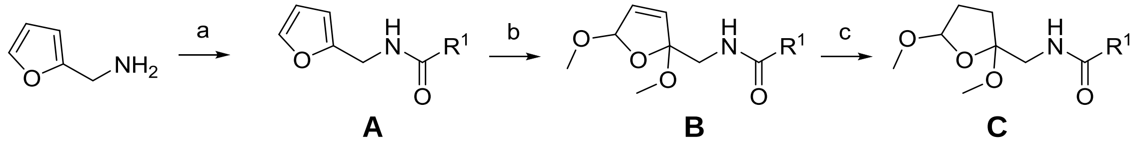

Reagents and Conditions: (a1) 6-caprolactone, (a2) R^1Cl, Et3N, DCM, (a3) R^1OH, EDC, DMAP, $NaHCO_3$, DCM, (b) Br_2, MeOH, Et_2O, (c) Pd/C, H_2 (g), MeOH

entry	compound	scaffold	R^1	method	yield	IC50 [µM]
1	**139**	A	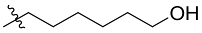	a1	98%	>100
2	**137**	B	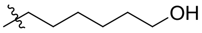	b	77%	15±2
3	**140**	C	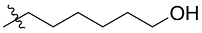	c	74%	>100
4	**141**	A	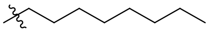	a2	83%	>100
5	**142**	B	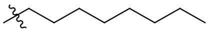	b	58%	>100
6	**143**	C	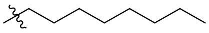	c	75%	>100
7	**144**	A	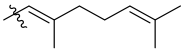	a3	91%	19±1
8	**145**	B	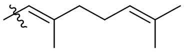	b	-	nd

The set of compounds was tested in the fluorescent RabGGTase assay[1]. As can be derived from Table 8.2, besides **137**, only one additional low µM inhibitor was found: **144** inhibited RabGGTase at an IC_{50} of 19 µM. Unfortunately, no hints toward more active furfurylamine inhibitors could be extracted from this series. It seems that the terminal alcohol together with the reactive 2,5-dimethoxy-dihydrofuran scaffold is necessary in order to obtain some activity but the mechanism behind this activity remains unclear. Since **144** is loosely based on the GGPP substrate, it could be speculated that this compound inhibits competitively with respect to the substrate. Attempts to co-crystallize these inhibitors with RabGGTase in order to obtain insights in the binding mode of these compounds were unsuccessful.

The disappointing activity results, together with the unsuccessful crystallization attempts and acid lability of this compound class, let to the decision to not further investigate the furfurylamine derivatives as potential RabGGTase inhibitors.

---

[1] At this point of the project, the radioactive assay had not been established yet

§ 8.3 Evaluation of benzoxazolone based RabGGTase inhibitors

Next, we wanted to evaluate the potential of the benzoxazolone based scaffold as RabGGTase inhibitor. In order to check the integrity of the assay results the initial hit was resynthesized (Table 8.3)

Table 8.3: Synthesis of the oxazole inhibitor

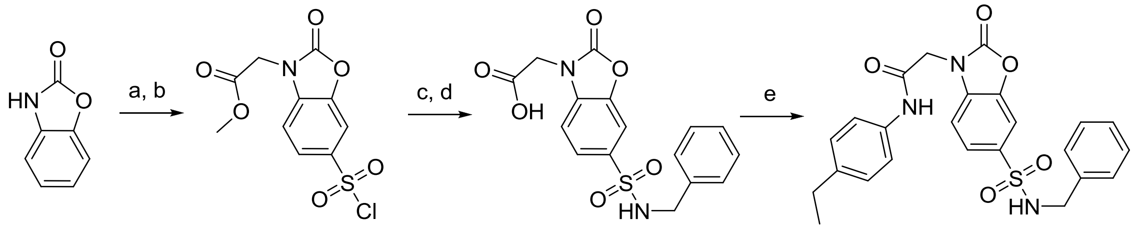

146 **147** **148** **138**

Reagents and Conditions: (a) NaH, methylbromoacetate, THF, 95% (b) SO_3HCl (c) benzylamine, pyridine, DCM (98%, 2 steps), (d) HCl (c), dioxane Δ, (e) 4-ethylaniline, EDC, DCM (75%, 2 steps)

Unsubstituted benzoxazolone **146** was treated with methylbromoacetate followed by the introduction of the sulfonylchloride with chlorosulfonic acid to furnish intermediate **147** according to a procedure in patent literature[199]. The sulfonamide functionality was obtained upon reaction with benzylamine in the presence of pyridine as a base. Hydrolysis of the ester then gave **148**. The final transformation involved the introduction of 4-ethylaniline employing standard coupling conditions. All steps were very high yielding and let to **138** in 70% overall yield.

The fresh batch was rescreened in the NBD-FPP assay and was found to inhibit RabGGTase with an IC_{50} of 18 µM. Co-crystallization attempts of **138** with RabGGTase were unsuccessful. As a counter screen, the compound was tested at the recently established radioactive substrate based assay established at the LDC. In the radioactive assay, no inhibitory activity could be determined for this substrate. Since the radioactive assay correlates better with potential cellular activity, no additional library was made around this compound class. Most probably, the initial activity found for this compound class could be related to the artificial NBD-FPP assay system.

§ 8.4 Evaluation of fluorescent NBD-FPP assay

Whereas the NBD-FPP assay has been rather useful as an aid in the development of our THB-based inhibitors as well as in the reported peptide based inhibitors (peptides and peptide analogs § 1.7.1), in the high-throughput screen it resulted, besides the identification of psoromic acid, mainly in false positives. In addition, there is no clear correlation between the NBD-FPP assay and cellular prenylation. These discrepancies are mainly related to the use of a fluorescent substrate instead of natural analog GGPP. In order to identify extra RabGGTase inhibitor hits, a HTS employing the newly established [^{3}H]-GGPP assay has successfully been carried out at the LDC.

In general, assay artifacts should be considered once employing a non-natural substrate. Although inhibitors can be successfully identified, a counterscreen is recommended in order to discard false positives before starting optimization rounds.

Chapter 9: De novo design of RabGGTase inhibitors

The solved crystal-structure of **BMS3** in complex with RabGGTase was a great opportunity to explore exit vectors around this THB structure and successfully led to low nanomolar selective inhibitors of RabGGTase. However, the possession of such a crystal structure also opens up possibilities to design structurally new inhibitors. In this chapter, the first attempts toward new RabGGTase inhibitor scaffolds will be discussed.

§ 9.1 Back to the FTase inhibitors

Besides **BMS3** there are many more FTIs known. Although these inhibitors have all been checked for cross inhibition with closely related GGTase I, none of these inhibitors have been tested against RabGGTase. The co-crystal structure analyses indicate that both for FTase and RabGGTase, interaction with the zinc ion and π-stacking with the nearby aromatic residues (Tyr361 and Phe289, respectively) are essential for binding. The FTIs listed in Scheme 9.1 all possess these common two structural features necessary for binding: an imidazole to coordinate to the zinc and an aromatic group to establish van der Waals interactions with the aromatic residues.

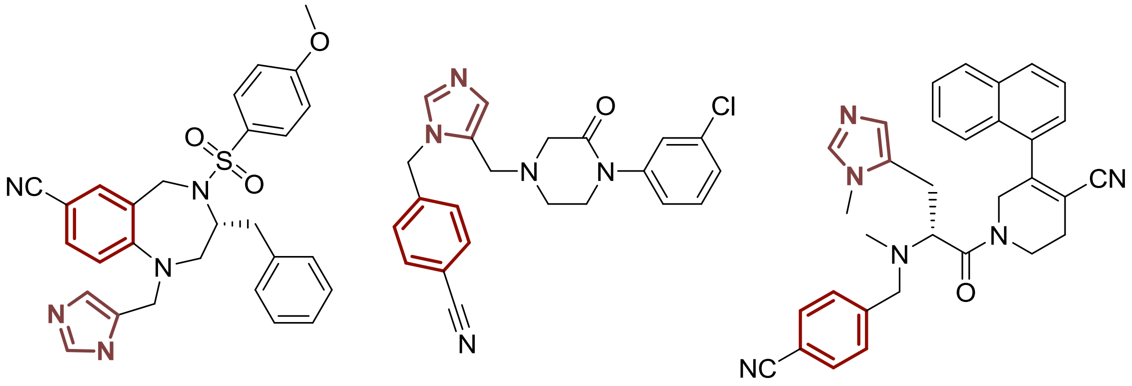

BMS3 (**23**)
IC_{50} FTase = 1.7 nM
IC_{50} GGTase I > 10 μM

L-778,123 (**4**)
IC_{50} FTase = 2nM
IC_{50} GGTase I = 98 nM

ABT-33 (**149**)
IC_{50} FTase = 1.2nM
IC_{50} GGTase I = 3.5 μM

Scheme 9.1: BMS3, L-778,123 and ABT are all FTase inhibitors with an imidazole.

Therefore, it was envisioned that L-778,123 and ABT-33[200, 201] could be potential RabGGTase inhibitors as well. L-778,123 and ABT-33 (Scheme 9.2) were synthesized according to literature procedures and were evaluated in the radioactive RabGGTase assay. It was found that ABT-33 indeed was a potent inhibitor of RabGGTase as well, whereas L-778,123 showed no inhibition of RabGGTase activity.

Synthesis of ABT-FTase inhibitor

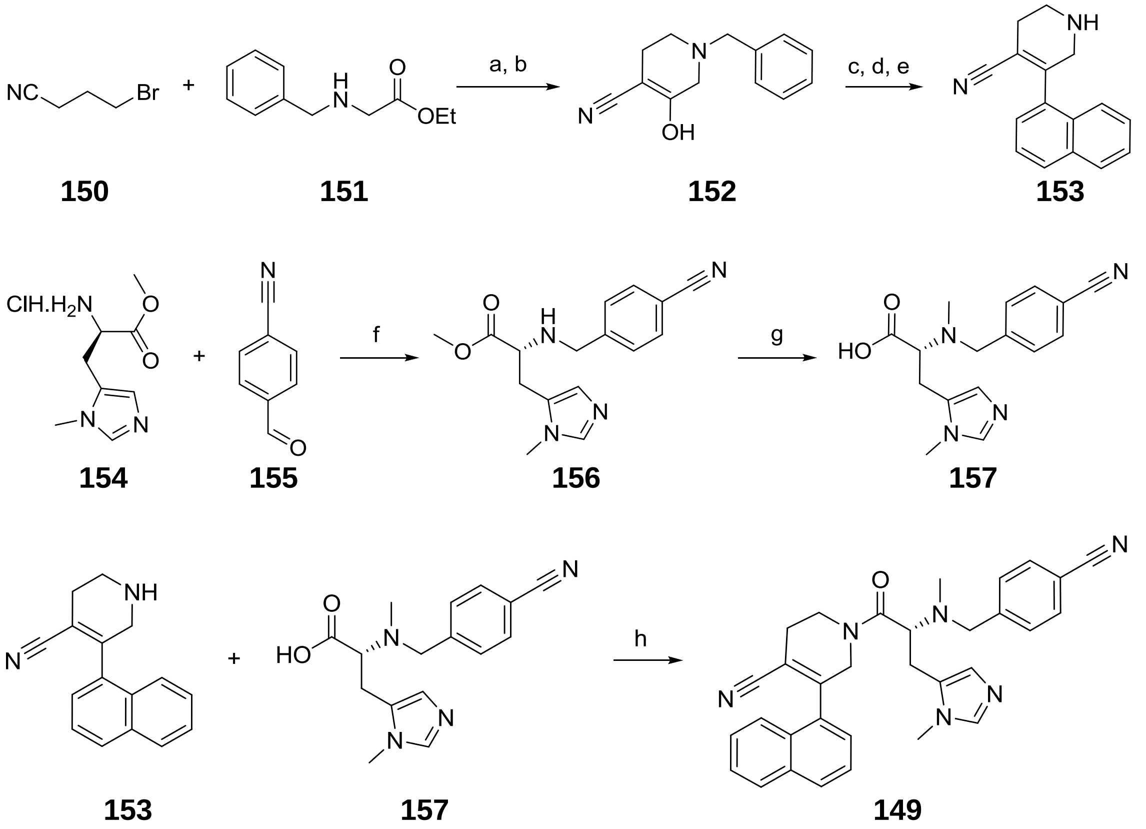

Reagents and Conditions: (a) K_2CO_3, neat (b) *t*BuOK, toluene (95%, 2 steps) (c) Tf_2O, pyridine, DCM, 15% (d) 1-naphtylboronic acid, K_3PO_4, $Pd(PPh_3)_4$, dioxane, Δ, 53%, (e) 1-chloroethylchloroformate, DCE, MeOH, Δ, 53%, (f) NaOAc, $NaBH_3(CN)$, MeOH, 81%, (g) i. paraformaldehyde, $NaBH_3(CN)$, MeOH, ii. LiOH, THF, 56%, (h) HATU, DIPEA, DMF, 32%.

Scheme 9.2: Synthesis of FTase inhibitor ABT-33 (**149**).

The co-crystal structure of ABT-33 in complex with RabGGTase could be solved. The imidazole was indeed binding to the zinc, whereas the benzyl ring was π-stacking with Phe289. Furthermore, the naphthalene moiety was T-stacking with Trp244. The additional nitrile showed a hydrogen bond interaction with Arg144. In contrast to **BMS3**, ABT-33 adapts a different orientation in FTase and RabGGTase. For FTase, besides the common imidazole-zinc and π-stacking features, an additional hydrogen bond interaction is formed between the nitrile and Tyr93. Further interaction is assured by T-stacking of the naphthalene moiety with Trp102.

Interestingly, an overlay of the crystal structures of **BMS3** with ABT-33 showed the hypothesized common binding features: the aromatic group and imidazole. Therefore, it seems that FTase and RabGGTase have a privileged scaffold in common (Figure 9.1).

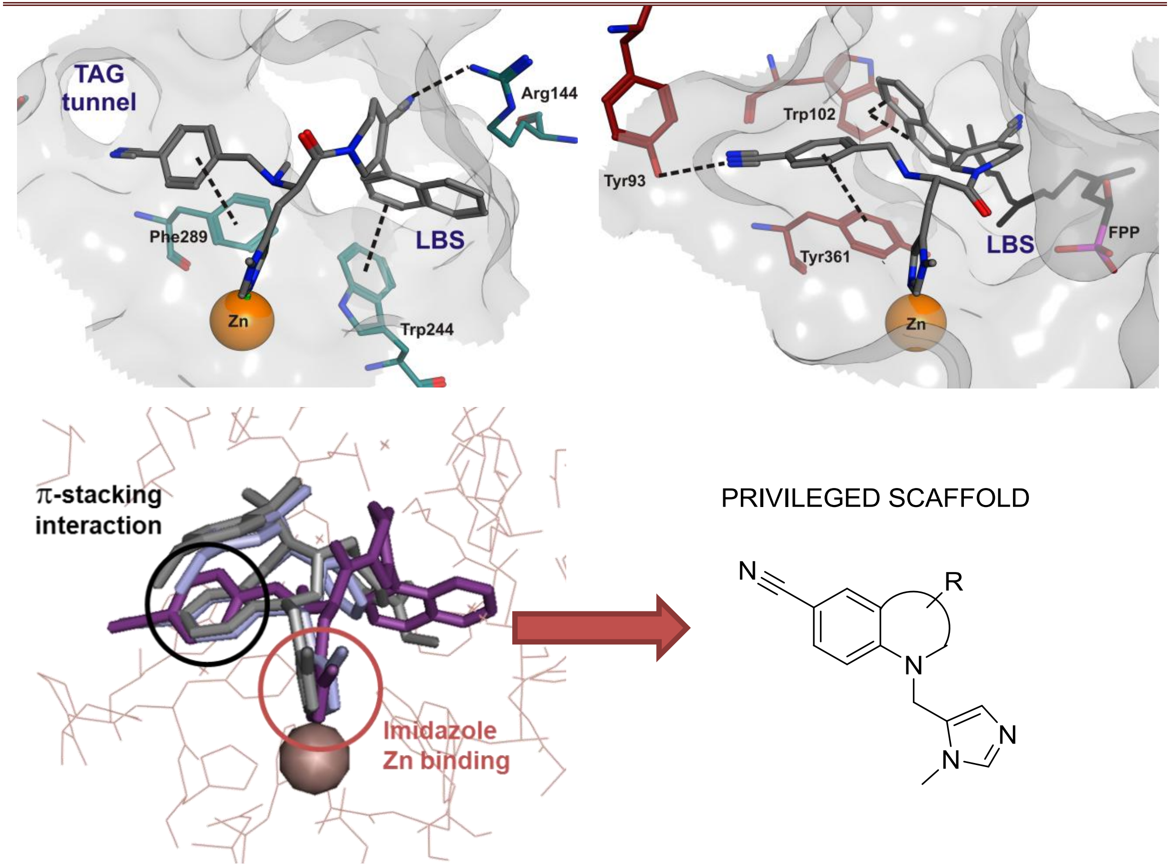
TAG tunnel
Arg144
Phe289
LBS
Zn
Trp244
Tyr93
Trp102
Tyr361
LBS
FPP
Zn
π-stacking interaction
Imidazole Zn binding
PRIVILEGED SCAFFOLD
N
R
N
N
N

Figure 9.1: a) Co-crystal structure of ABT-33 (**149**) in RabGGTase, b) Co-crystal structure of ABT (**149**) in FTase, c) Overlay of **BMS3**, ABT-33 and **93** shows a similar binding mode in RabGGTase, leading to a privileged scaffold.

In order to investigate which interactions are necessary for RabGGTase and/or FTase activity, some of the intermediates of the synthesis were screened as well. In addition, **157** was coupled to benzylamine (Scheme 9.3) in order to evaluate the importance of the naphthalene part of the inhibitor for RabGGTase inhibition.

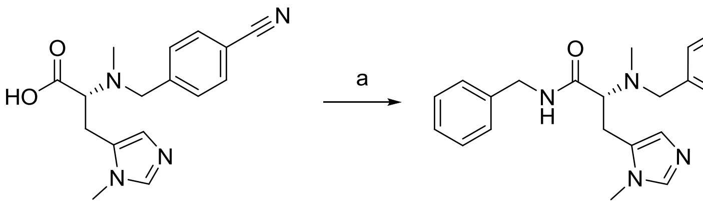
HO
O
N
N
N
N
a
O
N
H
N
N
N
N

157 **158**

Reagents and Conditions: (a) benzylamine, HATU, DIPEA, DMF.

Scheme 9.3: Synthesis of analog **158**.

Table 9.1: Biological evaluation of ABT, building blocks and analogs

Entry	Substance	RabGGTase	FTase	GGTase I
1	**156**	>10 000	9,395±6,205	>30 000
2	**157**	>10 000	nd	>30 000
3	**ABT-33(149)**	10.5±0.5	<5[§]	>30 000
4	**158**	9,272±729	2,605±176	>30 000

[§] lower detection limit, nd=not determined

From Table 9.1 it is clear that the privileged core scaffold alone, represented by building blocks **156** & **157**, is not sufficient to provide RabGGTase inhibition. The introduction of an additional benzyl (**158**) gives a weakly active dual FTase/RabGGTase inhibitor. However, extra interactions, like realized with the naphthalene moiety in ABT-33, seem necessary to obtain potent inhibitors.

§ 9.2 General strategy to identify prenyl transferase inhibitors

The common privileged scaffold of FTase and RabGGTase inhibitors presented a potential access to dual and/or selective inhibitors. Although the privileged scaffold itself was not sufficient to obtain activity, it was envisioned that the introduction of a proper extra group could lead to new inhibitors. The generation of a library around this scaffold thus, would present an opportunity to find new FTase and RabGGTase inhibitors, either dual or selective (*e.g.* **159a-c**). The generation of an intermediate such as **160**, would give access to several heterocyclic core structures with 'inhibitor potential'. It was envisioned that **160** was available by a Mitsunobu reaction between **161** and 5-hydroxymethyl-1-methyl-1H-imidazole (**162**), or by alkylation of **161** with 5-(chloromethyl)-1-methyl-1H-imidazole (**163**).

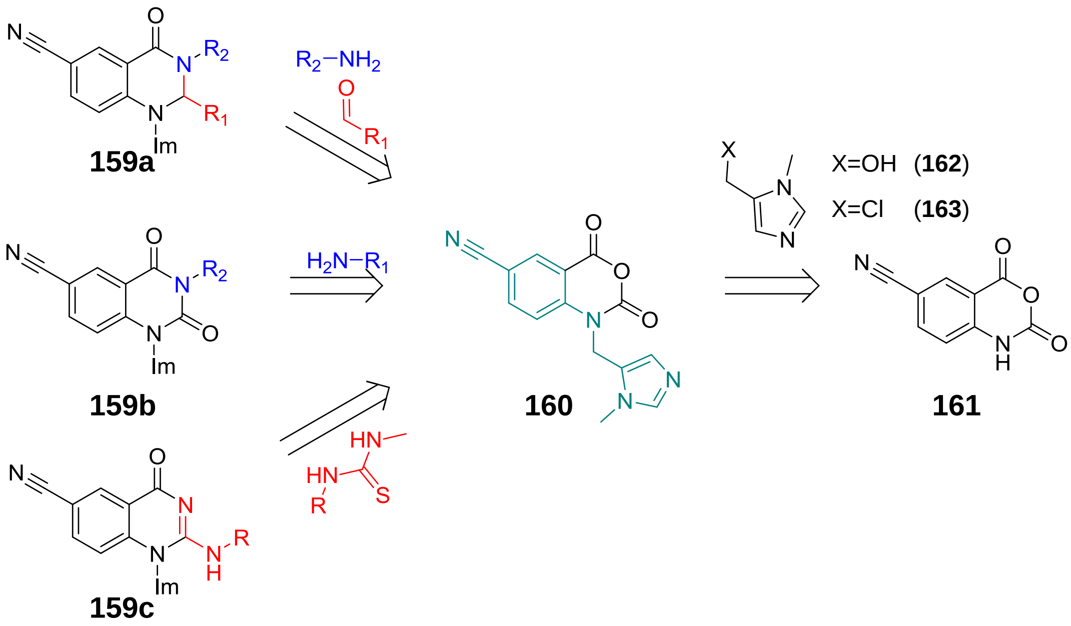

Scheme 9.4: Retrosynthesis of quickly accessible predicted inhibitors. Im=imidazoylmethyl

Isatoic anhydrides, such as **161**, are valuable building blocks in heterocyclic chemistry, due to their reactivity toward both electrophiles and nucleophiles[202, 203]. Since **161** is not commercially available, a synthetic route was established to obtain the isatoic anhydride. The synthesis is outlined in Scheme 9.5. First, 4-aminobenzonitrile **164** was selectively brominated with NBS in DMF and subsequently protected with Boc anhydride to give intermediate **165**. The halogen-lithium exchange with n-BuLi resulted in a rearrangement of the Boc substituent into intermediate **166** in analogy with the literature[204]. The Boc and tBu were deprotected in one step by addition of 20 equiv. of TFA in DCM. First attempts to obtain **161** by treatment of **166** with triphosgene failed and only gave recovered starting material, probably due to unsuitable workup conditions.

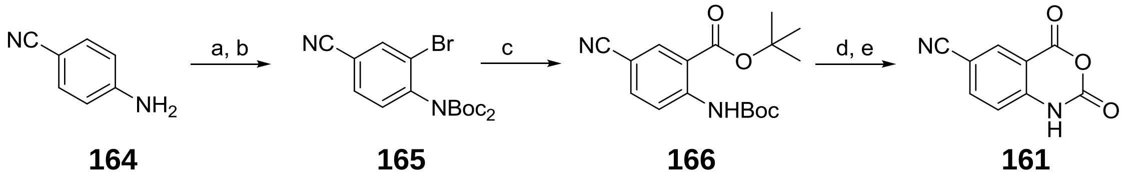

Reagents and Conditions: (a) NBS, DMF, 99%, (b) Boc_2O, DMAP, THF, Δ, (c) n-BuLi in hexane, THF, -78°C, 82%, (d) TFA, DCM, 99%, (e) triphosgene, THF, Δ, failed.

Scheme 9.5: Synthesis of 5-cyano-isatoic anhydride.

Parallel to the development of a synthetic route towards **161**, the introduction of the imidazole on commercially available 5-bromo isatoic anhydride was investigated. First, 5-hydroxymethyl-1-methyl-1H-imidazole (**162**) was synthesized using a modified

Rapoport's procedure (Scheme 9.6)[205]. **162** was then converted to 5-(chloromethyl)-1-methyl-1H-imidazole (**163**) by treatment with thionyl chloride in DMF. Then, several reactions conditions were screened to obtain compound **169** (Table 9.2).

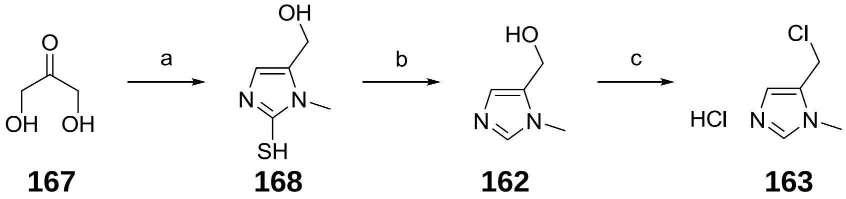

Reagents & Conditions: (a) KNCS, $MeNH_2$*HCl, AcOH, $MeCN/H_2O$ Δ, (b) H_2O_2, $AcOH/H_2O$, 75% (2 steps) (c) $SOCl_2$, DMF, 99%.

Scheme 9.6: Synthesis of hydroxymethyl- and chloromethyl -1-methyl-1H-imidazole.

Table 9.2: Conditions toward privileged building block **169**.

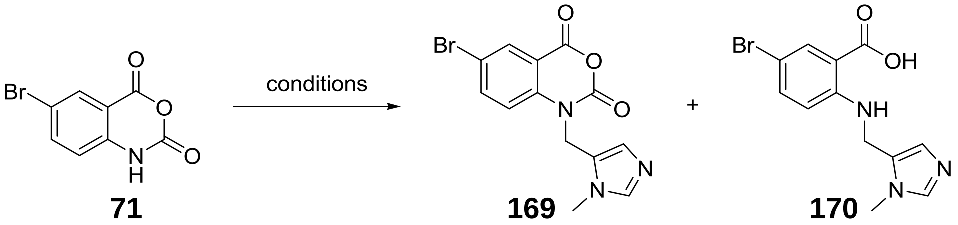

entry	reactant	reagents	solvent	temperature	**169**	**170**
a	**162**	DIAD, PPh_3	THF	0°C → rt	complex mixture	
b	**163**	K_2CO_3	DMF	0°C → rt	25	40
c	**163**	NaH	DMF	0°C → rt	30	50
d	**163**	Et_3N, KI	DMF	60°C	5	60

Employing typical Mitsunobu conditions, in analogy to patent literature[206] resulted in a complex mixture of products (entry a). Analysis of the product mixture showed mainly anthranilic acid products like **170** and addition products with DIAD. In order to prevent addition of DIAD, reversed addition of reagents was investigated but was unsuccessful as well. Therefore, different alkylation conditions with reactant **163** were examined. Prestirring isatoic anhydride **71** with base (either K_2CO_3 or NaH, entries b and c) for 1 h, followed by slow addition of **163** showed the most promising results, but nonetheless resulted in low yields of **169**. In all cases a mixture of **169**, **170** and unreacted starting material were observed, which were difficult to separate using column chromatography, partially due to their low solubility in organic solvents. Therefore, other strategies will have to be considered.

§ 9.3 First example of successful scaffold hopping

Due to the difficulties in the synthesis of privileged building blocks **160** and **169** and time constraints in the project, it was decided to investigate another approach to obtain molecules with **159a** as core scaffold. The retrosynthesis is depicted in Scheme 9.7

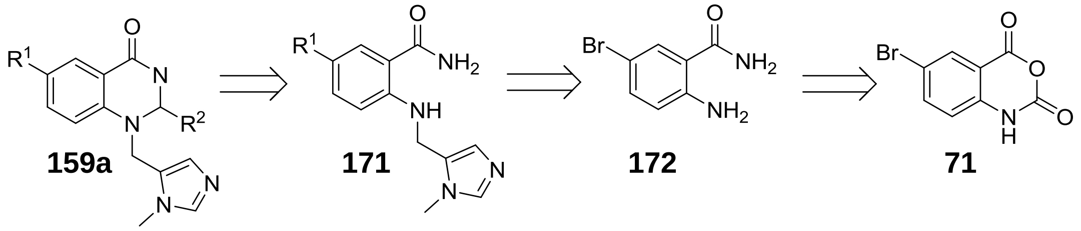

Scheme 9.7: Retrosynthesis II of **159a**

The synthesis starts again with 5-bromo isatoic anhydride **71**, which is allowed to react with aqueous ammonia to give 2-amino-5-bromobenzamide (**172**) as a precipitate (Scheme 9.8)[207]. This precipitate is then subjected to reductive amination conditions suited for electro-deficient arylamines[208] with N-methylimidazole-5-carboxaldehyde (**76**) to obtain substrate **171**a. The bromide was then converted to a nitrile under Rosenmund-von Braun conditions in 22% to obtain **171**b. The low yield was mainly caused due to degradation and loss of product into the water layer promoted by NMP. **171a** and **171**b were subjected to condensation with substituted aldehydes in order to obtain a small library of dihydroquinazolinones (**173**).

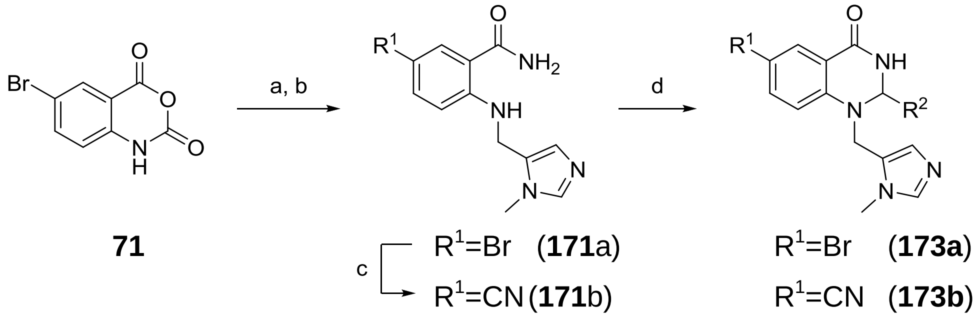

Reagents and Conditions: (a) NH_4OH (b) N-methylimidazole 5-carboxaldehyde **76**, TFA, $NaBH(OAc)_3$, THF (73%, 2 steps), (c) CuCN, NMP, Δ, 22% (d) R^2CHO, $HCl_{(c)}$, EtOH (69-72%).

Scheme 9.8: Synthesis of potential RabGGTase inhibitors

A small set of compounds was synthesized following the route outlined in Scheme 9.8 and screened for RabGGTase and FTase activity. The results are summarized in Table 9.3.

Table 9.3: Biological evaluation of a small set of dihydroquinazolinones.

				In vitro IC_{50} [nM]		
Entry	Substance	R1	R2	RabGGTase	FTase	GGTase I
1	**171a**	Br	-	>10000	9703	>99 500
2	**174**	Br	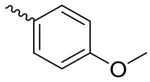	>10000	683#	4399±2784
5	**175**	CN	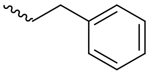	731±143	52.4±11.4	>99 500

Although only a few substances have been synthesized, Table 9.3 clearly shows the potential of the privileged scaffold for prenyl transferase inhibitors. Interestingly, compound **174** appears to be a weak dual inhibitor of FTase and GGTase I, whereas the simple building block **171**a displays weak inhibition against FTase. Substance **175** shows even nanomolar inhibitory activity against both FTase and RabGGTase.

§ 9.4 Scaffold Hopping Future Prospective

The small set of inhibitors presented in Table 9.3 shows the potential of scaffolds containing the 5-anilinomethyl-imidazole core structure. Rather unexpected, a low µM GGTase I inhibitor was identified among this set of inhibitors. Since a GGTase I inhibitor would also profit from the imidazole zinc binding, this inhibitor class is apparently also available via this privileged core scaffold. Therefore, it would be worthwhile to investigate more into the general route toward different scaffolds via isatoic anhydride. Since the introduction of the cyanide function was problematic, one could imagine introducing other groups, such as furan nitrile by Suzuki coupling reactions, which is known to give RabGGTase and FTase inhibitory activity as well. An alternative construction of the general building block is presented in Scheme 9.9.

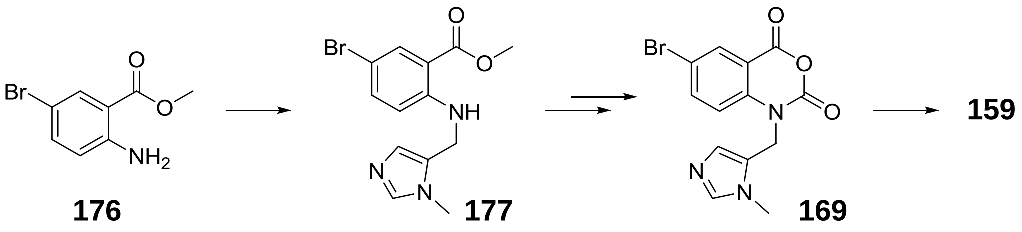

Scheme 9.9: Different synthetic strategies toward building block **169**.

Intermediate **177** can be obtained by a reductive amination with methyl 2-amino-5-bromobenzoate (**176**) and N-methylimidazole-5-carboxaldehyde (**76**), in analogy with the reaction in Scheme 9.8. After saponification of the ester, the free acid could be treated with triphosgene to obtain **169**, which would give access to many different heterocyclic and open scaffolds, privileged to inhibit any of the prenyltransferases. Subsequent transition-metal catalyzed coupling to the aryl bromide would give access to many more potential selective prenyl transferase inhibitors. In order to prevent many purification steps, the synthesis can also be carried out on solid phase. The imidazole could be coupled to a trityl-resin and cleaved after generation of the final products. Altogether, this process could lead to a fast generation of various prenyl transferase inhibitors.

Chapter 10: Concluding Remarks

Several approaches to obtain selective inhibitors of RabGGTase have been described in this thesis; structure based design, *in vitro* screening and *de novo* design. These approaches, besides their starting points, all follow the same design cycle. The development of active compounds has often been described as an iterative cycle of design, synthesis, screening, structure-activity-relationship (with or without structural information of the target) followed by the next step of design. Following these steps carefully, many successes can be reached within the optimization and tuning of activity and selectivity. Interestingly, depending on the starting point or approach, different insights could be obtained.

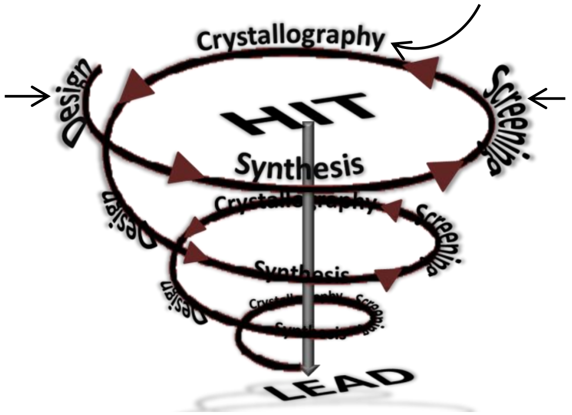
Dual Inhibitor Approach

De novo Approach

Structure-based drug design is a powerful tool to identify new possibilities to tune potency and selectivity. By using the co-crystal structures of **BMS3**, the dual inhibitor, in both FTase and RabGGTase, it was possible to identify many exit vectors to increase selectivity for RabGGTase. Substituents that were meant to increase selectivity were identified by virtual screening. However, as clear from Chapter 4 even virtual screening needs careful optimization. The first set of compounds generated and synthesized did not show the expected activity and often were not active at all against RabGGTase. In contrast, FTase was more ‘adaptive’ than expected toward changes of the ligands. Additional crystallization of some of these dual inhibitors gave interesting insights. It seemed that RabGGTase requires an exact π-binding with the THB core and the tyrosine in order to establish activity, therefore rigid modifications were not allowed. Interestingly, FTase showed an adjustment in its active site in order to allow the larger ligands to bind. Its bulky Trp102 flipped around by 90 degrees, opening up a larger pocket. Since this tryptophan is known to be responsible for the substrate selectivity[197] and GGPP is known to be an inhibitor of FTase[54] it could be speculated that GGPP induces a similar shift of this tryptophan. This shift, then, would allow GGPP to bind, but renders the enzyme inactive toward its substrates.

The observations from the co-crystal structures have been taken into account in the next cycle of design. An extra binding constraint was set in order to fix the core of the ligand in the RabGGTase binding site. It was clear that varying one position of the ligand was not sufficient in order to obtain selectivity so it was necessary to additionally identify groups which targeted the TAG tunnel. By introducing heteroaromatic five or six-membered rings, some groups could be identified that successfully targeted the TAG tunnel. The principle was shown by the introduction of a furan moiety. Crystallization studies showed that this group was oriented to the TAG tunnel as designed. In FTase though, the furan pointed away from the surface into the exit groove therefore this group was not sufficient to assure complete selectivity. The combination of the furan with a benzylcarbamate showed the potential of combining those two exit vectors in order to obtain a selective inhibitor which was also successfully co-crystallized with RabGGTase (Figure 10.1).

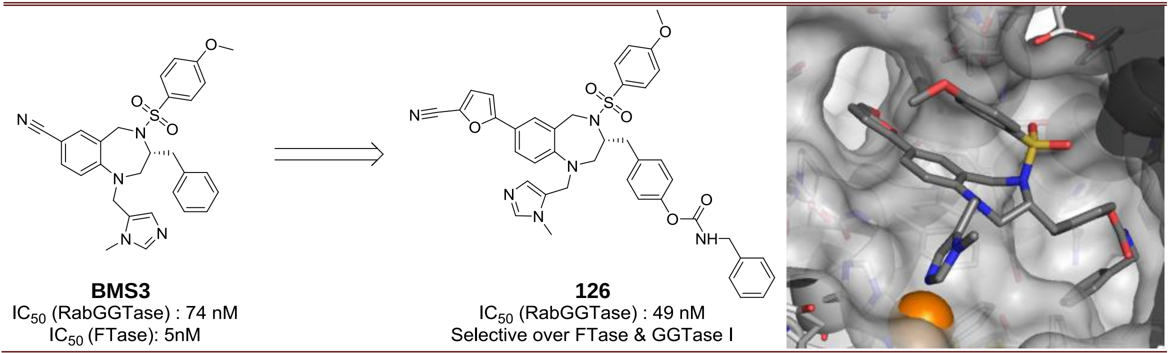

BMS3
IC_{50} (RabGGTase) : 74 nM
IC_{50} (FTase): 5nM

126
IC_{50} (RabGGTase) : 49 nM
Selective over FTase & GGTase I

Figure 10.1: From dual inhibitor **BMS3** to a selective RabGGTase inhibitor.

The parallel development of other RabGGTase assays rendered new challenges. Different assay systems were shown to give different trends, which seemed to be a consequence of the prenyldonor (GGPP or NBD-FPP). Therefore, the design needed to be reconsidered once more. It was hypothesized that different binding modes within one compound class could result in different types of binding respective to the prenylpyrophosphate; competitive, non-competitive or even cooperative. Since GGPP binds with a very high affinity to RabGGTase, it was speculated that non-competitive or cooperative compounds would be superior in activity to competitive compounds. This meant that selectivity should be obtained from the lipid binding site, without reaching the GGPP pocket. In order to obtain promising candidates, an additional virtual screening was carried out with GGPP in the binding site. It could be shown that the introduction of aromatic groups such as pyridine, indeed resulted in highly active *in* *vitro* RabGGTase inhibitors. However, no selectivity against FTase was gained. In order to verify the binding mode hypothesis, it will be interesting to have the binding mode of these compounds determined, both by competition experiments with GGPP and NBD-FPP and to have some of these compounds co-crystallized with RabGGTase in complex with GGPP.

Attempts to discover new RabGGTase inhibitors using our fluorometric NBD-FPP assay resulted mainly in false positives, which clearly showed the need for evaluation of hit compounds in a counter assay. Else, such an inhibitor development process could end up in a negative spiral leading to an inactive compound class, based on an artificial assay system.

The initial results of the *de novo* design shows the potential for a structure based development program to quickly obtain prenyl transferase inhibitors and more efforts on the synthesis of such inhibitors together with crystallization studies could certainly lead to new interesting FTase-, GGTase I- or RabGGTase inhibitors. Furthermore, the identification of the 'PTase privileged scaffold' also uncovered ABT-33 as a RabGGTase inhibitor.

These results also indicate that RabGGTase-THB co-crystal structures might be a valuable starting point for more extensive structure-based design of selective RabGGTase inhibitors, for example using computational methods such as growing/linking approaches or *de novo* design. It would especially be interesting to grow the inhibitors within the TAG tunnel, in order to find new anchor points for selective RabGGTase inhibitor design. Furthermore, several other interaction partners that were not approachable by the THB scaffold could be explored using such an approach. In addition, it would be interesting to use the RabGGTase crystal construct for fragment based screening. Such an approach potentially lead to new molecular interaction partners and would give a deeper understanding of potential binders.

Finally, the low nM THB inhibitors were tested in cells; they were screened for cellular reprenylation and for inhibition of proliferation of several cancer cell lines. Interestingly, the IC_{50} values for prenylation of RabGGTase correlated generally with the proliferation data for the cancer cell lines. It could also be shown that the selective RabGGTase inhibitor **126** successfully inhibited proliferation of cancer cells as potently as dual inhibitor **BMS3**. Combined, these results indicate that RabGGTase should be regarded as a relevant target for anti-cancer therapy. However, before additional conclusions about the therapeutic role of RabGGTase can be drawn, more studies will be necessary to study the effect of RabGGTase inhibition *in vivo.* It would be interesting to know if these inhibitors really show an apoptotic effect, in addition to the viability studies conducted in the cancer cell lines.

Besides their therapeutic relevance, the selective RabGGTase inhibitors described here represent valuable tools to study the effect of Rab GTPase in vesicular trafficking and in cancer from a chemical biology perspective.

Experimental Section

§ 10.1 Virtual screening procedure for RabGGTase and FTase

§ 10.1.1 General procedure for virtual screening

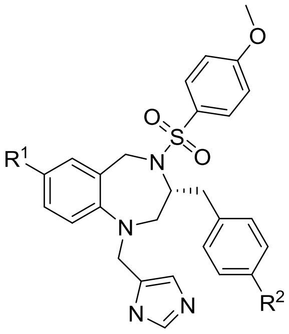

THB core

The virtual library was prepared by decoration of the tetrahydrobenzodiazepine (THB) core with 62 different R^1 and 62 different R^2 groups (62 x 62, see supplementary data). The library was prepared in Pipeline Pilot, the structures were assembled and stereoisomers and tautomers were enumerated. This database was minimized in MOE (version 2009.10)[179] using database minimize, with MMFF94x forcefield and an RMS gradient of 0.1. The crystal structures of RabGGTase and FTase were prepared for docking by removal of the **BMS3** inhibitor and the prenylpyrophosphates, followed by the addition of hydrogens using the Protonate3D function in MOE. Ligands were docked into the proteins using GOLD (version 4.1.1)[180, 181]. Since the imidazole is known to bind to the zinc atom, we set a binding constraint by defining an imidazole substructure with defined distance to the zinc atom (min 1.5 Å, max 3.5 Å, spring constant = 5). Further, the binding site was defined by a sphere of radius 15 Å around the phenylalanine/tyrosine residue. The ChemScore scoring function was used in combination with most accurate automatic genetic algorithm settings (autoscale = 1). Ten solutions were generated for all inhibitors. The scores for RabGGTase and FTase were compared for each inhibitor, assuming that an inhibitor with a high score for RabGGTase and a low score for FTase would be most selective. The compounds that satisfied these conditions and showed a preserved binding mode in RabGGTase were further evaluated for their synthetic feasibility and synthesized.

§ 10.1.2 Specific binding constraints in RabGGTase VHS:

1st virtual screening: imidazole-zinc constraint, no GGPP

constraint substructure protein 9654 imidazole.mol2 4 3.5 1.5 5.0

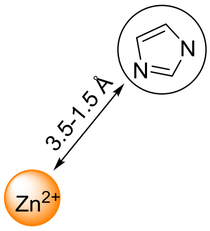
N
N
3.5-1.5 Å
Zn2+

2nd virtual screening: imidazole-zinc constraint &THB-tyrosine constraint, no GGPP

constraint distance protein 9259 ligand 4 4.5800 4.3800 5.0000 on

constraint distance protein 9914 ligand 34 2.1800 1.9800 5.0000 on

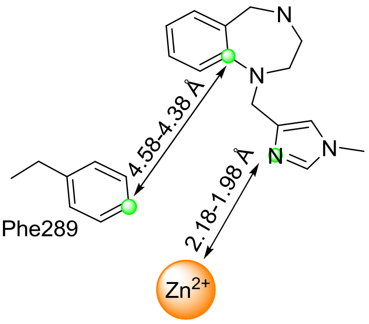
N
N
N
N
4.58-4.38 Å
2.18-1.98 Å
Phe289
Zn2+

3rd virtual screening: imidazole-zinc constraint & THB-tyrosine constraint, with GGPP

constraint distance protein 9259 ligand 4 4.5800 4.3800 5.0000 on

constraint distance protein 9914 ligand 34 2.1800 1.9800 5.0000 on

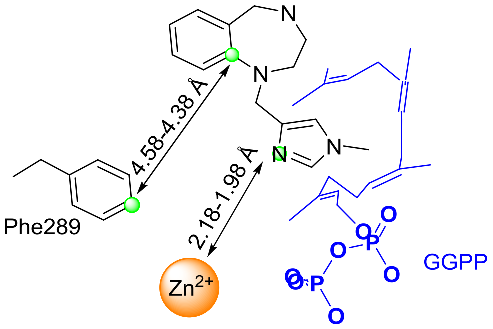
N
N
N
N
4.58-4.38 Å
2.18-1.98 Å
Phe289
Zn2+
O
O
O
P
O
O
O
P
O
GGPP

§ 10.2 Assay procedures

§ 10.2.1 Solution based fluorometric biochemical RabGGTase assay procedure for IC_{50} determination of THBs.

All IC_{50} values were measured using black 96-well plates under the following conditions: 37 °C, *buffer:* 50 mM Hepes, pH 7.4, 50 mM NaCl, 2 mM $MgCl_2$, 2 mM DTE (added freshly), 20 µM GDP (added freshly), 0.01% Triton X-100. *Final concentrations:* 2 µM Rab, 2 µM REP, 50 nM RabGGTase, 2 µM NBD-FPP **1**. 50 µM THB (from a 10 mM solution in DMSO). For the 100% activity control, instead of THB solution, 0.5% of DMSO was added. A 0% activity control for the correction for bleaching of fluorescence was measured. The 0% activity control wells contained 100 nM RabGGTase and 1.5 µM NBD-FPP. In every screening session the IC_{50} of **BMS3** was measured as a reference. After mixing of the fluorescent substrate, the enzyme and the THB solutions (or DMSO), the reaction mixtures were incubated for 5 minutes at 37 °C. Then, the protein substrates (Rab7 and REP1) were added and fluorescence intensity was recorded for 30 minutes at intervals of 14 seconds (λ_{ex} = 479 nm, λ_{em} = 520 nm). Data were evaluated using Microsoft Excel. The fluorescence intensity on individual time points was normalised with respect to the 0% activity control and reaction rates were determined from the linear parts of the progress curve. Concentration dependent inhibition of RabGGTase was measured using different concentrations of inhibitors resulting from two-fold dilution series. Reaction progress at every concentration of inhibitor was measured in triplicates. IC_{50} values were calculated using 4-parameter log fits using XL Fit curve fitting software for Excel using the following equation:

$$y = A + \frac{B - A}{1 + \left(\frac{x}{\mathrm{IC}_{50}}\right)^{slope}}$$

where *y* is the remaining enzyme activity (in %) and *x* is the corresponding concentration. The fitted IC_{50} parameter is the relative IC_{50}, and is defined as the concentration giving a response half way between the fitted top (B) and bottom (A) of the curve. (measured at the MPI and at the LDC)

§ 10.2.2 Solution-based fluorometric FTase assay.

Inhibition of FTase was measured according to procedures described by Pompliano *et al.*[175, 176], mainly measured at the LDC.

§ 10.2.3 Solution-based fluorometric GGTase I assay.

Inhibition of GGTase I was measured according to the procedure described by Goossens *et al.* [177],measured at the LDC.

§ 10.2.4 Cell culture

HCT 116 (DSMZ) cells were maintained in McCoy's 5a medium with 1.5 mM glutamine + 10% FCS, A2780 (ECACC) and HeLa (DSMZ) cells in RPMI1640 medium with 1.5 mM glutamine + 10% FCS. PBMC cells were freshly isolated from buffy coats (DRK Hagen, Germany) and seeded in RPMI medium with 1.5 mM glutamine + 10 % FCS.

§ 10.2.5 Reprenylation assay

Cells: HeLa; Medium: RPMI1640, 10% FCS, 1% glutamine; Plates: 96 well, sterile

Protocol: The HeLa cells were trypsinized and counted. Then 1.2 x 10^4 cells per well were seeded in 100 µL medium and incubated at 37°C/5%CO_2 for 24 h. The compounds were added to the cells (2 wells for each concentration), followed by the addition of **BMS3** at a final concentration of 1 µM as positive control. After incubation for 6 h at 37°C/5%CO_2, the medium was removed and the cells were washed with cold PBS (2x). Then the prenylation buffer (20 µL/well) was added [50 mM HEPES (NaOH pH 7.2), 50 mM, 2 mM $MgCl_2$, 0.5% NP-40, 0.7 mM DTT, 50 µM GDP, Roche Protease Inhibitor Cocktail, 0.4 µM RabGGTase 0.4 µM REP1, 2 µM biotin-GPP] and shaken (320 rpm) at room temperature for 1h, after which the lysates were frozen overnight. The lysates were thawed, and 10 µL of each lysate were placed in a 96 well plate and mixed with 10 µL gel loading buffer [5 µL E-page loading-buffer (EPBUF01; Invitrogen), 2 µL NU-page sample reducing agent (NP0009; Invitrogen), 3 µL H_2O)]. The plate was sealed and heated at 75°C for 10 minutes and spun at 3800 rpm for 10 min. An E-Page gel (EP09606; Invitrogen) was prepared and placed in the Mother E-Base gel running device (EBM03EU; Invitrogen). The gel was loaded with 10 µl of the prepared samples and protein standards were added at designated positions. The gel was run in EP-mode for 15 min. Then the gel was washed in A.dest and gel pieces were removed from the pockets. The gel was transferred to PVDF-membrane stacks (IB401001; Invitrogen) and a gel-sandwich was prepared according to manufactures instructions. The blot was runned on the IBlot gel transfer device (IB1001EU; Invitrogen) for 7 min and allowed to dry for 1h. The membrane was then incubated in MeOH for 2 min and washed with A.dest and blocked with Odyssey Blocking-Buffer (927-40000;LI-COR) for 1h. This was incubated with monoclonal anti α-tubulin (T5168; Sigma) 1:3000 in Odyssey Blocking Buffer at 4°C overnight. The membrane was washed 3x with PBS-T for 5 min and incubated with goat αmouse IR800 (926-32210) 1:10,000 and streptavidin IR680 (926-32231; LI-COR9) 1:2000 in Odyssey Blocking Buffer for 1h. The membrane was washed 3x with PBS-T for 5 min, once with PBS and analyzed employing Odyssey Infrared Imaging System. The signals obtained from the positive controls were set as 100 % RabGGTase inhibition and rel. IC_{50}´s were calculated accordingly employing algorithm 205 by XLfit software (ID Business Solutions Ltd). [We choose 1 µM BMS 3 as 100 % determinant because we observed a saturated reprenylation signal at this concentration]. Measured at the LDC.

§ 10.2.6 Alamar Blue Assay

Cells were trypsinized and seeded in 100 µl/well with the appropriate cell culture medium in µclear 96well-Plates (Greiner) at the following densities: HCT116 cells at $2x10^3$ cells/well, A2780 cells at $3x10^3$ cells/well, HeLa cells at $2x10^3$ cells/well and PBMC at $2x10^5$ cells/well. After incubation at 37°C/5%CO_2 for 24 h compounds or DMSO as negative control diluted in 100 µl of the appropriate medium were added. Plates were further incubated at 37°C/5%CO2 in boxes with wet paper to get a humid environment and avoid loss of cell culture medium for 72 h. Then 100 µl of medium was removed from each well and 10 µl of Alamar Blue reagent (Invitrogen) was added followed by further incubation at 37°C/5%CO2 for 3h. Subsequently fluorescence was measured at an excitation wavelength of 530 nm and an emission wavelength of 595 nm in each well employing a Victor plate reader (Perkin Elmer). The fluorescence signals of DMSO treated cells were set as 100% viability and IC_{50}´s of compound treated cells were calculated accordingly employing algorithm 205 by XLfit software (ID Business Solutions Ltd). Measured at the LDC

§ 10.3 Synthetic procedures

§ 10.3.1 General Information

All reactions were carried out under an inert atmosphere of argon. Standard syringe techniques were applied for transfer of air sensitive reagents and dry solvents. Microwave-assisted reactions were performed in a Discover (CEM Corporation) single-mode microwave instrument producing controlled irradiation at 2450 MHz, using standard sealed microwave glass vials. Reaction temperatures were monitored with an IR sensor on the outside wall of the reaction vials. Reaction times refer to hold times at the indicated temperatures, not to total irradiation times. ^{1}H and ^{13}C nuclear magnetic resonance (NMR) spectra were recorded on a Varian Mercury 400 or a Bruker DRX 500, with chemical shifts (δ) reported in ppm relative to the solvent residual signals of $CDCl_3$ (δ_H = 7.26 ppm, δ_C = 77.16 ppm), MeOD (δ_H = 3.31 ppm, δ_C = 49.0 ppm) DMSO-d_6 (δ_H = 2.50 ppm, δ_C = 39.5 ppm) or acetone-d_6 (δ_H = 2.05 ppm, δ_C = 29.8 ppm) and coupling constants reported in Hz. Peak assignment was also done with the aid of gCOSY, gHSQC and gHMBC measurements. High resolution mass spectra (HR-MS, 70 eV) were measured on a Thermo Orbitrap coupled to Thermo Accela HPLC machine using electron spray ionization technique (ESI). Analytical HPLC-MS data were recorded on an Agilent HPLC (1100 series) coupled to a Finnigan LCQ ESI spectrometer, using a CC 125/4 Nucleodur C4 Gravity 3 μM column. The standard gradient began at 10% acetonitrile and was raised to 90% over 15 min. After 3 min at 90% acetonitrile, the column was washed for 5 min with 100% acetonitrile. The column was then equilibrated for 3 min with 10% acetonitrile. TFA (0.1% v/v) was added to the HPLC solvents. Chromatographic purification refers to flash chromatography using the indicated solvent (mixture) and Merck silica gel 60. For biochemical and biological testing, compounds were optionally purified by preparative HPLC-MS using an Agilent HPLC (1100 series) and a VP 125/21 NUCLEODUR C4 Gravity, 5 μm column until they were >98% pure. Compounds on TLC were visualized by UV detection or $KMnO_4$ staining. DCM was dried and distilled from CaH_2 prior to use. Other commercially available reagents and dry solvents were used as purchased. FTase inhibitors **BMS3** (**23**), BMS-214662 (3)[17, 191, 192] and ABT (**149**)[200, 201, 209] and fluorescent analog NBD-FPP (**27**)[66, 182, 183] as well as starting material **147**[199] and **163** were synthesized according to literature procedure. Compounds **23**, **87**, **88**, **90**, **94**, **96**-**103** and **115**-**118** were synthesized by Dr. Robin Bon; the synthesis is included here for completion.

(2E)-2-methyl-4-(oxan-2-yloxy)but-2-enal (52)

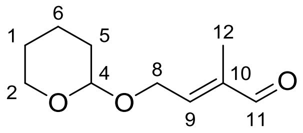

To a solution of dimethylallyl alcohol (5 g, 58 mmol) in DCM was added DHP (7.3 g, 87 mmol) and PPTS (1.5 g, 5.8 mmol) and the mixture was stirred overnight at room temperature and poured onto Et_2O. The organic phase was washed with brine, dried over $MgSO_4$ and concentrated *in vacuo* to obtain THP protected dimethylallyl alcohol **50**.

70% *t*BuOOH (12 mL, 88 mmol) was diluted with 3 volumes DCM, saturated with $MgSO_4$ and filtered. The filtrate was dried once more over $MgSO_4$ and filtered again. To the filtrate, **50** (3 g, 18 mmol) was added, followed by the addition of SeO_2 (195 mg, 1.8 mmol) and tetrazole (4 mL of 0.45 M solution in MeCN, 1.8 mmol). The mixture was stirred overnight at room temperature and coevaporated three times with toluene. The residue was taken up in Et_2O, the organic phase washed with $NaHCO_3$ and dried over $MgSO_4$ to give a 2 : 1 mixture of alcohol and aldehyde. Flash chromatography yielded **178** (1.6 g, 49%) and **52** (1 g, 28%).

A fraction of unpurified mixture (20 mg, 0.11 mmol) in DCM was added to a stirred solution of Na_2CO_3 (80 mg, 0.75 mmol) and MnO_2 (93 mg, 1 mmol) and stirred overnight. Et_2O was added, the mixture filtered through a plug of silica gel to give **52**(77% over all steps).**^{1}H NMR**(400 MHz, $CDCl_3$) δ = 9.45 (s, 1H, H-*11*), 6.62-6.58 (m, 1H, H-*9*), 4.69-4.66 (m, 1H, H-*4*), 4.60 – 4.53 (m, 1H, H-*8*), 4.39 – 4.30 (m, 1H, H-*8*), 3.91 – 3.83 (m, 1H, H-*2*), 3.61 – 3.49 (m, 1H, H-*2*), 1.89 – 1.47 (m, 6H, H-*1, 5, 6*), 1.76 (s, 3H, H-*12*).

[(2E)-2-methyl-4-(oxan-2-yloxy)but-2-en-1-yl](prop-2-en-1-yl)amine (53)

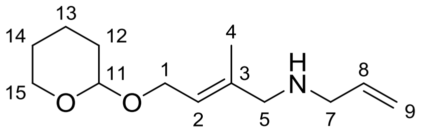

To a solution of aldehyde **52** (500 mg, 2.7 mmol) in DCM (10 mL) was added allylamine (0.24 mL, 3.3 mmol), $NaBH(OAc)_3$ (1.15 g, 5.4 mmol) and AcOH (0.28 mL, 4.9 mmol). The reaction mixture was stirred overnight and quenched by the addition of $NaHCO_3$. The aqueous phase was extracted with Et_2O (4 times) and the combined organic layers were dried over Na_2SO_4 and concentrated *in vacuo.* The crude was purified by flash chromatography (10% MeOH in DCM) to give **179** as a yellow oil (360 mg, 60%). **1H NMR** (400 MHz, $CDCl_3$) δ = 5.92 (ddt, *J*=16.5, 10.3, 6.1, 1H, H-*8*), 5.60 – 5.53 (m, 1H, H-*2*), 5.21 (dd, *J*=16.6, 1.6, 1H, H-*9*), 5.13 (dd, *J*=10.2, 1.6, 1H, H-*9*), 4.63 – 4.59 (m, 1H, H-*11*), 4.27 (dd, *J*=12.2, 6.3, 1H, H-*1*), 4.05 (dd, *J*=12.3, 7.1, 1H, H-*1*), 3.99 – 3:77 (m, 1H, H-*15*), 3.62 – 3.38 (m, 1H, H-*15*), 3.26 (d, *J*=6.1, 2H, H-*7*), 3.23 (s, 2H, H-*5*), 3.19 – 3.08 (m, 1H, H-*6*), 1.73 (s, 3H, H-*4*), 1.96 – 1.35 (m, 6H, H-*12, 13, 14*).

Ethyl (2Z)-2-hydroxy-3-(pyridin-3-yl)prop-2-enoate (57)

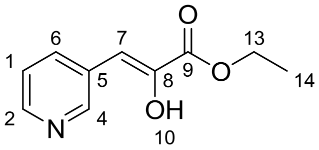

Following a procedure reported in the literature[186], 0.5 mL EtOH was added to a solution of NaH (2.24 g, 0.09 mol) in 50 mL Et_2O. The reaction mixture was cooled down to 0 °C, and under vigorously stirring N,N-dimethylglycine ethyl ester **56** (19.8 mL, 0.14 mol) and nicotinaldehyde **55** (4.4 mL, 0.05 mol) were added. The released hydrogen-gas was captured in a balloon filled with argon to keep the reaction inert. The reaction was allowed to warm up to room temperature and was stirred overnight. The mixture was diluted with EtOAc and washed with water. The organic layer was extracted with 1 N HCl and discarded. The aqueous layer was neutralized by addition of saturated $NaHCO_3$ solution and extracted three times with ethyl acetate. The combined organic layers were concentrated to give **57**, which was precipitated by addition of EtOAc (7.6 g, 74%). ^{1}**H NMR** (400 MHz, DMSO) δ = 9.89 (s, 1H, H-*10*), 8.84 (d, *J*=2.1, 1H, H-*4*), 8.41 (dd, *J*=4.8, 1.7, 1H, H-*2*), 8.22 (ddd, *J*=8.0, 2.2, 1.7, 1H, H-*6*), 7.38 (dd, *J*=8.0, 4.8, 1H, H-*1*), 6.43 (s, 1H, H-*7*), 4.28 (q, *J*=7.1, 2H, H-*13*), 1.30 (t, *J*=7.1, 3H, H-*14*). ^{13}**C NMR** (101 MHz, DMSO) δ = 164.13 (C-9), 150.10 (C-2), 147.79 (C-4), 143.12 (C-8), 135.70 (C-6), 130.76 (C-5), 123.48 (C-1), 106.76 (C-7), 61.53 (C-13), 14.08 (C-14).

Ethyl 2-(diethoxyphosphoryl)-2-hydroxy-3-(pyridin-3-yl)propanoate (59)

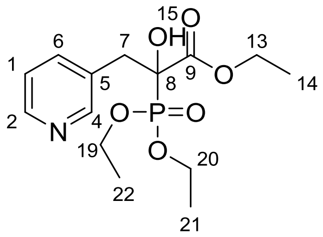

A procedure from the literature[189] was modified as follows: to a solution of **57** (1 g, 5.18 mmol) and triethylphosphite (1.3 mL, 7.76 mmol) in DCM at -10 °C was added 4M HCl in dioxane (1.9 mL, 7.75 mmol) The reaction mixture was stirred 1 h and then kept in the refrigerator overnight. The solvent and volatile by-products were evaporated *in vacuo* in a warm water bath (below 40 °C) to give the crude product. Flash chromatography with EtOAc/acetone (4: 1) gave the product as a yellow oil (1.2 g, 70%). **^{1}H NMR**(400 MHz, MeOD) δ = 8.47 (dd, *J*=2.3, 0.9, 1H, H-*4*), 8.45 (dd, *J*=4.9, 1.7, 1H, H-*2*), 7.79 (ddd, *J*=7.9, 2.3, 1.7, 1H, H-*6*), 7.41 (ddd, *J*=7.9, 4.9, 0.8, 1H, H-*1*), 5.02 (ddd, *J*=8.0, 8.0, 4.5, 1H, H-*15*), 4.23 (q, *J*=7.1, 2H, H-*13*), 4.16 – 4.03 (m, 2H, H-*19*), 3.91 (dq, *J*=14.2, 7.1, 2H, H-*20*), 3.31 (ddd, *J*=14.5, 4.4, 2.1, 1H, H-*7*), 3.18 (dd, *J*=14.5, 7.9, 1H, H-*7*), 1.28 (td, *J*=7.1, 1.1, 3H, H-*22*), 1.26 (t, *J*=7.2, 3H, H-*14*), 1.19 (td, *J*=7.1, 1.1, 3H, H-*21*)**^{13}C NMR** (101 MHz, MeOD) δ = 169.17 (d, *J*=2.9, C-9), 150.07 (C-4), 147.70 (C-2), 138.36 (C-6), 132.42 (C-5), 124.00 (C-1), 75.71 (d, *J*=5.8, C-8),64.67 (d, *J*=6.2, C-19), 64.39 (d, *J*=6.2, C-20), 61.81 (C-13), 35.92 (d, *J*=7.0, C-7), 15.15 (d, *J*=6.9, C-21, C-22), 13.27 (C-14). **LC-MS** (C18, ESI_MS): 331.96 [M+H]$^+$, 662.49 [2M+H]$^+$; R$_t$=5.63 min.

2-hydroxy-2-phosphono-3-(pyridin-3-yl)propanoic acid (3-PEHPC, 5)

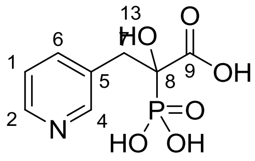

A procedure from the literature[158] was modified as follows: **59** (0.56 g, 1.7 mmol) was dissolved in 12 N HCl (5 mL) and the solution was heated at reflux for 5 hours. The solution was concentrated on a rotary evaporator to yield a viscous oil. This was dissolved in 0.2 ml water. EtOH was added to precipitate 5. The solid was transferred to an eppendorf tube, and washed several times with EtOH via centrifugation to yield the desired product 5 as a white solid (0.2 g, 50%).**^{1}H NMR** (400 MHz, D$_2$O) δ = 8.77 (d, *J*=1.8, 1H, H-*4*), 8.75 – 8.71 (m, 1H, H-*2*), 8.61-8.56 (m, 1H, H-*6*), 8.07 (ddd, *J*=8.1, 5.9, 0.9, 1H, H-*1*), 4.94 (ddd, *J*=9.3, 6.5, 4.4, 1H, H-*13*), 3.52 (dd, *J*=14.6, 4.4, 1H, H-*7*), 3.39 (dd, *J*=14.6, 6.5, 1H, H-*7*). **LC-MS** (C18, ESI_MS): 247.96 [M+H]$^+$, 494.82 [2M+H]$^+$; R$_t$=1.38 min.

Imidazo[1,2-a]pyridine-3-carbaldehyde (61)

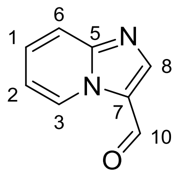

A procedure from the literature[190] was modified as follows: to a stirred solution of imidazo[1,2-a]pyridine **60** (3 g, 25 mmol) and dry DMF (2.4 mL, 32 mmol) in DCE (8 mL) was added $POCl_3$ (2.9 mL, 31 mmol) at 0 °C. The cooling bath was removed and the solution was stirred for 1h at room temperature. The reaction was allowed to warm up to room temperature and then put to reflux for 3 hours. The reaction mixture was poured on ice (50ml), neutralized by addition of 2N sodium hydroxide solution, and extracted with dichloromethane (3x40ml). The combined organic phases were dried over sodium sulfate and concentrated *in vacuo* to obtain **61** as a yellow solid which was used as a crude in the next step.**^{1}H NMR** (400 MHz, DMSO) δ = 9.91 (s, 1H, H-*10*), 9.37 (ddd, *J*=6.8, 1.2, 1.2 1H, H-*3*), 8.51 (s, 1H, H-*8*), 7.85 (ddd, *J*=9.0, 1.1, 1.1 1H, H-*6*), 7.67 (ddd, *J*=9.0, 6.9, 1.3, 1H, H-*1*), 7.29 (ddd, *J*=6.9, 6.9, 1.2, 1H, H-*2*).

Ethyl (2Z)-2-hydroxy-3-{imidazo[1,2-a]pyridin-3-yl}prop-2-enoate (62)

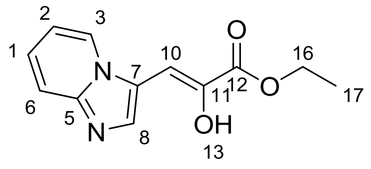

In analogy to the synthesis of **57**, 0.5 mL absolute EtOH was added to a solution of washed NaH (310 mg, 7.8 mmol) in 8 mL Et_2O. The reaction mixture was cooled down to 0 °C, and under vigorously stirring N,N-Dimethylglycine ethyl ester **56** (1.53 g, 11.7 mmol) and **61** (570 mg, 3.9 mmol) were added. The released hydrogen-gas was captured in a balloon filled with argon to keep the reaction inert. The reaction was allowed to warm up to room temperature and was stirred overnight. The reaction mixture was heated at 30 °C for 1 h, cooled down to 0°C and was quenched with water (4 mL). The mixture was diluted with 5 mL EtOAc. The organic phase was collected in a beaker which was made acidic with 1N HCl (5 mL) and stirred for 10 min. The mixture was checked for pH = 1 and was made alkaline by the addition of solid $NaHCO_3$. By this the expected product precipitated out and was collected by filtration to give **62** as a white solid (851 mg, 94%) **^{1}H NMR** (400 MHz, DMSO) δ = 9.69 (s, 1H, H-*13*), 8.69 (ad, *J*=7.0, 1H, H-*3*), 8.09 (s, 1H, H-*10*), 7.61 (ad, *J*=9.0, 1H, H-*6*), 7.31 (ddd, *J*=8.9, 6.9, 1.1, 1H, H-*1*), 7.00 (ddd, *J*=6.8, 6.8,1.2, 1H, H-*2*), 6.90 (s, 1H, H-*8*), 4.29 (q, *J*=7.1, 2H, H-*16*), 1.33 (t, *J*=7.1, 3H, H-*17*).**^{13}C NMR** (101 MHz, DMSO) δ = 163.96 (C-12), 139.62 (C-5), 136.09 (C-8), 125.05 (C-3), 124.92 (C-1), 120.14 (C-7), 117.17 (C-2), 112.73 (C-6), 97.03 (C-10), 61.17 (C-16), 14.18 (C-17).

Ethyl 2-(diethoxyphosphoryl)-2-hydroxy-3-{imidazo[1,2-a]pyridin-3-yl}propanoate (65)

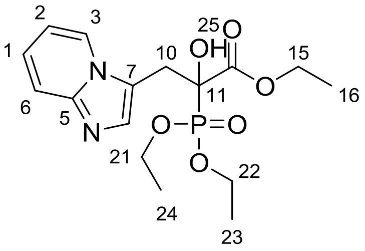

In analogy to the synthesis of **59**, to a solution of **62** (370 mg, 1.59 mmol) and triethylphosphite (0.41 mL, 2.4 mmol) in DCM (2 mL) and DMF (0.5 mL) at -10 °C was added 4M HCl in dioxane (0.6 mL, 2.4 mmol) The reaction mixture was stirred 1 h and then kept in the refrigerator overnight. The solvents were evaporated *in vacuo* to give an oily residue, which was purified by flash chromatography (EtOAc/Acetone 4:1) to give **65** as a yellow oil (437 mg, 74%) **R_f**: 0.18 (EtOAc/Acetone 4:1) **^{1}H NMR** (400 MHz, $CDCl_3$) δ = 8.14 (ddd, *J*=6.9, 1.1, 1.1, 1H, H-*3*), 7.60 (ddd, *J*=9.1, 1.1, 1.1, 1H, H-*6*), 7.53 (s, 1H, H-*8*), 7.17 (ddd, *J*=9.1, 6.7, 1.2, 1H, H-*1*), 6.85 (ddd, *J*=6.8, 6.8 1.2, 1H, H-*2*), 5.08 (ddd, *J*=8.6, 6.8, 5.3, 1H, H-*25*), 4.20 (q, *J*=7.1, 2H, H-*15*), 4.14 – 3.99 (m, 2H, H-*21*), 3.93 – 3.78 (m, 2H, H-*22*), 3.57 – 3.45 (m, 2H, H-*10*), 1.27 (td, *J*=7.1, 1.2, 3H, H-*23*), 1.23 (t, *J*=7.1, 3H, H-*16*), 1.16 (td, *J*=7.1, 1.1, 3H, H-*24*). **LC-MS** (C18, ESI_MS): 371.07 $[M+H]^+$, 740.49 $[2M+H]^+$; R_t=4.57 min.

2-hydroxy-3-{imidazo[1,2-a]pyridin-3-yl}-2-phosphonopropanoic acid (7)

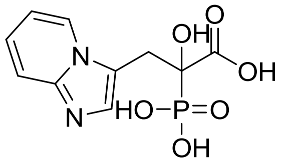

Analogous with the synthesis of 5, **65** (200 mg, 0.54 mmol) was dissolved in 12 N HCl (2.3 mL) and the solution was heated at reflux for 5 hours. The solution was concentrated on a rotary evaporator to yield a viscous oil. This was dissolved in 0.1 ml water. EtOH was added to precipitate 7. The solid was transferred to an eppendorf tube, and washed several times with EtOH via centrifugation to yield the desired product 7 as a white solid (93 mg, 60%). **LC-MS** (C18, ESI_MS): 286.93 $[M+H]^+$, 572.82 $[2M+H]^+$; R_t=1.39 min.

(3R)-7-bromo-3-[(4-hydroxyphenyl)methyl]-2,3,4,5-tetrahydro-1H-1,4-benzodiazepine-2,5-dione (180)

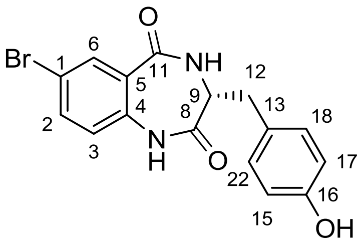

A stirred solution of 5-bromoisatoic anhydride **71** (5.57 g, 23 mmol), D-tyrosine methyl ester hydrochloride **72** (5.33 g, 23 mmol) and DMAP (60 mg, 0.5 mmol) in anhydrous pyridine (50 mL) was heated under reflux for 4 days. The reaction mixture was allowed to cool to room temperature and the solvents were evaporated. The residue was dissolved in EtOAc, washed with 10% HCl, brine, dried over Na_2SO_4 and concentrated *in vacuo*, giving crude **180** (7.7 g) as a dark brown solid. This crude material could immediately be used in the next step. For analysis, **180** was purified by flash column chromatography (cyclohexane:EtOAc 3:1 → EtOAc), affording pure **180** as a light brown solid (5.7 g, 68%) **R_f** 0.12 (EtOAc c-hexane [1:1]) **Mp**126.1 °C, **^{1}H NMR** (400 MHz, MeOD) δ = 7.89 (d, *J*=2.4, 1H, H-*6*), 7.64 (dd, *J*=8.6, 2.4, 1H, H-*2*), 7.05 (d, *J*=8.5, 2H, H-*18,* H-*22*), 7.02 (d, *J*=8.7, 1H, H-*3*), 6.66 (d, *J*=8.5, 2H, H-*15,* H-*17*), 3.97 (dd, *J*=8.8, 6.0, 1H, H-*9*), 3.14 (dd, *J*=14.3, 6.0, 1H, H-*12*), 2.84 (dd, *J*=14.4, 8.9, 1H, H-*12*).**^{13}C NMR** (101 MHz, MeOD)δ = 173.06 (C-8), 169.40 (C-11), 157.31 (C-16), 137.33 (C-4), 136.88 (C-2), 134.18 (C-6), 131.24 (C-18, C-22), 128.97 (C-13), 128.82 (C-5), 124.22 (C-3), 118.34 (C-1), 116.32 (C-15, C-17), 55.85 (C-9), 34.04 (C-12).**LC-MS** (C18, ESI_MS): 361.01 $[M+H]^+$, 722.59 $[2M+H]^+$; R_t=8.40 min. **HRMS (ESI):** calculated for $C_{16}H_{13}BrN_2O_3$ $[M+H]^+$: 361.0182, found: 361.0184.

4-{[(3R)-7-bromo-2,3,4,5-tetrahydro-1H-1,4-benzodiazepin-3-yl]methyl}phenol (**70**a)

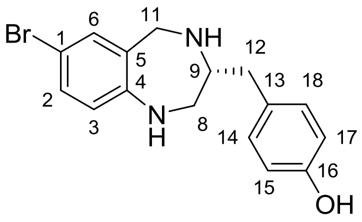

A solution of borane in THF (1M, 25 mL, 25 mmol) was slowly added to a stirred solution of crude **180** (1.78 g) in dry THF (45 mL). The reaction mixture was heated under reflux for 18h. After cooling to 0 °C, MeOH (9 mL) was added carefully, the solvents were evaporated and the residue was dissolved in MeOH (20 mL). To this solution, 7N HCl (5 mL) was added and the mixture was heated to dryness on a steam bath. The resulting solid was suspended in $NaHCO_3$ (sat, 100 mL) and the suspension was brought to pH 9 with 5N NaOH. The product was extracted with EtOAc (3×100 mL) and the combined organic layers were washed with brine, dried over Na_2SO_4 and concentrated *in vacuo*. Purification by flash column chromatography (EtOAc/acetone, 3:1) afforded **70**a as a light brown solid (672 mg, 67%) **R$_f$** 0.89 (EtOAc/acetone, 1:1) ; **Mp** 175.7 °C, **^{1}H NMR** (400 MHz, MeOD) δ = 7.21 (d, *J*=2.2, 1H, H-*6*), 7.14 (dd, *J*=8.4, 2.2, 1H, H-*2*), 7.04 (d, *J*=8.6, 2H, H-*14,* H-*18*), 6.73 (d, *J*=8.6, 1H, H-*3*), 6.72 (d, *J*=8.4, 2H, H-*15,* H-*17*), 3.83 (d, *J*=14.4, 1H, H-*11*), 3.71 (d, *J*=14.4, 1H, H-*11*), 3.25 (dd, *J*=13.3, 2.4, 1H, H-*8*), 2.99 (dddd, *J*=9.0, 7.7, 6.6, 2.4, 1H, H-*9*), 2.63 (dd, *J*=13.3, 6.7, 1H, H-*8*), 2.59 – 2.50 (m, 2H, H-*12*).**^{13}C NMR** (101 MHz, MeOD)δ = 155.97 (C-16), 150.03 (C-4), 133.19 (C-13), 132.03 (C-6), 130.22 (C-2), 130.12 (C-14, C-18), 129.14 (C-5), 120.29 (C-3), 115.24 (C-15, C-17), 111.86 (C-1), 62.50 (C-9), 52.74 (C-8), 51.66 (C-11), 38.95 (C-12). **LC-MS** (C18, ESI_MS): 333.03 $[M+H]^+$, R$_t$=5.92min **HRMS** (ESI)**:** calculated for $C_{16}H_{18}N_2Br$ 333.0597 $[M+H]^+$, found: 333.05997. $[\alpha]_D^{20}$+47.5 (*c*=1, MeOH/$CHCl_3$).

(3R)-3-[(4-hydroxyphenyl)methyl]-2,3,4,5-tetrahydro-1H-1,4-benzodiazepine-7-carbonitrile (**70**b)

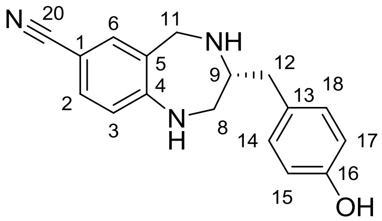

Three dry microwave tubes were charged with THB **70**a (400 mg, 1.2 mmol per tube) and CuCN (323 mg, 3.6 mmol per tube). The vessels were flushed with argon and sealed. Dry DMF (4 mL per tube) was added through the septum and the reaction mixtures were irradiated in the microwave at 200 ºC for 30 minutes. After cooling, the content of the 3 tubes was poured into 200 mL of a mixture of NH_4Cl (sat) and NH_4OH (25%) (pH = 8.6). EtOAc (200 mL) was added and the mixture was stirred for 1 h. The layers were separated, the aqueous layer was extracted with EtOAc (2×200 mL) and the combined organic layers were washed with a mixture of NH_4Cl (sat.) and NH_4OH (25%) (pH =

8.6) (2×100 mL), brine, dried over Na_2SO_4 and concentrated *in vacuo*. Purification by flash column chromatography (cyclohexane:EtOAc:Et_3N 74:25:1 → EtOAc:Et_3N 99:1) afforded **70**b as a light brown solid (672 mg, 67%) **R_f** 0.56 (EtOAc/DCM [1:10]); **Mp** 179.9 °C,**^{1}H NMR** (400 MHz, MeOD) δ = 7.36 (d, *J*=2.0, 1H, H-*6*), 7.32 (dd, *J*=8.3, 2.0, 1H, H-*2*), 7.05 (d, *J*=8.6, 2H, H-*14,* H-*18*), 6.80 (d, *J*=8.3, 1H, H-*3*), 6.74 (d, *J*=8.6, 2H, H-*15,* H-*17*), 3.99 (d, *J*=15.1, 1H, H-*11*), 3.84 (d, *J*=15.0, 1H, H-*11*), 3.41 (dd, *J*=13.9, 2.8, 1H, H-*8*), 3.16 – 3.08 (m, 1H, H-*9*), 2.81 (dd, *J*=13.9, 7.3, 1H, H-*8*), 2.70 (dd, *J*=13.6, 6.3, 1H, H-*12*), 2.63 (dd, *J*=13.6, 8.1, 1H, H-*12*).**^{13}C NMR** (101 MHz, MeOD) δ = 156.02 (C-16), 155.10 (C-4), 133.85 (C-2), 131.70 (C-6), 130.15 (C-14, C-18), 128.91 (C-13), 128.43 (C-5), 119.70 (C-20), 118.04 (C-3), 115.28 (C-15, C-17), 100.37 (C-1), 61.66 (C-9), 50.36 (C-8), 50.04 (C-11), 38.50 (C-12). **LC-MS** (C18, ESI_MS): 280.02 $[M+H]^+$, R_t=4.49 min **HRMS (ESI):** calculated for $C_{17}H_{18}N_3O$ $[M+H]^+$ 280.1444, found 280.1445. $[\boldsymbol{\alpha}]_{\boldsymbol{D}}^{\mathbf{20}}$ +47.5 (*c*=1, MeOH/$CHCl_3$).

4-{[(3R)-7-bromo-4-[(4-methoxybenzene)sulfonyl]-2,3,4,5-tetrahydro-1H-1,4-benzodiazepin-3-yl]methyl}phenol (73a)

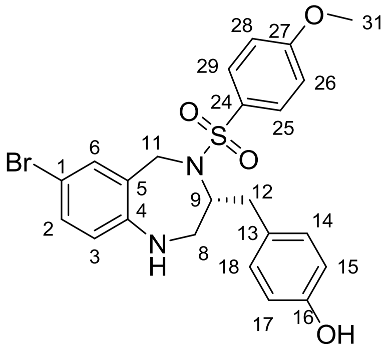

4-Methoxybenzenesulfonyl chloride (710 mg, 3.44 mmol) was added to a solution of THB **70**a (915 mg, 2.75 mmol) in anhydrous pyridine (12 mL) at 0 °C. The reaction mixture was allowed to warm to room temperature and stirred overnight. The solvent was evaporated, the residue was taken in a mixture of EtOAc and NH_4Cl (sat.) and stirred for 10 minutes. The layers were separated and the aqueous layer was extracted with EtOAc twice more. The combined organic layers were washed with brine, dried over Na_2SO_4 and concentrated *in vacuo*. Purification by flash column chromatography (DCM:EtOAc 95:5 → 80:20) afforded **73**a as a white solid (987 mg, 71%). **R_f** 0.56 (EtOAc/DCM [1:10]); **Mp** 179.9 °C, **^{1}H NMR** (400 MHz, MeOD) δ = 7.37 (d, *J*=9.0, 2H, H-*25,* H-*29*), 7.04 (d, *J*=8.4, 2H, H-*14,* H-*18*), 6.96 (d, *J*=2.1, 1H, H-*6*), 6.87 (dd, *J*=8.5, 2.2, 1H, H-*2*), 6.71 (d, *J*=8.5, 2H, H-*15,* H-*17*), 6.68 (d, *J*=9.0, 2H, H-*26,* H-*28*), 6.07 (d, *J*=8.5, 1H, H-*3*), 4.62 (d, *J*=17.2, 1H, H-*11*), 4.38 (d, *J*=17.2, 1H, H-*11*), 4.18 (ddd, *J*=13.9, 9.3, 4.7, 1H, H-*9*), 3.75 (s, 3H, H-*31*), 3.40 – 3.26 (m, 1H, H-*8*), 2.94 – 2.76 (m, 3H, H-*8,* H-*12*).**^{13}C NMR** (101 MHz, MeOD)δ = 161.40 (C-27), 154.62 (C-16), 146.47 (C-4), 130.49 (C-6), 130.29 (C-24), 128.84 (C-14, C-18), 128.71 (C-2), 127.95 (C-25, C-29), 127.26 (C-13), 122.45 (C-5), 116.67 (C-3), 113.73 (C-15, C-17), 111.69 (C-26, C-28), 107.59 (C-1), 60.75 (C-9), 53.45 (C-31), 46.03 (C-8), 44.29 (C-11), 37.05 (C-12). **LC-MS** (C18, ESI_MS):502.97 [M+H]$^+$ R$_t$=10.17min **HRMS (ESI):** calculated for $C_{23}H_{23}BrN_2O_4$ [M+H]$^+$ 503.0635, found 503.0630 $[\alpha]_D^{20}$+18.5 (*c*=1, MeOH/$CHCl_3$).

(3R)-3-[(4-hydroxyphenyl)methyl]-4-[(4-methoxybenzene)sulfonyl]-2,3,4,5-tetrahydro-1H-1,4-benzodiazepine-7-carbonitrile (73b)

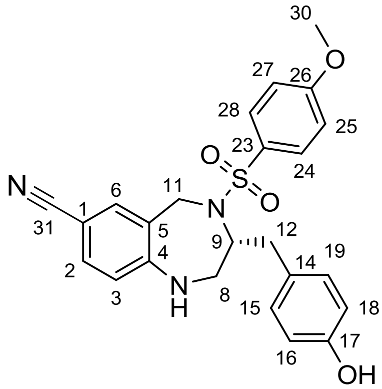

4-Methoxybenzenesulfonyl chloride **75** (234 mg, 1.13 mmol) was added to a solution of THB **70**b (301 mg, 1.1 mmol) in anhydrous pyridine (4 mL) at 0 °C. The reaction mixture was allowed to warm to room temperature and stirred overnight. Then, the solvent was evaporated. The residue was taken in a mixture of EtOAc and NH_4Cl (sat.) and stirred for 10 minutes. The layers were separated and the aqueous layer was extracted with EtOAc twice more. The combined organic layers were washed with brine, dried over Na_2SO_4 and concentrated *in vacuo*. Purification by flash column chromatography (DCM:EtOAc 95:5 → 80:20) afforded **(73**b**)** as a white solid (294 mg, 61%) **R*f*** 0.653 (DCM/MeOH, 10:1); **Mp** 123.8°C,**^{1}H NMR** (500 MHz, MeOD) δ = 7.38 (d, *J*=8.8, 2H, H-*24,* H-*28*), 7.13 (d, *J*=1.5, 1H, H-*6*), 7.09 (d, *J*=8.3, 2H, H-*15,* H-*19*), 7.03 (dd, *J*=8.4, 1.4, 1H, H-*2*), 6.74 (d, *J*=8.3, 2H, H-*16,* H-*18*), 6.69 (d, *J*=8.9, 2H, H-*25,* H-*27*), 6.10 (d, *J*=8.4, 1H, H-*3*), 4.69 (d, *J*=17.5, 1H, H-*11*), 4.44 (d, *J*=17.5, 1H, H-*11*), 4.35 – 4.27 (m, 1H, H-*9*), 3.76 (s, 3H, H-*30*), 3.53 (dd, *J*=15.0, 11.2, 1H, H-*8*), 3.02 (dd, *J*=15.0, 4.9, 1H, H-*8*), 2.92 (dd, *J*=13.5, 4.0, 1H, H-*12*), 2.79 (dd, *J*=13.4, 9.0, 1H, H-*12*).**^{13}C NMR** (126 MHz, MeOD) δ = 164.05 (C-26), 157.32 (C-17), 153.48 (C-4), 135.20 (C-6), 132.85 (C-23), 132.74 (C-2), 131.45 (C-15, C-19), 130.38 (C-24, C-28), 129.42 (C-14, C-18), 121.91 (C-5), 121.05 (C-31), 117.12 (C-3), 116.36 (C-16, C-18), 114.34 (C-25, C-27), 99.37 (C-1), 63.68 (C-9), 56.05 (C-30), 47.48 (C-8), 46.94 (C-11), 40.52 (C-12) **LC-MS** (C18, ESI_MS): 450.0 [M+H]$^+$R$_t$=9.23 min. **HRMS (ESI):** calculated for $C_{24}H_{24}N_3O_4S$ [M+H]$^+$ 450.1482, found 450.1477.$[\alpha]_D^{20}$ +133.4 (*c*=1, MeOH).

4-{[(3R)-7-bromo-4-[(4-methoxybenzene)sulfonyl]-1-[(1-methyl-1H-imidazol-5-yl)methyl]-2,3,4,5-tetrahydro-1H-1,4-benzodiazepin-3-yl]methyl}phenol (74a)

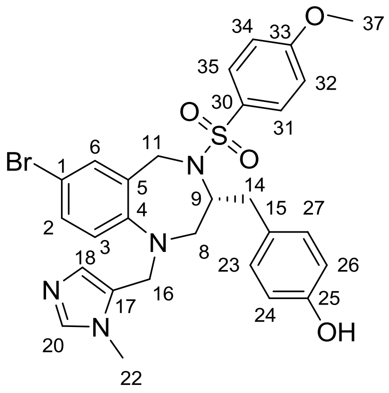

THB **73**a (2.1 g, 4.2 mmol) and N-methylimidazole carboxaldehyde **76** (574 mg, 5.2 mmol) were mixed in dry toluene (30 mL). To this stirred slurry, TFA (2.17 mL, 29.2 mmol) and TFAA (1.86 mL, 13.4 mmol) were added sequentially, while maintaining the temperature below 30 °C. The biphasic mixture was stirred vigorously for 2h at rt. Triethylsilane (1 mL, 6.3 mmol) was added and the reaction mixture was stirred overnight at rt. The reaction mixture was quenched with $NaHCO_3$ (sat.) and extracted with 3 times with EtOAc. The combined organic layers were washed with brine, dried over Na_2SO_4 and concentrated *in vacuo*. Purification by flash column chromatography (DCM:MeOH 98:2 → 90:10) afforded **74**a as a white solid (2.0 g, 80%). **R*f*** 0.67(DCM/MeOH [10:1]) **Mp** 286.4 °C; **^{1}H NMR** (500 MHz, DMSO) δ = 7.53 (s, 1H, H-*20*), 7.33 (d, *J*=8.8, 2H, H-*31,* H-*35*), 7.22 (d, *J*=1.7, 1H, H-*6*), 7.11 (d, *J*=8.3, 1H, H-*2*), 6.86 (d, *J*=8.2, 2H, H-*23,* H-*27*), 6.80 (d, *J*=8.9, 2H, H-*32,* H-*34*), 6.61 (d, *J*=8.2, 2H, H-*24,* H-*26*), 6.55 (s, 1H, H-*18*), 6.42 (bs, 1H, H-*3*), 4.58 (d, *J*=17.0, 1H, H-*16*), 4.41 (d, *J*=17.1, 1H, H-*16*), 4.33 – 4.09 (m, 1H, H-*9*), 4.04 (d, *J*=16.0, 1H, H-*11*), 3.77 (s, 3H, H-*37*), 3.76 (d, *J*=16.0, 1H, H-*11*), 3.49 (s, 3H, H-*22*), 3.47 – 3.41 (m, 1H, H-*8*), 2.82 (dd, *J*=14.9, 3.4, 1H, H-*8*), 2.66 (dd, *J*=13.8, 6.2, 1H, H-*14*), 2.44 – 2.05 (m, 1H, H-*14*). **^{13}C NMR** (101 MHz, DMSO) δ = 162.58 (C-33), 156.40 (C-25), 149.09 (C-4), 139.20 (C-20), 132.49 (C-6), 132.39 (C-17), 132.23 (C-30), 130.71 (C-2), 130.64 (C-23, C-27), 130.49 (C-15), 129.51 (C-31, C-35), 128.29 (C-5), 128.10 (C-18), 118.17 (C-3), 115.71 (C-24, C-26), 114.17 (C-32, C-34), 110.88 (C-1), 58.75 (C-9), 56.21 (C-37), 53.82 (C-8), 46.58 (C-11), 46.20 (C-16), 37.11 (C-14), 31.55 (C-22). **LC-MS** (C18, ESI_MS): 597.07 $[M+H]^+$ R_t=7.92min; **HRMS (ESI):** calculated for $C_{28}H_{30}BrN_4O_4S$ $[M+H]^+$: 597.1166, found: 597.1162, $[\alpha]_D^{20}$+18.5 (*c*=1, MeOH/$CHCl_3$).

(3R)-3-[(4-hydroxyphenyl)methyl]-4-[(4-methoxybenzene)sulfonyl]-1-[(1-methyl-1H-imidazol-5-yl)methyl]-2,3,4,5-tetrahydro-1H-1,4-benzodiazepine-7-carbonitrile (74b)

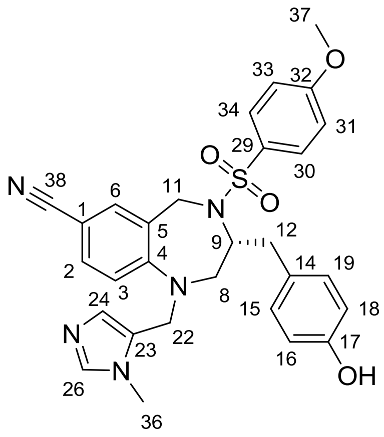

In analogy to the procedure described for **73a**, THB **73**b (389 mg, 0.87 mmol) and N-methylimidazole carboxaldehyde **76** (119 mg, 1.08 mmol) were mixed in dry toluene (8 mL). To this stirred slurry, TFA (450 µL, 6.1 mmol) and TFAA (384 µL, 2.8 mmol) were added sequentially, while maintaining the temperature below 30 °C. The biphasic mixture was stirred vigorously for 2h at rt. Triethylsilane (207 µL, 1.3 mmol) was added and the reaction mixture was stirred overnight at rt. The reaction mixture was quenched with $NaHCO_3$ (sat.) and extracted with three times EtOAc. The combined organic layers were washed with brine, dried over Na_2SO_4 and concentrated *in vacuo*. Purification by flash column chromatography (DCM:MeOH 98:2 → 90:10) afforded **74**b as a white solid (391 mg, 83%) **R_f** 0.53 (DCM/MeOH [10:1]); **Mp** 159.6 °C, **^{1}H NMR** (500 MHz, MeOD) δ = 7.57 (s, 1H, H-*26*), 7.41 (d, *J*=8.9, 2H, H-*30,* H-*34*), 7.36 (d, *J*=2.1, 1H, H-*6*), 7.27 (dd, *J*=8.6, 2.1, 1H, H-*2*), 7.00 (d, *J*=8.4, 2H, H-*15,* H-*19*), 6.82 (d, *J*=8.9, 2H, H-*31,* H-*33*), 6.71 (d, *J*=8.4, 2H, H-*16,* H-*18*), 6.58 (s, 1H, H-*24*), 6.44 (d, *J*=8.5, 1H, H-*3*), 4.69 (d, *J*=17.5, 1H, H-*22*), 4.59 (d, *J*=17.6, 1H, H-*22*), 4.32 – 4.25 (m, 1H, H-*9*), 4.18 (d, *J*=16.6, 1H, H-*11*), 3.82 (s, 3H, H-*37*), 3.82 (d, *J*=16.6, 1H, H-*11*), 3.73 (dd, *J*=15.6, 10.9, 1H, H-*8*), 3.55 (s, 3H, H-*36*), 3.07 (dd, *J*=15.5, 4.4, 1H, H-*8*), 2.84 (dd, *J*=13.6, 4.8, 1H, H-*12*), 2.68 (dd, *J*=13.6, 8.3, 1H, H-*12*). **^{13}C NMR** (126 MHz, $CDCl_3$ + 10% MeOD) δ = 162.78 (C-32), 155.90 (C-17), 152.05 (C-4), 138.95 (C-26), 137.54 (C-23), 133.83 (C-6), 132.43 (C-2), 131.74 (C-29), 129.95 (C-15, C-19), 129.16 (C-30, C-34), 128.06 (C-24), 127.28 (C-14), 126.53 (C-5), 119.35 (C-38), 115.74 (C-16, C-18), 114.83 (C-3), 113.81 (C-31, C-33), 107.47 (C-1), 58.65 (C-9), 55.68 (C-37), 52.61 (C-8), 46.79 (C-22), 45.35 (C-11), 38.02 (C-12), 31.63 (C-36). **LC-MS** (C18, ESI_MS): 544.14 $[M+H]^+$ R_t=6.91 min; **HRMS (ESI):** calculated for $C_{29}H_{30}N_5O_4S$ $[M+H]^+$: 544.2013, found: 544.1999. $[\alpha]_D^{20}$ +161.7 (*c*=1, $CHCl_3$).

General Remark about ^{13}C NMR of THBs

For many of the THBs, the highlighted quaternary carbons cannot be identified in regular ^{13}C NMR measurements even in concentrated samples with many scans. Therefore, these carbons have either been assigned using 2D techniques like HSQC, or in case of no clear long range correlations the structures are assigned by analogy.

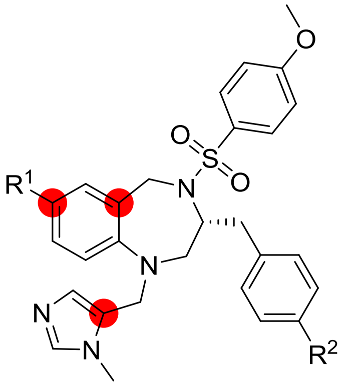

General Procedure I for O-methylation of THBs:

All reactions were carried out at a concentration of 50 mM of THB, 55 mM of alkyl halide and 75 mM of NaH in dry DMF. To a solution of 1 equiv. of THB in DMF, 1.5 equiv. of NaH and 1.1 equiv. of alkyl halide were added at 0 °C. The reaction mixture was allowed to warm up to room temperature and stirred overnight. The reaction mixture was quenched by the addition of brine and extracted three times with DCM. The combined organic layers were washed with brine, dried over Na_2SO_4 and concentrated *in vacuo*. The crude product was purified by column chromatography (DCM:MeOH 97:3).

(3R)-3-[(4-butoxyphenyl)methyl]-4-[(4-methoxybenzene)sulfonyl]-1-[(1-methyl-1H-imidazol-5-yl)methyl]-2,3,4,5-tetrahydro-1H-1,4-benzodiazepine-7-carbonitrile(87)

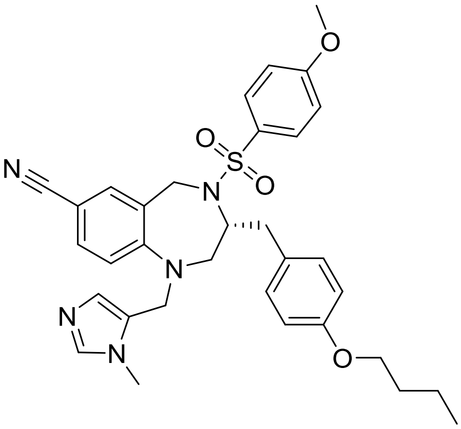

According to General Procedure I, reaction between THB **74**b (40 mg, 74 µmol) and n-butyl bromide (9 µL, 81 µmol) afforded **87** as a white solid (40 mg, 92%). **^{1}H NMR** (400 MHz, $CDCl_3$) δ 7.44 (s, 1H), 7.37 (d, J = 8.8 Hz, 2H), 7.27 (s, 1H), 7.24 (d, J = 8.6 Hz, 1H), 6.99 (d, J = 8.5 Hz, 2H), 6.80 (d, J = 8.5 Hz, 2H), 6.71 (d, J = 8.9 Hz, 2H), 6.67 (s, 1H), 6.37 (d, J = 8.5 Hz, 1H), 4.57

(d, *J* = 17.6 Hz, 1H), 4.39 (d, *J* = 17.6 Hz, 1H), 4.27 – 4.12 (m, *J* = 7.4 Hz, 1H), 3.95 (d, *J* = 16.3 Hz, 1H), 3.94 (t, *J* = 6.6 Hz, 2H), 3.79 (s, 3H), 3.71 (d, *J* = 16.3 Hz, 1H), 3.60 – 3.48 (m, 1H), 3.49 (s, 3H), 3.05 (dd, *J* = 15.4, 4.3 Hz, 1H), 2.83 (dd, *J* = 13.8, 4.6 Hz, 1H), 2.65 (dd, *J* = 13.7, 8.1 Hz, 1H), 1.82 – 1.69 (m, 2H), 1.58 – 1.41 (m, 2H), 0.98 (t, *J* = 7.4 Hz, 3H); **^{13}C NMR** (101 MHz, $CDCl_3$) δ 162.68 (C), 158.31 (C), 152.03 (C), 139.28 (CH), 133.92 (CH), 132.40 (CH), 131.85 (C), 130.33 (2×CH), 129.28 (2×CH), 128.64 (CH), 128.17 (C), 119.41 (C), 115.23 (CH), 114.82 (2×CH), 113.67 (2×CH), 101.88 (C,), 67.85 (CH_2), 58.21 (CH), 55.76 (CH_3), 53.34 (CH_2), 46.94 (CH_2), 46.38 (CH_2), 38.26 (CH_2), 31.57 (CH_3), 31.47 (CH_2), 19.37 (CH_2), 13.99 (CH_3); **LC-MS** (C4, ESI_MS) 600.2 $[M+H]^+$; R_t = 7.93 min; **HRMS (ESI):**calculated for $C_{33}H_{38}N_5O_4S$ $[M+H]^+$ 600.2632, found 600.2639.

(3R)-4-[(4-methoxybenzene)sulfonyl]-1-[(1-methyl-1H-imidazol-5-yl)methyl]-3-({4-[(3-methylbut-2-en-1-yl)oxy]phenyl}methyl)-2,3,4,5-tetrahydro-1H-1,4-benzodiazepine-7-carbonitrile(88)

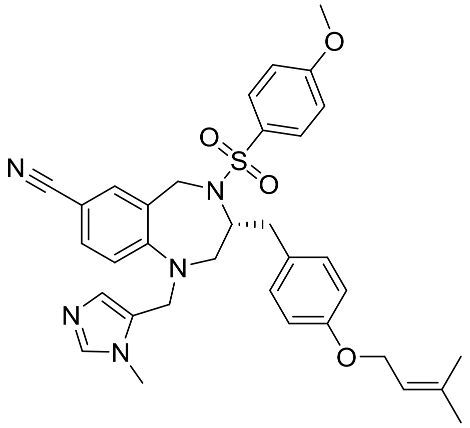

According to General Procedure I, reaction between THB **74**b (50 mg, 92 µmol) and 1-bromo-3-methylbut-2-ene (12 µL, 101 µmol) afforded **88** as a white solid (53 mg, 94%). **^{1}H NMR** (400 MHz, $CDCl_3$) δ 7.40 (s, 1H), 7.33 (d, *J* = 8.7 Hz, 2H), 7.23 (s, 1H), 7.19 (d, *J* = 8.6 Hz, 1H), 6.95 (d, *J* = 8.5 Hz, 2H), 6.78 (d, *J* = 8.4 Hz, 2H), 6.67 (d, *J* = 8.7 Hz, 2H), 6.63 (s, 1H), 6.33 (d, *J* = 8.5 Hz, 1H), 5.45 (t, *J* = 6.7 Hz, 1H), 4.53 (d, *J* = 17.7 Hz, 1H), 4.45 (d, *J* = 6.7 Hz, 2H), 4.36 (d, *J* = 17.5 Hz, 1H), 4.20 – 4.09 (m, *J* = 10.5, 7.8 Hz, 1H), 3.94 (d, *J* = 16.3 Hz, 1H), 3.75 (s, 3H), 3.67 (d, *J* = 16.3 Hz, 1H), 3.50 (dd, *J* = 15.3, 10.9 Hz, 1H), 3.45 (s, 3H), 3.01 (dd, *J* = 15.4, 4.4 Hz, 1H), 2.79 (dd, *J* = 13.7, 4.6 Hz, 1H), 2.61 (dd, *J* = 13.6, 7.9 Hz, 1H), 1.76 (s, 3H), 1.71 (s, 3H); **^{13}C NMR** (101 MHz, $CDCl_3$) δ 162.68 (C), 158.01 (C), 152.02 (C), 138.35 (C), 133.92 (CH), 132.39 (CH), 131.81 (C), 130.32 (2×CH), 129.26 (2×CH), 128.50 (CH), 128.32 (C), 126.48 (C), 124.61 (C), 119.68 (CH), 119.41 (C), 115.23 (CH), 114.97 (2×CH), 113.66 (2×CH), 109.89 (CH), 101.85 (C), 64.92 (CH_2), 58.22 (CH), 55.75 (CH_3), 53.34 (CH_2), 46.92 (CH_2), 46.36 (CH_2), 38.26 (CH_2), 31.57 (CH_3), 25.94 (CH_3), 18.33 (CH_3); **LC-MS** (C4, ESI_MS) 612.2 $[M+H]^+$; R_t = 7.88 min; **HRMS (ESI):**calculated for $C_{34}H_{38}N_5O_4S$ $[M+H]^+$ 612.2639, found 612.2633.

(3R)-3-{[4-(benzyloxy)phenyl]methyl}-4-[(4-methoxybenzene)sulfonyl]-1-[(1-methyl-1H-imidazol-5-yl)methyl]-2,3,4,5-tetrahydro-1H-1,4-benzodiazepine-7-carbonitrile (89)

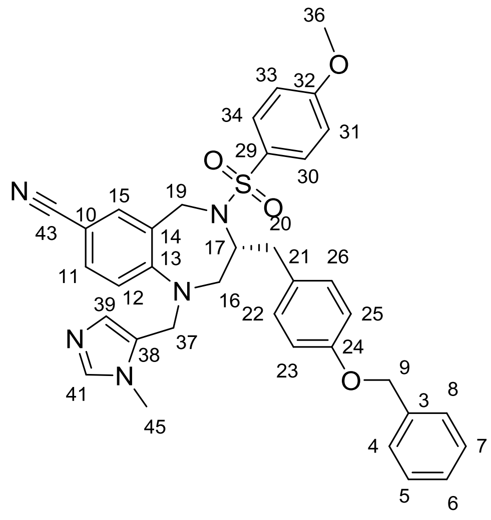

According to General Procedure I, reaction between THB **74**b (50 mg, 92 µmol) and benzyl bromide (12 µL, 101 µmol) afforded **89** as a white solid (50 mg, 85%). **R_f** 0.36 (DCM/MeOH [10:1]); **^{1}H NMR** (400 MHz, MeOD) δ = 7.51 (s, 1H, H-*41*), 7.43 – 7.40 (m, 2H, H-*5,* H-*7*), 7.37 (d, *J*=9.0, 2H, H-*30,* H-*34*), 7.39 – 7.32 (m, 3H, H-*4, 6, 8*), 7.30 (d, *J*=2.0, 1H, H-*15*), 7.22 (dd, *J*=8.6, 2.0, 1H, H-*11*), 7.06 (d, *J*=8.7, 2H, H-*22,* H-*26*), 6.88 (d, *J*=8.7, 2H, H-*23,* H-*25*), 6.77 (d, *J*=9.0, 2H, H-*31,* H-*33*), 6.55 (s, 1H, H-*39*), 6.39 (d, *J*=8.6, 1H, H-*12*), 5.03 (s, 2H, H-*9*), 4.63 (d, *J*=17.6, 1H, H-*19*), 4.54 (d, *J*=17.6, 1H, H-*19*), 4.31 – 4.20 (m, 1H, H-*17*), 4.14 (d, *J*=16.5, 1H, H-*37*), 3.77 (d, *J*=16.5, 2H, H-*37*), 3.77 (s, 3H, H-*36*), 3.69 (dd, *J*=15.5, 11.0, 1H, H-*16*), 3.49 (s, 3H, H-*45*), 3.04 (dd, *J*=15.5, 4.5, 1H, H-*16*), 2.82 (dd, *J*=13.7, 4.5, 1H, H-*20*), 2.66 (dd, *J*=13.7, 8.1, 1H, H-*20*). **^{13}C NMR** (101 MHz, MeOD) δ = 163.01 (C-32), 157.91 (C-24), 146.69 (C-13)139.00 (C-41), 137.60 (C-3), 133.82 (C-15), 132.05 (C-11), 131.82 (C-29), 130.25 (C-22, C-26), 129.51 (C-21), 129.13 (C-5, C-7), 128.30 (C-4, C-8), 127.67 (C-6), 127.43 (C-30, C-34), 126.56 (C-39), 119.37 (C-43), 115.03 (C-12), 114.90 (C-31, C-33), 113.56 (C-23, C-25), 100.47 (C-10), 69.80 (C-9), 59.12 (C-17), 55.03 (C-36), 53.10 (C-16), 46.52 (C-19), 45.78 (C-37), 37.92 (C-20), 30.62 (C-45). **LC-MS** (C18, ESI_MS): 634.05 $[M+H]^+$, R_t=8.01 min. **HRMS(ESI):** calculated for $C_{36}H_{36}N_5O_4S$ $[M+H]^+$ 634.2483, found 634.2470.

(3R)-3-[(4-{[(2E)-3,7-dimethylocta-2,6-dien-1-yl]oxy}phenyl)methyl]-4-[(4-methoxybenzene)sulfonyl]-1-[(1-methyl-1H-imidazol-5-yl)methyl]-2,3,4,5-tetrahydro-1H-1,4- benzodiazepine-7-carbonitrile (90)

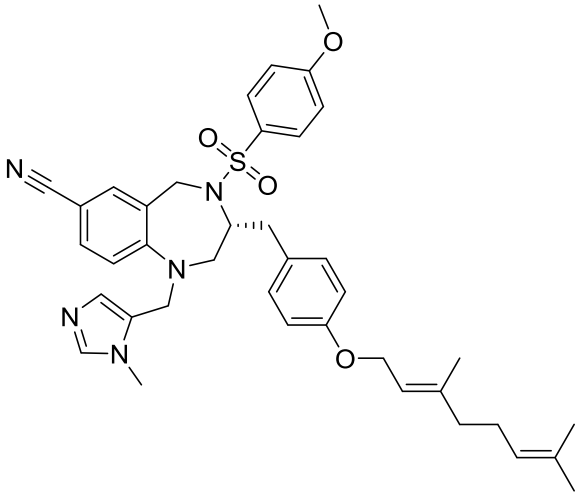

According to General Procedure I, reaction between THB **74**b (50 mg, 92 µmol) and geranyl bromide (21 µL, 101 µmol) afforded **90** as a white solid (59 mg, 94%). **^{1}H NMR** (400 MHz, CDCl$_3$) δ 7.39 (s, 1H), 7.30 (d, *J* = 8.8 Hz, 2H), 7.20 (s, 1H), 7.16 (d, *J* = 8.6 Hz, 1H), 6.92 (d, *J* = 8.4 Hz, 2H), 6.74 (d, *J* = 8.3 Hz, 2H), 6.64 (d, *J* = 8.8 Hz, 2H), 6.60 (s, 1H), 6.30 (d, *J* = 8.5 Hz, 1H), 5.41 (t, *J* = 6.2 Hz, 1H), 5.02 (t, *J* = 6.0 Hz, 1H), 4.49 (d, *J* = 17.7 Hz, 1H), 4.44 (d, *J* = 6.3 Hz, 2H), 4.32 (d, *J* = 17.5 Hz, 1H), 4.16 – 4.06 (m, 1H), 3.91 (d, *J* = 16.2 Hz, 1H), 3.71 (s, 3H), 3.68 – 3.60 (m, 1H), 3.52 – 3.44 (m, *J* = 15.4 Hz, 1H), 3.42 (s, 3H), 2.98 (dd, *J* = 15.3, 4.0 Hz, 1H), 2.76 (dd, *J* = 14.0, 4.4 Hz, 1H), 2.58 (dd, *J* = 13.7, 7.9 Hz, 1H), 2.14 – 1.92 (m, *J* = 15.5 Hz, 4H), 1.66 (s, 3H), 1.61 (s, 3H), 1.53 (s, 3H); **^{13}C NMR** (101 MHz, CDCl$_3$) δ 162.70 (C), 158.06 (C), 152.04 (C), 141.41 (C), 139.58 (C), 133.94 (CH), 132.42 (CH), 131.94 (C), 131.83 (C), 130.33 (2×CH), 129.28 (2×CH), 128.30 (C), 126.56 (C), 123.90 (CH), 119.50 (CH), 119.27 (C), 115.23 (CH), 115.03 (2×CH), 113.69 (2×CH), 113.32 (CH), 109.89 (CH), 101.87 (C), 65.04 (CH$_2$), 58.22 (CH), 55.77 (CH$_3$), 53.36 (CH$_2$), 46.93 (CH$_2$), 46.35 (CH$_2$), 39.68 (CH$_2$), 38.25 (CH$_2$), 31.63 (CH$_3$), 26.45 (CH$_2$), 25.81 (CH$_3$), 17.83 (CH$_3$), 16.81 (CH$_3$); **LC-MS** (C4, ESI_MS) 680.2 [M+H]$^+$; R$_t$ = 8.82 min; **HRMS (ESI):**calculated for $C_{39}H_{46}N_5O_4S$ [M+H]$^+$ 680.3265, found 680.3261.

General Procedure II for O-aminoacylation of THBs**:**

All reactions were carried out at a concentration of 100 mM of THB and 110 mM of isocyanate in dichloromethane. To a solution of 1 equiv. of THB and 1.1 equiv. of Et$_3$N at 0 °C was added 1.1 equiv. of isocyanate. The reaction mixture was stirred overnight, diluted with dichloromethane, washed with NaHCO$_3$ (sat), dried over Na$_2$SO$_4$ and concentrated *in vacuo*. The crude product was purified by column chromatography (DCM:MeOH 98:3).

4-{[(3R)-7-cyano-4-[(4-methoxybenzene)sulfonyl]-1-[(1-methyl-1H-imidazol-5-yl)methyl]-2,3,4,5-tetrahydro-1H-1,4-benzodiazepin-3-yl]methyl}phenyl-N-hexylcarbamate (91)

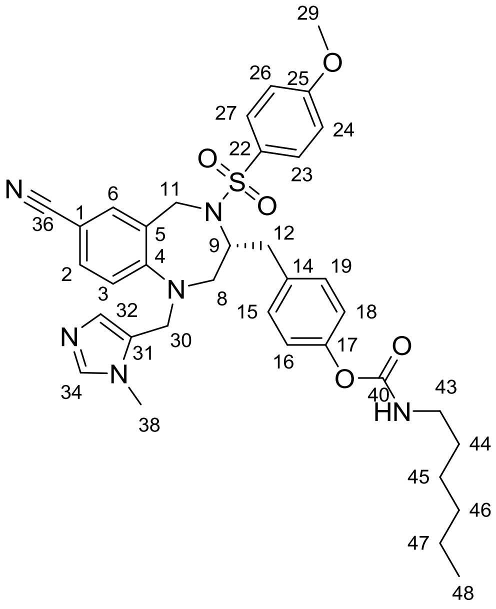

According to General Procedure **II**, reaction between THB **74**b (50 mg, 92 µmol) and hexylisocyanate (15 µL, 110 µmol) afforded **91** as a white solid (43 mg, 72%) **R_f**: 0.49 (DCM/MeOH, 10:1) **Mp** 98.3 °C, **^{1}H NMR** (400 MHz, MeOD) δ = 7.60 – 7.53 (m, 1H, H-*34*), 7.38 (d, *J*=9.0, 2H, H-*23,* H-*27*), 7.31 (d, *J*=1.9, 1H, H-*6*), 7.23 (dd, *J*=8.6, 2.0, 1H, H-*2*), 7.15 (d, *J*=8.4, 2H, H-*15,* H-*19*), 7.00 (d, *J*=8.5, 2H, H-*16,* H-*18*), 6.79 (d, *J*=9.0, 2H, H-*24,* H-*26*), 6.58 (s, 1H, H-*32*), 6.40 (d, *J*=8.6, 1H, H-*3*), 4.70 (d, *J*=17.6, 1H, H-*11*), 4.57 (d, *J*=17.7, 1H, H-*11*), 4.35 – 4.22 (m, 1H, H-*9*), 4.15 (d, *J*=16.5, 1H, H-*30*), 3.79 (s, 3H, H-*29*), 3.78 (d, *J*=16.5, 1H, H-*30*), 3.73 (dd, *J*=15.4, 10.1, 2H, H-*8*), 3.50 (s, 3H, H-*38*), 3.16 (t, *J*=7.1, 2H, H-*43*), 3.04 (dd, *J*=15.5, 4.3, 1H, H-*8*), 2.89 (dd, *J*=13.6, 5.0, 1H, H-*12*), 2.73 (dd, *J*=13.5, 8.0, 1H, H-*12*), 1.60 – 1.49 (m, 2H, H-*44*), 1.41 – 1.26 (m, 6H, H-*45*), 0.92 (t, *J*=6.9, 3H, H-*48*).**^{13}C NMR** (101 MHz, MeOD) δ = 164.23 (C-25), 157.20 (C-40), 153.43 (C-4), 151.51 (C-17), 139.84 (C-34*), 135.43 (C-14), 135.01 (C-6), 133.24 (C-2), 132.85 (C-22), 131.23 (C-15, C-19), 130.35 (C-23, C-27), 128.71 (C-31''), 127.14 (C-32*), 125.42 (C-5''), 122.90 (C-16, C-18), 120.58 (C-36), 116.08 (C-3), 114.78 (C-24, C-26), 101.56 (C-1), 60.35 (C-9), 56.23 (C-29), 54.07 (C-8), 47.72 (C-11), 46.80 (C-30), 42.04 (C-43), 39.38 (C-12), 32.66 (C-46), 30.75 (C-38), 27.56 (C-45), 23.65 (C-47), 14.39 (C-48). (*assigned with HSQC, **''**assigned with HMBC). **LC-MS** (C18, ESI_MS) 672.29 $[M+H]^+$ R_t=8.80 min **HRMS (ESI)** calculated for $C_{36}H_{42}N_6O_5S$ $[M+H]^+$: 671.3010, found:671.3005. $[\alpha]_D^{20}$ +48.7(*c*=1, MeOH).

4-{[(3R)-7-cyano-4-[(4-methoxybenzene)sulfonyl]-1-[(1-methyl-1H-imidazol-5-yl)methyl]-2,3,4,5-tetrahydro-1H-1,4-benzodiazepin-3-yl]methyl}phenyl-N-benzylcarbamate (92)

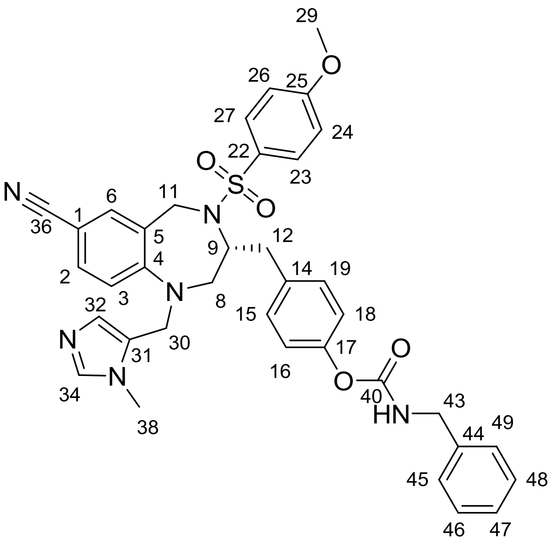

According to General Procedure **II**, reaction between THB **74**b (50 mg, 92 µmol) and benzylisocyanate (12 µL, 110 µmol) afforded **92** as a white solid (60 mg, 96%) **R_f** 0.5 (DCM/MeOH, 10:1) **Mp** 116.8 °C, **^{1}H NMR** (500 MHz, MeOD) δ = 7.60 (s, 1H, H-*34*), 7.38 (d, *J*=8.8, 2H, H-*23*, H-*27*), 7.36 – 7.31 (m, 4H, H-*6*, H-*45*, H-*47*, H-*49*), 7.30 – 7.21 (m, 3H, H-*2*, H-*46*, H-*48*), 7.16 (d, *J*=8.2, 2H, H-*15*, H-*19*), 7.03 (d, *J*=8.3, 2H, H-*16*, H-*18*), 6.80 (d, *J*=8.8, 2H, H-*24*, H-*26*), 6.60 (s, 1H, H-*32*), 6.42 (d, *J*=8.4, 1H, H-*3*), 4.71 (d, *J*=17.7, 1H, H-*11*), 4.58 (d, *J*=17.7, 1H, H-*11*), 4.36 (s, 2H, H-*43*), 4.31 – 4.24 (m, 1H, H-*9*), 4.17 (d, *J*=16.4, 1H, H-*30*), 3.83 – 3.75 (m, 1H, H-*30*), 3.78 (s, 3H, H-*29*), 3.73 (dd, *J*=15.6, 11.1, 1H, H-*8*), 3.51 (s, 3H, H-*38*), 3.04 (dd, *J*=15.5, 4.1, 1H, H-*8*), 2.90 (dd, *J*=13.6, 5.1, 1H, H-*12*), 2.74 (dd, *J*=13.7, 8.0, 1H, H-*12*). **^{13}C NMR** (126 MHz, MeOD) δ = 164.28 (C-25), 157.50 (C-40), 153.45 (C-4), 151.51 (C-17), 140.37 (C-44), 139.97 (C-34), 135.61 (C-14), 135.04 (C-6), 133.26 (C-2), 132.88 (C-22), 131.26 (C-15, C-19), 130.38 (C-23, C-27), 129.58 (C-45, C-49),129.06(C-31), 128.41 (C-46, C-48), 128.29 (C-47), 127.51 (C-32), 125.89 (C-5), 122.93 (C-16, C-18), 120.53 (C-36), 116.11 (C-3), 114.80 (C-26, C-28), 101.70 (C-1), 60.39 (C-9), 56.22 (C-29), 54.08 (C-8), 47.72 (C-11), 46.75 (C-30), 45.72 (C-43), 39.36 (C-12), 31.91 (C-38). **LC-MS** (C18, ESI_MS): 677.23 $[M+H]^+$ R_t=8.14 min. **HRMS (ESI)** calculated for $C_{34}H_{38}N_6O_5S$ $[M+H]^+$: 677.2541, found: 677.2536. $[\boldsymbol{\alpha}]_{\boldsymbol{D}}^{\mathbf{20}}$ +36.9 (*c*=1, MeOH).

4-{[(3R)-7-cyano-4-[(4-methoxybenzene)sulfonyl]-1-[(1-methyl-1H-imidazol-5-yl)methyl]-2,3,4,5-tetrahydro-1H-1,4-benzodiazepin-3-yl]methyl}phenyl-N,N-diethylcarbamate (93)

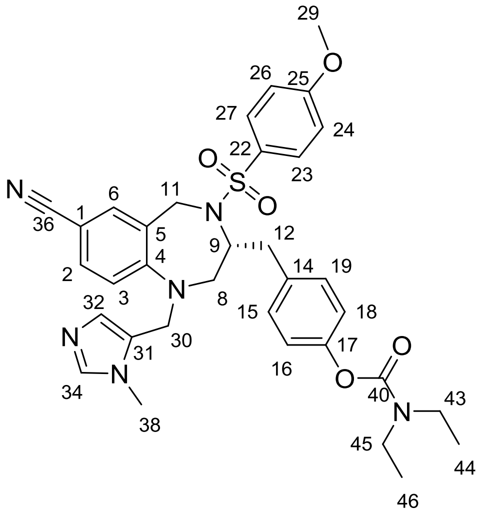

According to General Procedure **II**, reaction between THB **74**b (50 mg, 92 µmol) and diethylcarbamoyl chloride (15 µL, 110 µmol) afforded **90** as a white solid (43 mg, 72%).**R_f** 0.56 (DCM/MeOH, 10:1) **Mp** 113.7 °C, **^{1}H NMR** (500 MHz, MeOD) δ = 7.69 (s, 1H, H-*34*), 7.39 (d, *J*=8.9, 2H, H-*27*), 7.32 (d, *J*=2.0, 1H, H-*6*), 7.23 (dd, *J*=8.6, 2.0, 1H, H-*2*), 7.18 (d, *J*=8.3, 2H, H-*19*), 7.01 (d, *J*=8.4, 2H, H-*18*), 6.81 (d, *J*=8.9, 2H, H-*26*), 6.64 (s, 1H, H-*32*), 6.41 (d, *J*=8.8, 1H, H-*3*), 4.71 (d, *J*=17.6, 1H, H-*11*), 4.58 (d, *J*=17.7, 1H, H-*11*), 4.40 – 4.25 (m, 1H, H-*9*), 4.19 (d, *J*=16.5, 1H, H-*30*), 3.79 (s, 3H, H-*29*), 3.88 – 3.68 (m, 2H, H-*8,* H-*30*), 3.54 (s, 3H, H-*38*), 3.39 (d, *J*=7.2, 2H, H-*43*), 3.38 (d, *J*=7.2, 2H, H-*45*), 3.06 (dd, *J*=15.4, 4.3, 1H, H-*8*), 2.90 (dd, *J*=13.3, 4.3, 1H, H-*12*), 2.76 (dd, *J*=13.3, 8.3, 1H, H-*12*), 1.27 (t, *J*=7.2, 3H, H-*46*), 1.19 (t, *J*=7.2, 3H, H-*44*).**^{13}C NMR** (126 MHz, MeOD) δ = 164.27 (C-25), 156.17 (C-40), 151.64 (C-4), 149.92 (C-17), 139.97 (C-34), 135.68 (C-6), 135.04 (C-14), 133.25 (C-2), 132.91 (C-22), 131.32 (C-15, C-19), 130.37 (C-23, C-27), 129.11 (C-31), 126.99 (C-32), 125.39 (C-5), 122.99 (C-16, C-18), 120.53 (C-36), 116.10 (C-3), 114.80 (C-24, C-26), 99.09 (C-1), 60.35 (C-9), 56.23 (C-29), 54.12 (C-8), 47.74 (C-11), 46.81 (C-30), 43.44 (C-45), 43.20 (C-43), 39.37 (C-12), 32.05 (C-38), 14.49 (C-46), 13.60 (C-44). **LC-MS** (C18, ESI_MS) 643.28 $[M+H]^+$ R_t=8.15 min **HRMS (ESI):** calculated for $C_{34}H_{39}N_6O_5S$ $[M+H]^+$: 643.2697, found: 643.2692.$[\alpha]_D^{20}$ + 63.5 (*c*=1, MeOH).

General Procedure III for O-triflation of THBs

All reactions were carried out at a concentration of 0.1 M of THB, 0.15 M of N-phenylbis(trifluoromethanesulfonimide) (**86**) and 0.3 M of Et$_3$N in dry DCM. To a solution of 1 equiv. of THB and 3 equiv. of Et$_3$N in DCM, 1.5 equiv. of **86** was added at 0 °C. The reaction mixture was allowed to warm up to room temperature and stirred overnight. The reaction mixture was quenched by the addition of NaHCO$_3$ (sat.) and extracted with DCM (3×). The combined organic layers were washed with brine, dried over Na$_2$SO$_4$ and concentrated *in vacuo*. The crude product was purified by column chromatography (DCM:MeOH 98:2 → 95:5).

4-{[(3R)-7-cyano-4-[(4-methoxybenzene)sulfonyl]-1-[(1-methyl-1H-imidazol-5-yl)methyl]-2,3,4,5-tetrahydro-1H-1,4-benzodiazepin-3-yl]methyl}phenyl-trifluoromethanesulfonate (83)

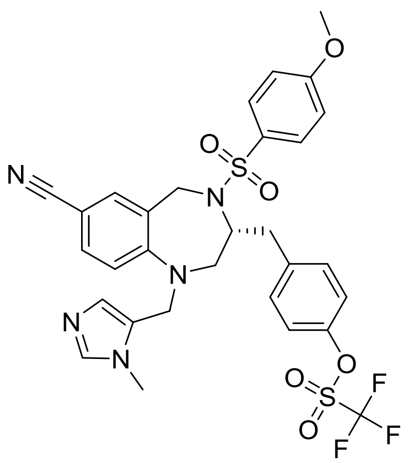

According to General Procedure **III**, reaction between THB **74**b (287 mg, 0.53 mmol) and **86** (283 mg, 0.79 mmol) afforded **83** as a white solid (336 mg, 94%).^{1}**H NMR** (500 MHz, $CDCl_3$) δ 7.53 (s, 1H), 7.36 (d, *J* = 8.9 Hz, 2H), 7.31 – 7.26 (m, *J* = 10.6 Hz, 2H), 7.19 (d, *J* = 8.7 Hz, 2H), 7.15 (d, *J* = 8.7 Hz, 2H), 6.76 – 6.69 (m, *J* = 8.8 Hz, 3H), 6.46 (d, *J* = 8.4 Hz, 1H), 4.59 (d, *J* = 17.4 Hz, 1H), 4.45 (d, *J* = 17.4 Hz, 1H), 4.24 – 4.13 (m, 1H), 4.03 (d, *J* = 15.9 Hz, 1H), 3.85 – 3.73 (m, *J* = 15.4 Hz, 1H), 3.79 (s, 3H), 3.51 (s, 3H), 3.56 – 3.46 (m, 1H), 3.02 (dd, *J* = 15.3, 4.3 Hz, 1H), 2.89 (dd, *J* = 13.8, 5.5 Hz, 1H), 2.62 (dd, *J* = 13.7, 7.7 Hz, 1H); ^{13}**C NMR** (126 MHz, $CDCl_3$) δ 162.98 (C), 152.11 (C), 148.51 (C), 139.19 (CH), 137.49 (C), 134.51 (C), 134.01 (CH), 132.66 (CH), 131.52 (C), 131.15 (2×CH), 129.31 (2×CH), 128.37 (CH), 126.59 (C), 121.83 (2×CH), 119.26 (C), 115.44 (CH), 113.87 (2×CH), 109.70 (C), 102.46 (C), 58.14 (CH), 55.83 (CH_3), 53.43 (CH_2), 46.70 (CH_2), 46.11 (CH_2), 38.09 (CH_2), 31.77 (CH_3); **LC-MS** (C4, ESI_MS) 676.1 $[M+H]^+$; R_t = 7.99 min; **HRMS (ESI):**calculated for $C_{30}H_{29}F_3N_5O_6S_2$ $[M+H]^+$ 676.1506, found 676.1501.

General Procedure IVa for Suzuki couplings of THBs and arylboronic acids:

All reactions were carried out at a concentration of 50 mM of THB, and 55 mM of arylboronic acid in dioxane/water (4/1). To a solution of 1 equiv. of THB and 1.1 equiv. of arylboronic acid (unless stated otherwise) in dioxane/water (4/1), 0.2 equiv. of $Pd(PPh_3)_4$ and 3 equiv. of Na_2CO_3 (solid) were added. The reaction mixture was purged with argon, heated to 80 °C and stirred overnight. After cooling to rt, the reaction mixture was diluted with DCM, washed three times with water and brine, dried over Na_2SO_4 and concentrated *in vacuo*. The crude product was purified by column chromatography (DCM:MeOH 98:2 → 92:8).

General Procedure IVb for Suzuki couplings of THBs and arylboronic acids:

All reactions were carried out at a concentration of 50 mM of THB and 55 mM of arylboronic acid in DME/water (2/1). To a solution of 1 equiv. THB and 1.1 equiv. of arylboronic acid 0.01 equiv. of $Pd(PPh_3)_4$ and 2 equiv. of K_2CO_3 (solid) were added. The reaction mixture was purged with argon and heated to 80 °C for 1 hour. The reaction was checked by TLC and in case of incompletion, 1 equiv. of arylboronic acid and 0.01 equiv. of $Pd(PPh_3)_4$ were added extra and stirred at 80 °C for 1 extra hour. Upon completion, the reaction mixture was diluted with DCM, washed three times with water and brine, dried over Na_2SO_4 and concentrated *in vacuo*. The crude product was purified by column chromatography (DCM:MeOH 98:2).

4-[(4-methoxybenzene)sulfonyl]-1-[(1-methyl-1H-imidazol-5-yl)methyl]-3-{[4-(pyridin-3-yl)phenyl]methyl}-2,3,4,5-tetrahydro-1H-1,4-benzodiazepine-7-carbonitrile (94)

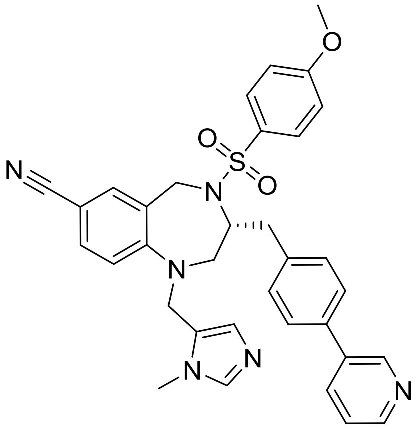

According to General Procedure **IVa**, reaction between THB **83** (50 mg, 74 µmol) and 3-pyridineboronic acid (27 mg, 222 µmol) afforded **94** as a white solid (42 mg, 94%). **^{1}H NMR** (400 MHz, $CDCl_3$) δ 8.85 (d, *J* = 1.9 Hz, 1H), 8.60 (dd, *J* = 4.8, 1.4 Hz, 1H), 7.88 (d, *J* = 8.0 Hz, 1H), 7.51 (d, *J* = 8.2 Hz, 2H), 7.44 (s, 1H), 7.42 – 7.34 (m, *J* = 8.3, 6.2 Hz, 4H), 7.30 (s, 1H), 7.20 (d, *J* = 8.0 Hz, 2H), 6.74 – 6.66 (m, 3H), 6.44 (d, *J* = 8.2 Hz, 1H), 4.61 (d, *J* = 17.4 Hz, 1H), 4.46 (d, *J* = 17.4 Hz, 1H), 4.33 – 4.21 (m, 1H), 4.02 (d, *J* = 16.2 Hz, 1H), 3.77 (d, *J* = 16.2 Hz, 1H), 3.75 (s, 3H), 3.57 (dd, *J* = 15.3, 10.4 Hz, 1H), 3.51 (s, 3H), 3.10 (dd, *J* = 15.5, 4.5 Hz, 1H), 2.94 (dd, *J* = 13.9, 5.1 Hz, 1H), 2.71 (dd, *J* = 13.4, 8.0 Hz, 1H); **LC-MS** (C4, ESI_MS) 605.1 $[M+H]^+$; R_t = 5.67 min; **HRMS (ESI):**calculated for $C_{34}H_{33}N_6O_3S$ $[M+H]^+$ 605.2329, found 605.2326.

7-bromo-3-[(4-butoxyphenyl)methyl]-4-[(4-methoxybenzene)sulfonyl]-1-[(1-methyl-1H-imidazol-5-yl)methyl]-2,3,4,5-tetrahydro-1H-1,4-benzodiazepine (96)

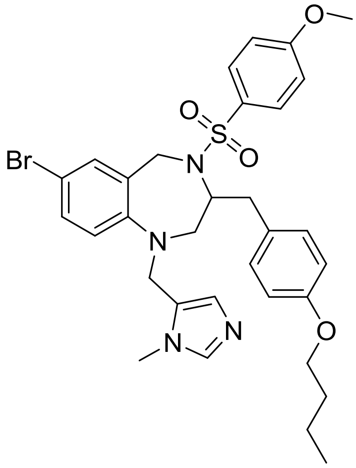

According to General Procedure I, reaction between THB **74**a (100 mg, 167 µmol) and n-butyl bromide (20 µL, 184 µmol) afforded **96** as a white solid (109 mg, 99%). **^{1}H NMR** (500 MHz, CDCl$_3$) δ 7.43 (s, 1H), 7.35 (d, *J* = 8.9 Hz, 2H), 7.23 (s, 1H), 7.16 (d, *J* = 8.6 Hz, 1H), 6.88 (d, *J* = 8.4 Hz, 2H), 6.78 (s, 1H), 6.74 (d, *J* = 8.5 Hz, 2H), 6.69 (d, *J* = 8.9 Hz, 2H), 6.47 (d, *J* = 8.3 Hz, 1H), 4.53 (d, *J* = 16.7 Hz, 1H), 4.36 (d, *J* = 16.7 Hz, 1H), 4.13 – 4.01 (m, 1H), 3.97 – 3.87 (m, 3H), 3.79 (s, *J* = 7.4 Hz, 3H), 3.84 – 3.73 (m, 1H), 3.53 (s, 3H), 3.32 (dd, *J* = 14.8, 7.8 Hz, 1H), 2.88 (dd, *J* = 14.8, 3.8 Hz, 1H), 2.78 (dd, *J* = 13.9, 5.9 Hz, 1H), 2.44 (dd, *J* = 13.3, 6.8 Hz, 1H), 1.81 – 1.69 (m, 2H), 1.54 – 1.41 (m, 2H), 0.98 (t, *J* = 7.4 Hz, 3H); **^{13}C NMR** (101 MHz, CDCl$_3$) δ 162.54 (C), 158.12 (C), 148.93 (C), 139.20 (CH), 132.72 (CH), 131.99 (C), 131.08 (CH), 130.22 (2×CH), 129.42 (2×CH), 128.89 (C), 127.59 (C), 123.05 (C), 117.86 (CH), 114.67 (2×CH), 113.66 (2×CH), 112.96 (C), 109.89 (CH), 67.80 (CH$_2$), 57.93 (CH), 55.67 (CH$_3$), 53.63 (CH$_2$), 46.84 (CH$_2$), 46.16 (CH$_2$), 37.19 (CH$_2$), 31.58 (CH$_3$), 31.57 (CH$_2$), 19.39 (CH$_2$), 13.99 (CH$_3$); **LC-MS** (C4, ESI_MS) 652.9 and 654.9 $[M+H]^+$; R_t = 7.71 min, **HRMS (ESI)**: calculated for $C_{32}H_{38}BrN_4O_4S$ $[M+H]^+$ 653.1792, found 653.1790.

4-{[7-(4-chlorophenyl)-4-[(4-methoxybenzene)sulfonyl]-1-[(1-methyl-1H-imidazol-5-yl)methyl]-2,3,4,5-tetrahydro-1H-1,4-benzodiazepin-3-yl]methyl}phenol (97)

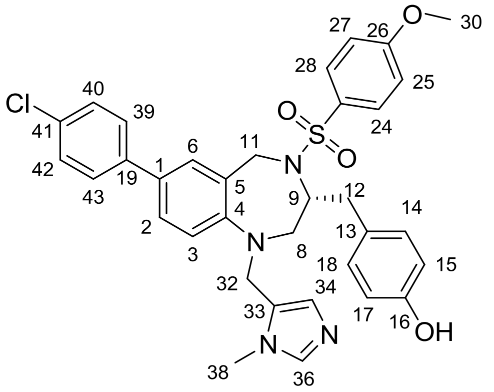

According to General Procedure **IVa**, reaction between THB **74**a (290 mg, 0.49 mmol) and 4-chlorophenylboronic acid (83 mg, 0.53 mmol) afforded **97** as a white solid (234 mg, 77%). **^{1}H NMR** (500 MHz, MeOD) δ = 7.70 (s, 1H, H-*36*), 7.49 (d, *J*=8.5, 2H, H-*39,* H-*43*), 7.37 (d, *J*=8.6, 4H, H-*24, 28, 40,42*), 7.30 (d, *J*=1.8, 1H, H-*6*), 7.27 (dd, *J*=8.4, 1.9, 1H, H-*2*), 7.14 (s, 1H, H-*34*), 6.94 (d, *J*=8.4, 2H, H-*14,* H-*18*), 6.75 (d, *J*=8.9, 2H, H-*25,* H-*27*), 6.69 (d, *J*=8.4, 2H, H-*15,* H-*17*), 6.56 (d, *J*=8.2, 1H, H-*3*), 4.61 (s, 2H, H-*32*), 4.28 (d, *J*=16.6, 1H, H-*11*), 4.25 – 4.19 (m, 1H, H-*9*), 3.98 (d, *J*=16.9, 1H, H-*11*), 3.79 (s, 3H, H-*38*), 3.77 (s, 3H, H-*30*), 3.55 (dd, *J*=15.1, 9.3, 1H, H-*8*), 3.05 (dd, *J*=15.2, 4.2, 1H, H-*8*), 2.80 (dd, *J*=13.8, 5.5, 1H, H-*12*), 2.64 (dd, *J*=13.6, 7.7, 1H, H-*12*). **^{13}C NMR** (126 MHz, MeOD) δ = 163.73 (C-26), 156.85 (C-16), 148.77 (C-4), 139.64 (C-19), 137.43 (C-36), 133.58 (C-41), 133.02 (C-1), 132.87 (C-33), 132.60 (C-23), 130.99 (C-14, C-18), 130.08 (C-24, C-28), 129.64 (C-40, C-42), 129.29 (C-6), 128.76 (C-13), 128.42 (C-39, C-43), 127.28 (C-2), 127.05(C-5)119.71(C-34)116.80 (C-3), 116.18 (C-15, C-17), 114.50 (C-25, C-27), 59.32 (C-9), 56.03 (C-30), 55.12 (C-8), 47.71 (C-32), 46.80 (C-11), 38.16 (C-12), 33.83 (C-38). **LC-MS** (C4, ESI_MS) 629.2 $[M+H]^+$; R_t = 8.34 min, **HRMS (ESI):** calculated for $C_{34}H_{34}ClN_4O_4S$ $[M+H]^+$ 629.1984, found 629.1982.

4-{[7-(4-chlorophenyl)-4-[(4-methoxybenzene)sulfonyl]-1-[(1-methyl-1H-imidazol-5-yl)methyl]-2,3,4,5-tetrahydro-1H-1,4-benzodiazepin-3-yl]methyl}phenyl trifluoromethanesulfonate (98)

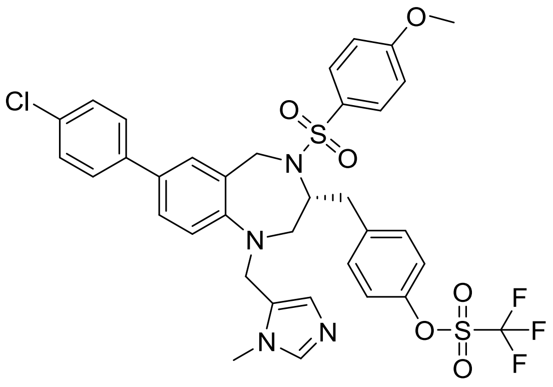

According to General Procedure **III**, reaction between THB **97** (165 mg, 0.26 mmol) and N- phenylbis(trifluoromethane-sulphonimide) **86** (141 mg, 0.39 mmol) afforded **98** as a white solid (144 mg, 72%). **LC-MS** (C4, ESI_MS) 761.1 and 763.0 $[M+H]^+$; R_t = 8.23 min; **HRMS (ESI)** calculated for $C_{35}H_{33}ClF_3N_4O_6S_2$ $[M+H]^+$ 761.1477, found 761.1477.

4-{[7-(3,4-dichlorophenyl)-4-[(4-methoxybenzene)sulfonyl]-1-[(1-methyl-1H-imidazol-5-yl)methyl]-2,3,4,5-tetrahydro-1H-1,4-benzodiazepin-3-yl]methyl}phenol (99)

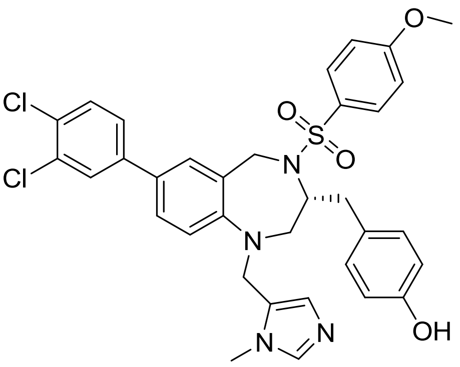

According to General Procedure **IVa**, reaction between THB **74**a (110 mg, 0.18 mmol) and 3,4-dichlorophenylboronic acid (39 mg, 0.20 mmol) afforded **99** as a white solid (109 mg, 89%). **^{1}H NMR** (400 MHz, $CDCl_3$) δ 7.60 (d, *J* = 2.1 Hz, 1H), 7.47 (d, *J* = 8.4 Hz, 2H), 7.41 – 7.31 (m, 3H), 7.30 – 7.22 (m, 2H), 6.86 – 6.77 (m, 3H), 6.74 (d, *J* = 8.2 Hz, 2H), 6.69 (d, *J* = 8.8 Hz, 2H), 6.63 (d, *J* = 8.1 Hz, 1H), 4.66 (d, *J* = 17.0 Hz, 1H), 4.48 (d, *J* = 17.0 Hz, 1H), 4.07 – 3.95 (m, *J* = 15.2 Hz, 2H), 3.86 (d, *J* = 15.7 Hz, 1H), 3.77 (s, 3H), 3.55 (s, 3H), 3.38 (dd, *J* = 14.1, 8.3 Hz, 1H), 2.93 (dd, *J* = 14.7, 3.4 Hz, 1H), 2.78 (dd, *J* = 13.8, 5.3 Hz, 1H), 2.45 – 2.33 (m, 1H), **LC-MS** (C4, ESI_MS) 663.0 and 665.0 $[M+H]^+$; R_t = 7.91 min **HRMS (ESI):** calculated for $C_{34}H_{33}Cl_2N_4O_4S$ $[M+H]^+$ 663.1594, found 663.1593.

4-{[7-(3,4-dichlorophenyl)-4-[(4-methoxybenzene)sulfonyl]-1-[(1-methyl-1H-imidazol-5-yl)methyl]-2,3,4,5-tetrahydro-1H-1,4-benzodiazepin-3-yl]methyl}phenyl trifluoromethanesulfonate (100)

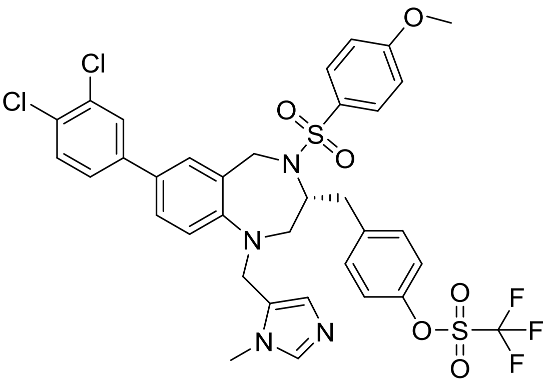

According to General Procedure **III**, reaction between THB **99** (338 mg, 0.51 mmol) and **86** (273 mg, 0.76 mmol) afforded **100** as a white solid (331 mg, 82%). **^{1}H NMR** (400 MHz, $CDCl_3$) δ 7.64 – 7.43 (m, 4H), 7.43 – 7.28 (m, 4H), 7.14 (d, *J* = 8.6 Hz, 2H), 7.07 (d, *J* = 8.5 Hz, 2H), 6.88 (s, 1H), 6.73 (d, *J* = 8.1 Hz, 1H), 6.68 (d, *J* = 8.8 Hz, 2H), 4.69 (d, *J* = 16.6 Hz, 1H), 4.48 (d, *J* = 16.5 Hz, 1H), 4.14 – 4.06 (m, 1H), 4.00 (dd, *J* = 29.0, 14.9 Hz, 2H), 3.76 (s, 3H), 3.59 (s, 3H), 3.37 (dd, *J* = 14.4, 7.5 Hz, 1H), 2.96 – 2.82 (m, 2H), 2.45 (dd, *J* = 14.0, 6.7 Hz, 1H); **LC-MS** (C4, ESI_MS) 795.0 and 797.0 $[M+H]^+$; R_t = 8.46 min; **HRMS (ESI)** calculated for $C_{35}H_{32}Cl_2F_3N_4O_6S_2$ $[M+H]^+$ 795.1087, found 795.1087.

7-(3,4-dichlorophenyl)-4-[(4-methoxybenzene)sulfonyl]-1-[(1-methyl-1H-imidazol-5-yl)methyl]-3-({4-[3-(morpholin-4-yl)prop-1-yn-1-yl]phenyl}methyl)-2,3,4,5-tetrahydro-1H-1,4-benzodiazepine (101)

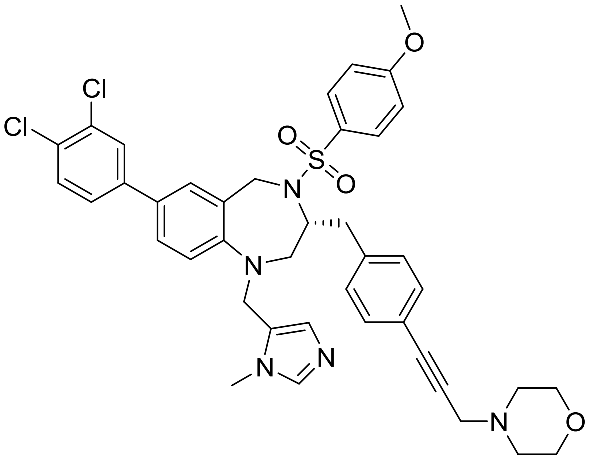

A dry Schlenk tube was charged with THB **100** (50 mg, 63 µmol), N-propargyl morpholine(47 mg, 377 µmol), Pd(PPh$_3$)$_4$ (18 mg, 16 µmol), CuI (1.2 mg, 6 µmol), Et$_3$N (26 µL, 189 µmol) and tetrabutylammonium iodide (35 mg, 94 µmol). Dry DMF (3 mL) was added and the reaction mixture was purged with argon and stirred at 70 °C overnight. After cooling, the reaction mixture was poured into water and extracted three times with EtOAc. The combined organic layers were washed with brine, dried over Na$_2$SO$_4$ and concentrated *in vacuo*. Purification by flash column chromatography (DCM:MeOH 98:2 → 90:10) afforded **101** as a white solid (27 mg, 56%). **LC-MS** (C4, ESI_MS) 770.1 and 772.1 $[M+H]^+$; R_t = 7.81 min; **HRMS (ESI):** calculated for $C_{41}H_{42}Cl_2N_5O_4S$ $[M+H]^+$ 770.2329, found 770.2341.

1-[4-(4-{[7-(3,4-dichlorophenyl)-4-[(4-methoxybenzene)sulfonyl]-1-[(1-methyl-1H-imidazol-5-yl)methyl]-2,3,4,5-tetrahydro-1H-1,4-benzodiazepin-3-yl]methyl}phenyl)piperazin-1-yl]ethan-1-one (102)

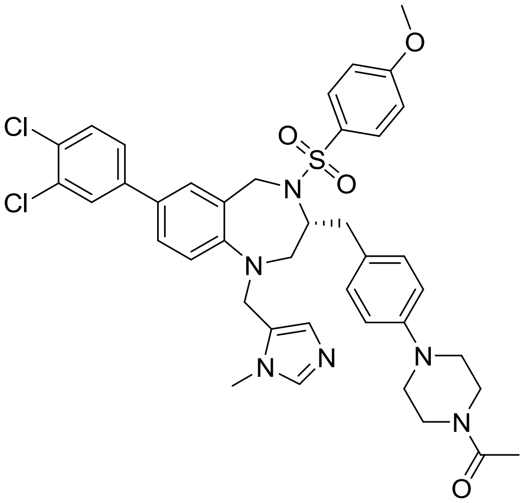

A dry Schleck tube was charged with THB **100** (100 mg, 126 µmol), ligand **95** (15 mg, 50 µmol), Pd(OAc)$_2$ (5.6 mg, 25 µmol) and Cs$_2$CO$_3$ (57 mg, 176 µmol). Dry THF (0.5 mL) was added, followed by piperazine (19 mg, 151 µmol). The reaction mixture was purged with argon and stirred at 60 °C overnight. After cooling, the solvent was evaporated and the product was purified by flash column chromatography (DCM:MeOH 98:2 → 90:10), affording **102** as a white solid (80 mg, 82%). **LC-MS** (C4, ESI_MS) 773.2 and 775.2 $[M+H]^+$; R_t = 7.57 min; **HRMS (ESI)**: calculated for $C_{40}H_{43}Cl_2N_6O_4S$ $[M+H]^+$773.2438, found 773.2443.

7-(3,4-dichlorophenyl)-4-[(4-methoxybenzene)sulfonyl]-1-[(1-methyl-1H-imidazol-5-yl)methyl]-3-{[4-(pyridin-3-yl)phenyl]methyl}-2,3,4,5-tetrahydro-1H-1,4-benzodiazepine (103)

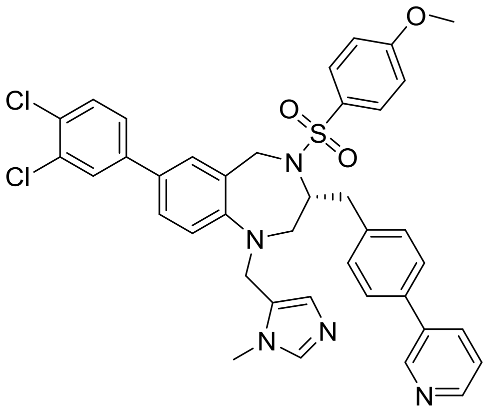

According to General Procedure **IVa**, reaction between THB **100** (50 mg, 63 µmol) and 3-pyridineboronic acid (23 mg, 189 µmol) afforded **103** as a white solid (41 mg, 57%). **LC-MS** (C4, ESI_MS) 724.1 and 726.0 $[M+H]^+$; R_t = 7.11 min; **HRMS (ESI)**: calculated for $C_{39}H_{36}Cl_2N_5O_3S$ $[M+H]^+$ 724.1910, found 724.1911.

4-{[(3R)-7-(3-chlorophenyl)-4-[(4-methoxybenzene)sulfonyl]-1-[(1-methyl-1H-imidazol-5-yl)methyl]-2,3,4,5-tetrahydro-1H-1,4-benzodiazepin-3-yl]methyl}phenol (104)

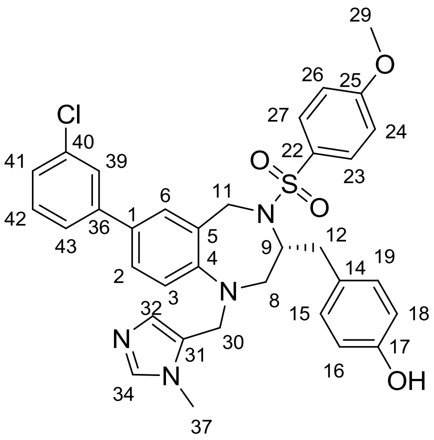

According to General Procedure **IVb** reaction between THB **74**a (200 mg, 0.33 mmol) and 3-chlorophenylboronic acid (63 mg, 0.40 mmol) afforded **104** as a white solid (210 mg, 68%), $\mathbf{R_f}$ 0.27 (5% MeOH in DCM) **Mp** 158.7 °C,^{1}**H NMR** (500 MHz, MeOD) δ = 7.57 (s, 1H, H-*34*), 7.54 (dd, *J*=2.1, 1.4, 1H, H-*39*), 7.47 (ddd, *J*=7.8, 1.4, 1.4, 1H, H-*41*), 7.36 (dd, *J*=7.9, 7.9, 1H, H-*42*), 7.33 (d, *J*=8.9, 2H, H-*23,* H-*27*), 7.30 (s, 1H, H-*6*), 7.28 (s, 1H, H-*2*), 7.26 (ddd, *J*=7.8, 2.2, 1.4, 1H, H-*43*), 6.88 (d, *J*=8.2, 2H, H-*15,* H-*19*), 6.71 (d, *J*=8.9, 2H, H-*24,* H-*26*), 6.70 (s, 1H, H-*32*), 6.66 – 6.63 (m, 1H, H-*3*), 6.65 (d, *J*=8.4, 2H, H-*16,* H-*18*), 4.65 (d, *J*=16.8, 1H, H-*30*), 4.59 (d, *J*=16.9, 1H, H-*30*), 4.16 – 4.09 (m, 1H, H-*9*), 4.06 (d, *J*=15.7, 1H, H-*11*), 3.92 (d, *J*=15.2, 1H, H-*11*), 3.74 (s, 3H, H-*29*), 3.56 (s, 3H, H-*37*), 3.47 (dd, *J*=14.9, 8.1, 1H, H-*8*), 2.93 (dd, *J*=15.0, 3.8, 1H, H-*8*), 2.79 (dd, *J*=13.8, 6.2, 1H, H-*12*), 2.49 – 2.34 (m, 1H, H-*12*). ^{13}**C NMR** (126 MHz, MeOD) δ = 164.05 (C-25), 157.11 (C-17), 150.95 (C-4), 143.81 (C-36), 139.91 (C-34), 135.72 (C-1), 133.10 (C-22), 132.43 (C-40), 131.31 (C-42), 131.25 (C-15, C-19), 130.46 (C-23, C-27), 130.10 (C-5), 130.06 (C-31), 129.66 (C-6), 129.60 (C-14), 128.25 (C-32), 127.64 (C-2), 127.49 (C-43), 127.16 (C-39), 125.66 (C-41), 117.53 (C-3), 116.30 (C-16, C-18), 114.69 (C-24, C-26), 60.01 (C-9), 56.11 (C-29), 54.90 (C-8), 47.87 (C-30), 47.27 (C-11), 38.25 (C-12), 31.92 (C-37). **LC-MS** (C18, ESI_MS) 629.2 $[M+H]^+$; R_t = 6.79 min

HRMS (ESI): calculated for $C_{34}H_{34}N_4O_4ClS$ $[M+H]^+$ 629.1983, found 629.1914. $[\alpha]_D^{20}$+251.0 (*c*=1, MeOH/$CHCl_3$, 1:1).

3-[(4-butoxyphenyl)methyl]-7-(3-chlorophenyl)-4-[(4-methoxybenzene)sulfonyl]-1-[(1-methyl-1H-imidazol-5-yl)methyl]-2,3,4,5-tetrahydro-1H-1,4-benzodiazepine (105)

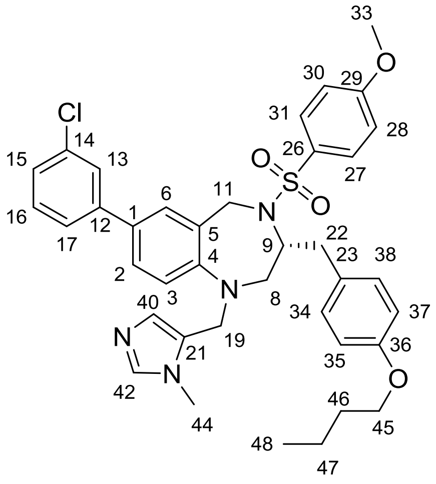

According to General Procedure I reaction between THB **104** (25 mg, 40 µmol) and n-butyl bromide (4.8 µL, 44 µmol) afforded **105** as a white solid (23 mg, 85%) **R$_f$** 0.39 (3% MeOH in DCM). **^{1}H NMR** (400 MHz, MeOD) δ = 7.55 (s, 1H, H-*42*), 7.52 (dd, *J*=2.1, 1.7, 1H, H-*13*), 7.45 (ddd, *J*=7.7, 1.8, 1.1, 1H, H-*15*), 7.35 (dd, *J*=7.8, 7.8 1H, H-*16*), 7.34 – 7.33 (m, 1H, H-*6*), 7.33 (d, *J*=9.1, 2H, H-*27,* H-*31*), 7.31 – 7.28 (m, 1H, H-*2*), 7.25 (ddd, *J*=7.9, 2.1, 1.1, 1H, H-*17*), 6.95 (d, *J*=8.6, 2H, H-*34,* H-*38*), 6.75 (d, *J*=8.8, 2H, H-*35,* H-*37*), 6.72 (s, 1H, H-*40*), 6.69 (d, *J*=9.1, 2H, H-*28,* H-*30*), 6.68 – 6.63 (m, 1H, H-*3*), 4.61 (s, 2H, H-*19*), 4.18 – 4.10 (m, 1H, H-*9*), 4.06 (d, *J*=15.6, 1H, H-*11*), 3.93 (t, *J*=6.5, 3H, H-*45*), 3.93 (d, *J*=15.6, 1H, H-*11*), 3.75 (s, 3H, H-*33*), 3.58 (s, 3H, H-*44*), 3.47 (dd, *J*=15.0, 7.8, 1H, H-*8*), 2.95 (dd, *J*=14.8, 3.9, 1H, H-*8*), 2.82 (dd, *J*=13.8, 6.2, 1H, H-*22*), 2.46 (dd, *J*=13.4, 6.8, 1H, H-*22*), 1.78 – 1.69 (m, 2H, H-*46*), 1.55 – 1.44 (m, 2H, H-*47*), 0.97 (t, *J*=7.4, 3H, H-*48*). **^{13}C NMR** (101 MHz, MeOD) δ = 163.68 (C-29), 159.02 (C-36), 150.05 (C-4), 143.37 (C-12), 139.61 (C-42), 135.50 (C-14), 132.66 (C-26), 130.99 (C-38, C-34), 130.24 (C-23), 130.17 (C-27, C-31), 129.62 (C-40), 129.43 (C-2), 128.15 (C-6),128.11(C-1),127.96(C-21), 127.53 (C-16), 127.35 (C-17), 127.06 (C-13), 125.42 (C-15), 119.23 (C-5), 117.38 (C-3), 115.32 (C-35, C-37), 114.45 (C-28, C-30), 68.49 (C-45), 59.44 (C-9), 56.02 (C-33), 54.72 (C-8), 47.75 (C-19), 47.26 (C-11), 37.99 (C-22), 32.31 (C-46), 31.93 (C-44), 20.09 (C-47), 14.18 (C-48). **LC-MS** (C18_ESI) 685.3 $[M+H]^+$, R$_t$ =7.81 **HRMS (ESI)**: calculated for $C_{38}H_{42}ClN_4O_4S$ $[M+H]^+$ 685.2610, found 685.2608.$[\alpha]_D^{20}$+80.0 (c=1, $CHCl_3$/MeOH, 1:1).

4-{[(3R)-7-(3-chlorophenyl)-4-[(4-methoxybenzene)sulfonyl]-1-[(1-methyl-1H-imidazol-5-yl)methyl]-2,3,4,5-tetrahydro-1H-1,4-benzodiazepin-3-yl]methyl}phenyl N-benzylcarbamate (106)

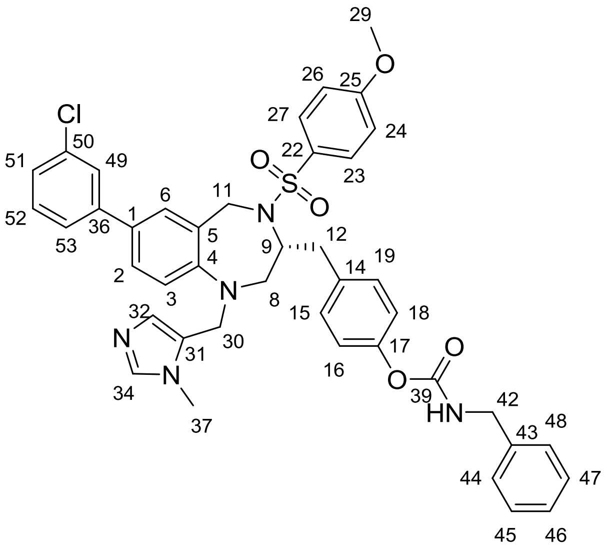

According to General Procedure **II**, reaction between THB **104** (15 mg, 24 µmol) and benzylisocyanate (4.8 mg, 36 µmol) afforded **106** as a white solid (16 mg, 88%) **R_f** 0.32 (3% MeOH in DCM) **Mp** 79.6 °C **^{1}H NMR** (500 MHz, MeOD) δ = 7.56 (s, 1H, H-*34*), 7.55 (dd, *J*=2.1, 1.7, 1H, H-*49*) 7.48 (ddd, *J*=7.8, 1.7, 1.1, 1H, H-*51*), 7.37 (dd, *J*=7.8, 7.8 1H, H-*52*), 7.35 (d, *J*=8.8, 2H, H-*23,* H-*27*), 7.35 – 7.32 (m, 4H, H-*44, 46, 48, 53*), 7.33 (d, *J*=2.3, 1H, H-*6*), 7.31 (dd, *J*=8.1, 2.4, 1H, H-*2*), 7.28 – 7.25 (m, 2H, H-*45,* H-*47*), 7.06 (d, *J*=8.2, 2H, H-*15,* H-*19*), 6.97 (d, *J*=8.4, 2H, H-*16,* H-*18*), 6.73 (d, *J*=8.9, 2H, H-*24,* H-*26*), 6.72 (s, 1H, H-*32*), 6.68 (d, *J*=8.0, 1H, H-*3*), 4.70 (d, *J*=16.8, 1H, H-*30*), 4.62 (d, *J*=16.8, 1H, H-*30*), 4.36 (s, 2H, H-*42*), 4.20 – 4.12 (m, 1H, H-*9*), 4.07 (d, *J*=15.6, 1H, H-*11*), 3.94 (d, *J*=15.2, 1H, H-*11*), 3.72 (s, 3H, H-*29*), 3.55 (s, 3H, H-*37*), 3.50 (dd, *J*=15.0, 8.0, 1H, H-*8*), 2.93 (dd, *J*=15.0, 3.7, 1H, H-*8*), 2.88 (dd, *J*=13.8, 6.4, 1H, H-*12*), 2.57 – 2.44 (m, 1H, H-*12*). **^{13}C NMR** (126 MHz, MeOD) δ = 164.12 (C-25), 157.36 (C-39), 151.35 (C-17), 150.98 (C-4), 143.82 (C-36), 140.27 (C-43), 140.03 (C-34), 136.07 (C-50), 135.73 (C-14), 132.94 (C-22), 132.50 (C-31), 131.33 (C-52), 131.12 (C-15, C-19), 130.54 (C-45, C-47), 129.99 (C-2), 129.66 (C-1), 129.58 (C-23, C-27), 128.50 (C-32), 128.42 (C-44, 46, 48), 128.29 (C-53), 127.68 (C-6), 127.51 (C-5), 127.17 (C-49), 125.67 (C-51), 122.75 (C-16, C-18), 117.50 (C-3), 114.77 (C-24, C-26), 59.89 (C-9), 56.13 (C-29), 54.84 (C-8), 47.86 (C-30), 47.17 (C-11), 45.71 (C-42), 38.36 (C-12), 31.88 (C-37). **LC-MS** (C18, ESI_MS)**:** 762.40 [M+H]$^+$ R_t=7.65min. **HRMS (ESI)** calculated for $C_{42}H_{42}N_5O_5ClS$ [M+H]$^+$: 763.2565, found: 763.2589.

4-{[(3R)-4-[(4-methoxybenzene)sulfonyl]-1-[(1-methyl-1H-imidazol-5-yl)methyl]-7-(pyridin-4-yl)-2,3,4,5-tetrahydro-1H-1,4-benzodiazepin-3-yl]methyl}phenol (107)

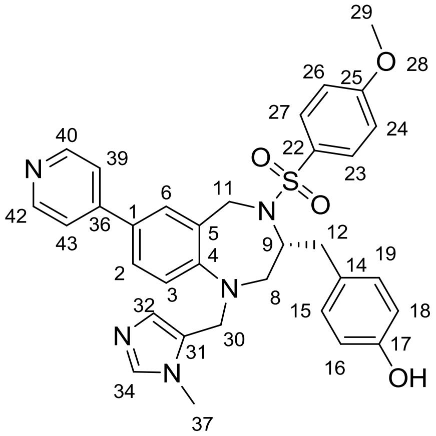

According to General Procedure **IVb** reaction between THB **74**a (150 mg, 0.25 mmol) and 4-pyridineboronic acid (34 mg, 0.28 mmol) afforded **107** as a white solid (210 mg, 68%) **R_f** 0.43 (DCM/MeOH, 10:1) **Mp** 148.8 °C **^{1}H NMR** (500 MHz, MeOD) δ = 8.52 (dd, *J*=4.7, 1.6, 2H, H-*40,* H-*42*), 7.67 (dd, *J*=4.8, 1.4, 2H, H-*43,* H-*39*), 7.59 (s, 1H, H-*34*), 7.51 (d, *J*=2.4, 1H, H-*6*), 7.48 (dd, *J*=8.4, 2.4, 1H, H-*2*), 7.39 (d, *J*=8.9, 2H, H-*23,* H-*27*), 6.96 (d, *J*=8.2, 2H, H-*16,* H-*19*), 6.76 (d, *J*=8.9, 2H, H-*24,* H-*26*), 6.69 (d, *J*=8.4, 2H, H-*16,* H-*18*), 6.68 – 6.66 (m, 1H, H-*32*), 6.64 (d, *J*=8.4, 1H, H-*3*), 4.73 (d, *J*=17.1, 1H, H-*30*), 4.68 (d, *J*=17.2, 1H, H-*30*), 4.25 – 4.18 (m, 1H, H-*9*), 4.13 (d, *J*=16.0, 1H, H-*11*), 3.92 (d, *J*=16.0, 1H, H-*11*), 3.78 (s, 3H, H-*29*), 3.64 – 3.57 (m, 1H, H-*8*), 3.59 (s, 3H, H-*37*), 3.02 (dd, *J*=15.2, 4.0, 1H, H-*8*), 2.84 (dd, *J*=13.7, 5.6, 1H, H-*12*), 2.61 – 2.52 (m, 1H, H-*12*). **^{13}C NMR** (126 MHz, MeOD) δ = 163.09 (C-25), 156.19 (C-17), 150.90 (C-4), 149.36 (C-40, C-42), 148.87 (C-36), 138.98 (C-34), 132.09 (C-22), 130.29 (C-15, C-19), 129.44 (C-23, C-27), 128.78 (C-1), 128.69 (C-14), 128.49 (C-6), 127.18 (C-32), 126.70 (C-2), 121.01 (C-39, C-43), 116.22 (C-3), 115.33 (C-16, C-18), 113.68 (C-24, C-26), 59.20 (C-9), 55.12 (C-29), 53.66 (C-8), 47.00 (C-30), 46.13 (C-11), 37.62 (C-12), 30.84 (C-37). **LC-MS** (C18_ESI)**:** 596.1 $[M+H]^+$ R_t=5.44 min; **HRMS (ESI)** calculated for $C_{33}H_{34}O_4N_5S$ $[M+H]^+$: 596.2326, found: 596.2323. $[\alpha]_D^{20}$ +26.8(*c*=1, $CHCl_3$).

5-[(3R)-3-[(4-hydroxyphenyl)methyl]-4-[(4-methoxybenzene)sulfonyl]-1-[(1-methyl-1H-imidazol-5-yl)methyl]-2,3,4,5-tetrahydro-1H-1,4-benzodiazepin-7-yl]furan-2-carbaldehyde (108)

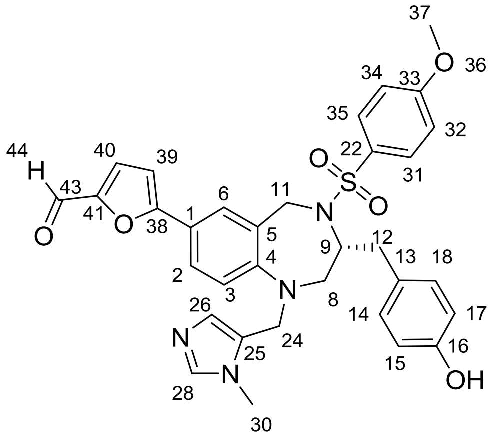

According to General Procedure **IVb** reaction between THB **74**a (300 mg, 0.5 mmol) and 5-formyl-2-furylboronic acid (2 × 84 mg, 1.2 mmol) afforded **108** as an orange solid (210 mg, 68%). **R_f** 0.64 (DCM/MeOH 10:1) **Mp** 152.7 °C **^{1}H NMR** (400 MHz, MeOD) δ = 9.46 (s, 1H, H-*44*), 7.54 (s, 1H, H-*28*), 7.51 (d, *J*=2.2, 1H, H-*6*), 7.46 (dd, *J*=8.6, 2.2, 1H, H-*2*), 7.43 (d, *J*=3.8, 1H, H-*40*), 7.34 (d, *J*=8.9, 2H, H-*31,* H-*35*), 6.92 (d, *J*=8.3, 2H, H-*14,* H-*18*), 6.81 (d, *J*=3.7, 1H, H-*39*), 6.71 (d, *J*=8.9, 2H, H-*32,* H-*34*), 6.68 (d, *J*=8.3, 2H, H-*15,* H-*17*), 6.63 (s, 1H, H-*26*), 6.47 (d, *J*=8.4, 1H, H-*3*), 4.62 (d, *J*=17.6, 1H, H-*11*), 4.57 (d, *J*=17.6, 1H, H-*11*), 4.21 – 4.09 (m, 1H, H-*9*), 4.03 (d, *J*=16.3, 1H, H-*24*), 3.76 (d, *J*=16.5, 1H, H-*24*), 3.74 (s, 3H, H-*37*), 3.59 – 3.53 (m, 1H, H-*8*), 3.53 (s, 3H, H-*30*), 2.99 (dd, *J*=15.3, 4.1, 1H, H-*8*), 2.81 (dd, *J*=13.7, 4.9, 1H, H-*12*), 2.57 (dd, *J*=13.5, 8.1, 1H, H-*12*). **^{13}C NMR** (101 MHz, MeOD) δ = 178.00 (C-43), 163.65 (C-33), 161.22 (C-38), 156.73 (C-16), 152.26 (C-41), 151.19 (C-4), 139.50 (C-28), 132.45 (C-22), 131.04 (C-14, C-18), 130.05 (C-31, C-35), 129.06 (C-25), 128.79 (C-13), 128.12 (C-6), 127.54 (C-2), 127.38 (C-26), 126.34 (C-40), 125.86 (C-5),121.11 (C-1), 116.46 (C-3), 116.15 (C-15, C-17), 114.42 (C-32, C-34), 107.23 (C-39), 59.59 (C-9), 56.03 (C-37), 54.12 (C-8), 47.78 (C-24), 46.81 (C-11), 38.56 (C-12), 31.92 (C-30). **LC-MS** (C18, ESI_MS) 613.1 $[M+H]^+$; R_t = 7.30 min; **HRMS (ESI):** calculated for $C_{33}H_{33}O_6N_4S$ $[M+H]^+$ 613.2115, found 613.2105.$[\alpha]_D^{20}$ +244.3 (*c*=1, MeOH).

4-{[(3R)-7-(5-formylfuran-2-yl)-4-[(4-methoxybenzene)sulfonyl]-1-[(1-methyl-1H-imidazol-5-yl)methyl]-2,3,4,5-tetrahydro-1H-1,4-benzodiazepin-3-yl]methyl}phenyl N-benzylcarbamate (109)

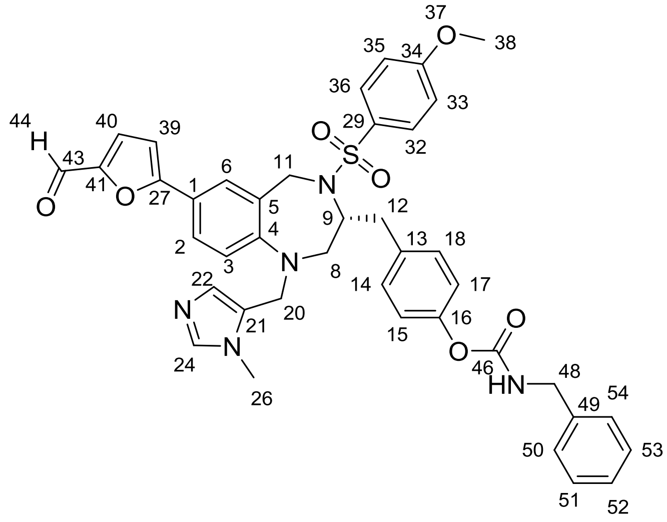

According to General Procedure **II**, reaction between THB **108** (20 mg, 33 µmol) and benzylisocyanate (4.8 mg, 36 µmol) afforded **109** as an orange solid (20 mg, 82%) **R_f** 0.23 (2% MeOH in DCM). **Mp** 121.8°C. **^{1}H NMR** (500 MHz, MeOD) δ = 9.48 (s, 1H, H-*44*), 7.75 (s, 1H, H-*24*), 7.55 (d, *J*=1.6, 1H, H-*6*), 7.51 (dd, *J*=8.3, 1.6, 1H, H-*2*), 7.46 (d, *J*=3.8, 1H, H-*40*), 7.36 (d, *J*=8.9, 2H, H-*32,* H-*36*), 7.34 – 7.30 (m, 4H, H-*50, 51, 53, 54*), 7.28 – 7.22 (m, 1H, H-*52*), 7.12 (d, *J*=8.3, 2H, H-*14,* H-*18*), 7.02 (d, *J*=8.4, 2H, H-*15,* H-*17*), 6.85 (d, *J*=3.8, 1H, H-*39*), 6.74 (d, *J*=8.9, 2H, H-*33,* H-*35*), 6.66 (s, 1H, H-*22*), 6.52 (d, *J*=8.3, 1H, H-*3*), 4.72 – 4.61 (m, 2H, H-*20*), 4.36 (s, 2H, H-*48*), 4.24 – 4.16 (m, 1H, H-*9*), 4.07 (d, *J*=16.1, 1H, H-*11*), 3.81 (d, *J*=16.1, 1H, H-*11*), 3.74 (s, 3H, H-*38*), 3.60 (dd, *J*=15.4, 10.1, 1H, H-*8*), 3.54 (s, 3H, H-*26*), 2.99 (dd, *J*=15.3, 4.1, 1H, H-*8*), 2.91 (dd, *J*=13.6, 5.4, 1H, H-*12*), 2.67 (dd, *J*=13.4, 7.6, 1H, H-*12*). **^{13}C NMR** (126 MHz, MeOD) δ = 178.15 (C-43), 163.86 (C-34), 161.33 (C-27), 157.05 (C-46), 152.44 (C-41), 151.16 (C-16), 151.13 (C-4), 139.77 (C-49), 139.76 (C-24), 135.34 (C-13), 132.48 (C-29), 130.92 (C-14, C-18), 130.20 (C-32, C-26), 129.35 (C-51, C-53), 192.25 (C-21), 128.26 (C-6), 128.20 (C-50, C-54), 128.09 (C-52), 127.38 (C-22), 127.33 (C-40), 126.44 (C-2), 122.68 (C-15, C-17), 120.93 (C-1), 116.49 (C-3), 114.55 (C-33, C-35), 107.31 (C-39), 59.76 (C-9), 56.10 (C-38), 54.07 (C-8), 47.81 (C-20), 46.67 (C-11), 45.59 (C-48), 38.85 (C-12), 31.94 (C-26). **LC-MS** (C18, ESI_MS) 746.2 $[M+H]^+$; R_t = 8.24 min; **HRMS (ESI):** calculated for $C_{41}H_{40}O_7N_5S$ $[M+H]^+$ 746.2643, found 746.2636. $[\boldsymbol{\alpha}]_{\boldsymbol{D}}^{\mathbf{20}}$ +156.8 (*c*=1, $CHCl_3$).

4-{[(3R)-4-[(4-methoxybenzene)sulfonyl]-7-(2-methoxypyridin-4-yl)-1-[(1-methyl-1H-imidazol-5-yl)methyl]-2,3,4,5-tetrahydro-1H-1,4-benzodiazepin-3-zl]methyl}phenol (111)

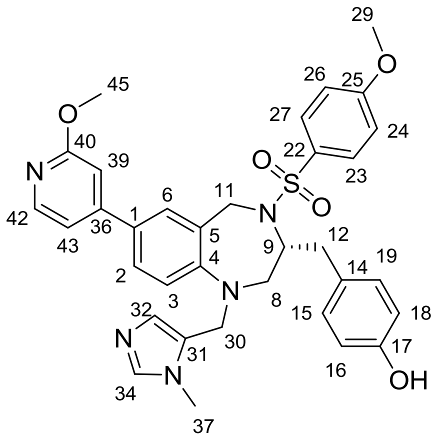

According to General Procedure **IVa** reaction between THB **74**a (150 mg, 0.25 mmol) and 2-methoxypyridine-4-boronic acid (42 mg, 0.28 mmol) afforded **111** as an offwhite solid (40 mg, 25%) **R$_f$** 0.72 (DCM/MeOH, 10:1) **Mp** 154.7 °C. **^{1}H NMR** (400 MHz, MeOD) δ = 8.10 (d, *J*=5.5, 1H, H-*42*), 7.56 (s, 1H, H-*34*), 7.41 (d, *J*=2.4, 2H, H-*6*), 7.40 – 7.37 (m, 1H, H-*2*), 7.35 (d, *J*=8.9, 2H, H-*27*), 7.18 (dd, *J*=5.5, 1.7, 1H, H-*43*), 6.97 (d, *J*=1.7, 1H, H-*39*), 6.91 (d, *J*=8.1, 2H, H-*15*), 6.72 (d, *J*=8.9, 2H, H-*26*), 6.68 (s, 1H, H-*32*), 6.66 (d, *J*=8.3, 2H, H-*18*), 6.61 (d, *J*=8.2, 1H, H-*3*), 4.68 (d, *J*=17.2, 1H, H-*11*), 4.62 (d, *J*=16.9, 1H, H-*11*), 4.22 – 4.12 (m, 1H, H-*9*), 4.09 (d, *J*=16.4, 1H, H-*30*), 3.94 (s, 3H, H-*45*), 3.90 (d, *J*=16.6, 1H, H-*30*), 3.75 (s, *J*=6.7, 3H, H-*29*), 3.56 (s, *J*=17.6, 3H, H-*37*), 3.54 – 3.48 (m, 1H, H-*8*), 2.97 (d, *J*=14.4, 1H, H-*8*), 2.80 (dd, *J*=12.9, 4.7, 1H, H-*12*), 2.56 – 2.45 (m, 1H, H-*12*). **^{13}C NMR** (101 MHz, MeOD) δ = 166.54 (C-40), 164.08 (C-25), 157.19 (C-17), 152.27 (C-36), 151.76 (C-4), 148.01 (C-42), 139.98 (C-34), 133.09 (C-22), 131.29 (C-15, C-19), 130.44 (C-23, C-27), 129.94 (C-1), 129.86 (C-31), 129.64 (C-6), 129.53 (C-14), 128.26 (C-32), 127.67 (C-2), 117.17 (C-3), 116.33 (C-16, C-18), 115.66 (C-43), 114.68 (C-24, C-26), 107.65 (C-39), 60.18 (C-9), 56.12 (C-29), 54.81 (C-8), 54.12 (C-45), 47.95 (C-30), 47.17 (C-11), 38.61 (C-12), 31.87 (C-37). **LC-MS** (C18-ESI): 626.13 [M+H]$^+$ R$_t$=7.67min. **HRMS (ESI)** calculated for $C_{34}H_{36}O_5N_5S$ [M+H]$^+$:626.2429, found: 626.2432. $[\alpha]_D^{20}$+84.5 (*c*=1.1, CHCl$_3$).

3-[(3R)-3-[(4-hydroxyphenyl)methyl]-4-[(4-methoxybenzene)sulfonyl]-1-[(1-methyl-1H-imidazol-5-yl)methyl]-2,3,4,5-tetrahydro-1H-1,4-benzodiazepin-7-yl]benzonitrile (112)

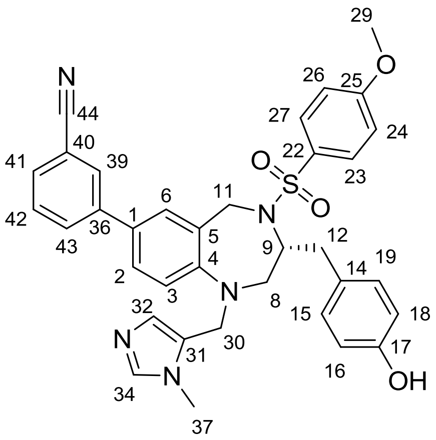

According to General Procedure **IVa** reaction between THB **74**a (150 mg, 0.25 mmol) and 3-cyanophenylboronic acid (41 mg, 0.28 mmol) afforded **112** as an yellow solid (81 mg, 52%) **R*f*** 0.54 (DCM/MeOH, 10:1) **Mp** 157.6 °C **^{1}H NMR** (500 MHz, MeOD) δ = 7.86 (dd, *J*=1.8, 1.8, 1H, H-*39*), 7.84 (ddd, *J*=7.5, 1.7, 1.7, 1H, H-*43*), 7.59 (ddd, *J*=7.7, 1.5, 1.5, 1H, H-*41*), 7.55 (s, 1H, H-*34*), 7.54 (dd, *J*=7.5, 7.5 1H, H-*42*), 7.34 (d, *J*=8.7, 2H, H-*23,* H-*27*), 7.34 (d, *J*=2.7, 1H, H-*6*), 7.31 (dd, *J*=6.5, 2.7, 1H, H-*2*), 6.89 (d, *J*=8.1, 2H, H-*15,* H-*19*), 6.72 (d, *J*=8.9, 2H, H-*24,* H-*26*), 6.68 (s, 1H, H-*32*), 6.66 – 6.64 (m, 1H, H-*3*), 6.65 (d, *J*=8.3, 2H, H-*16,* H-*18*), 4.67 (d, *J*=17.0, 1H, H-*11*), 4.61 (d, *J*=16.9, 1H, H-*11*), 4.18 – 4.10 (m, 1H, H-*9*), 4.07 (d, *J*=15.8, 1H, H-*30*), 3.90 (d, *J*=15.8, 1H, H-*30*), 3.74 (s, 3H, H-*29*), 3.55 (s, 3H, H-*37*), 3.50 (dd, *J*=14.7, 8.4, 1H, H-*8*), 2.96 (dd, *J*=15.1, 4.2, 1H, H-*8*), 2.79 (dd, *J*=13.9, 6.1, 1H, H-*12*), 2.51 – 2.39 (m, 1H, H-*12*).**^{13}C NMR** (126 MHz, MeOD) δ = 164.06 (C-25), 157.14 (C-17), 151.17 (C-4), 143.03 (C-36), 139.98 (C-34), 133.08 (C-22), 131.82 (C-43), 131.27 (C-23, C-27), 131.00 (C-42), 130.96 (C-39), 130.65 (C-41), 130.47 (C-15, C-19), 129.96 (C-6), 129.87 (C-31), 129.62 (C-14), 129.60 (C-2), 128.35 (C-32), 127.67 (C-1), 119.93 (C-44), 117.53 (C-3), 116.33 (C-16, C-18), 114.71 (C-24, C-26), 113.85 (C-40), 60.06 (C-9), 56.14 (C-29), 54.93 (C-8), 47.91 (C-11), 47.24 (C-30), 38.33 (C-12), 31.89 (C-37). **LC-MS** (C18-ESI): 620.18 $[M+H]^+$ R_t=8.05 min. **HRMS (ESI)** calculated for $C_{35}H_{34}O_4N_5S$ $[M+H]^+$: 620.2319, found: 620.2326. $[\boldsymbol{\alpha}]_{\boldsymbol{D}}^{\mathbf{20}}$+78.5 (*c*=1.5, $CHCl_3$).

4-{[(3R)-7-(3,5-difluorophenyl)-4-[(4-methoxybenzene)sulfonyl]-1-[(1-methyl-1H-imidazol-5-yl)methyl]-2,3,4,5-tetrahydro-1H-1,4-benzodiazepin-3-yl]methyl}phenol (113)

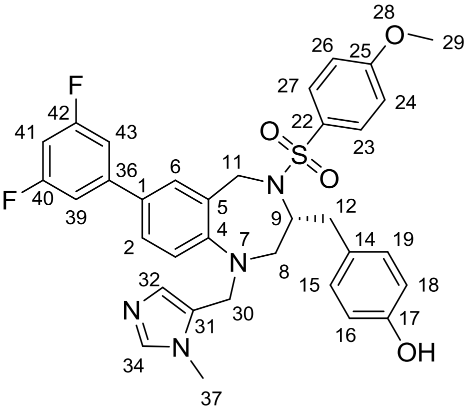

According to General Procedure **IVa** reaction between THB **74**a (150 mg, 0.25 mmol) and 3,5-difluorophenyl boronic acid (44 mg, 0.28 mmol) afforded **113** as an orange solid (112 mg, 71%) **R_f** 0.68 (DCM/MeOH, 10:1) **Mp** 160.6 °C, **^{1}H NMR** (500 MHz, MeOD) δ = 7.54 (s, 1H, H-*34*), 7.33 (d, *J*=9.0, 2H, H-*23,* H-*27*), 7.31 (s, 1H, H-*6*), 7.30 – 7.27 (m, 1H, H-*2*), 7.14 (dd, *J*=8.9, 2.2, 2H, H-*39,* H-*43*), 6.88 (d, *J*=8.2, 2H, H-*15,* H-*19*), 6.81 (tt, *J*=9.0, 2.4, 1H, H-*41*), 6.72 (d, *J*=9.0, 2H, H-*24,* H-*26*), 6.65 (d, *J*=8.2, 2H, H-*16,* H-*18*), 6.64 – 6.63 (m, 1H, H-*3*), 6.62 (s, 1H, H-*32*), 4.65 (d, *J*=17.6, 1H, H-*11*), 4.59 (d, *J*=17.6, 1H, H-*11*), 4.18 – 4.10 (m, 1H, H-*9*), 4.06 (d, *J*=15.7, 1H, H-*30*), 3.89 (d, *J*=15.7, 1H, H-*30*), 3.75 (s, 3H, H-*29*), 3.54 (s, 3H, H-*37*), 3.51 – 3.44 (m, 1H, H-*8*), 2.94 (d, *J*=13.4, 1H, H-*8*), 2.77 (d, *J*=8.2, 1H, H-*12*), 2.51 – 2.38 (m, 1H, H-*12*).**^{13}C NMR** (126 MHz, MeOD) δ = 164.94 (d, *J*=-246.3 (C-40)), 164.83 (d, *J*=-246.6 (C-42)), 164.08 (C-25), 157.16 (C-17), 151.46 (C-4), 134.75 (C-34), 133.07 (C-22), 131.28 (C-15, C-19), 131.11 (C-14), 130.46 (C-23, C-27), 130.00 (C-31), 129.55 (d, *J*=5.4 (C-36)), 128.84 (C-6), 128.25 (C-32), 127.59 (C-2), 118.68 (C-3), 117.36 (d, *J*=4.0 (C-1)) 116.35 (C-16, C-18), 114.73 (C-24, C-26), 109.78 (d, *J*=26.1, (C-39, C-43)), 102.23 (d, *J*=24.3 (C-41)) 60.04 (C-9), 56.13 (C-29), 54.10 (C-8), 47.88 (C-30), 47.20 (C-11), 37.63 (C-12), 31.59 (C-37). **LC-MS** (C18_ESI)**:** 631.18 $[M+H]^+$ R_t = 8.84; **HRMS (ESI)** calculated for $C_{34}H_{33}O_4N_4F_2S$ $[M+H]^+$: 631.2185, found: 631.2183. $[\alpha]_D^{20}$ +49.4 (*c*=0.5, $CHCl_3$).

4-{[(3R)-7-(furan-2-yl)-4-[(4-methoxybenzene)sulfonyl]-1-[(1-methyl-1H-imidazol-5-yl)methyl]-2,3,4,5-tetrahydro-1H-1,4-benzodiazepin-3-yl]methyl}phenol (114)

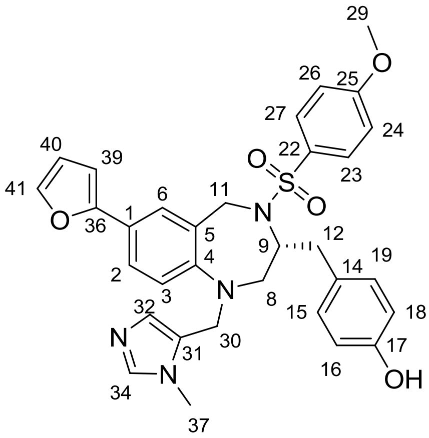

According to General Procedure **IVa** reaction between THB **74**a (150 mg, 0.25 mmol) and 2-furylboronic acid (31 mg, 0.28 mmol) afforded **114** as a redbrown solid (104 mg, 71%) **R$_f$** 0.48 (DCM/MeOH, 10:1), **Mp** 186.5 °C **^{1}H NMR** (500 MHz, MeOD) δ = 7.56 (s, 1H, H-*34*), 7.49 (d, *J*=1.9, 1H, H-*41*), 7.41 (s, 1H, H-*6*), 7.38 (d, *J*=8.6, 1H, H-*2*), 7.34 (d, *J*=8.9, 2H, H-*23,* H-*27*), 6.89 (d, *J*=8.2, 2H, H-*15,* H-*19*), 6.73 (d, *J*=8.9, 2H, H-*24,* H-*26*), 6.69 (s, 1H, H-*32*), 6.65 (d, *J*=8.3, 2H, H-*16,* H-*18*), 6.63 – 6.61 (m, 1H, H-*3*), 6.60 (d, *J*=3.2, 1H, H-*39*), 6.47 (dd, *J*=3.3, 1.8, 1H, H-*40*), 4.65 (d, *J*=16.7, 1H, H-*11*), 4.59 (d, *J*=16.8, 1H, H-*11*), 4.15 – 4.06 (m, 1H, H-*9*), 4.03 (d, *J*=15.6, 1H, H-*30*), 3.90 (d, *J*=15.6, 1H, H-*30*), 3.75 (s, 3H, H-*29*), 3.57 (s, 3H, H-*37*), 3.45 (dd, *J*=14.8, 8.2, 1H, H-*8*), 2.89 (dd, *J*=14.9, 3.5, 1H, H-*8*), 2.80 (dd, *J*=13.8, 6.1, 1H, H-*12*), 2.47 – 2.39 (m, 1H, H-*12*).**^{13}C NMR** (126 MHz, MeOD) δ = 164.08 (C-25), 157.11 (C-17), 155.25 (C-36), 150.48 (C-4), 142.59 (C-41), 139.96 (C-31), 139.93 (C-34), 133.10 (C-22), 131.23 (C-23, C-27), 130.49 (C-15, C-19), 130.44 (C-3), 129.73 (C-14), 128.43 (C-32), 126.78 (C-5), 126.65 (C-6), 124.77 (C-2), 120.77 (C-1), 116.29 (C-24, C-26), 114.71 (C-16, C-18), 112.61 (C-40), 104.36 (C-39), 59.95 (C-9), 56.09 (C-29), 54.76 (C-8), 47.81 (C-11), 47.23 (C-30), 38.20 (C-12), 30.66 (C-37). **LC-MS** (C18_ESI): 585.15 $[M+H]^+$ R_t = 7.96min **HRMS (ESI)** calculated for $C_{32}H_{33}O_5N_4S$ $[M+H]^+$: 585.2162, found: 585.2166. $[\alpha]_D^{20}$ -28.3 (*c*=1, MeOH).

(3R)-N-benzyl-3-[(4-hydroxyphenyl)methyl]-4-[(4-methoxybenzene)sulfonyl]-1-[(1-methyl-1H-imidazol-5-yl)methyl]-2,3,4,5-tetrahydro-1H-1,4-benzodiazepine-7-carboxamide (115)

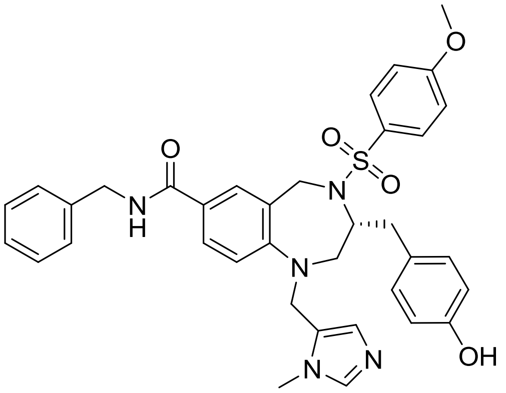

A dry microwave tube was charged with THB **74**a (100 mg, 167 µmol), benzylamine (55 µL, 502 µmol), $Mo(CO)_6$ (44 mg, 167 µmol), Herrmann's palladacycle (7 mg, 8 µmol), tri(tert-butyl)phosphonium tetrafluoroborate (Fu's salt, 73 mg, 251 µmol) and DBU (75 µL, 502 µmol). Dry THF (2 mL) was added, the reaction mixture was purged with argon and irradiated in the microwave at 160 ºC for 30 minutes. After cooling, the reaction mixture was taken up in DCM:MeOH (90:10), filtered through Celite, washed with NH_4Cl (sat.) and brine, dried over Na_2SO_4 and concentrated *in vacuo*. Purification by flash column chromatography (DCM:MeOH 99:1 → 92:8) afforded **115** as a white solid (17 mg, 16%). **^{1}H NMR** (400 MHz, DMSO) δ 8.73 (t, *J* = 6.0 Hz, 1H), 7.58 (s, 1H), 7.46 (d, *J* = 8.7 Hz, 1H), 7.36 – 7.28 (m, 7H), 7.23 (t, *J* = 6.6 Hz, 1H), 7.05 (s, 1H), 6.96 (d, *J* = 8.3 Hz, 2H), 6.74 (d, *J* = 8.9 Hz, 2H), 6.67 (d, *J* = 8.2 Hz, 2H), 6.31 (d, *J* = 7.8 Hz, 1H), 4.59 (d, *J* = 17.5 Hz, 1H), 4.51 – 4.41 (m, 3H), 4.35 – 4.23 (m, *J* = 17.0 Hz, 2H), 3.84 – 3.74 (m, *J* = 16.9, 10.9 Hz, 1H), 3.74 (s, 3H), 3.66 (s, 3H), 3.15 – 3.06 (m, 1H), 3.02 – 2.90 (m, *J* = 12.2 Hz, 1H), 2.75 – 2.57 (m, 2H). **LC-MS** (C4, ESI_MS) 652.2 $[M+H]^+$; R_t = 7.49 min. **HRMS (ESI)**: calculated for $C_{36}H_{38}N_5O_5S$ $[M+H]^+$ 652.2588, found 652.2585.

(R)-N-hexyl-3-(4-hydroxybenzyl)-4-(4-methoxyphenylsulfonyl)-1-((1-methyl-1H-imidazol-5-yl)methyl)-2,3,4,5-tetrahydro-1H-benzo[e][1,4]diazepine-7-carboxamide(116).

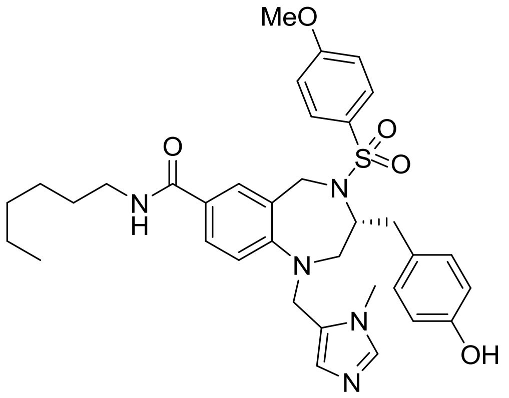

A dry microwave tube was charged with THB **74**a (100 mg, 167 µmol), hexylamine (36 µL, 502 µmol), $Mo(CO)_6$ (44 mg, 167 µmol), Herrmann's palladacycle (7 mg, 8 µmol), tri(tert-butyl)phosphonium tetrafluoroborate (Fu's salt, 73 mg, 251 µmol) and DBU (75 µL, 502 µmol). Dry THF (2 mL) was added, the reaction mixture was purged with argon and irradiated in the microwave at 160 ºC for 30 minutes. After cooling, the reaction mixture was taken into DCM:MeOH (90:10), filtered through celite, washed with NH_4Cl (sat.) and brine, dried over Na_2SO_4 and concentrated *in vacuo*. Purification by flash column chromatography (DCM:MeOH 99:1 → 92:8) afforded **116** as a white solid (14 mg, 13%). **^{1}H NMR** (400 MHz, DMSO) δ 9.23 (s, 1H), 8.39 (br s, 1H), 8.11 (t, *J* = 5.6 Hz, 1H), 7.52 (s, 1H), 7.41 (d, *J* = 8.8 Hz, 1H), 7.31 (d, *J* = 8.9 Hz, 2H), 6.98 – 6.88 (m, 3H), 6.74 (d, *J* = 9.0 Hz, 2H), 6.66 (d, *J* = 8.5 Hz, 2H), 6.31 (d, J = 8.8 Hz, 1H), 4.59 (d, *J* = 17.5 Hz, 1H), 4.45 (d, *J* = 17.7 Hz, 1H), 4.30 – 4.15 (m, *J* = 16.8 Hz, 2H), 3.81 – 3.68 (m, 5H), 3.62 (s, 4H), 3.23 – 3.17 (m, 1H), 3.13 – 3.06 (m, 1H), 2.93 (d, *J* = 10.9 Hz, 1H), 2.74 – 2.55 (m, 1H), 1.49 (d, *J* = 7.0 Hz, 2H), 1.28 (t, *J* = 6.0 Hz, 6H), 0.86 (t, *J* = 6.6 Hz, 3H). **LC-MS** (C4, ESI_MS) 646.2 $[M+H]^+$, 668.3 $[M+Na]^+$; R_t = 8.07 min. **HRMS (ESI)**: calculated for $C_{35}H_{44}N_5O_5$ $[M+H]^+$ 646.3058, found 646.3054.

1-{4-[(3R)-3-[(4-hydroxyphenyl)methyl]-4-[(4-methoxybenzene)sulfonyl]-1-[(1-methyl-1H-imidazol-5-yl)methyl]-2,3,4,5-tetrahydro-1H-1,4-benzodiazepin-7-yl]piperazin-1-yl}ethan-1-one (117)

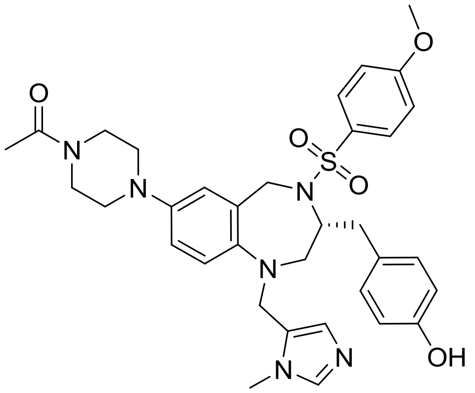

A dry microwave tube was charged with THB **74**a (200 mg, 335 µmol), ligand **95** (10 mg, 33 µmol), $Pd_2(dba)_3$ (15 mg, 17 µmol) and NaO^tBu (64 mg, 669 µmol). Dry THF (2 mL) was added, followed by piperazine (51 mg, 402 µmol). The reaction mixture was purged with argon and irradiated in the microwave at 100 ºC for 8h. After cooling, the reaction mixture was poured into water and the pH was adjusted to 7-8 using NH_4Cl (sat). The aqueous layer was extracted three times with DCM, the combined organic layers were washed with brine, dried over Na_2SO_4 and concentrated *in vacuo*. Purification by flash column chromatography (DCM:MeOH 98:2 → 90:10) afforded **117** as a white solid (65 mg, 30%). **^{1}H NMR** (400 MHz, DMSO) δ 7.39 (s, 1H), 7.35 – 7.29 (m, *J* = 8.9 Hz, 2H), 6.88 (d, *J* = 8.4 Hz, 2H), 6.79 (d, *J* = 9.0 Hz, 4H), 6.69 (d, *J* = 9.0 Hz, 1H), 6.63 (d, *J* = 8.4 Hz, 2H), 6.56 – 6.47 (m, 1H), 4.51 (d, *J* = 16.7 Hz, 1H), 4.38 (d, *J* = 16.9 Hz, 1H), 4.19 (d, *J* = 16.2 Hz, 1H), 4.16 – 4.09 (m, 1H), 4.03 – 3.91 (m, *J* = 15.0 Hz, 1H), 3.77 (s, 3H), 3.76 (s, 3H), 3.62 – 3.56 (m, *J* = 9.4, 4.3 Hz, 4H), 3.37 – 3.28 (m, *J* = 8.5 Hz, 1H), 3.09 – 3.02 (m, *J* = 4.9 Hz, 2H), 3.02 – 2.90 (m, *J* = 13.1, 6.6 Hz, 2H), 2.81 – 2.72 (m, 1H), 2.66 (dd, *J* = 13.8, 6.2 Hz, 1H), 2.49 – 2.41 (m, *J* = 6.1 Hz, 1H), 2.05 (s, 3H); **LC-MS** (C4, ESI_MS) 645.2 $[M+H]^+$; R_t = 6.37 min. **HRMS (ESI):** calculated for $C_{34}H_{41}N_6O_5S$ $[M+H]^+$ 645.2854, found 645.2851.

4-{[(3R)-4-[(4-methoxybenzene)sulfonyl]-1-[(1-methyl-1H-imidazol-5-yl)methyl]-7-(phenylamino)-2,3,4,5-tetrahydro-1H-1,4-benzodiazepin-3-yl]methyl}phenol (118)

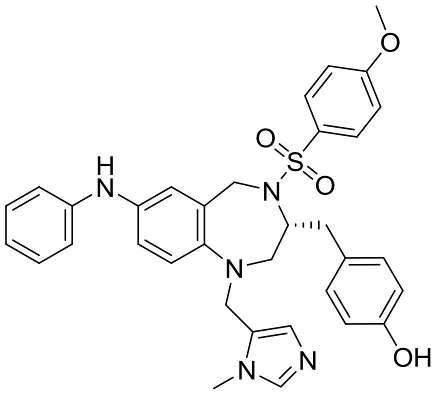

A dry Schlenk tube was charged with THB **74**a (200 mg, 335 µmol), ligand **95** (10 mg, 33 µmol), $Pd_2(dba)_3$ (15 mg, 17 µmol) and NaO^tBu (64 mg, 669 µmol). Dry THF (2 mL) was added, followed by aniline (37 µL, 402 µmol). The reaction mixture was purged with argon and stirred under reflux overnight. After cooling, the reaction mixture was poured into water and the pH was adjusted to 7–8 using NH_4Cl (sat). The aqueous layer was extracted three times with DCM, the combined organic layers were washed with brine, dried over Na_2SO_4 and concentrated *in vacuo*. Purification by flash column chromatography (DCM:MeOH 98:2 → 90:10) afforded **118** as a white solid (170 mg, 83%). **^{1}H NMR** (400 MHz, DMSO) δ 7.42 (s, 1H), 7.31 (d, *J* = 8.8 Hz, 2H), 7.16 (t, *J* = 7.7 Hz, 2H), 6.93 (d, *J* = 8.1 Hz, 2H), 6.90 – 6.77 (m, 7H), 6.71 (t, *J* = 7.3 Hz, 1H), 6.63 – 6.56 (m, *J* = 8.3 Hz, 3H), 4.54 (d, *J* = 16.5 Hz, 1H), 4.31 (d, *J* = 16.5 Hz, 1H), 4.18 (d, *J* = 15.9 Hz, 1H), 4.13 – 3.97 (m, 2H), 3.77 (s, 3H), 3.75 (s, 3H), 3.35 – 3.26 (m, *J* = 13.8 Hz, 1H), 2.82 – 2.71 (m, *J* = 11.6 Hz, 1H), 2.65 (dd, *J* = 13.6, 6.8 Hz, 1H), 2.46 – 2.37 (m, 1H); **LC-MS** (C4, ESI_MS) 610.1 $[M+H]^+$,; R_t = 7.73 min; **HRMS (ESI):** calculated for $C_{34}H_{36}N_5O_4S$ $[M+H]^+$ 610.2483, found 610.2479.

§ 10.3.8 Synthesis of 5th Generation THBs

4-{[(3R)-7-{5-[(1E)-(hydroxyimino)methyl]furan-2-yl}-4-[(4-methoxybenzene)-sulfonyl]-1-[(1-methyl-1H-imidazol-5-yl)methyl]-2,3,4,5-tetrahydro-1H-1,4-benzodiazepin-3-yl]methyl}phenol (119)

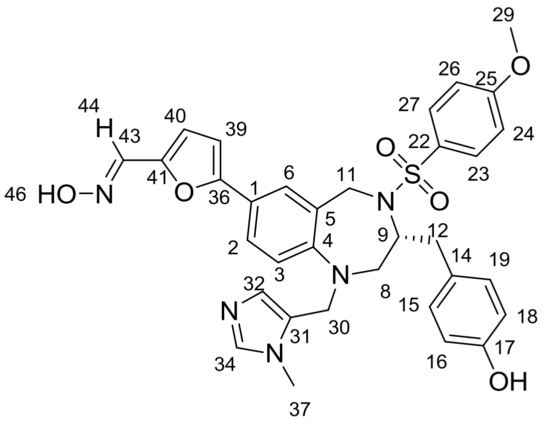

A mixture of THB **108** (25 mg, 163 µmol), $NH_4OH.HCl$ (4.3 mg, 61.2 µmol) and Et_3N (0.1 mL) in 0.5 mL DCM and 0.5 mL MeOH was stirred in a closed flask at 25°C for 3 h after which the solvent was evaporated. The residue was purified by flash chromatography (3% MeOH in DCM) to give **119** (25 mg, 97%) **R_f** 0.25 (6% MeOH in DCM) **Mp** 96.5 °C **^{1}H NMR** (400 MHz, MeOD) δ = 7.99 (s, 1H, H-*44*), 7.55 (s, 1H, H-*46*), 7.49 (d, *J*=2.2, 1H, H-*6*), 7.48 (s, 1H, H-*34*), 7.43 (dd, *J*=8.5, 2.4, 1H, H-*2*), 7.36 (d, *J*=9.0, 2H, H-*23,* H-*27*), 6.92 (d, *J*=8.4, 2H, H-*15,* H-*19*), 6.74 (d, *J*=9.0, 2H, H-*24,* H-*26*), 6.72 (d, *J*=3.5, 1H, H-*39*), 6.69 (d, *J*=3.5, 1H, H-*40*), 6.66 (d, *J*=8.4, 2H, H-*16,* H-*18*), 6.66 (s, 1H, H-*32*), 6.56 (d, *J*=8.4, 1H, H-*3*), 4.67 (d, *J*=16.9, 1H, H-*11*), 4.61 (d, *J*=16.9, 1H, H-*11*), 4.18 – 4.11 (m, 1H, H-*9*), 4.04 (d, *J*=15.9, 1H, H-*30*), 3.85 (d, *J*=16.0, 1H, H-*30*), 3.75 (s, 3H, H-*29*), 3.55 (s, 3H, H-*37*), 3.51 (dd, *J*=15.2, 8.6, 1H, H-*8*), 2.93 (dd, *J*=15.1, 3.7, 1H, H-*8*), 2.81 (dd, *J*=14.1, 6.1, 1H, H-*12*), 2.49 (dd, *J*=13.9, 7.4, 1H, H-*12*).**^{13}C NMR** (126 MHz, MeOD) δ = 164.11 (C-25), 157.13 (C-17), 156.74 (C-36), 150.40 (C-4), 147.83 (C-41), 140.81 (C-43), 137.16 (C-34), 133.06 (C-22), 131.29 (C-15, C-19), 130.46 (C-23, C-27),130.36(C-31), 129.57 (C-14), 127.15 (C-6), 126.82(C-32), 125.37 (C-5), 125.28 (C-2), 120.73 (C-1), 117.02 (C-3), 116.33 (C-16, C-18), 115.82 (C-39), 114.73 (C-24, C-26), 106.31 (C-40), 60.08 (C-9), 56.14 (C-29), 54.75 (C-8), 47.88 (C-30), 47.10 (C-11), 32.24 (C-12), 30.68 (C-37). **LC-MS** (C18_ESI)**:** 628.15 $[M+H]^+$ R_t=6.06min. **HRMS (ESI)** calculated for $C_{33}H_{34}O_6N_5S$ $[M+H]^+$: 628.2224, found: 628.2220. $[\alpha]_D^{20}$+44.6 (*c*=1, MeOH).

5-[(3R)-3-[(4-hydroxyphenyl)methyl]-4-[(4-methoxybenzene)sulfonyl]-1-[(1-methyl-1H-imidazol-5-yl)methyl]-2,3,4,5-tetrahydro-1H-1,4-benzodiazepin-7-yl]furan-2-carbonitrile(120)

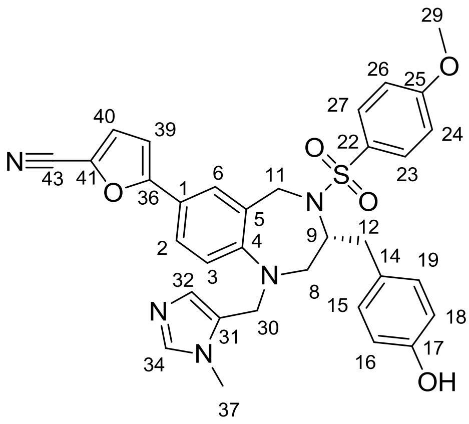

A mixture of THB **108** (100 mg, 163 µmol), $NH_4OH.HCl$ (13.6 mg, 196 µmol) and Et_3N (68 µL, 489 µmol) in 0.5 mL DCM and 0.5 ml MeOH was stirred in a closed flask at 25°C for 3 h after which the solvent was evaporated. The residue was dissolved in DCM and cooled to 0°C. TFAA (23 µL, 163 µmol) and Et_3N (136 µL, 978 µmol) were added and the mixture was allowed to come to room temperature. After stirring for 2 h an extra equiv. of TFAA was added. After stirring another 2 h, the reaction was quenched with $NaHCO_3$ (sat) and extracted three times with DCM. The combined organic layers were washed with brine, dried over Na_2SO_4 and concentrated *in vacuo*. The crude product was purified by column chromatography (DCM: MeOH 98:2). $\mathbf{R_f}$ 0.28, **Mp** 136 °C, ^{1}**H NMR** (500 MHz, MeOD) δ = 7.56 (s, 1H, H-*34*), 7.46 (d, *J*=2.2, 1H, H-*6*), 7.41 (dd, *J*=8.5, 2.2, 1H, H-*2*), 7.36 (d, *J*=8.9, 2H, H-*27*), 7.34 (d, *J*=3.7, 1H, H-*40*), 6.94 (d, *J*=8.3, 2H, H-*19*), 6.78 (d, *J*=3.7, 1H, H-*39*), 6.75 (d, *J*=8.9, 2H, H-*26*), 6.67 (d, *J*=8.4, 2H, H-*18*), 6.63 (s, 1H, H-*32*), 6.55 (d, *J*=8.5, 1H, H-*3*), 4.68 (d, *J*=17.2, 1H, H-*30*), 4.62 (d, *J*=17.3, 1H, H-*30*), 4.18 (s, 1H, H-*9*), 4.08 (d, *J*=16.1, 1H, H-*11*), 3.84 (d, *J*=15.8, 1H, H-*11*), 3.76 (s, 3H, H-*29*), 3.61 – 3.54 (m, 1H, H-*8*), 3.55 (s, 3H, H-*37*), 2.99 (dd, *J*=15.2, 4.1, 1H, H-*8*), 2.82 (dd, *J*=13.7, 5.6, 1H, H-*12*), 2.60 – 2.49 (m, 1H, H-*12*). ^{13}**C NMR** (126 MHz, MeOD) δ = 164.13 (C-25), 160.47 (C-36), 157.20 (C-17), 151.61 (C-4), 139.99 (C-34), 133.06 (C-22), 131.30 (C-15, C-19), 130.43 (C-23, C-27), 129.68 (C-31), 129.46 (C-14), 128.09 (C-32), 127.86 (C-6), 125.93 (C-2), 125.81 (C-40), 125.14 (C-41), 121.53 (C-1), 116.89 (C-3), 116.35 (C-16, C-18), 114.72 (C-24, C-26), 113.07 (C-43), 105.62 (C-39), 60.19 (C-9), 56.14 (C-29), 54.58 (C-8), 47.89 (C-30), 47.06 (C-11), 38.74 (C-12), 31.84 (C-37). **LC-MS** (C18_ESI): 610.2 $[M+H]^+$ R_t = 6.43min **HRMS (ESI)** calculated for $C_{33}H_{32}O_5N_5S$ $[M+H]^+$: 610.2119, found: 610.2113. $[\alpha]_D^{20}$ +34.2 (*c*=1, MeOH).

4-{[(3R)-7-(2-chloropyridin-4-yl)-4-[(4-methoxybenzene)sulfonyl]-1-[(1-methyl-1H-imidazol-5-yl)methyl]-2,3,4,5-tetrahydro-1H-1,4-benzodiazepin-3-yl]methyl}phenol (123)

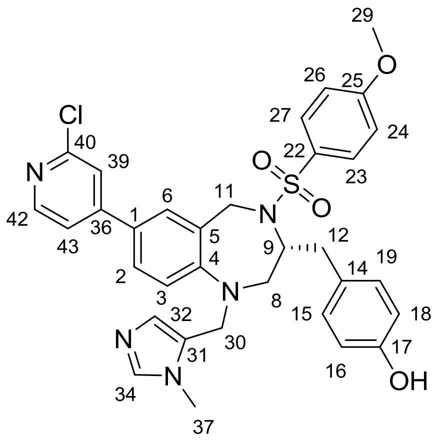

A dry Schlenk tube was charged with THB **74**a (0.5 g, 0.84 mmol), bis(pinacolato)diboron (0.32 g, 1.26 mmol), PdCl$_2$(dppf) (34 mg, 42 µmol), and potassium acetate (0.8 g, 8.4 mmol) in DMSO. The mixture was degassed and heated to 95°C overnight. The resulting mixture was diluted with ethyl acetate, and the solution was filtered and washed with brine. The resulting organic layer was dried and concentrated. The resulting boronate **122** was used as a crude in the next step. Following General Procedure **IVb**, a solution of boronate **122** (0.2 g, 31 µmol) in DME/water was allowed to react with 4-bromo-2-chloropyridine (66 mg, 34 µmol) to give **123** as a white solid(109 mg, 56%) **R$_f$** 0.27 (5% MeOH in DCM), **Mp** 136 °C. **^{1}H NMR**(400 MHz, MeOD) δ = 8.24 (d, *J*=5.4, 1H, H-*42*), 7.54 (d, *J*=1.8, 1H, H-*39*), 7.50 (s, 1H, H-*34*), 7.46 (dd, *J*=5.4, 1.8, 1H, H-*43*), 7.37 (d, *J*=2.3, 1H, H-*6*), 7.33 (dd, *J*=8.7, 2.1, 1H, H-*2*), 7.32 (d, *J*=8.9, 2H, H-*23,* H-*27*), 6.90 (d, *J*=8.4, 2H, H-*15,* H-*19*), 6.68 (d, *J*=9.0, 2H, H-*24,* H-*26*), 6.67 (d, *J*=8.4, 2H, H-*16,* H-*18*), 6.63 (s, 1H, H-*32*), 6.52 (d, *J*=8.8, 1H, H-*3*), 4.61 (s, 2H, H-*11*), 4.19 – 4.10 (m, 1H, H-*9*), 4.04 (d, *J*=16.2, 1H, H-*30*), 3.80 (d, *J*=16.2, 1H, H-*30*), 3.72 (s, 3H, H-*29*), 3.59 – 3.52 (m, 1H, H-*8*), 3.51 (s, 3H, H-*37*), 2.98 (dd, *J*=15.2, 4.0, 1H, H-*8*), 2.78 (dd, *J*=13.7, 5.3, 1H, H-*12*), 2.52 (dd, *J*=13.5, 7.3, 1H, H-*12*).**^{13}C NMR** (101 MHz, MeOD) δ = 163.70 (C-25), 156.85 (C-17), 152.63 (C-40), 152.17 (C-4), 151.74 (C-36), 150.38 (C-42), 139.69 (C-34), 132.59 (C-22), 131.11 (C-15, C-19), 130.14 (C-23, C-27), 129.54 (C-6), 129.14 (C-31), 128.94 (C-14), 127.96 (C-32), 127.64 (C-1), 121.49 (C-39), 120.48 (C-43), 116.88 (C-3), 116.22 (C-24, C-26), 114.48 (C-16, C-18), 59.74 (C-9), 56.08 (C-29), 54.36 (C-8), 47.88 (C-30), 46.93 (C-11), 38.50 (C-12), 31.88 (C-37).**LC-MS** (C18_ESI): 630.19 [M+H]$^+$ R$_t$ = 6.25min **HRMS (ESI)** calculated for $C_{33}H_{33}O_4N_5ClS$ [M+H]$^+$: 630.19363, found: 630.1932. $[\boldsymbol{\alpha}]_{\boldsymbol{D}}^{\mathbf{20}}$ +251 (*c*=1, MeOH/CHCl$_3$, 1:1).

4-{[(3R)-7-(5-formylfuran-2-yl)-4-[(4-methoxybenzene)sulfonyl]-1-[(1-methyl-1H-imidazol-5-yl)methyl]-2,3,4,5-tetrahydro-1H-1,4-benzodiazepin-3-yl]methyl}phenyl trifluoromethanesulfonate (124)

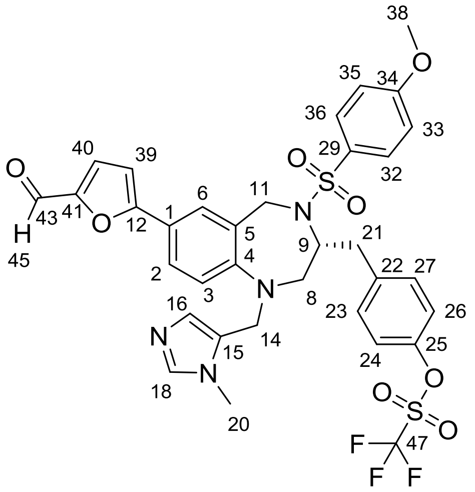

According to General Procedure **III**, reaction between THB **108** (200 mg, 0.33 mmol) and **86** (175 mg, 0.49 mmol) afforded **124** as an orange solid. (210 mg, 86%) **R*f*** 0.72 (10% MeOH in DCM), **Mp** 144.6 °C. **^{1}H NMR** (500 MHz, MeOD) δ = 9.52 (s, 1H, H-*45*), 7.61 (d, *J*=2.2, 1H, H-*6*), 7.60 (s, 1H, H-*18*), 7.55 (dd, *J*=8.5, 2.0, 1H, H-*2*), 7.52 (d, *J*=3.7, 1H, H-*40*), 7.39 (d, *J*=8.8, 2H, H-*32,* H-*36*), 7.32 (d, *J*=8.5, 2H, H-*23,* H-*27*), 7.26 (d, *J*=8.5, 2H, H-*24,* H-*26*), 6.93 (d, *J*=3.7, 1H, H-*39*), 6.76 (d, *J*=8.8, 2H, H-*33,* H-*35*), 6.70 (s, 1H, H-*16*), 6.62 (d, *J*=8.5, 1H, H-*3*), 4.78 (d, *J*=17.1, 1H, H-*11*), 4.69 (d, *J*=17.2, 1H, H-*11*), 4.33 – 4.26 (m, 1H, H-*9*), 4.17 (d, *J*=16.0, 1H, H-*14*), 3.93 (d, *J*=16.0, 1H, H-*14*), 3.76 (s, 3H, H-*38*), 3.65 (dd, *J*=15.5, 9.4, 1H, H-*8*), 3.60 (s, 3H, H-*20*), 3.03 (dd, *J*=15.2, 3.9, 1H, H-*8*), 2.95 (dd, *J*=13.8, 6.9, 1H, H-*21*), 2.69 – 2.60 (m, 1H, H-*21*). **^{13}C NMR** (126 MHz, MeOD) δ = 178.47 (C-43), 164.20 (C-34), 160.22 (C-12), 152.46 (C-41), 152.08 (C-4), 149.79 (C-25), 140.08 (C-18), 140.02 (C-22), 133.08 (C-29), 132.47 (C-23, C-27), 130.48 (C-32, C-36), 128.48 (C-6), 128.17 (C-16), 127.28 (C-40), 126.62 (C-2), 122.32 (C-24, C-26), 121.69(C-1), 117.11 (C-3), 114.74 (C-33, C-35), 107.55 (C-39), 59.91 (C-9), 56.12 (C-38), 54.32(C-8), 47.72 (C-14), 47.13 (C-11), 37.45 (C-21), 31.82 (C-20). **LC-MS** (C18_ESI)**:** 745.15 $[M+H]^+$, R_t=8.99min; **HRMS (ESI)** calculated for $C_{34}H_{32}O_6N_4F_3S_2$ $[M+H]^+$: 745.16082, found: 745.15982. $[\alpha]_D^{20}$+144.2 (*c*=0.42, $CHCl_3$).

5-[(3R)-3-{[4-(4-chlorophenyl)phenyl]methyl}-4-[(4-methoxybenzene)sulfonyl]-1-[(1-methyl-1H-imidazol-5-yl)methyl]-2,3,4,5-tetrahydro-1H-1,4-benzodiazepin-7-yl]furan-2-carbaldehyde(125)

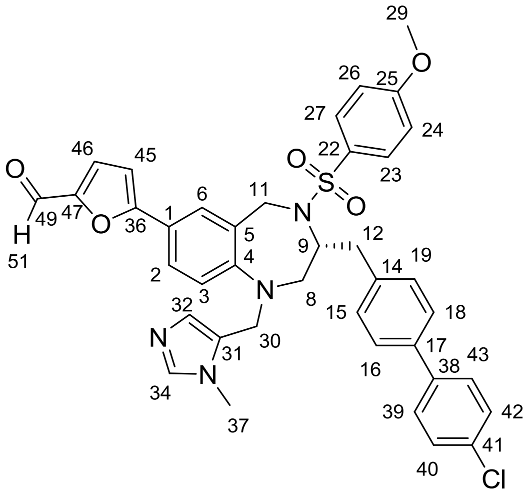

According to General Procedure **IVb** reaction between THB **124** (50 mg, 0.075 mmol) and parachlorobenzylboronic acid (12 mg, 0.07 mmol) afforded**125** as an orange solid (40 mg, 84%). **R_f** 0.29 (3% MeOH in DCM), **Mp** 114.7 °C. **^{1}H NMR** (500 MHz, MeOD) δ = 9.50 (s, 1H, H-*51*), 7.61 (d, *J*=8.6, 2H, H-*43*), 7.60 (d, *J*=2.3, 1H, H-*6*), 7.56 (s, 1H, H-*34*), 7.54 (dd, *J*=8.6, 2.3, 1H, H-*2*), 7.50 (d, *J*=8.0, 2H, H-*18*), 7.50 (d, *J*=3.8, 1H, H-*46*), 7.43 (d, *J*=8.6, 2H, H-*40*), 7.38 (d, *J*=8.9, 2H, H-*27*), 7.22 (d, *J*=8.0, 2H, H-*15*), 6.91 (d, *J*=3.8, 1H, H-*45*), 6.72 (d, *J*=8.9, 2H, H-*26*), 6.67 (s, 1H, H-*32*), 6.60 (d, *J*=8.6, 1H, H-*3*), 4.76 (d, *J*=17.1, 1H, H-*11*), 4.68 (d, *J*=17.2, 1H, H-*11*), 4.34 – 4.25 (m, 1H, H-*9*), 4.14 (d, *J*=16.0, 1H, H-*30*), 3.90 (d, *J*=16.0, 1H, H-*30*), 3.69 (s, 3H, H-*29*), 3.72 – 3.61 (m, 1H, H-*8*), 3.57 (s, 3H, H-*37*), 3.06 (dd, *J*=15.2, 4.1, 1H, H-*8*), 2.95 (dd, *J*=13.6, 6.1, 1H, H-*12*), 2.72 – 2.61 (m, 1H, H-*12*).**^{13}C NMR** (126 MHz, MeOD) δ = 178.49 (C-49), 164.14 (C-25), 161.62 (C-47), 152.86 (C-36), 152.61 (C-4), 140.75 (C-38), 140.04 (C-34), 139.35 (C-17), 138.47 (C-14), 134.30 (C-41), 133.08 (C-22), 131.02 (C-15, C-19), 130.43 (C-23, C-27), 129.94 (C-40, C-42), 129.71(C-31), 129.66 (C-6), 129.35 (C-39, C-43), 128.49 (C-46), 128.19 (C-32), 127.94 (C-16, C-18), 126.59 (C-2), 121.67(C-1), 117.05 (C-3), 114.73 (C-24, C-26), 107.52 (C-45), 60.02 (C-9), 56.08 (C-29), 54.81 (C-8), 47.90 (C-30), 47.13 (C-11), 38.99 (C-12), 31.86 (C-37). **LC-MS (C18_ESI):** 707.16 [M+H]$^+$ R_t=7.46min; **HRMS (ESI)** calculated for $C_{39}H_{36}O_5N_4ClS$ [M+H]$^+$: 707.20895, found: 707.20863. $[\alpha]_D^{20}$ +72.3 (*c*=0.6, $CHCl_3$/MeOH 1:1).

4-{[(3R)-7-(5-cyanofuran-2-yl)-4-[(4-methoxybenzene)sulfonyl]-1-[(1-methyl-1H-imidazol-5-yl)methyl]-2,3,4,5-tetrahydro-1H-1,4-benzodiazepin-3-yl]methyl}phenyl N-benzylcarbamate (126)

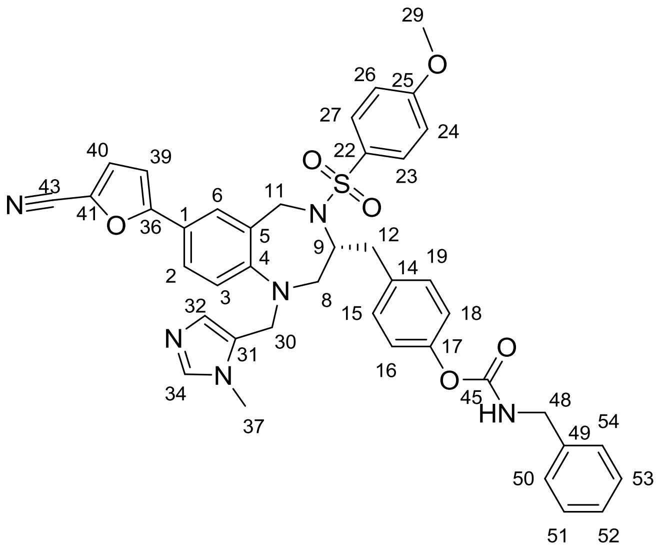

According to General Procedure **II**, reaction between THB **120** (22 mg, 36 µmol) and benzyl-isocyanate (5.4 mg, 40 µmol) afforded **126** as an orange solid (19 mg, 71%) **R_f** 0.24 (3% MeOH in DCM), **Mp** 155 °C. **^{1}H NMR** (500 MHz, MeOD)δ = 7.57 (s, 1H, H-*34*), 7.47 (d, *J*=2.3, 1H, H-*6*), 7.42 (dd, *J*=8.6, 2.3, 1H, H-*2*), 7.36 (d, *J*=8.8, 2H, H-*23,* H-*27*), 7.34 (d, *J*=3.7, 1H, H-*40*) 7.35 – 7.31 (m, 4H, H-*50, 51, 53, 54*), 7.31 – 7.26 (m, 1H, H-*52*), 7.12 (d, *J*=8.2, 2H, H-*15,* H-*19*), 7.00 (d, *J*=8.4, 2H, H-*16,* H-*18*), 6.78 (d, *J*=3.7, 1H, H-*39*), 6.76 (d, *J*=8.9, 2H, H-*24,* H-*26*), 6.65 (s, 1H, H-*32*), 6.56 (d, *J*=8.0, 1H, H-*3*), 4.72 (d, *J*=17.2, 1H, H-*30*), 4.63 (d, *J*=17.2, 1H, H-*30*), 4.36 (s, 2H, H-*48*), 4.25 – 4.16 (m, 1H, H-*9*), 4.09 (d, *J*=16.0, 1H, H-*11*), 3.85 (d, *J*=15.9, 1H, H-*11*), 3.74 (s, 3H, H-*29*), 3.61 (dd, *J*=15.3, 9.4, 1H, H-*8*), 3.54 (s, 3H, H-*37*), 2.99 (dd, *J*=15.2, 4.0, 1H, H-*8*), 2.90 (dd, *J*=13.7, 5.6, 1H, H-*12*), 2.73 – 2.55 (m, 1H, H-*12*).**^{13}C NMR** (126 MHz, MeOD) δ = 164.18 (C-25), 160.45 (C-36), 157.40 (C-45), 151.58 (C-4), 151.43 (C-17), 140.26 (C-49), 140.03 (C-34), 135.89 (C-14), 132.91 (C-22), 131.17 (C-15, C-19), 130.49 (C-23, C-27), 129.57 (C-5), 129.45 (C-31), 128.41 (C-50, C-54), 128.29 (C-51, C-53),128.19 (C-52), 128.04 (C-32), 127.90 (C-6), 125.96 (C-40), 125.81 (C-2), 125.16 (C-41), 122.83 (C-16, C-18), 121.58 (C-1), 116.86 (C-3), 114.78 (C-24, C-26), 113.06 (C-43), 105.64 (C-39), 60.11 (C-9), 56.16 (C-29), 54.44 (C-8), 47.89 (C-30), 46.91 (C-11), 45.72 (C-48), 38.83 (C-12), 31.84 (C-37). **LC-MS** (C18, ESI_MS) 743.30 [M+H]$^+$; R_t = 8.48 min; **HRMS (ESI)** calculated for $C_{41}H_{40}O_6N_6S$ [M+H]$^+$ 744.2725, found 744.2693. $[\boldsymbol{\alpha}]_{\boldsymbol{D}}^{\boldsymbol{20}}$+172.84 (*c*=0.84, MeOH).

5-[(3R)-3-{[4-(benzyloxy)phenyl]methyl}-4-[(4-methoxybenzene)sulfonyl]-1-[(1-methyl-1H-imidazol-5-yl)methyl]-2,3,4,5-tetrahydro-1H-1,4-benzodiazepin-7-yl]furan-2-carbonitrile(127)

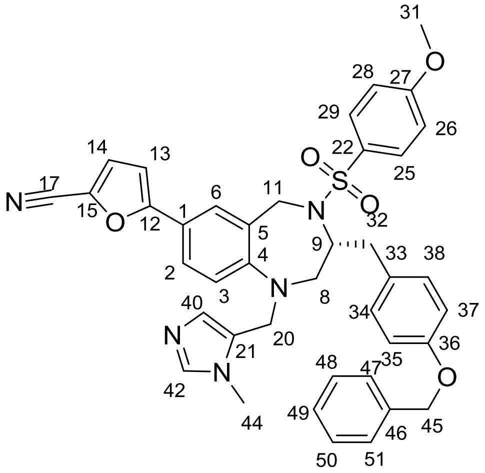

According to General Procedure I, reaction between THB **120** (20 mg, 33 µmol) and benzyl bromide (6.2 mg, 36 µmol) afforded **127**as a white solid (16 mg, 69%). **R_f** 0.28 (3% MeOH in DCM), **Mp** 92 °C **^{1}H NMR** (500 MHz, MeOD) δ = 7.52 (s, 1H, H-*42*), 7.46 (d, *J*=2.3, 1H, H-*6*), 7.44 – 7.40 (m, 2H, H-*47,* H-*51*), 7.42 (dd, *J*=7.6, 2.4, 1H, H-*2*) 7.38 – 7.34 (m, 2H, H-*48,* H-*50*), 7.36 (d, *J*=8.9, 2H, H-*25,* H-*29*), 7.31 (d, *J*=3.7, 1H, H-*14*), 7.31 – 7.27 (m, 1H, H-*49*), 7.02 (d, *J*=8.4, 2H, H-*34,* H-*38*), 6.87 (d, *J*=8.5, 2H, H-*35,* H-*37*), 6.75 (d, *J*=3.7, 1H, H-*13*), 6.73 (d, *J*=8.9, 2H, H-*26,* H-*28*), 6.64 (s, 1H, H-*40*), 6.56 (d, *J*=7.6, 1H, H-*3*), 5.05 (s, 2H, H-*45*), 4.62 (s, 2H, H-*11*), 4.22 – 4.12 (m, 1H, H-*9*), 4.07 (d, *J*=16.1, 1H, H-*20*), 3.84 (d, *J*=15.9, 1H, H-*20*), 3.75 (s, 3H, H-*31*), 3.59 – 3.55 (m, 1H, H-*8*), 3.54 (s, 3H, H-*44*), 3.04 – 2.95 (m, 1H, H-*8*), 2.84 (dd, *J*=13.5, 5.4, 1H, H-*32*), 2.63 – 2.51 (m, 1H, H-*32*). **^{13}C NMR** (126 MHz, MeOD) δ = 163.92 (C-27), 160.20 (C-12), 158.84 (C-36), 151.47 (C-4), 139.87 (C-42), 138.52 (C-46), 132.81 (C-22), 131.19 (C-34, C-38), 130.73 (C-33), 130.26 (C-25, C-29), 129.37 (C-48, C-50), 129.02(C-21), 128.74 (C-49), 128.46 (C-47, C-51), 128.15 (C-40), 127.74 (C-6), 125.88 (C-2), 125.75 (C-15), 125.64 (C-14), 125.03 (C-1), 116.84 (C-3), 115.92 (C-35, C-37), 114.60 (C-26, C-28), 112.95 (C-17), 105.53 (C-13), 70.91 (C-45), 59.79 (C-9), 56.10 (C-31), 54.49 (C-8), 47.83 (C-11), 47.03 (C-20), 38.43 (C-32), 31.84 (C-44). **LC-MS** (C18_ESI)**:** 700.2 [M+H]$^+$, R_t=7.22min; **HRMS (ESI)** calculated for $C_{40}H_{38}O_5N_5S$ [M+H]$^+$: 700.25882, found: 700.25871. $[\boldsymbol{\alpha}]_{\boldsymbol{D}}^{\boldsymbol{20}}$ +40.6 (*c*=0.6, $CHCl_3$).

4-{[(3R)-7-(5-cyanofuran-2-yl)-4-[(4-methoxybenzene)sulfonyl]-1-[(1-methyl-1H-imidazol-5-yl)methyl]-2,3,4,5-tetrahydro-1H-1,4-benzodiazepin-3-yl]methyl}phenyl trifluoromethanesulfonate (128)

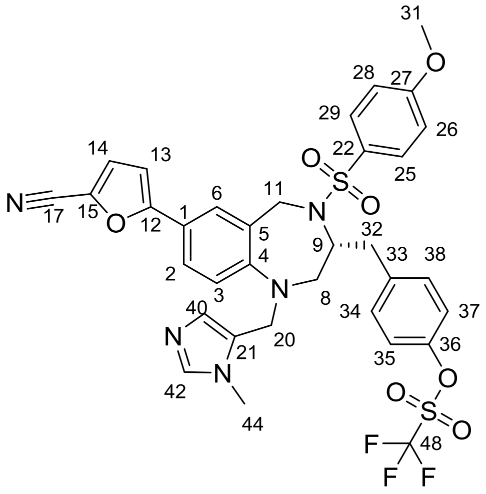
31
O
28
27
29
26
22
O
S
O
25
14
13
N
17
15
O
12
6
11
1
5
N
4
9
32
33
38
2
3
N
8
34
37
40
N
21
20
36
35
O
42
N
44
O
S
O
F
48
F
F

According to General Procedure **III**, reaction between THB **120** (400 mg, 0.66 mmol) and **86** (352 mg, 0.89 mmol) afforded **128** as a white solid which was used as a crude in the subsequent steps. **^{1}H NMR** (400 MHz, MeOD) δ = 7.58 (s, 1H, H-*42*), 7.48 (d, *J*=2.2, 1H, H-*6*), 7.43 (dd, *J*=8.4, 2.2, 1H, H-*2*), 7.36 (d, *J*=8.9, 2H, H-*25,* H-*29*), 7.34 (d, *J*=3.7, 1H, H-*14*), 7.28 (d, *J*=8.5, 2H, H-*34,* H-*38*), 7.22 (d, *J*=8.7, 2H, H-*35,* H-*37*), 6.79 (d, *J*=3.7, 1H, H-*13*), 6.73 (d, *J*=8.8, 2H, H-*26,* H-*28*), 6.69 (s, 1H, H-*40*), 6.61 (d, *J*=8.4, 1H, H-*3*), 4.74 (d, *J*=16.8, 1H, H-*11*), 4.65 (d, *J*=16.7, 1H, H-*11*), 4.29 – 4.20 (m, 1H, H-*9*), 4.13 (d, *J*=15.8, 1H, H-*20*), 3.90 (d, *J*=15.9, 1H, H-*20*), 3.75 (s, 3H, H-*31*), 3.66 – 3.59 (m, 1H, H-*8*), 3.58 (s, 3H, H-*44*), 3.00 (dd, *J*=15.1, 4.1, 1H, H-*8*), 2.92 (dd, *J*=13.8, 6.8, 1H, H-*32*), 2.65 – 2.53 (m, 1H, H-*32*). **LC-MS** (C18_ESI): 742.08 $[M+H]^+$, R_t=7.19min.

5-[(3R)-4-[(4-methoxybenzene)sulfonyl]-1-[(1-methyl-1H-imidazol-5-yl)methyl]-3-{[4-(pyridin-3-yl)phenyl]methyl}-2,3,4,5-tetrahydro-1H-1,4-benzodiazepin-7-yl]furan-2-carbonitrile(129)

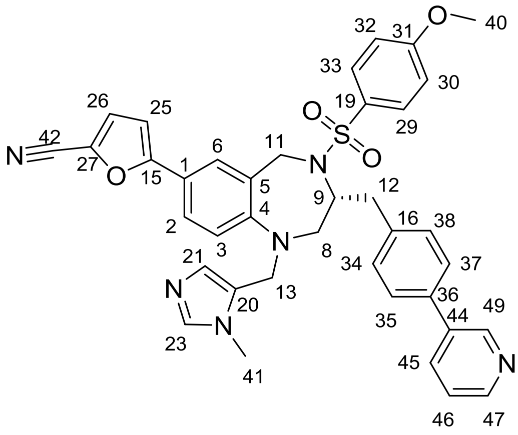
O
40
32
31
33
30
19
O
S
O
29
26
25
N
42
27
O
15
6
11
1
5
N
4
9
12
16
38
2
21
3
N
8
34
37
N
20
13
36
44
49
35
23
N
41
45
N
46
47

According to General Procedure **IVb** reaction between THB **128** (50 mg, 0.075 mmol) and 3-pyridineboronic acid (9.1 mg, 0.07 mmol) afforded **129** as an yellow solid (32 mg, 68%) **R_f** 0.24 (3% MeOH in DCM), **Mp** 114 °C. **^{1}H NMR** (500 MHz, MeOD) δ = 8.80 (dd, *J*=2.4, 0.9, 1H, H-*49*), 8.51 (dd, *J*=4.9, 1.5, 1H, H-*47*), 8.09 (ddd, *J*=8.0, 2.3, 1.6, 1H, H-*45*) 7.58 (s, 1H, H-*23*), 7.55 (d, *J*=8.1, 2H, H-*29,* H-*33*), 7.51 (ddd, *J*=7.9, 4.8, 0.8, 1H, H-*46*), 7.50 (s, 1H, H-*6*), 7.45 (d, *J*=8.4, 1H, H-*2*), 7.38 (d, *J*=8.9, 2H, H-*35,* H-*37*), 7.35 (d, *J*=3.7, 1H, H-*26*), 7.27 (d, *J*=8.0, 2H, H-*34,* H-*38*), 6.80 (d, *J*=3.7, 1H, H-*25*), 6.72 (d, *J*=8.9, 2H, H-*30,* H-*32*), 6.69 (s, 1H, H-*21*), 6.63 (d, *J*=8.5, 1H, H-*3*), 4.77 (d, *J*=17.0, 1H, H-*11*), 4.68 (d, *J*=17.1, 1H, H-*11*), 4.29 (s, 1H, H-*9*), 4.14 (d, *J*=16.0, 1H, H-*13*), 3.93 (d, *J*=16.0, 1H, H-*13*), 3.70 (s, 3H, H-*40*), 3.69 – 3.61 (m, 1H, H-*8*), 3.59 (s, 3H, H-*41*), 3.06 (dd, *J*=15.2, 4.0, 1H, H-*8*), 2.96 (dd, *J*=13.6, 6.4, 1H, H-*12*), 2.69 – 2.59 (m, 1H, H-*12*).^{13}C NMR (126 MHz, MeOD) δ = 164.14 (C-31), 160.41 (C-15), 151.95 (C-4), 148.62 (C-47), 148.26 (C-49), 140.06 (C-23), 139.40 (C-16), 138.32 (C-44), 136.77 (C-36), 136.37 (C-45), 133.11 (C-19), 131.30 (C-34, C-38), 130.44 (C-35, C-37), 129.74 (C-20), 128.25 (C-21), 128.14 (C-29, C-33), 127.93 (C-6), 126.01 (C-27), 125.80 (C-2), 125.46 (C-26), 125.23 (C-46), 117.14 (C-3), 114.73 (C-30, C-32), 113.04 (C-42), 105.76 (C-25), 59.94 (C-9), 56.08 (C-40), 54.94 (C-8), 47.82 (C-13), 47.21 (C-11), 38.76 (C-12), 31.87 (C-41).**LC-MS** (C18_ESI)**:** 670.98 $[M+H]^+$, R$_t$=5.29min; **HRMS (ESI)** calculated for $C_{38}H_{35}O_4N_6S$ $[M+H]^+$: 671.24350, found: 671.24217. $[\boldsymbol{\alpha}]_{\boldsymbol{D}}^{\mathbf{20}}$ + 66.1 (*c*=0.5, MeOH/CHCl$_3$,1:1).

5-[(3R)-4-[(4-methoxybenzene)sulfonyl]-1-[(1-methyl-1H-imidazol-5-yl)methyl]-3-{[4-(phenylamino)phenyl]methyl}-2,3,4,5-tetrahydro-1H-1,4-benzodiazepin-7-yl]furan-2-carbonitrile (130)

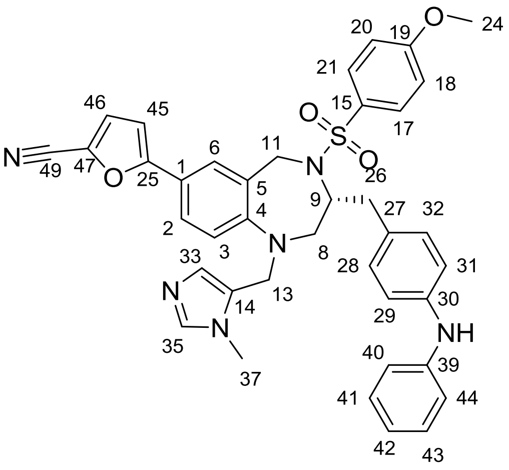

A dry Schlenk tube was charged with THB **128** (50 mg, 67 µmol), ligand **95** (6 mg, 20 µmol), Pd(OAc)$_2$ (1.5 mg, 6.7 µmol) and Cs$_2$CO$_3$ (44 mg, 135 µmol). Dry toluene (0.5 mL) was added, followed by aniline (8 mg, 86 µmol). The reaction mixture was purged with argon and stirred at reflux overnight. After cooling, the solvent was evaporated and the product was purified by flash column chromatography (2% MeOH in DCM) affording **130** as a white solid (20 mg, 43%). ^{1}**H NMR** (500 MHz, MeOD) δ = 7.56 (s, 1H, H-*35*), 7.49 (d, *J*=2.5, 1H, H-*6*), 7.44 (dd, *J*=8.4, 2.3, 1H, H-*2*), 7.38 (d, *J*=8.9, 2H, H-*17,* H-*21*), 7.35 (d, *J*=3.7, 1H, H-*46*), 7.21 (dd, *J*=8.6, 7.4, 2H, H-*41,* H-*43*), 7.06 (ddd, *J*=8.5, 1.3, 1.3, 2H, H-*40,* H-*44*) 6.98 (s, 4H, H-*28, 29, 31, 32*), 6.83 (ddd, *J*=7.5, 1.3, 1.3, 1H, H-*42*), 6.80 (d, *J*=3.7, 1H, H-*45*), 6.76 (d, *J*=8.9, 2H, H-*18,* H-*20*), 6.66 (s, 1H, H-*33*), 6.59 (d, *J*=8.5, 1H, H-*3*), 4.73 (d, *J*=17.1, 1H, H-*11*), 4.64 (d, *J*=17.1, 1H, H-*11*), 4.25 – 4.17 (m, 1H, H-*9*), 4.11 (d, *J*=16.1, 1H, H-*13*), 3.88 (d, *J*=16.1, 1H, H-*13*), 3.74 (s, 3H, H-*24*), 3.66 – 3.58 (m, 1H, H-*8*), 3.57 (s, 3H, H-*37*), 3.03 (dd, *J*=15.3, 4.0, 1H, H-*8*), 2.85 (dd, *J*=13.7, 5.7, 1H, H-*26*), 2.61 – 2.51 (m, 1H, H-*26*).^{13}**C NMR** (126 MHz, MeOD) δ = 164.14 (C-19), 160.56 (C-25), 151.63 (C-4), 145.30 (C-39), 143.89 (C-30), 139.82 (C-35), 133.09 (C-15), 131.01 (C-28, C-32), 130.47 (C-17, C-21), 130.21 (C-27), 130.12 (C-41, C-43), 129.62 (C-14), 128.23 (C-33), 127.89 (C-6), 125.95 (C-2), 125.81 (C-46), 125.18 (C-47), 121.07 (C-42), 118.50 (C-29, C-31), 118.24 (C-40, C-44), 116.72 (C-3), 114.70 (C-18, C-20), 113.05 (C-49), 105.65 (C-45), 60.18 (C-9), 56.13 (C-24), 54.38 (C-8), 47.52 (C-11), 46.76 (C-13), 38.39 (C-26), 31.82 (C-37). **LC-MS** (C18_ESI)**:** 685.18 [M+H]$^+$, R$_t$=7.05min; **HRMS (ESI)** calculated for $C_{39}H_{37}O_4N_6S$ [M+H]$^+$: 685.25915, found: 685.25908.

4-{[(3R)-4-[(4-methoxybenzene)sulfonyl]-7-(2-methoxypyridin-4-yl)-1-[(1-methyl-1H-imidazol-5-yl)methyl]-2,3,4,5-tetrahydro-1H-1,4-benzodiazepin-3-yl]methyl}phenyl N-benzylcarbamate(131)

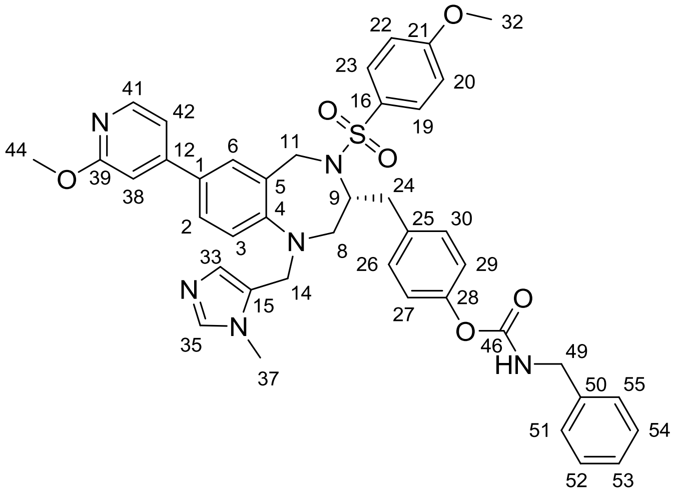

According to General Procedure **II**, reaction between THB **111** (20 mg, 32 µmol) and benzylisocyanate (4.7 mg, 35 µmol) afforded **131** as a off white solid (21 mg, 86%) **R*f*** 0.25 (3% MeOH in DCM) **Mp** 97.4 °C **^{1}H NMR** (500 MHz, MeOD) δ = 8.11 (d, *J*=5.5, 1H, H-*41*), 7.57 (s, 1H, H-*35*), 7.45 (d, *J*=2.3, 1H, H-*6*), 7.42 (dd, *J*=8.4, 2.3, 1H, H-*2*), 7.36 (d, *J*=9.0, 2H, H-*19,* H-*23*), 7.36 – 7.35 (m, 2H, H-*52,* H-*54*), 7.35 – 7.33 (m, 2H, H-*51,* H-*55*), 7.29 – 7.24 (m, 1H, H-*53*), 7.21 (dd, *J*=5.5, 1.5, 1H, H-*42*), 7.12 (d, *J*=8.6, 2H, H-*26,* H-*30*), 7.00 (d, *J*=8.8, 2H, H-*27,* H-*29*), 7.00 (d, *J*=1.5, 1H, H-*38*), 6.75 (d, *J*=8.9, 2H, H-*20,* H-*22*), 6.69 (s, 1H, H-*33*), 6.65 (d, *J*=8.4, 1H, H-*3*), 4.75 (d, *J*=17.0, 1H, H-*11*), 4.66 (d, *J*=17.0, 1H, H-*11*), 4.37 (s, 2H, H-*49*), 4.24 – 4.18 (m, 1H, H-*9*), 4.12 (d, *J*=15.8, 1H, H-*14*), 3.95 (s, 3H, H-*44*), 3.94 (d, *J*=15.8, 1H, H-*14*), 3.74 (s, 3H, H-*32*), 3.63 – 3.57 (m, 1H, H-*8*), 3.57 (s, 3H, H-*37*), 2.98 (dd, *J*=15.1, 4.2, 1H, H-*8*), 2.91 (dd, *J*=13.8, 6.1, 1H, H-*24*), 2.64 – 2.56 (m, 1H, H-*24*). **^{13}C NMR** (126 MHz, MeOD) δ = 166.57 (C-39), 164.17 (C-21), 157.41 (C-46), 152.35 (C-12), 151.86 (C-4), 151.42 (C-28), 148.02 (C-41), 140.28 (C-50), 140.03 (C-35), 136.00 (C-25), 132.95 (C-16), 131.16 (C-26, C-30), 130.52 (C-19, C-23), 130.00 (C-1), 129.88(C-15), 129.71 (C-6), 129.58 (C-52, C-54), 128.42 (C-51, C-55), 128.35 (C-33), 128.29 (C-53), 127.73 (C-2), 122.81 (C-27, C-29), 117.12 (C-3), 115.69 (C-42), 114.75 (C-20, C-22), 107.67 (C-38), 60.10 (C-9), 56.13 (C-32), 54.61 (C-8), 54.19 (C-44), 47.95 (C-11), 47.05 (C-14), 45.72 (C-49), 38.31 (C-24), 31.82 (C-37).**LC-MS** (C18_ESI)**:** 759.16 [M+H]$^+$, R$_t$=6.87min; **HRMS (ESI)** calculated for $C_{42}H_{43}O_6N_6S$ [M+H]$^+$: 759.29593, found: 759.29696.$[\boldsymbol{\alpha}]_{\boldsymbol{D}}^{\mathbf{20}}$+96.6 (*c*=0.6, MeOH/CHCl$_3$,1:1).

(3R)-3-{[4-(benzyloxy)phenyl]methyl}-4-[(4-methoxybenzene)sulfonyl]-7-(2-methoxypyridin-4-yl)-1-[(1-methyl-1H-imidazol-5-yl)methyl]-2,3,4,5-tetrahydro-1H-1,4-benzodiazepine (132)

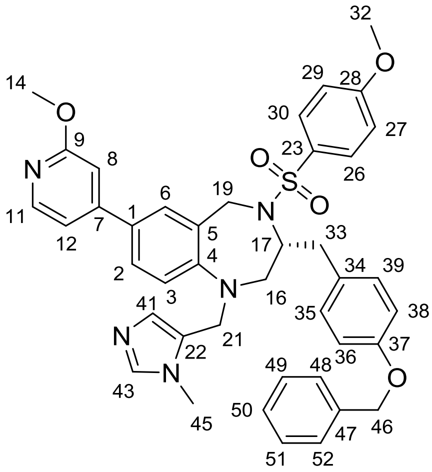

According to General Procedure I, reaction between THB **111** (20 mg, 32 µmol) and benzyl bromide (6.2 mg, 36 µmol) afforded **132** as a white solid (18 mg, 81%). **R$_f$** 0.26 (3% MeOH in DCM). **Mp** 99°C **^{1}H NMR** (500 MHz, MeOD) δ = 8.11 (d, *J*=5.5, 1H, H-*11*), 7.55 (s, 1H, H-*43*), 7.45 (d, *J*=2.1, 1H, H-*6*), 7.44 – 7.43 (m, 2H, H-*48,* H-*52*), 7.41 (dd, *J*=8.2, 2.3, 1H, H-*2*), 7.39 – 7.33 (m, 2H, H-*49,* H-*51*), 7.36 (d, *J*=8.8, 2H, H-*26,* H-*30*), 7.32 – 7.28 (m, 1H, H-*50*), 7.20 (dd, *J*=5.5, 1.5, 1H, H-*12*), 7.01 (d, *J*=8.4, 2H, H-*35,* H-*39*), 6.99 (d, *J*=1.5, 1H, H-*8*), 6.86 (d, *J*=8.5, 2H, H-*36,* H-*38*), 6.72 (d, *J*=8.9, 2H, H-*27,* H-*29*), 6.68 (s, 1H, H-*41*), 6.65 (d, *J*=8.4, 1H, H-*3*), 5.05 (s, 2H, H-*46*), 4.69 (d, *J*=17.0, 1H, H-*19*), 4.64 (d, *J*=17.0, 1H, H-*19*), 4.19 (dd, *J*=16.5, 10.0, 1H, H-*17*), 4.11 (d, *J*=15.9, 1H, H-*21*), 3.95 (s, 3H, H-*14*), 3.93 (d, *J*=15.9, 1H, H-*21*), 3.74 (s, 3H, H-*32*), 3.60 – 3.52 (m, 1H, H-*16*), 3.56 (s, 3H, H-*45*), 3.04 – 2.93 (m, 1H, H-*16*), 2.89 – 2.81 (m, 1H, H-*33*), 2.59 – 2.46 (m, 1H, H-*33*). **^{13}C NMR** (126 MHz, MeOD) δ = 166.58 (C-9), 164.10 (C-28), 159.02 (C-37), 152.35 (C-7), 151.89 (C-4), 148.03 (C-11), 140.03 (C-43), 138.85 (C-47), 133.15 (C-23), 131.32 (C-35, C-39), 131.16 (C-34), 130.45 (C-26, C-30), 129.86 (C-1), 129.81(C-22), 129.69 (C-6), 129.50 (C-49, C-51), 128.86 (C-50), 128.63 (C-48, C-52), 128.38 (C-41), 127.72 (C-2), 117.30 (C-3), 116.01 (C-36, C-38), 115.70 (C-12), 114.71 (C-27, C-29), 107.69 (C-8), 71.01 (C-46), 60.10 (C-17), 56.13 (C-32), 54.86 (C-16), 54.20 (C-14), 47.92 (C-19), 47.19 (C-21), 38.39 (C-33), 31.84 (C-45). **LC-MS** (C18_ESI)**:** 716.22 [M+H]$^+$, R$_t$=7.05min; **HRMS (ESI)** calculated for $C_{41}H_{42}O_5N_5S$ [M+H]$^+$: 716.29012, found: 716.29110.$[\boldsymbol{\alpha}]_{\boldsymbol{D}}^{\mathbf{20}}$ +67.37 (*c*=0.49, MeOH : $CHCl_3$ [1:1]).

4-{[(3R)-4-[(4-methoxybenzene)sulfonyl]-7-(2-methoxypyridin-4-yl)-1-[(1-methyl-1H-imidazol-5-yl)methyl]-2,3,4,5-tetrahydro-1H-1,4-benzodiazepin-3-yl]methyl}phenyl trifluoromethanesulfonate(133)

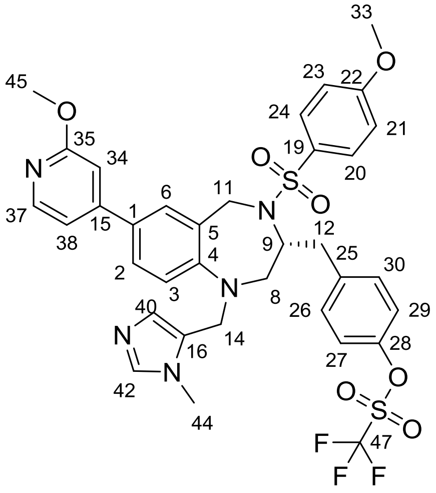

According to General Procedure **III**, reaction between THB **111** (60 mg, 959 µmol) and **86** (38 mg, 105 µmol) afforded **133** as a white solid. (65 mg, 90%) ^{1}**H NMR** (500 MHz, MeOD) δ = 8.14 (d, *J*=5.4, 1H, H-*37*), 7.62 (s, 1H, H-*42*), 7.48 (d, *J*=2.5, 1H, H-*6*), 7.46 (dd, *J*=8.4, 2.5, 1H, H-*2*), 7.39 (d, *J*=9.0, 2H, H-*20,* H-*24*), 7.29 (d, *J*=8.8, 2H, H-*26,* H-*30*), 7.24 (d, *J*=8.8, 2H, H-*27,* H-*29*), 7.23 (dd, *J*=5.5, 1.5, 1H, H-*38*), 7.02 (d, *J*=1.7, 1H, H-*34*), 6.75 – 6.74 (m, 1H, H-*3*), 6.75 (d, *J*=9.0, 2H, H-*21,* H-*23*), 6.71 (s, 1H, H-*40*), 4.78 (d, *J*=16.8, 1H, H-*11*), 4.70 (d, *J*=16.9, 1H, H-*11*), 4.30 – 4.23 (m, 1H, H-*9*), 4.17 (d, *J*=15.7, 1H, H-*14*), 4.02 (d, *J*=15.4, 1H, H-*14*), 3.97 (s, 3H, H-*45*), 3.77 (s, 3H, H-*33*), 3.63 (s, 3H, H-*44*), 3.59 (dd, *J*=14.9, 8.1, 1H, H-*8*), 3.00 (dd, *J*=15.1, 3.8, 1H, H-*8*), 2.95 (dd, *J*=13.8, 7.3, 1H, H-*12*), 2.61 – 2.52 (m, 1H, H-*12*). ^{13}**C NMR**: (126 MHz, MeOD) δ = 166.57 (C-35), 164.18 (C-22), 152.28 (C-15), 152.13 (C-4), 149.76 (C-28), 148.06 (C-37), 140.19 (C-25), 140.08 (C-42), 139.66 (C-16), 133.07 (C-19), 132.43 (C-26, C-30), 130.51 (C-20, C-24), 130.45 (C-1), 129.89(C-16), 129.75 (C-6), 128.46 (C-40), 127.83 (C-2), 122.28 (C-27, C-29), 118.91 (C-47), 117.47 (C-3), 115.72 (C-38), 114.71 (C-21, C-23), 107.78 (C-34), 59.80 (C-9), 56.10 (C-33), 55.05 (C-8), 54.20 (C-45), 47.72 (C-11), 47.26 (C-14), 37.97 (C-12), 31.84 (C-44). **LC-MS** (C18_ESI)**:** 758.08 $[M+H]^+$*,* R_t=6.93min; **HRMS (ESI)** calculated for $C_{35}H_{34}O_7N_5F_3NaS_2$ $[M+Na]^+$: 780.17440, found: 780.17436. $[\alpha]_D^{20}$ + 35.8 (*c*=0.9, CHCl$_3$).

(3R)-4-[(4-methoxybenzene)sulfonyl]-7-(2-methoxypyridin-4-yl)-1-[(1-methyl-1H-imidazol-5-yl)methyl]-3-{[4-(pyridin-3-yl)phenyl]methyl}-2,3,4,5-tetrahydro-1H-1,4-benzodiazepine(134)

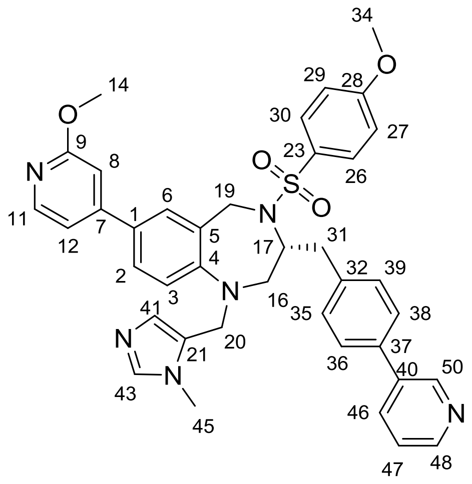

According to General Procedure **IVb** reaction between THB **133** (23.5 mg, 31 µmol) and 3-pyridineboronic acid (4.2 mg, 34µmol) afforded **134** as an yellow solid (18 mg, 84%) **R_f** 0.23 (3% MeOH in DCM), **Mp** 100 °C **^{1}H NMR** (500 MHz, MeOD) δ = 8.81 (d, *J*=2.5, 1H, H-*50*), 8.51 (dd, *J*=4.9, 1.6, 1H, H-*48*), 8.12 (d, *J*=5.4, 1H, H-*11*), 8.10 (ddd, *J*=8.0, 2.4, 1.7, *46*), 7.62 (s, 1H, H-*43*), 7.54 (d, *J*=8.1, 2H, H-*36,* H-*38*), 7.52 (dd, *J*=8.1, 5.2, 1H, H-*47*), 7.47 (s, 1H, H-*6*), 7.44 (d, *J*=8.4, 1H, H-*2*), 7.38 (d, *J*=8.9, 2H, H-*26,* H-*30*), 7.26 (d, *J*=7.9, 2H, H-*35,* H-*39*), 7.21 (dd, *J*=5.5, 1.5, 1H, H-*12*), 7.00 (d, *J*=1.5, 1H, H-*8*), 6.74 (s, 1H, H-*41*), 6.71 (d, *J*=8.4, 1H, H-*3*), 6.70 (d, *J*=8.9, 2H, H-*27,* H-*29*), 4.78 (d, *J*=16.9, 1H, H-*19*), 4.70 (d, *J*=16.9, 1H, H-*19*), 4.34 – 4.24 (m, 1H, H-*17*), 4.17 (d, *J*=15.8, 1H, H-*20*), 4.01 (d, *J*=16.2, 1H, H-*20*), 3.95 (s, 3H, H-*14*), 3.69 (s, 3H, H-*34*), 3.66 – 3.63 (m, 1H, H-*16*), 3.62 (s, 3H, H-*45*), 3.05 (dd, *J*=15.0, 3.7, 1H, H-*16*), 2.97 (dd, *J*=13.7, 6.7, 1H, H-*31*), 2.67 – 2.54 (m, 1H, H-*31*).**^{13}C NMR** (126 MHz, MeOD) δ = 166.58 (C-9), 164.14 (C-28), 152.32 (C-7), 152.04 (C-4), 148.61 (C-48), 148.26 (C-50), 148.04 (C-11), 139.57 (C-43), 139.49 (C-32), 138.34 (C-40), 136.73 (C-37), 136.37 (C-46, C-50), 133.17 (C-23), 131.29 (C-35, C-39), 130.46 (C-26, C-30), 130.38(C-1), 129.96 (C-21),129.76 (C-6), 128.11 (C-36, C-38), 127.94 (C-41), 127.79 (C-2), 125.47 (C-47), 117.47 (C-3), 115.73 (C-12), 114.70 (C-27, C-29), 107.76 (C-8), 59.92 (C-17), 56.05 (C-34), 55.12 (C-16), 54.20 (C-14), 47.89 (C-19), 47.31 (C-20), 38.63 (C-31), 31.95 (C-45).**LC-MS** (C18_ESI)**:** 687.05 $[M+H]^+$, R_t=5.54min; **HRMS (ESI)** calculated for $C_{39}H_{39}O_4N_6S$ $[M+H]^+$: 687.27480, found: 687.27493.

4-{[(3R)-4-[(4-methoxybenzene)sulfonyl]-7-(2-methoxypyridin-4-yl)-1-[(1-methyl-1H-imidazol-5-yl)methyl]-2,3,4,5-tetrahydro-1H-1,4-benzodiazepin-3-yl]methyl}-N-phenylaniline (135)

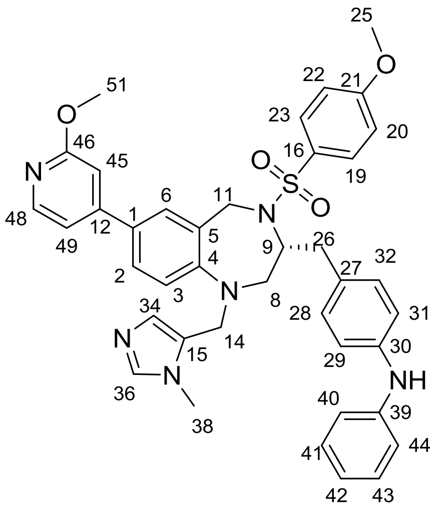

A dry Schlenk tube was charged with THB **133** (20 mg, 26 µmol), ligand **95** (2 mg, 8 µmol), Pd(OAc)$_2$ (1 mg, 4 µmol) and Cs$_2$CO$_3$ (18 mg, 52 µmol). Dry toluene (0.2 mL) was added, followed by aniline (8 mg, 86 µmol). The reaction mixture was purged with argon and stirred at 100 °C overnight. After cooling, the solvent was evaporated and the product was purified by flash column chromatography (2% MeOH in DCM) affording **135** as a white solid (14.2 mg, 75%).**^{1}H NMR** (400 MHz, MeOD) δ = 8.11 (dd, *J*=5.5, 0.8, 1H, H-*48*), 7.57 (s, 1H, H-*36*), 7.45 (d, *J*=2.2, 1H, H-*6*), 7.42 (dd, *J*=8.2, 2.4, 1H, H-*2*), 7.37 (d, *J*=9.0, 2H, H-*19,* H-*23*), 7.22 (dd, *J*=5.5, 1.6, 1H, H-*49*), 7.21 – 7.17 (m, 2H, H-*41,* H-*43*), 7.09 – 7.04 (m, 2H, H-*40,* H-*44*), 7.00 (dd, *J*=1.6, 0.8, 1H, H-*45*), 6.97 (s, 4H, H-*28, 29, 31, 32*), 6.85 – 6.80 (m, 1H, H-*42*), 6.74 (d, *J*=9.1, 2H, H-*20,* H-*22*), 6.70 (s, 1H, H-*34*), 6.66 (d, *J*=8.1, 1H, H-*3*), 4.74 (d, *J*=17.0, 1H, H-*11*), 4.65 (d, *J*=17.0, 1H, H-*11*), 4.23 – 4.17 (m, 1H, H-*9*), 4.13 (d, *J*=15.8, 1H, H-*14*), 3.95 (d, *J*=15.9, 2H, H-*14*), 3.94 (s, 3H, H-*51*), 3.73 (s, 3H, H-*25*), 3.59 (s, 3H, H-*38*), 3.63 – 3.53 (m, 1H, H-*8*), 3.02 (dd, *J*=15.3, 3.9, 1H, H-*8*), 2.85 (dd, *J*=13.7, 5.9, 1H, H-*26*), 2.57 – 2.47 (m, 1H, H-*26*). **LC-MS** (C18_ESI): 701.13 [M+H]$^+$, R$_t$=6.90min; **HRMS (ESI)** calculated for C$_{40}$H$_{41}$O$_4$N$_6$S [M+H]$^+$: 701.29045, found: 701.29052.

§ 10.3.9 Synthesis of furfuranyl analogs

General Procedure V for oxidation of furan

All reactions were carried out at a concentration of 70 mM furfuryl and 84 mM of bromine in dry methanol/ether (2/1) under argon atmosphere. A solution of bromine (1.2 equiv) in methanol was slowly added via an addition funnel to a stirred solution of furfuryl (1 equiv) in methanol/ether (1/1) maintaining an internal temperature between -35 and -45°C. Upon completion of addition, stirring was continued for a further 2 h at reduced temperature. The reaction mixture was quenched with $Na_2S_2O_3$ (aq) and the solvent was removed under reduced pressure. The residue was dissolved in DCM, washed with water (3×) and brine, dried over Na_2SO_4 and concentrated *in vacuo*. The crude product was purified by column chromatography

General Procedure VI for hydrogenation

All reactions were carried out at a concentration of 750 mM furfuryl in methanol. Furfuryl (1 equiv) was prestirred with activated carbon for 30 min in methanol. After filtration, 5% Pd/C (10 weight%) was added to the filtrate and the flask was evacuated and filled with H_2 gas (3 cycles). The reaction was stirred overnight, the solution was filtered and evaporated to yield the product.

N-(furan-2-ylmethyl)-6-hydroxyhexanamide (139)

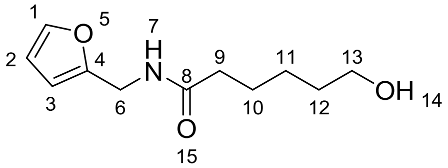

In a 20 mL, one neck round bottom flask, 6-Caprolactone (5 mL, 46.34 mmol) was added slowly to furfuryl amine (0.5 g, 5.15 mmol) over 1 h at rt. The reaction was stirred overnight after which an attempt was made to concentrate the 6-caprolactone under reduced pressure (as reported in the literature) however almost no caprolactone could be removed using this method. Flash chromatography (EtOAc) resulted in **139** a slightly brown solid. **R*f*** 0.25 (EtOAc) ^{1}**H NMR** (400 MHz, MeOD) δ = 7.40 (dd, *J*=1.9, 0.8, 1H, H-*1*), 6.33 (dd, *J*=3.2, 1.9, 1H, H-*2*), 6.22 (dd, *J*=3.2, 0.8, 1H, H-*3*), 4.33 (s, 2H, H-*6*), 3.53 (t, *J*=6.6, 2H, H-*13*), 2.21 (t, *J*=7.5, 2H, H-*9*), 1.69 – 1.58 (m, 2H, H-*12*), 1.58 – 1.48 (m, 2H, H-*10*), 1.41 – 1.31 (m, 2H, H-*11*). ^{13}**C NMR** (101 MHz, MeOD) δ = 175.92 (C-8), 153.16 (C-1), 143.22 (C-4), 111.31 (C-2), 107.99 (C-3), 62.75 (C-13), 37.09 (C-6), 36.90 (C-9), 33.29 (C-12), 26.75 (C-10), 26.49 (C-11). **LC-MS** (C18_ESI): 212.0 $[M+H]^+$ R_t=5.77min.

N-[(2,5-dimethoxy-2,5-dihydrofuran-2-yl)methyl]-6-hydroxyhexanamide (137)

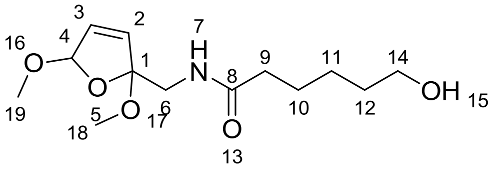

According to General Procedure V, reaction with furfuryl **139** (0.2 g, 95 mmol) followed by flash chromatography (1% Et_3N in EtOAc) afforded **137** (0.2g 77%) mixtures of isomers 1 : 2 (minor*, major). ^{1}**H NMR** (400 MHz, MeOD) δ = 6.12 (dd, *J*=5.9, 1.1, 1H, H-*4*), 6.08 (dd, *J*=5.9, 1.2, 1H, H-*4**), 5.90 (dd, *J*=5.9, 1.3, 1H, H-*3*), 5.88 (dd, *J*=5.9, 1.2, 1H, H-*3**), 5.76 (t, *J*=1.2, 1H, H-*2*), 5.50 (t, *J*=1.2, 1H, H-*2**), 3.66 (d, *J*=13.7, 1H, H-*6**), 3.59 (d, *J*=13.7, 1H, H-*6*), 3.54 (t, *J*=6.6, 2H, H-*14*), 3.48 (s, 3H, H-*19**), 3.46 (s, 3H, H-*19*), 3.30 (d, *J*=13.8, 1H, H-*6*), 3.22 (d, *J*=13.7, 1H, H-*6**), 3.18 (s, 3H, H-*18**), 3.13 (s, 3H, H-*18*), 2.22 – 2.12 (m, 2H, H-*9*), 1.67 – 1.48 (m, 4H, H-*10,* H-*12*), 1.43 – 1.30 (m, 2H, H-*11*).^{13}**C NMR** (101 MHz, MeOD) δ = 176.28 (C-8*), 176.13 (C-8), 133.66 (C-3), 133.32 (C-3*), 132.88 (C-2), 132.49 (C-2*), 115.44 (C-1), 114.42 (C-1*), 110.03 (C-4), 108.76 (C-4*), 62.75 (C-14), 62.73 (C-14*), 56.53 (C-19*), 56.23 (C-19), 50.81 (C-18*), 50.22 (C-18), 46.22 (C-6*), 46.19 (C-6), 37.14 (C-9*), 36.87 (C-9), 33.30 (C-12), 33.28 (C-12*), 26.83 (C-10*), 26.59 (C-10), 26.53 (C-11), 26.50 (C-11*).

N-[(2,5-dimethoxyoxolan-2-yl)methyl]-6-hydroxyhexanamide (140)

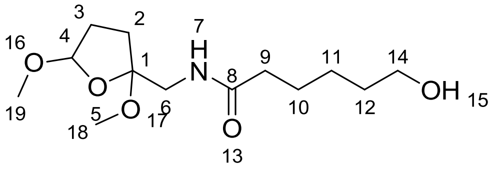

According to General Procedure **VI**, reaction with furfuryl **137** (40 mg, 0.15 mmol) gave **140**as a yellow oil (30 mg, 75%). mixtures of isomers 3 : 4 (minor*, major) ^{1}**H NMR** (400 MHz, MeOD) δ = 5.12 – 5.09 (m, 1H, H-*4**), 5.05 (dd, *J*=5.3, 2.7, 1H, H-*4*), 3.54 (t, *J*=6.6, 2H, H-*14*), 3.48 (d, *J*=13.5, 1H, H-*6*), 3.39 (s, 3H, H-*19**), 3.39 (d, *J*=13.3, 1H, H-*6*), 3.35 (s, 3H, H-*19*), 3.30 (s, 3H, H-*18**), 3.24 (s, 3H, H-*18*), 2.23 (t, *J*=7.5, 2H, H-*9*), 2.16 – 1.96 (m, 2H, H-*3*), 1.93 – 1.80 (m, 2H, H-*2*), 1.69 – 1.59 (m, 2H, H-*10*), 1.55 (dt, *J*=13.9, 6.8, 2H, H-*12*), 1.44 – 1.33 (m, 2H, H-*11*).^{13}**C NMR** (101 MHz, MeOD) δ = 176.39 (C-8), 176.20 (C-8*), 110.95 (C-1*), 110.52 (C-1), 107.74 (C-4*), 107.25 (C-4), 62.75 (C-14), 55.87 (C-19*), 55.27 (C-19), 49.77 (C-18*), 49.49 (C-18), 45.45 (C-6), 44.15 (C-6*), 37.00 (C-9), 36.90 (C-9*), 33.32 (C-12), 32.56 (C-2*), 32.45 (C-2), 31.86 (C-3*), 31.71 (C-3), 26.85 (C-10*), 26.82 (C-10), 26.53 (C-11).

N-(furan-2-ylmethyl)octanamide (141)

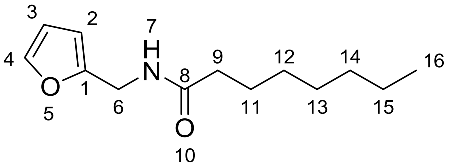

Furfuryl amine (0.30 g, 3.1 mmol) was dissolved in DCM (5 mL) in a 10 mL one necked round bottom flask and the reaction mixture was cooled down to 0°C, then octanoyl chloride (0.55 mL, 3.7 mmol) and Et_3N (0.52 mL, 3.7 mmol) were added. The reaction was followed on TLC and after complete consumption of furfuryl amine the solution was poured into water (10 mL) and extracted with DCM (3 x 15 mL). The organic layer was washed with brine, dried over Na_2SO_4 and concentrated. Flash chromatography (EtOAc/cyclohexane 1:3) resulted in **141** as a white solid.^{1}**H NMR** (400 MHz, MeOD) δ = 7.40 (dd, *J*=2.1, 0.9, 1H, H-*4*), 6.33 (dd, *J*=3.3, 1.9, 1H, H-*3*), 6.22 (dd, *J*=3.2, 0.8, 1H, H-*2*), 4.34 (s, 2H, H-*6*), 2.23 – 2.16 (m, 2H, H-*9*), 1.85 – 1.38 (m, 2H, H-*11*), 1.38 – 1.21 (m, 8H, H-*12,13,14,15*), 0.90 (t, *J*=5.9, 3H, H-*16*).^{13}**C NMR** (101 MHz, MeOD) δ = 176.06 (C-8), 153.20 (C-1), 143.21 (C-4), 111.30 (C-3), 107.98 (C-2), 37.08 (C-6), 36.96 (C-9), 32.89 (C-14), 30.19 (C-12), 30.10 (C-13), 26.98 (C-11), 23.64 (C-15), 14.41 (C-16).

N-[(2,5-dimethoxy-2,5-dihydrofuran-2-yl)methyl]octanamide(142)

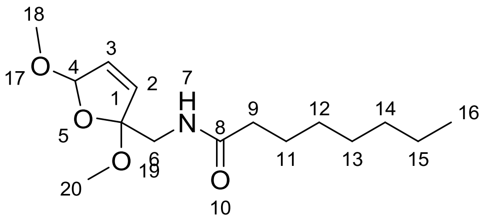

According to General Procedure **V**, reaction with furfuryl **141** (50 mg, 270 µmol) followed by flash chromatography (1% Et_3N in EtOAc) afforded **142** (46 mg, 72%) mixtures of isomers 5 : 6 (minor*, major) ^{1}**H NMR** (400 MHz, MeOD) δ = 6.11 (dd, *J*=5.9, 1.1, 1H, H-*4*), 6.07 (dd, *J*=5.9, 1.2, 1H, H-*4**), 5.89 (dd, *J*=5.9, 1.3, 1H, H-*3*), 5.87 (dd, *J*=5.9, 1.2, 1H, H-*3**), 5.75 (t, *J*=1.2, 1H, H-*2*), 5.49 (t, *J*=1.2, 1H, H-*2**), 3.65 (d, *J*=13.7, 1H, H-*6**), 3.59 (d, *J*=13.7, 1H, H-*6*), 3.48 (s, 3H, H-*18**), 3.47 (s, 3H, H-*18*), 3.30 (d, *J*=13.7, 1H, H-*6*), 3.22 (d, *J*=13.7, 1H, H-*6**), 3.18 (s, 3H, H-*20**), 3.13 (s, 3H, H-*20*), 2.19 – 2.11 (m, 2H, H-*9*), 1.63 – 1.50 (m, 2H, H-*11*), 1.37 – 1.24 (m, 8H, H-*12,13,14,15*), 0.90 (t, *J*=6.9, 3H, H-*16*). ^{13}**C NMR** (101 MHz, MeOD) δ = 176.40 (C-8*), 176.26 (C-8), 133.64 (C-3), 133.25 (C-3*), 132.89 (C-2), 132.54 (C-2*), 115.45 (C-1), 114.44 (C-1*), 110.02 (C-4), 108.77 (C-4*), 56.53 (C-18*), 56.23 (C-18), 50.81 (C-20*), 50.22 (C-20), 46.23 (C-6), 46.20 (C-6*), 37.21 (C-9), 36.93 (C-9*), 32.90 (C-14*), 32.87 (C-14), 30.27 (C-12), 30.21 (C-12*), 30.11 (C-13), 27.06 (C-11*), 26.80 (C-11), 23.66 (C-15), 14.41 (C-16).

N-[(2,5-dimethoxyoxolan-2-yl)methyl]octanamide (143)

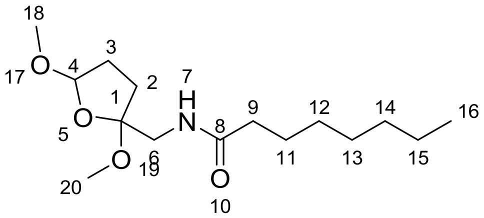

According to General Procedure **VI**, reaction with furfuryl **142** (80 mg, 0.28 mmol) gave **143** as a yellow oil (60 mg, 74%). mixtures of isomers 5 : 6 (minor*, major) ^{1}**H NMR** (400 MHz, MeOD) δ = 5.12 – 5.08 (m, 1H, H-4*), 5.04 (dd, *J*=5.3, 2.6, 1H, H-*4*), 3.53 (d, *J*=13.8, 1H, H-6*), 3.48 (d, *J*=13.9, 1H, H-*6*), 3.39 (s, 3H, H-*18*), 3.38 (d, *J*=13.7, 1H, H-6*), 3.34 (s, 3H, H-18*), 3.32 (d, *J*=13.9, 1H, H-*6*), 3.30 (s, 3H, H-*20*), 3.24 (s, 3H, H-20*), 2.21 (t, *J*=7.4, 2H, H-*9*), 2.15 – 1.97 (m, 2H, H-*3*), 1.96 – 1.81 (m, 2H, H-*2*), 1.66 – 1.55 (m, 2H, H-*11*), 1.38 – 1.24 (m, 8H, H-*12,13,14,15*), 0.90 (t, *J*=6.9, 3H, H-*16*). ^{13}**C NMR** (101 MHz, MeOD) δ = 176.48 (C-8), 176.29 (C-8*), 110.95 (C-1), 110.51 (C-1*), 107.71 (C-4), 107.24 (C-4*), 55.86 (C-18), 55.27 (C-18*), 49.76 (C-20), 49.48 (C-20*), 45.42 (C-6*), 44.14 (C-6), 37.09 (C-9*), 36.94 (C-9), 32.89 (C-14), 32.57 (C-2), 32.45 (C-2*), 31.84 (C-3), 31.73 (C-3*), 30.23 (C-12), 30.12 (C-13), 27.07 (C-11), 23.65 (C-15), 14.41 (C-16).

(2E)-N-(furan-2-ylmethyl)-3,7-dimethylocta-2,6-dienamide (144)

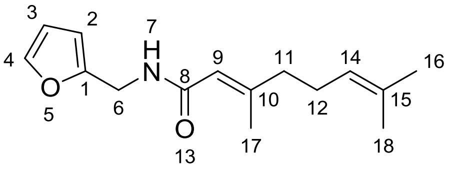

To a mixture of sodium bicarbonate (1.3 g, 15.5 mmol) and geranyl acid (1.07 mL, 6.18 mmol) in dichloromethane (20 mL) was added furfurylamine (0.3 g, 3.1 mmol). EDC (1.2 g, 6.18 mmol) and 4-DMAP (0.189 g, 1.54 mmol) under argon. The reaction mixture was stirred for 8h. Brine (25 mL) was added to the yellow reaction mixture, which resulted in the formation of a white precipitate. The precipitate was filtered off and the filtrate was extracted with dichloromethane (3 x 40 mL). The organic layer was washed with 1N HCl, water and brine and dried over Na$_2$SO$_4$. After concentration of the solvent under reduced pressure the residue was purified by column chromatography which provided **144** as a yellow oil. ^{1}**H NMR** (400 MHz, MeOD) δ = 7.40 (dd, *J*=1.9, 0.9, 1H, H-*4*), 6.33 (dd, *J*=3.2, 1.9, 1H, H-*3*), 6.23 (dd, *J*=3.2, 0.8, 1H, H-*2*), 5.69 (q, *J*=1.2, 1H, H-*9*), 5.15 – 5.06 (m, 1H, H-*14*), 4.36 (s, *J*=6.2, 2H, H-*6*), 2.21 – 2.11 (m, 4H, H-*11,12*), 2.11 (d, *J*=1.3, 3H, H-*17*), 1.68 (d, *J*=1.0, 3H, H-*18*), 1.61 (d, *J*=0.7, 3H, H-*16*).^{13}**C NMR** (101 MHz, MeOD) δ = 169.46 (C-8), 155.47 (C-10), 153.32 (C-1), 143.17 (C-4), 133.14 (C-15), 124.41 (C-14), 118.97 (C-9), 111.30 (C-3), 107.92 (C-2), 41.79 (C-6), 36.80 (C-11), 27.24 (C-12), 25.84 (C-16), 18.56 (C-18), 17.74 (C-17).

Methyl 2-[6-(benzylsulfamoyl)-2-oxo-2,3-dihydro-1,3-benzoxazol-3-yl]acetate(181)

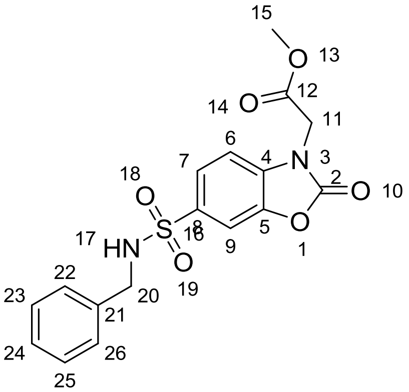

147 (200 mg, 0.65 mmol) was added to a solution of benzylamine (71 µL, 0.65 mmol) and pyridine (182 µL, 1.96 mmol) in DCM (5 mL). After stirring at 23 °C for 1 h, the reaction was quenched with three pieces of ice and diluted with water (0.5 mL). The whole was extracted with EtOAc (10 mL), and the organic layer was washed with water (2 mL) and brine (2 × 2 mL), and dried over anhydrous Na_2SO_4. Filtration and evaporation *in vacuo* gave the crude. Flash chromatography (cHex/EtOAc 1 : 1) gives the product as a white solid (260 mg, 97%) **R_f** 0.44 (cHex/EtOAc, 1:1) **Mp** 139.4 °C. **^{1}H NMR** (400 MHz, $CDCl_3$) δ = 7.64 (dd, *J*=8.2, 1.6, 1H, H-*6*), 7.59 (d, *J*=1.5, 1H, H-*9*), 7.22 – 7.08 (m, 5H, H-*22, 23, 24, 25, 26*), 6.94 (d, *J*=8.2, 1H, H-*7*), 4.57 (s, 2H, H-*20*), 4.02 (s, 2H, H-*11*), 3.76 (s, 3H, H-*15*). **^{13}C NMR** (101 MHz, $CDCl_3$) δ = 167.28 (C-12), 154.34 (C-2), 142.49 (C-21), 136.59 (C-5), 135.65 (C-8), 134.40 (C-4), 128.87 (C-23, C-25), 128.18 (C-22, C-26), 128.07 (C-24), 124.33 (C-7), 109.63 (C-6), 108.87 (C-9), 53.44 (C-15), 47.38 (C-11), 43.43 (C-20). **LC-MS** (C18_ESI)**:** 376.80 $[M+H]^+$, R_t=8.13min; **HRMS (ESI)** calculated for $C_{17}H_{17}O_6N_2S$ $[M+H]^+$: 377.08018, found: 377.08028.

2-[6-(benzylsulfamoyl)-2-oxo-2,3-dihydro-1,3-benzoxazol-3-yl]acetic acid (148)

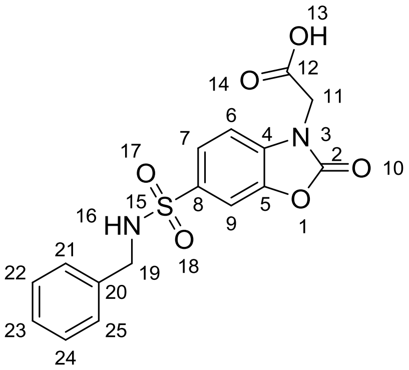

181 (0.2 g, 0.53 mmol) was refluxed in a mixture of dioxane and concentrated HCl (1:1, 1 mL) for 2 h. The reaction mixture was evaporated to dryness to yield the product, which was used as a crude in the following steps. **^{1}H NMR** (400 MHz, DMSO) δ = 8.15 (t, *J*=6.3, 1H, H-*13*), 7.72 (d, *J*=1.9, 1H, H-*9*), 7.70 (dd, *J*=8.0, 2.1, 1H, H-*6*), 7.50 (d, *J*=8.2, 1H, H-*7*), 7.30 – 7.17 (m, 5H, H-*21, 22, 23, 24, 25*), 4.71 (s, 2H, H-*19*), 3.99 (d, *J*=6.3, 2H, H-*11*). **^{13}C NMR** (101 MHz, DMSO) δ = 168.49 (C-12), 153.74 (C-2), 141.44 (C-20), 137.50 (C-5), 134.93 (C-8), 134.43 (C-4), 128.22 (C-22, C-24), 127.63 (C-21, C-25), 127.15 (C-23), 123.32 (C-7), 109.68 (C-6), 108.14 (C-9), 46.20 (C-11), 43.28 (C-19). **LC-MS** (C18_ESI)**:** 360.90 $[M+H]^+$, R_t=7.39min; **HRMS (ESI)** calculated for $C_{16}H_{15}O_6N_2S$ $[M+H]^+$: 363.06453, found: 363.06457.

2-[6-(benzylsulfamoyl)-2-oxo-2,3-dihydro-1,3-benzoxazol-3-yl]-N-(4-ethylphenyl)acetamide (138)

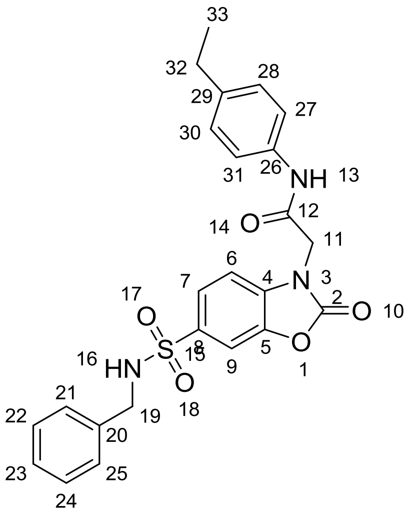

The crude carboxylic acid **148** (50 mg, 0.14 mmol) was dissolved in DCM (15 ml), then EDC.HCl (31 mg) was added and the mixture was stirred for 30 min. Next, 4-ethylaniline was added and the reaction mixture was stirred overnight under argon. The orange/yellow reaction mixture was quenched by addition of $NaHCO_3$ (sat) and extracted with DCM (3x) The combined organic layers were washed with brine, dried over anhydrous $MgSO_4$, filtered and evaporated to yield the crude, which was purified by flash chromatography to obtain **138** (48 mg, 75%). **^{1}H NMR**(400 MHz, acetone) δ = 7.77 (dd, *J*=8.2, 1.9, 1H, H-*7*), 7.72 (d, *J*=1.9, 1H, H-*9*), 7.55 (d, *J*=8.4, 2H, H-*27,* H-*31*), 7.42 (d, *J*=8.2, 1H, H-*6*), 7.31 – 7.20 (m, 5H, H-*21, 22, 23, 24, 25*), 7.17 (d, *J*=8.4, 2H, H-*28,* H-*30*), 4.85 (s, 2H, H-*19*), 4.14 (s, 2H, H-*11*), 2.59 (q, *J*=7.7, 2H, H-*32*), 1.18 (t, *J*=7.6, 3H, H-*33*).**LC-MS** (C18_ESI)**:** 465.92 $[M+H]^+$, R_t=9.27min; **HRMS (ESI)** calculated for $C_{24}H_{24}O_5N_3S$ $[M+H]^+$: 466.14312, found: 466.14254.

(2R)-N-benzyl-2-{[(4-cyanophenyl)methyl](methyl)amino}-3-(1-methyl-1H-imidazol-5-yl)propanamide (158)

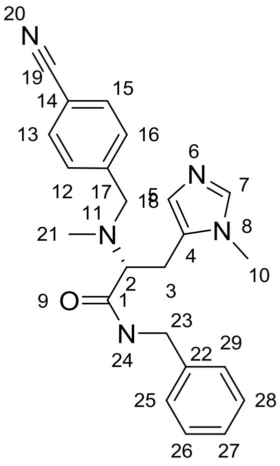

To a prestirred mixture of **157** (17 mg, 56 µmol), HATU (26 mg, 68 µmol) and DIPEA (20 µL, 114 mmol) in dry DMF, was added benzylamine (9 mg, 85 µmol). The reaction mixture was stirred overnight and partitioned between with EtOAc and $NaHCO_3$ (sat) the aqueous layer was extracted 3 times with EtOAc. The organic layer was dried over Na_2SO_4, filtrated and concentrated to yield the crude. Purification by flash chromatography (0.5% NH_4OH and 5% MeOH in EtOAc) gave **158** (12 mg, 54%) **^{1}H NMR** (400 MHz, MeOD) δ = 7.64 (d, *J*=8.5, 2H, H-*13,* H-*15*), 7.62 (s, 1H, H-*7*), 7.45 (d, *J*=8.5, 2H, H-*12,* H-*16*), 7.34 – 7.20 (m, 3H, H-*25, 27, 29*), 7.19 – 7.15 (m, 2H, H-*26,* H-*28*), 6.82 (s, 1H, H-*5*), 4.39 (d, *J*=14.7, 1H, H-*23*), 4.33 (d, *J*=14.8, 1H, H-*23*), 3.86 (d, *J*=14.4, 1H, H-*18*), 3.71 (d, *J*=14.4, 1H, H-*18*), 3.62 (s, 3H, H-*10*), 3.56 (dd, *J*=9.6, 5.3, 1H, H-*2*), 3.19 (dd, *J*=15.0, 9.5, 1H, H-*3*), 3.00 (dd, *J*=15.0, 5.3, 1H, H-*3*), 2.31 (s, 3H, H-*21*). **LC-MS** (C18_ESI): 388.2 $[M+H]^+$ R_t=5.57min.

tert-butyl N-(2-bromo-4-cyanophenyl)-N-[(tert-butoxy)carbonyl]carbamate (165)

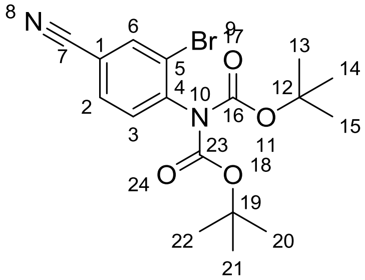

165 was synthesized according to literature procedure[204]. To a solution of 4-amino-3-bromobenzonitrile (1 g, 5.1 mmol) in anhydrous THF (50 mL) was added boc anhydride (3.3 g, 15.2 mmol) and DMAP (62 mg, 0.51 mmol). The solution was stirred at reflux overnight and concentrated to dryness. The precipitate was partitioned between 0.5 N HCl (100 mL) and EtOAc (100 mL). The aqueous layer was extracted with EtOAc (2 x 50 mL) and the combined organic phases were washed with brine (50mL), dried over Na_2SO_4, filtered and concentrated to afford crude **165**, which was used as such in the following steps.**^{1}H NMR** (400 MHz, $CDCl_3$) δ = 7.92 (d, *J*=1.8, 1H, H-*6*), 7.63 (dd, *J*=8.2, 1.8, 1H, H-*2*), 7.34 (d, *J*=8.2, 1H, H-*3*), 1.40 (s, 18H, H-*13, 14, 15, 20, 21, 22*).**LC-MS** (C18_ESI):396.5 $[M+H]^+$ R_t=10.25min.

Tert-butyl 2-{[(tert-butoxy)carbonyl]amino}-5-cyanobenzoate (166)

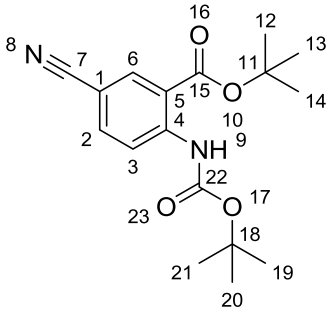

166 was synthesized according to literature procedure[204]. A solution of n-BuLi in hexane (340 µL of 1.6 M) were added dropwise at -78 °C under argon to a solution of **165** (200 mg, 0.5 mmol) in THF (5 mL). The reaction was stirred for 15 min at -78 °C and treated with sat. NH_4Cl solution. The reaction was warmed to room temperature, diluted with water and extracted twice with Et_2O. The combined organic layers were washed with brine, dried over Na_2SO_4, filtered and the solvent was evaporated to yield **166**, which was subsequently purified by flash chromatography (130 mg, 82%). **^{1}H NMR** (400 MHz, MeOD) δ = 8.56 (d, *J*=8.9, 1H, H-*3*), 8.25 (d, *J*=2.2, 1H, H-*6*), 7.81 (dd, *J*=8.9, 2.1, 1H, H-*2*), 1.64 (s, 9H, H-*12, 13, 14*), 1.55 (s, 9H, H-*19, 20, 21*).**^{13}C NMR** (101 MHz, MeOD) δ = 166.79 (C-15), 153.25 (C-22), 146.72 (C-4), 137.66 (C-2), 136.48 (C-6), 119.92 (C-3), 119.03 (C-7), 117.20 (C-5), 105.01 (C-1), 84.76 (C-11), 82.45 (C-18), 28.43 (C-12,13,14), 28.35 (C-19,20,21).

(1-methyl-2-sulfanyl-1H-imidazol-5-yl)methanol (168)

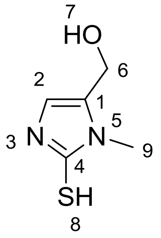

A procedure was adapted from the literature[205] as follows; a mixture of methylamine hydrochloride (14 g, 208.2mmol), dihydroxyacetone dimer (15 g, 166.5 mmol as monomer), potassium thiocyanate (24.3 g, 25.0 mmol) and acetic acid (19 mL, 333 mmol) in acetonitrile (163 mL) and water (3.0 mL) was stirred for 18 h at 55 °C. The mixture was cooled to 20 °C and filtered. The filter cake was washed with acetonitrile (50 mL), water (100 mL) and EtOAc (50 mL). The solid was dried under vacuum to give crude **168**. **^{1}H NMR** (400 MHz, DMSO) δ = 12.08 – 11.81 (m, 1H, H-*8*), 6.80 (s, 1H, H-*2*), 5.16 (t, *J*=5.2, 1H, H-*7*), 4.33 (d, *J*=5.1, 2H, H-*6*), 3.45 (s, 3H, H-*9*).

(1-methyl-1H-imidazol-5-yl)methanol (162)

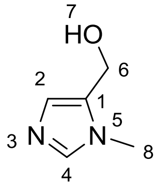

A procedure was adapted from the literature[205] as follows; a solution of 30% aqueous hydrogen peroxide (3.4 mL, 33.0 mmol) was gradually added over 30 min to a suspension of **168** (1.44 g, 10.0 mmol) in acetic acid (5.0 mL) and water (1.0 mL) while maintaining the temperature at 35-45 °C. The homogeneous mixture was stirred for 30 min at 40 °C and then cooled to 20 °C. The mixture was quenched by addition of 10% aqueous sodium sulfite (1 mL) at 25 °C. The mixture was treated with activated carbon (0.1 g) for 30 min at 20 °C and filtered over filter paper. The filtrate was basified to pH = 9.0 with 25% aqueous ammonia (10 mL) and extracted 3 times with $CHCl_3$/iPrOH (3 :1). The organic layer was dried over Na_2SO_4 filtered and concentrated *in vacuo* to give **162** (4.2 g, 75%).^{1}**H NMR** (400 MHz, DMSO) δ = 7.51 (s, 1H, H-*4*), 6.76 (s, 1H, H-*2*), 4.97 (bs, 1H, H-*7*), 4.40 (s, 2H, H-*6*), 3.59 (s, 3H, H-*8*).

5-bromo-2-{[(1-methyl-1H-imidazol-5-yl)methyl]amino}benzamide (172a)

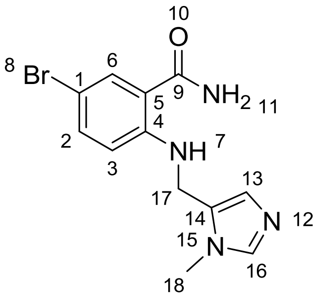

To 5.00 g (116 mmol) of 5-bromisatoic acid anhydride was added 3 ml of a 25 % aqueous ammonia solution and the mixture was kept at room temperature for 1 h. The precipitate was filtered, washed with a 5% aqueous ammonia solution, dried, and recrystallized from a water/EtOH (1:10) mixture to give 2-amino-5-bromo-benzamide[207].

A small fraction of obtained 2-amino-5-bromobenzamide (300 mg, 1.4 mmol) was stirred with N-methylimidazole 5-carboxaldehyde **76** (169 mg, 1.5 mmol) in THF (5 mL), followed by the addition of TFA (207 µL, 2.8 mmol) and $NaBH(OAc)_3$.(0.36 g, 1.7 mmol)[208]. After completion of the reaction, indicated by TLC, the reaction mixture was quenched by the addition of $NaHCO_3$ (sat). The aqueous layer was extracted with DCM (3x). The organic layer was dried over Na_2SO_4 filtered and concentrated *in vacuo* to give **172**, which was purified by flash chromatography (10% MeOH in DCM) ^{1}**H NMR** (400 MHz, MeOD) δ = 7.73 (d, *J*=2.3, 1H, H-*6*), 7.59 (s, 1H, H-*16*), 7.41 (dd, *J*=8.9, 2.4, 1H, H-*2*), 6.94 (s, 1H, H-*13*), 6.81 (d, *J*=9.0, 1H, H-*3*), 4.40 (s, 2H, H-*17*), 3.70 (s, 3H, H-*18*).

5-cyano-2-{[(1-methyl-1H-imidazol-5-yl)methyl]amino}benzamide (172b)

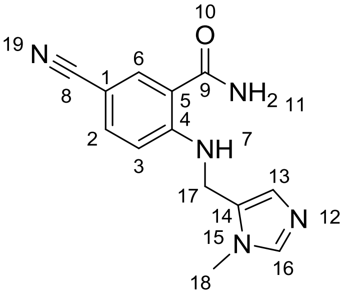

CuCN (250 mg, 2.8 mmol) was added to a stirred solution of **172a** (200 mg, 0.65 mmol) in NMP (2.0 mL) at room temperature. The reaction mixture was heated at 220 °C for 20 min using microwave irradiation, and the solvent was then removed by lyophilization from deionized water. The residue was thoroughly extracted with DCM, dried, and concentrated. Purification by silica gel chromatography (10% MeOH in DCM) gave **172b** as a white solid (36 mg, 22%). ^{1}**H NMR** (400 MHz, DMSO) δ = 9.06 (t, *J*=5.5, 1H,

H-*7*), 8.05 (d, *J*=1.9, 2H, H-*6*), 7.62 (dd, *J*=8.8, 1.9, 1H, H-*2*), 7.54 (s, 1H, H-*16*), 6.93 (d, *J*=8.9, 1H, H-*3*), 6.84 (s, 1H, H-*13*), 4.45 (d, *J*=5.4, 2H, H-*17*), 3.57 (s, 3H, H-*18*).

General Procedure VII for synthesis of tetrahydroquinazolinones

All reactions were carried out at a concentration of 160 mM of benzamide, 180 mM of aldehyde 320 mM of 34% HCl in EtOH. To a solution of 1 equiv. of benzamide in EtOH, 1.1 equiv. of aldehyde and 2 equiv. of 34% HCl were added. The reaction mixture was refluxed for ~5 h. After completion of the reaction, indicated by TLC, the reaction mixture was cooled down and evaporated. The crude product was purified by column chromatography (3% MeOH in DCM)

6-bromo-2-(4-methoxyphenyl)-1-[(1-methyl-1H-imidazol-5-yl)methyl]-1,2,3,4-tetrahydroquinazolin-4-one (174)

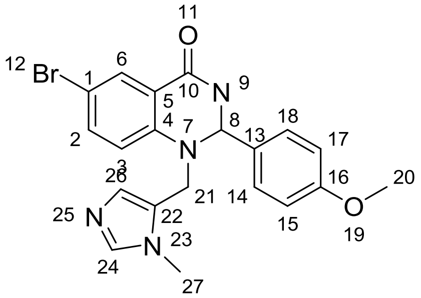

According to General Procedure **VII**, reaction of **172a** (100 mg, 0.32 mmol) with anisaldehyde (43 µL, 0.36 mmol) gave **174** (95 mg, 69%) **^{1}H NMR** (400 MHz, MeOD) δ = 8.87 (d, *J*=1.1, 1H, H-*24*), 7.96 (d, *J*=2.5, 1H, H-*6*), 7.53 (dd, *J*=8.8, 2.5, 1H, H-*2*), 7.39 (d, *J*=1.3, 1H, H-*26*), 7.28 (d, *J*=8.7, 2H, H-*14,18*), 6.89 (d, *J*=8.8, 2H, H-*15,17*), 6.83 (d, *J*=8.9, 1H, H-*3*), 5.82 (s, 1H, H-*8*), 4.77 (d, *J*=16.9, 1H, H-*21*), 4.53 (d, *J*=17.0, 1H, H-*21*), 3.86 (s, 3H, H-*20*), 3.77 (s, 3H, H-*27*). **LC-MS** (C18_ESI)**:** 427.15 [M+H]$^+$, R$_t$=5.58min; **HRMS (ESI)** calculated for C$_{20}$H$_{20}$O$_2$N$_4$Br [M+H]$^+$: 427.07642, found: 427.07524.

1-[(1-methyl-1H-imidazol-5-yl)methyl]-4-oxo-2-(2-phenylethyl)-1,2,3,4-tetrahydroquinazoline-6-carbonitrile(175)

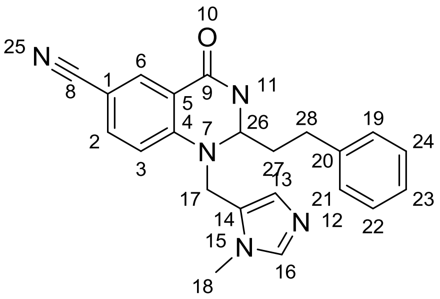

According to General Procedure **VII**, reaction of **172b** (20 mg, 78 µmol) with 3-phenylpropionaldehyde (12 mg, 86 µmol) gave **175** as a white solid (21 mg, 72%) **^{1}H NMR** (400 MHz, MeOD) δ = 8.11 (d, *J*=2.0, 1H, H-*6*), 7.69 (dd, *J*=8.7, 2.0, 1H, H-*2*), 7.65 (s, 1H, H-*16*), 7.29 – 7.21 (m, 2H, H-*22,* H-*24*), 7.20 – 7.13 (m, 3H, H-*19, 21, 23*), 7.11 (d, *J*=8.8, 1H, H-*3*), 6.85 (s, 1H, H-*13*), 4.88 (d, *J*=15.6, 1H, H-*17*), 4.62 (dd, *J*=8.5, 4.2, 1H, H-*26*), 4.42 (d, *J*=15.8, 1H, H-*17*), 3.61 (s, 3H, H-*18*), 2.74 – 2.65 (m, 1H, H-*28*), 2.60 – 2.51 (m, 1H, H-*28*), 2.10 – 1.92 (m, 2H, H-*27*). **^{13}C NMR** (101 MHz, MeOH) δ = 163.93 (C-9), 150.49 (C-4), 141.86 (C-20), 140.87 (C-16), 138.29 (C-2), 133.84 (C-6), 130.00 (C-13), 129.63 (C-22, C-24), 129.31 (C-19, C-21), 127.50 (C-14), 127.27 (C-23), 119.88 (C-8), 118.16 (C-5), 115.23 (C-3), 101.52 (C-1), 68.72 (C-26), 42.52 (C-17), 36.39 (C-27), 32.07 (C-18), 31.26 (C-28). **LC-MS** (C18_ESI)**:** 372.17 [M+H]$^+$, R$_t$=5.47min; **HRMS (ESI)** calculated for $C_{22}H_{22}ON_5$ [M+H]$^+$: 372.18189, found: 372.18300.

List of Abbreviations

αsyn	α-Synuclein
AAK1	AP2-associated kinase 1
AP2	Adaptor-related protein complex 2
Arf	ADP-ribosylation factor
CBR	C-terminal binding region,
CCVs	clathrin-coated vesicles
CIM	CBR interacting motif
COPI	coat protein complex I
COPII	coat protein complex II
EEA1	early endosome antigen 1
ER	endoplasmatic reticulum
FDA	Food and Drug Administration
FPP	farnesylpyrophosphate
FTase	farnesyl transferase
FTI	farnesyl transferase inhibitor
G Proteins	Guanine nucleotide-binding proteins
GAP	GTPase activating protein
GAPVD1	GTPase-activating protein and VPS9 domain-containing protein 1
GDI	guanosine nucleotide dissociation inhibitor
GDP	guanosine diphosphate
GEF	guanine nucleotide exchange factor
GGPP	geranylgeranylpyrophosphate
GGPPS	geranylgeranylpyrophosphate synthase
GGTase I	geranylgeranyl transferase I
GGTI	geranylgeranyl transferase inhibitor
GPCR	G-protein coupled receptors
GTP	guanosine-5'-triphosphate
GTPase	guanosine triphosphatase
HTS	High Throughput Screening
IC	intermediate compartment)
IF	improvement factor
LBS	lipid binding site
LRR	leucine-rich repeat
M6PRs	M6P receptors
MAP	mitogen-activated protein
MTOC	microtubule organizing center
mTOR	mammalian target of rapamycines
NSF	N-ethyl-maleimide-sensitive fusion protein
PI	phosphoinositide
PM	plasma membrane
PPP	prenylpyrophosphate
PRA1	prenylated Rab acceptor 1
PTase	prenyltransferase
PTI	prenyltransferase inhibitor
QT	Q and T wave in the heart's electrical cycle
Rab	Ras-like proteins in brain
RabF	Rab specific residues
RabGGTase	Rab geranylgeranyl transferase
RabSF	Rab subfamily specific motifs
Ran	Ras-like nuclear
Ras	Ras sarcoma
RBD	Rab-binding domain
RCE1	RAS converting enzyme 1
REP	Rab Escort Protein
Rho	Ras homologous
RNA*i*	Ribonucleic acid interference
RUN	RPIP8, UNC-14, NESCA
SCV	Salmonella containing vesicles

SNARE	Soluble NSF attachment protein receptor
TAG	Tunnel adjacent to ggpp binding site
TBC	Trec2/Cdc16/Bub2
THB	tetrahydrobenzodiazepine
TIP47	47-kDa tail interacting protein
VEGFR	Vascular endothelial growth factor receptor
ad	apparent doublet
Ac	acetyl
AcOH	acetic acid
aq.	aqueous
Bn	benzyl
Boc	*tert*-butoxycarbonyl
br	broad
Bu	butyl
ºC	degrees Celcius (centigrade)
CDI	carbonyldiimidazole
compd	compound
d	days
d (NMR)	doublet
dba	dibenzylidene acetone
DBU	1,8-diazabicyclo [5.4.0]undec-7-ene
dd (NMR)	doublet of doublets
DCM	dichloromethane
DCE	dichloroethene
DHP	dihydropyran
DIAD	Diisopropyl azodicarboxylate
DIPEA	diisopropylethylamine
DMAP	4-dimethylaminopyridine
DMF	*N*,*N*-dimethylformamide
DMSO	dimethyl sulfoxide
dt (NMR)	doublet of triplets
e.g.	*exempli gratia* (for example)
equiv.	equivalents
ESI	electrospray ionization
Et	ethyl
et al.	*et alia*(and others)
h	hours
HOBt	*N*-hydroxybenzotriazole
HPLC	high performance liquid chromatography
HRMS	high resolution mass spectrometry
i.e.	*id est* (that is)
IR	infrared
m (NMR)	multiplet
M	molar
MALDI	matrix-assisted laser desorption ionization
Me	methyl
MeCN	acetonitrile
min	minutes
mp	melting point
MS	mass spectrometry
N	normal (equivalents per liter)
NBS	*N*-bromosuccinimide
NBD-FPP	3,7,11-trimethyl-12-(7-nitrobenzo[1,2,5] oxadiazo-4-ylamino)dodeca-2,6,10-trienyl pyrophosphate
NCS	*N*-chlorosuccinimide
NHS	*N*-Hydroxysuccinimide
NMR	nuclear magnetic resonance
NVoc	Nitroveratryloxycarbonyl
o	ortho
p	para
PEG	polyethyleneglycol
Ph	Phenyl
ppm	parts per million
PPTS	Pyridinium p-toluenesulfonate
q	quartet
R_f	retention factor
rt	room temperature
s	singlet (NMR)
sat.	saturated

t (NMR)	triplet
t-Bu	*tert*-butyl
TEA	triethylamine
Tf	trifluoromethanesulfonyl
TFA	trifluoroacetic acid
TFAA	trifluoroacetic anhydride
THF	tetrahydrofuran
THP	tetrahydropyran
TLC	thin layer chromatography
Trt	trityl (triphenylmethyl)
Ts	*p*-toluenesulfonyl
TTBAP	tris tetrabutylammonium pyrophosphate

Amino acids

Ala	alanine (A)
Arg	arginine (R)
Asn	asparagine (N)
Asp	aspartate (D)
Cys	cysteine (C)
Gly	glycine (G)
Glu	glutamate (E)
Gln	glutamine (Q)
His	histidine (H)
Ile	isoleucine (I)
Leu	leucine (L)
Lys	lysine (K)
Met	methionine (M)
Phe	phenylalanine (F)
Pro	proline (P)
Ser	serine (S)
Thr	threonine (T)
Trp	tryptophane (W)
Tyr	tyrosine (Y)
Val	valine (V)

References

[1] A. Jemal, F. Bray, M. M. Center, J. Ferlay, E. Ward, D. Forman, *CA: A Cancer Journal for Clinicians* **2011**, n/a.
[2] H. Ovaa, C. Kuijl, J. Neefjes, *Drug Discovery Today: Technologies* **2009**, *6*, e3.
[3] B. Rosenberg, L. Van Camp, T. Krigas, *Nature* **1965**, *205*, 698.
[4] D. A. Fuchs, R. K. Johnson, *Cancer Treatment Reports* **1978**, *62*, 1219.
[5] V. C. Jordan, *Nat. Rev. Drug Discovery* **2003**, *2*, 205.
[6] N. Fleshner, A. R. Zlotta, *Cancer* **2007**, *110*, 1889.
[7] H. Reuveni, N. Livnah, T. Geiger, S. Klein, O. Ohne, I. Cohen, M. Benhar, G. Gellerman, A. Levitzki, *Biochemistry* **2002**, *41*, 10304.
[8] A. Quintas-Cardama, H. Kantarjian, J. Cortes, *Nat. Rev. Drug Discovery* **2007**, *6*, 834.
[9] D. R. Senger, L. Van De Water, L. F. Brown, J. A. Nagy, K. T. Yeo, T. K. Yeo, B. Berse, R. W. Jackman, A. M. Dvorak, H. F. Dvorak, *Cancer Metastasis Rev.* **1993**, *12*, 303.
[10] L. Sun, C. Liang, S. Shirazian, Y. Zhou, T. Miller, J. Cui, J. Y. Fukuda, J. Y. Chu, A. Nematalla, X. Wang, H. Chen, A. Sistla, T. C. Luu, F. Tang, J. Wei, C. Tang, *J. Med. Chem.* **2003**, *46*, 1116.
[11] N. Ferrara, K. J. Hillan, H.-P. Gerber, W. Novotny, *Nature Reviews. Drug Discovery* **2004**, *3*, 391.
[12] K. M. Sane, M. Mynderse, D. T. LaLonde, I. S. Dean, J. W. Wojtkowiak, F. Fouad, R. F. Borch, J. J. Reiners, R. A. Gibbs, R. R. Mattingly, *J. Pharmacol. Exp. Ther.* **2010**, *333*, 23.
[13] K. L. Dunn, P. S. Espino, B. Drobic, S. He, J. R. Davie, *Biochem. Cell Biol.* **2005**, *83*, 1.
[14] L. Sistonen, K. Alitalo, *Annals of Clinical Research* **1986**, *18*, 297.
[15] N. M. G. M. Appels, J. H. Beijnen, J. H. M. Schellens, *Oncologist* **2005**, *10*, 565.
[16] P. A. Konstantinopoulos, M. V. Karamouzis, A. G. Papavassiliou, *Nat. Rev. Drug Discovery* **2007**, *6*, 540.
[17] M. R. Lackner, R. M. Kindt, P. M. Carroll, K. Brown, M. R. Cancilla, C. Chen, H. de Silva, Y. Franke, B. Guan, T. Heuer, T. Hung, K. Keegan, J. M. Lee, V. Manne, C. O Brien, D. Parry, J. J. Perez-Villar, R. K. Reddy, H. Xiao, H. Zhan, M. Cockett, G. Plowman, K. Fitzgerald, M. Costa, P. Ross-Macdonald, *Cancer Cell* **2005**, *7*, 325.
[18] H. Stenmark, *Nat. Rev. Mol. Cell Biol.* **2009**, *10*, 513.
[19] K. Hubel, T. Lessmann, H. Waldmann, *Chem. Soc. Rev.* **2008**, *37*, 1361.
[20] F. Kugawa, M. Watanabe, F. Tamanoi, *Chem-Bio Informatics Journal* **2007**, *7*, 49.
[21] W. M. Oldham, N. Van Eps, A. M. Preininger, W. L. Hubbell, H. E. Hamm, *Nat. Struct. Mol. Biol.* **2006**, *13*, 772.
[22] A. G. Gilman, *Annu. Rev. Biochem.* **1987**, *56*, 615.
[23] Y. Takai, T. Sasaki, T. Matozaki, *Physiol. Rev.* **2001**, *81*, 153.
[24] J. Colicelli, *Sci. STKE* **2004**, *2004*, re13.
[25] K. Wennerberg, K. L. Rossman, C. J. Der, *J. Cell Sci.* **2005**, *118*, 843.
[26] G. A. Repasky, E. J. Chenette, C. J. Der, *Trends Cell Biol.* **2004**, *14*, 639.
[27] N. Fehrenbacher, D. Bar-Sagi, M. Philips, *Molecular Oncology* **2009**, *3*, 297.
[28] K. Rajalingam, R. Schreck, U. R. Rapp, S. Albert, *Biochimica et Biophysica Acta (BBA) - Molecular Cell Research* **2007**, *1773*, 1177.
[29] S. Etienne-Manneville, A. Hall, *Nature* **2002**, *420*, 629.
[30] A. J. Ridley, *Trends Cell Biol.* **2001**, *11*, 471.
[31] S. Y. Moon, Y. Zheng, *Trends Cell Biol.* **2003**, *13*, 13.
[32] A. Schmidt, A. Hall, *Genes Dev.* **2002**, *16*, 1587.
[33] A. L. Bishop, A. Hall, *Biochem. J.* **2000**, *348*, 241.
[34] J. B. Pereira-Leal, M. C. Seabra, *Journal of Molecular Biology* **2001**, *313*, 889.
[35] M. Zerial, H. McBride, *Nature Rev. Mol. Cell Biol.* **2001**, *2*, 107.
[36] K. Weis, *Cell* **2003**, *112*, 441.
[37] H. Y. Li, K. Cao, Y. Zheng, *Trends Cell Biol.* **2003**, *13*, 553.
[38] M.-P. Stein, J. Dong, A. Wandinger-Ness, *Adv. Drug Delivery Rev.* **2003**, *55*, 1421.

[39] S. L. Schwartz, C. Cao, O. Pylypenko, A. Rak, A. Wandinger-Ness, *J. Cell Sci.* **2007**, *120*, 3905.

[40] T. E. Dever, M. J. Glynias, W. C. Merrick, *Proceedings of the National Academy of Sciences of the United States of America* **1987**, *84*, 1814.

[41] H. R. Bourne, D. A. Sanders, F. McCormick, *Nature* **1991**, *349*, 117.

[42] J. B. Pereira-Leal, M. C. Seabra, *J. Mol. Biol.* **2000**, *301*, 1077.

[43] C. Ostermeier, A. T. Brunger, *Cell* **1999**, *96*, 363.

[44] A. Rak, *Science* **2003**, *302*, 646.

[45] A. Rak, *Cell* **2004**, *117*, 749.

[46] Y.-W. Wu, R. S. Goody, R. Abagyan, K. Alexandrov, *J. Biol. Chem.* **2009**, *284*, 13185.

[47] Y. Reiss, M. C. Seabra, S. A. Armstrong, C. A. Slaughter, J. L. Goldstein, M. S. Brown, *J. Biol. Chem.* **1991**, *266*, 10672.

[48] M. C. Seabra, Y. Reiss, P. J. Casey, M. S. Brown, J. L. Goldstein, *Cell* **1991**, *65*, 429.

[49] M. C. Seabra, J. L. Goldstein, T. C. Sudhof, M. S. Brown, *J. Biol. Chem.* **1992**, *267*, 14497.

[50] S. T. Withers, J. D. Keasling, *Appl. Microbiol. Biotechnol.* **2007**, *73*, 980.

[51] K. F. Leung, R. Baron, M. C. Seabra, *J. Lipid Res.* **2006**, *47*, 467.

[52] J. B. Pereira-Leal, A. N. Hume, M. C. Seabra, *FEBS Lett.* **2001**, *498*, 197.

[53] H. W. Fu, P. J. Casey, *Recent Prog. Horm. Res.* **1999**, *54*, 315.

[54] K. T. Lane, L. S. Beese, *J. Lipid Res.* **2006**, *47*, 681.

[55] E. C. Lerner, T. T. Zhang, D. B. Knowles, Y. M. Qian, A. D. Hamilton, S. M. Sebti, *Oncogene* **1997**, *15*, 1283.

[56] C. C. Huang, P. J. Casey, C. A. Fierke, *J. Biol. Chem.* **1997**, *272*, 20.

[57] K. E. Hightower, C. C. Huang, P. J. Casey, C. A. Fierke, *Biochemistry* **1998**, *37*, 15555.

[58] M. J. Saderholm, K. E. Hightower, C. A. Fierke, *Biochemistry* **2000**, *39*, 12398.

[59] Y. Reiss, M. S. Brown, J. L. Goldstein, *J. Biol. Chem.* **1992**, *267*, 6403.

[60] H. L. Hartman, K. E. Bowers, C. A. Fierke, *J. Biol. Chem.* **2004**, *279*, 30546.

[61] J. S. Taylor, T. S. Reid, K. L. Terry, P. J. Casey, L. S. Beese, *EMBO J.* **2003**, *22*, 5963.

[62] S. B. Long, P. J. Casey, L. S. Beese, *Nature* **2002**, *419*, 645.

[63] J. M. Troutman, T. Subramanian, D. A. Andres, H. P. Spielmann, *Biochemistry* **2007**, *46*, 11310.

[64] J. L. Hougland, C. L. Lamphear, S. A. Scott, R. A. Gibbs, C. A. Fierke, *Biochemistry* **2009**, *48*, 1691.

[65] J. S. Anant, L. Desnoyers, M. Machius, B. Demeler, J. C. Hansen, K. D. Westover, J. Deisenhofer, M. C. Seabra, *Biochemistry* **1998**, *37*, 12559.

[66] B. Dursina, R. Reents, C. Delon, Y. W. Wu, M. Kulharia, M. Thutewohl, A. Veligodsky, A. Kalinin, V. Evstifeev, D. Ciobanu, S. E. Szedlacsek, H. Waldmann, R. S. Goody, K. Alexandrov, *Journal of the American Chemical Society* **2006**, *128*, 2822.

[67] K. Alexandrov, I. Heinemann, T. Durek, V. Sidorovitch, R. S. Goody, H. Waldmann, *J. Am. Chem. Soc.* **2002**, *124*, 5648.

[68] T. Durek, K. Alexandrov, R. S. Goody, A. Hildebrand, I. Heinemann, H. Waldmann, *J. Am. Chem. Soc.* **2004**, *126*, 16368.

[69] Y. W. Wu, H. Waldmann, R. Reents, F. H. Ebetino, R. S. Goody, K. Alexandrova, *ChemBioChem* **2006**, *7*, 1859.

[70] Z. Guo, Y.-W. Wu, D. Das, C. Delon, J. Cramer, S. Yu, S. Thuns, N. Lupilova, H. Waldmann, L. Brunsveld, R. S. Goody, K. Alexandrov, W. Blankenfeldt, *EMBO J.* **2008**, *27*, 2444.

[71] N. H. Thoma, A. Niculae, R. S. Goody, K. Alexandrov, *J. Biol. Chem.* **2001**, *276*, 48631.

[72] N. H. Thoma, A. Iakovenko, A. Kalinin, H. Waldmann, R. S. Goody, K. Alexandrov, *Biochemistry* **2001**, *40*, 268.

[73] U. T. T. Nguyen, R. S. Goody, K. Alexandrov, *ChemBioChem* **2010**, *11*, 1194.

[74] A. Bernards, J. Settleman, *Trends Cell Biol.* **2004**, *14*, 377.

[75] A. L. Bishop, A. Hall, *Biochem. J.* **2000**, *348*, 241.

[76] C. T. Farrar, C. J. Halkides, D. J. Singel, *Structure* **1997**, *5*, 1055.

[77] Y. Ito, K. Yamasaki, J. Iwahara, T. Terada, A. Kamiya, M. Shirouzu, Y. Muto, G. Kawai, S. Yokoyama, E. D. Laue, M. Walchli, T. Shibata, S. Nishimura, T. Miyazawa, *Biochemistry* **1997**, *36*, 9109.
[78] M. Kjeldgaard, J. Nyborg, B. F. Clark, *FASEB J.* **1996**, *10*, 1347.
[79] S. R. Sprang, *Annu. Rev. Biochem.* **1997**, *66*, 639.
[80] I. R. Vetter, A. Wittinghofer, *Science* **2001**, *294*, 1299.
[81] C. Klebe, H. Prinz, A. Wittinghofer, R. S. Goody, *Biochemistry* **1995**, *34*, 12543.
[82] C. Lenzen, R. H. Cool, H. Prinz, J. Kuhlmann, A. Wittinghofer, *Biochemistry* **1998**, *37*, 7420.
[83] J. L. Bos, H. Rehmann, A. Wittinghofer, *Cell* **2007**, *129*, 865.
[84] L. Renault, B. Guibert, J. Cherfils, *Nature* **2003**, *426*, 525.
[85] C. Thomas, I. Fricke, A. Scrima, A. Berken, A. Wittinghofer, *Mol. Cell* **2007**, *25*, 141.
[86] A. Delprato, D. G. Lambright, *Nat. Struct. Mol. Biol.* **2007**, *14*, 406.
[87] A. Itzen, O. Pylypenko, R. S. Goody, K. Alexandrov, A. Rak, *EMBO J.* **2006**, *25*, 1445.
[88] G. Dong, M. Medkova, P. Novick, K. M. Reinisch, *Mol. Cell* **2007**, *25*, 455.
[89] Y. Cai, H. F. Chin, D. Lazarova, S. Menon, C. Fu, H. Cai, A. Sclafani, D. W. Rodgers, E. M. De La Cruz, S. Ferro-Novick, K. M. Reinisch, *Cell* **2008**, *133*, 1202.
[90] S. Schoebel, L. K. Oesterlin, W. Blankenfeldt, R. S. Goody, A. Itzen, *Mol. Cell* **2009**, *36*, 1060.
[91] F. Barr, D. G. Lambright, *Curr. Opin. Cell Biol.* **2010**, *22*, 461.
[92] L. Penengo, M. Mapelli, A. G. Murachelli, S. Confalonieri, L. Magri, A. Musacchio, P. P. Di Fiore, S. Polo, T. R. Schneider, *Cell* **2006**, *124*, 1183.
[93] R. Mattera, Y. C. Tsai, A. M. Weissman, J. S. Bonifacino, *J. Biol. Chem.* **2006**, *281*, 6874.
[94] M. T. G. Lee, A. Mishra, D. G. Lambright, *Traffic* **2009**, *10*, 1377.
[95] V. Wixler, L. Wixler, A. Altenfeld, S. Ludwig, R. S. Goody, A. Itzen, *Biol. Chem.* **2011**, *392*, 239.
[96] T. Murata, A. Delprato, A. Ingmundson, D. K. Toomre, D. G. Lambright, C. R. Roy, *Nat. Cell Biol.* **2006**, *8*, 971.
[97] K. Scheffzek, M. R. Ahmadian, W. Kabsch, L. WiesmÃ¼ller, A. Lautwein, F. Schmitz, A. Wittinghofer, *Science* **1997**, *277*, 333.
[98] K. Rittinger, P. A. Walker, J. F. Eccleston, S. J. Smerdon, S. J. Gamblin, *Nature* **1997**, *389*, 758.
[99] X. Pan, S. Eathiraj, M. Munson, D. G. Lambright, *Nature* **2006**, *442*, 303.
[100] M. Kukimoto-Niino, A. Sakamoto, E. Kanno, K. Hanawa-Suetsugu, T. Terada, M. Shirouzu, M. Fukuda, S. Yokoyama, *Structure* **2008**, *16*, 1478.
[101] L. M. G. Chavas, K. Ihara, M. Kawasaki, S. Torii, T. Uejima, R. Kato, T. Izumi, S. Wakatsuki, *Structure* **2008**, *16*, 1468.
[102] M. Wu, T. Wang, E. Loh, W. Hong, H. Song, *EMBO J.* **2005**, *24*, 1491.
[103] A. S. Burguete, T. D. Fenn, A. T. Brunger, S. R. Pfeffer, *Cell* **2008**, *132*, 286.
[104] S. Eathiraj, A. Mishra, R. Prekeris, D. G. Lambright, *J. Mol. Biol.* **2006**, *364*, 121.
[105] S. Eathiraj, X. Pan, C. Ritacco, D. G. Lambright, *Nature* **2005**, *436*, 415.
[106] G. Zhu, P. Zhai, J. Liu, S. Terzyan, G. Li, X. C. Zhang, *Nature Structural and Molecular Biology* **2004**, *11*, 975.
[107] A. Itzen, R. S. Goody, *Semin. Cell Dev. Biol.*, *In Press, Uncorrected Proof*.
[108] R. N. Collins, *Mol. Cell* **2003**, *12*, 1064.
[109] A. Alfonso, G. S. Payne, J. Donaldson, N. Segev, *Trafficking Inside Cells: Pathways, Mechanisms and Regulation*, Springer, **2009**.
[110] R. Vazquez-Martinez, M. M. Malagon, *Frontiers in Endocrinology* **2011**, *2*.
[111] J. H. Hurley, E. Boura, L.-A. Carlson, B. Rózycki, *Cell* **2010**, *143*, 875.
[112] H. Stenmark, *Nat. Rev. Mol. Cell Biol.* **2009**, *10*, 513.
[113] K. S. Carroll, J. Hanna, I. Simon, J. Krise, P. Barbero, S. R. Pfeffer, *Science* **2001**, *292*, 1373.

[114] H. McLauchlan, J. Newell, N. Morrice, A. Osborne, M. West, E. Smythe, *Curr. Biol.* **1998**, *8*, 34.

[115] S. Semerdjieva, B. Shortt, E. Maxwell, S. Singh, P. Fonarev, J. Hansen, G. Schiavo, B. D. Grant, E. Smythe, *The Journal of Cell Biology* **2008**, *183*, 499.

[116] I. Jordens, M. Marsman, C. Kuijl, J. Neefjes, *Traffic* **2005**, *6*, 1070.

[117] R. I. Tuxworth, M. A. Titus, *Traffic* **2000**, *1*, 11.

[118] N. Hirokawa, *Science* **1998**, *279*, 519.

[119] R. D. Vale, *Cell* **2003**, *112*, 467.

[120] A. Echard, F. Jollivet, O. Martinez, J. J. Lacapere, A. Rousselet, I. Janoueix-Lerosey, B. Goud, *Science* **1998**, *279*, 580.

[121] B. Short, C. Preisinger, J. Schaletzky, R. Kopajtich, F. A. Barr, *Curr. Biol.* **2002**, *12*, 1792.

[122] D. F. Markgraf, K. Peplowska, C. Ungermann, *FEBS Letters* **2007**, *581*, 2125.

[123] J. R. C. Whyte, S. Munro, *Journal of Cell Science* **2002**, *115*, 2627.

[124] W. Guo, D. Roth, C. Walch-Solimena, P. Novick, *Embo Journal* **1999**, *18*, 1071.

[125] W. Guo, F. Tamanoi, P. Novick, *Nat Cell Biol* **2001**, *3*, 353.

[126] B. B. Allan, B. D. Moyer, W. E. Balch, *Science* **2000**, *289*, 444.

[127] A. Simonsen, R. Lippe, S. Christoforidis, J. M. Gaullier, A. Brech, J. Callaghan, B. H. Toh, C. Murphy, M. Zerial, H. Stenmark, *Nature* **1998**, *394*, 494.

[128] E. Nielsen, S. Christoforidis, S. Uttenweiler-Joseph, M. Miaczynska, F. Dewitte, M. Wilm, B. Hoflack, M. Zerial, *Journal of Cell Biology* **2000**, *151*, 601.

[129] R. Jahn, R. H. Scheller, *Nat Rev Mol Cell Biol* **2006**, *7*, 631.

[130] T. Ohya, M. Miaczynska, U. Coskun, B. Lommer, A. Runge, D. Drechsel, Y. Kalaidzidis, M. Zerial, *Nature* **2009**, *459*, 1091.

[131] W. Wickner, R. Schekman, *Nat Struct Mol Biol* **2008**, *15*, 658.

[132] A. B. DiracSvejstrup, T. Sumizawa, S. R. Pfeffer, *Embo Journal* **1997**, *16*, 465.

[133] A. H. Hutagalung, P. J. Novick, *Physiol. Rev.* **2011**, *91*, 119.

[134] W. J. Chia, B. L. Tang, *Biochimica et Biophysica Acta (BBA) - Reviews on Cancer* **2009**, *1795*, 110.

[135] M. von Zastrow, A. Sorkin, *Curr. Opin. Cell Biol.* **2007**, *19*, 436.

[136] Y. Mosesson, G. B. Mills, Y. Yarden, *Nat. Rev. Cancer* **2008**, *8*, 835.

[137] K. W. Cheng, J. P. Lahad, W.-l. Kuo, A. Lapuk, K. Yamada, N. Auersperg, J. Liu, K. Smith-McCune, K. H. Lu, D. Fishman, J. W. Gray, G. B. Mills, *Nat. Med.* **2004**, *10*, 1251.

[138] X. Y. Wang, R. Kumar, J. Navarre, J. E. Casanova, J. R. Goldenring, *J. Biol. Chem.* **2000**, *275*, 29138.

[139] P. T. Caswell, H. J. Spence, M. Parsons, D. P. White, K. Clark, K. W. Cheng, G. B. Mills, M. J. Humphries, A. J. Messent, K. I. Anderson, M. W. McCaffrey, B. W. Ozanne, J. C. Norman, *Dev. Cell* **2007**, *13*, 496.

[140] P. K. Wright, *Recent Pat. Anti-Cancer Drug Discovery* **2008**, *3*, 137.

[141] D. Jenkins, D. Seelow, F. S. Jehee, C. A. Perlyn, L. G. Alonso, D. F. Bueno, D. Donnai, D. Josifiova, I. M. J. Mathijssen, J. E. V. Morton, K. Helene Ørstavik, E. Sweeney, S. A. Wall, J. L. Marsh, P. Nürnberg, M. Rita Passos-Bueno, A. O. M. Wilkie, *The American Journal of Human Genetics* **2007**, *80*, 1162.

[142] M. G. Spillantini, M. Goedert, *Ann. N. Y. Acad. Sci.* **2000**, *920*, 16.

[143] E. Dalfo, T. Gomez-Isla, J. L. Rosa, M. N. Bodelon, M. C. Tejedor, M. Barrachina, S. Ambrosio, I. Ferrer, *J. Neuropathol. Exp. Neurol.* **2004**, *63*, 302.

[144] A. A. Cooper, A. D. Gitler, A. Cashikar, C. M. Haynes, K. J. Hill, B. Bhullar, K. Liu, K. Xu, K. E. Strathearn, F. Liu, S. Cao, K. A. Caldwell, G. A. Caldwell, G. Marsischky, R. D. Kolodner, J. LaBaer, J.-C. Rochet, N. M. Bonini, S. Lindquist, *Science* **2006**, *313*, 324.

[145] A. D. Gitler, B. J. Bevis, J. Shorter, K. E. Strathearn, S. Hamamichi, L. J. Su, K. A. Caldwell, G. A. Caldwell, J.-C. Rochet, J. M. McCaffery, C. Barlowe, S. Lindquist, *Proceedings of the National Academy of Sciences* **2008**, *105*, 145.

[146] M. A. Bakowski, V. Braun, J. H. Brumell, *Traffic* **2008**, *9*, 2022.

[147] E. Boucrot, T. Henry, J.-P. Borg, J.-P. Gorvel, S. Meresse, *Science* **2005**, *308*, 1174.

[148] O. Steele-Mortimer, *Curr. Opin. Microbiol.* **2008**, *11*, 38.

[149] J. H. Brumell, M. A. Scidmore, *Microbiol. Mol. Biol. Rev.* **2007**, *71*, 636.

[150] R. H. Valdivia, *Curr. Opin. Microbiol.* **2008**, *11*, 53.

[151] M. P. Machner, R. R. Isberg, *Science* **2007**, *318*, 974.

[152] J. L. Bos, *Cancer Res.* **1989**, *49*, 4682.

[153] A. D. Basso, P. Kirschmeier, W. R. Bishop, *J. Lipid Res.* **2006**, *47*, 15.

[154] H. Mabuchi, A. Nohara, J. Kobayashi, M. Kawashiri, A. Inazu, *Current Drug Therapy* **2007**, *2*, 39.

[155] S. Rao, D. Cunningham, A. de Gramont, W. Scheithauer, M. Smakal, Y. Humblet, G. Kourteva, T. Iveson, T. Andre, J. Dostalova, A. Illes, R. Belly, J. J. Perez-Ruixo, Y. C. Park, P. A. Palmer, *Journal of Clinical Oncology* **2004**, *22*, 3950.

[156] R. B. Lobell, D. Liu, C. A. Buser, J. P. Davide, E. DePuy, K. Hamilton, K. S. Koblan, Y. Lee, S. Mosser, S. L. Motzel, J. L. Abbruzzese, C. S. Fuchs, E. K. Rowinsky, E. H. Rubin, S. Sharma, P. J. Deutsch, K. E. Mazina, B. W. Morrison, L. Wildonger, S.-L. Yao, N. E. Kohl, *Mol. Cancer Ther.* **2002**, *1*, 747.

[157] F. P. Coxon, M. H. Helfrich, B. Larijani, M. Muzylak, J. E. Dunford, D. Marshall, A. D. McKinnon, S. A. Nesbitt, M. A. Horton, M. C. Seabra, F. H. Ebetino, M. J. Rogers, *J. Biol. Chem.* **2001**, *276*, 48213.

[158] M. S. Marma, Z. Xia, C. Stewart, F. Coxon, J. E. Dunford, R. Baron, B. A. Kashemirov, F. H. Ebetino, J. T. Triffitt, R. G. G. Russell, C. E. McKenna, *J. Med. Chem.* **2007**, *50*, 5967.

[159] R. A. Baron, R. Tavare, A. C. Figueiredo, K. M. Blazewska, B. A. Kashemirov, C. E. McKenna, F. H. Ebetino, A. Taylor, M. J. Rogers, F. P. Coxon, M. C. Seabra, *J. Biol. Chem.* **2009**, *284*, 6861.

[160] C. E. McKenna, B. A. Kashemirov, K. M. Blazewska, I. Mallard-Favier, C. A. Stewart, J. Rojas, M. W. Lundy, F. H. Ebetino, R. A. Baron, J. E. Dunford, M. L. Kirsten, M. C. Seabra, J. L. Bala, M. S. Marma, M. J. Rogers, F. P. Coxon, *J. Med. Chem.* **2010**, *53*, 3454.

[161] M. Watanabe, H. D. G. Fiji, L. Guo, L. Chan, S. S. Kinderman, D. J. Slamon, O. Kwon, F. Tamanoi, *J. Biol. Chem.* **2008**, *283*, 9571.

[162] U. T. T. Nguyen, Z. Guo, C. Delon, Y. W. Wu, C. Deraeve, B. Fraenzel, R. S. Bon, W. Blankenfeldt, R. S. Goody, H. Waldmann, D. Wolters, K. Alexandrov, *Nat. Chem. Biol.* **2009**, *5*, 227.

[163] Z. Guo, Y. W. Wu, K. T. Tan, R. S. Bon, E. Guiu-Rozas, C. Delon, U. T. Nguyen, S. Wetzel, S. Arndt, R. S. Goody, W. Blankenfeldt, K. Alexandrov, H. Waldmann, *Angewandte Chemie-International Edition* **2008**, *47*, 3747.

[164] K. T. Tan, E. Guiu-Rozas, R. S. Bon, Z. Guo, C. Delon, S. Wetzel, S. Arndt, K. Alexandrov, H. Waldmann, R. S. Goody, Y. W. Wu, W. Blankenfeldt, *J. Med. Chem.* **2009**, *52*, 8025.

[165] W. C. Rose, F. Y. F. Lee, C. R. Fairchild, M. Lynch, T. Monticello, R. A. Kramer, V. Manne, *Cancer Res.* **2001**, *61*, 7507.

[166] G. M. Keseru, G. M. Makara, *Drug Discov. Today* **2006**, *11*, 741.

[167] K. H. Bleicher, H.-J. Bohm, K. Muller, A. I. Alanine, *Nature Reviews. Drug Discovery* **2003**, *2*, 369.

[168] L. M. Mayr, D. Bojanic, *Curr. Opin. Pharmacol.* **2009**, *9*, 580.

[169] Y. Etzion, A. J. Muslin, *Trends in Cardiovascular Medicine* **2009**, *19*, 207.

[170] G. Schneider, O. Clément-Chomienne, L. Hilfiger, P. Schneider, S. Kirsch, H.-J. Böhm, W. Neidhart, *Angewandte Chemie International Edition* **2000**, *39*, 4130.

[171] G. Schneider, *Nature Reviews. Drug Discovery*, *9*, 273.

[172] A. A. Patchett, R. P. Nargund, in *Annual Reports in Medicinal Chemistry, Vol 35, Vol. 35*, Academic Press Inc, San Diego, **2000**, pp. 289.

[173] K. H. Bleicher, *Curr. Med. Chem.* **2002**, *9*, 2077.

[174] J. Hodgson, *Nat Biotech* **2001**, *19*, 722.

[175] D. L. Pompliano, R. P. Gomez, N. J. Anthony, *J. Am. Chem. Soc.* **1992**, *114*, 7945.

[176] D. L. Pompliano, E. Rands, M. D. Schaber, S. D. Mosser, N. J. Anthony, J. B. Gibbs, *Biochemistry* **1992**, *31*, 3800.
[177] L. Goossens, S. Deweer, J. Pommery, J.-P. Hénichart, J.-F. Goossens, *J. Pharm. Biomed. Anal.* **2005**, *37*, 417.
[178] Z. Guo, PhD thesis, TU Dortmund **2008**.
[179] T. Sasaki, *J. Biol. Chem.* **1990**, *265*, 2333.
[180] T. Sasaki, K. Kaibuchi, A. K. Kabcenell, P. J. Novick, Y. Takai, *Mol. Cell. Biol.* **1991**, *11*, 2909.
[181] G. Jones, P. Willett, R. C. Glen, A. R. Leach, R. Taylor, *J. Mol. Biol.* **1997**, *267*, 727.
[182] Y. W. Wu, K. Alexandrov, L. Brunsveld, *Nat. Protoc.* **2007**, *2*, 2704.
[183] Y.-W. Wu, K.-T. Tan, H. Waldmann, R. S. Goody, K. Alexandrov, *Proceedings of the National Academy of Sciences* **2007**, *104*, 12294.
[184] S. E. Sen, S. L. Roach, *Synthesis* **1995**, *1995*, 756.
[185] T. Subramanian, Z. Wang, J. M. Troutman, D. A. Andres, H. P. Spielmann, *Org. Lett.* **2005**, *7*, 2109.
[186] K. Yager, S. Chu, K. Appelt, X. Li, **2005**, US, 2005054697
[187] F. H. Ebetino, A. V. Bayless, S. M. Dansereau, **1993**, 93-US4993
[188] L. Horner, E.-O. Renth, *Justus Liebigs Annalen der Chemie* **1967**, *703*, 37.
[189] W. Goldeman, M. Soroka, *Synthesis* **2006**, *2006*, 3019.
[190] J. Quiroga, J. Trilleras, B. Insuasty, R. Abonía, M. Nogueras, J. Cobo, *Tetrahedron Lett.* **2008**, *49*, 2689.
[191] B. C. Chen, J. E. Sundeen, P. Guo, M. S. Bednarz, R. Zhao, *Tetrahedron Lett.* **2001**, *42*, 1245.
[192] J. T. Hunt, C. Z. Ding, R. Batorsky, M. Bednarz, R. Bhide, Y. Cho, S. Chong, S. Chao, J. Gullo-Brown, P. Guo, S. H. Kim, F. Y. F. Lee, K. Leftheris, A. Miller, T. Mitt, M. Patel, B. A. Penhallow, C. Ricca, W. C. Rose, R. Schmidt, W. A. Slusarchyk, G. Vite, V. Manne, *J. Med. Chem.* **2000**, *43*, 3587.
[193] Z. Gao, C.-K. Chen, **2002**, WO, 2002085819
[194] M. R. Lackner, R. M. Kindt, P. M. Carroll, K. Brown, M. R. Cancilla, C. Y. Chen, H. de Silva, Y. Franke, B. Guan, T. Heuer, T. Hung, K. Keegan, J. M. Lee, V. Manne, C. O'Brien, D. Parry, J. J. Perez-Villar, R. K. Reddy, H. J. Xiao, H. J. Zhan, M. Cockett, G. Plowman, K. Fitzgerald, M. Costa, P. Ross-Macdonald, *Cancer Cell* **2005**, *7*, 325.
[195] http://www.licor.com/bio/applications/odyssey_applications/in_cell_western.jsp
[196] H. M. Sampath Kumar, B. V. Subba Reddy, P. Tirupathi Reddy, J. S. Yadav, *Synthesis* **1999**, *1999*, 586.
[197] K. DelVillar, H. Mitsuzawa, W. L. Yang, I. Sattler, F. Tamanoi, *J. Biol. Chem.* **1997**, *272*, 680.
[198] H. Tong, S. A. Holstein, R. J. Hohl, *Anal. Biochem.* **2005**, *336*, 51.
[199] L. D. Bratton, X.-M. Cheng, N. Erasga, G. F. Filzen, A. G. Geyer, C. Lee, B. K. Trivedi, P. C. Unangst, **2004**, US, 20040209936
[200] S. L. Gwaltney, S. J. O'Connor, L. T. J. Nelson, G. M. Sullivan, H. Imade, W. Wang, L. Hasvold, Q. Li, J. Cohen, W.-Z. Gu, S. K. Tahir, J. Bauch, K. Marsh, S.-C. Ng, D. J. Frost, H. Zhang, S. Muchmore, C. G. Jakob, V. Stoll, C. Hutchins, S. H. Rosenberg, H. L. Sham, *Bioorg. Med. Chem. Lett.* **2003**, *13*, 1359.
[201] S. L. Gwaltney, S. J. O'Connor, L. T. J. Nelson, G. M. Sullivan, H. Imade, W. Wang, L. Hasvold, Q. Li, J. Cohen, W.-Z. Gu, S. K. Tahir, J. Bauch, K. Marsh, S.-C. Ng, D. J. Frost, H. Zhang, S. Muchmore, C. G. Jakob, V. Stoll, C. Hutchins, S. H. Rosenberg, H. L. Sham, *Bioorg. Med. Chem. Lett.* **2003**, *13*, 1363.
[202] Y. Brouillette, J. Martinez, V. Lisowski, *Eur. J. Org. Chem.* **2009**, 3487.
[203] G. M. Coppola, *Synthesis-Stuttgart* **1980**, 505.
[204] S. Herzig, S. Kritter, T. Labbers, N. Marquardt, J.-U. Peters, S. Weber, *Synlett* **2005**, *2005*, 3107.

[205] P. E. Maligres, M. S. Waters, S. A. Weissman, J. C. McWilliams, S. Lewis, J. Cowen, R. A. Reamer, R. P. Volante, P. J. Reider, D. Askin, *J. Heterocycl. Chem.* **2003**, *40*, 229.

[206] J. Fensholdt, J. Thorhauge, B. Norremark, **2005**, WO, 2005054179

[207] A. V. Dolzhenko-Podchezertseva, L. M. Korkodinova , M. V. Vasilyuk, V. P. Kotegov, *Pharmaceutical Chemistry Journal* **2002**, *36*, 647.

[208] M. McLaughlin, M. Palucki, I. W. Davies, *Org. Lett.* **2006**, *8*, 3307.

[209] S. L. Gwaltney, L. T. j. Nelson, S. J. O'Connor, H. L. Sham, G. M. Sullivan, W. Wang, **2003**, US, 20030216441

Supplementary Data

Virtual Screening Input data

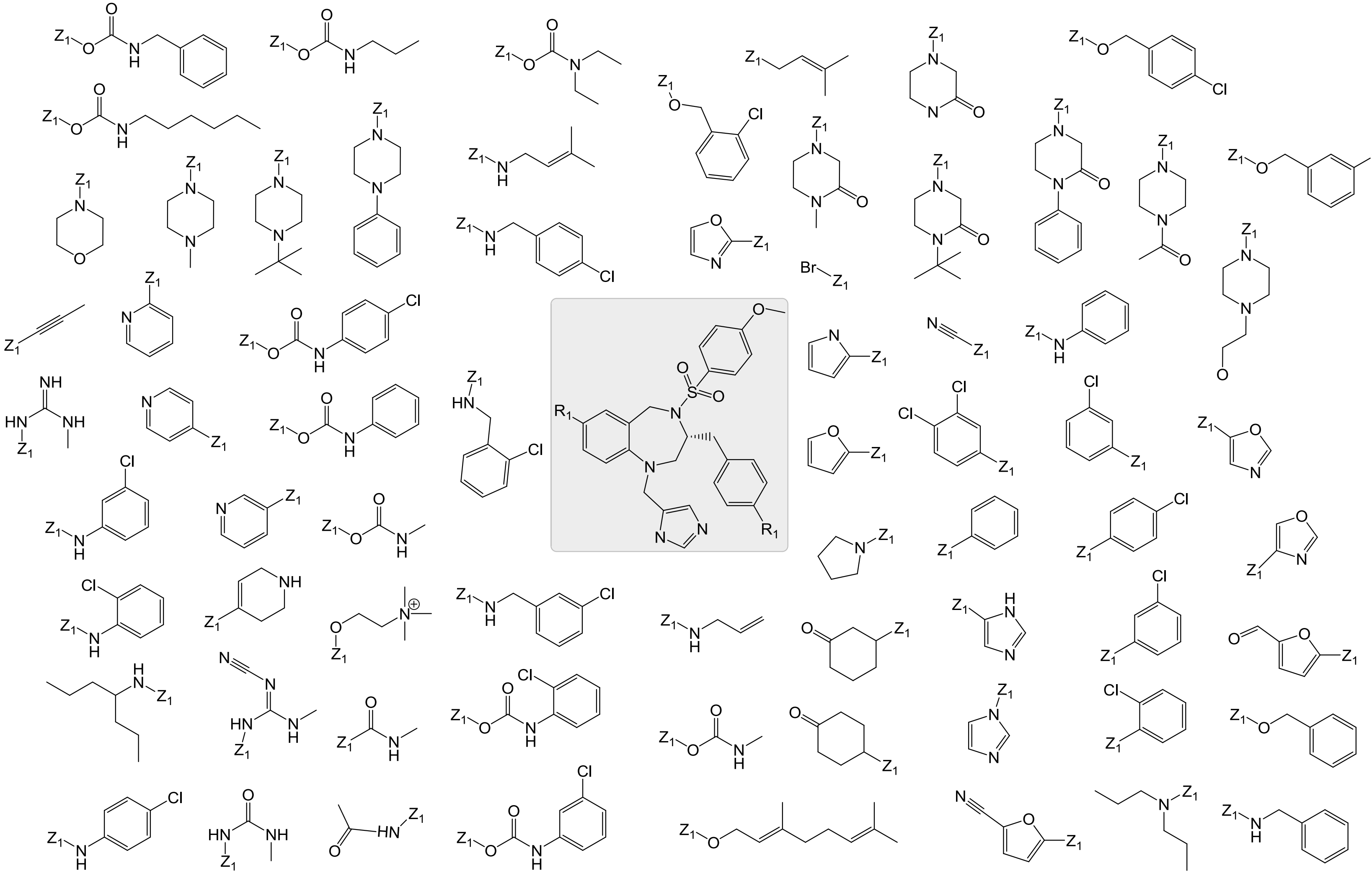

Cellular data of all tested compounds and cell lines

	RabGGTase (NBD-FPP)	RabGGTase (GGPP)	Cellular Reprenylation	FTase	HCT116	HELA	A2780	A549	DU145	PBMC
74b	1011±465	4	114.9±42.1	5.2±0.2	172	130	100	315	162	>10000
93	38±7	122.7±21.7	343±29	<5	75±10	745±303	43±9	412	nd	3836
89	441	180.5±13.5	nd	99.3±59	1048	372	265	655	756	>10000
83	18629±13202	1495.5±99.5	>10000	10.5±3.9	1049	1960	92	2223	3097	>10000
91	243±20	15.5±1.5	77.3±1.7	9.2±4.2	355	nd	233	281	201	>10000
92	72.2±1.7	6±4	81±32	<5	231	151	130	338	142	>10000
23	724±321	6.4±4.8	74±34	6±3	63±8	101±2	43	99	70	>10000
90	2072	23.5±4.5	278	1,012±688	1434±484	nd	1381±280	593	nd	>10000
88	39±10	63±24	43±12	15±8	112	59	116	74	90	8028
87	162±10	156±49	307±40	10±7	264	154	165	216	241	8686
94	353±158.1	11±2	466±345	4.3±2.2	308	409	399	442	413	>10000
99	>30000	>10000	nd	120.5±84.9	640	901	1002	774	828	>10000
97	>9,500	706±246	>30	194±78	4705±2385	8062	1740±648	2593	3126	>10000
101	>30000	>10000	>10000	>10000	4974	9308	3261	3206	10000	>10000
102	>30000	2827±977	nd	979±262	5572	5893	4652	2776	6455	6404
103	>30000	8490.5±1509.5	nd	>10000	4292		3541	2244	12720	>10000
109	616.2±415.7	1547±101	311±193	>10000	443±173	797±330	589±199	nd	nd	>10000
126	41.6±9	379	49±32	>10000	35±1	101±11	115±3	nd	nd	>10000
120	62.5±1.6	14	11±5	26.9±20	2±1	21±4	18±1	nd	nd	>10000
129	nd	59	54	151	71±10	130±11	222±1	nd	nd	>10000

Standard deviations available at the LDC

Assignment by analogy, NMR example of compound 91

1H NMR

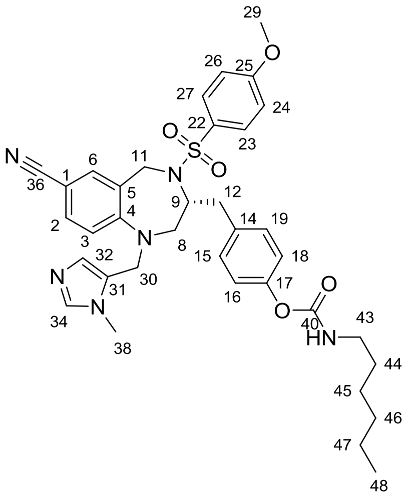
29
O
26
25
27
24
22
23
O
S
O
N
6
11
N
36
1
5
4
9
12
2
3
N
14
19
32
8
15
18
N
31
30
17
O
34
N
16
O
40
43
38
HN
44
45
46
47
48

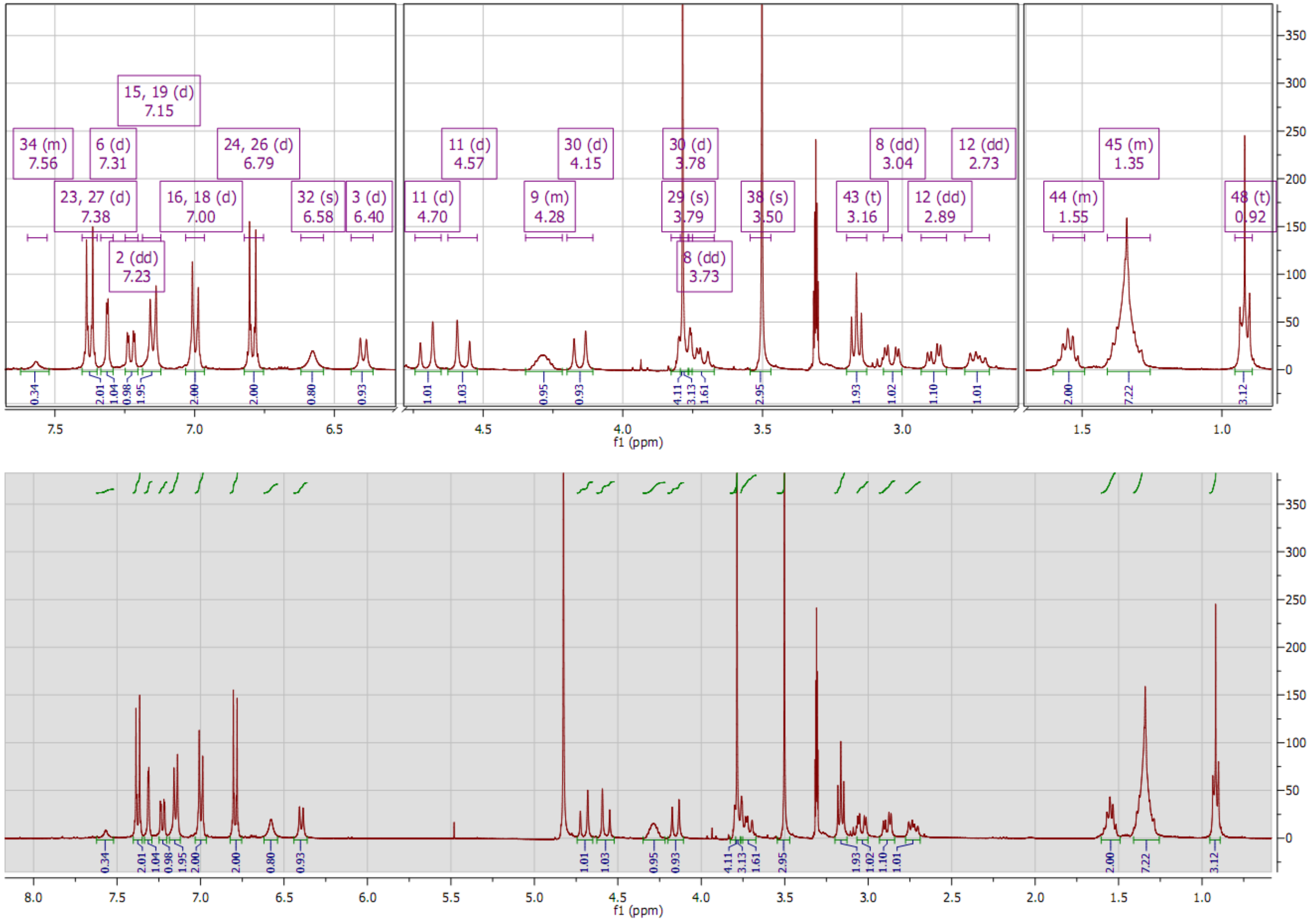

COSY

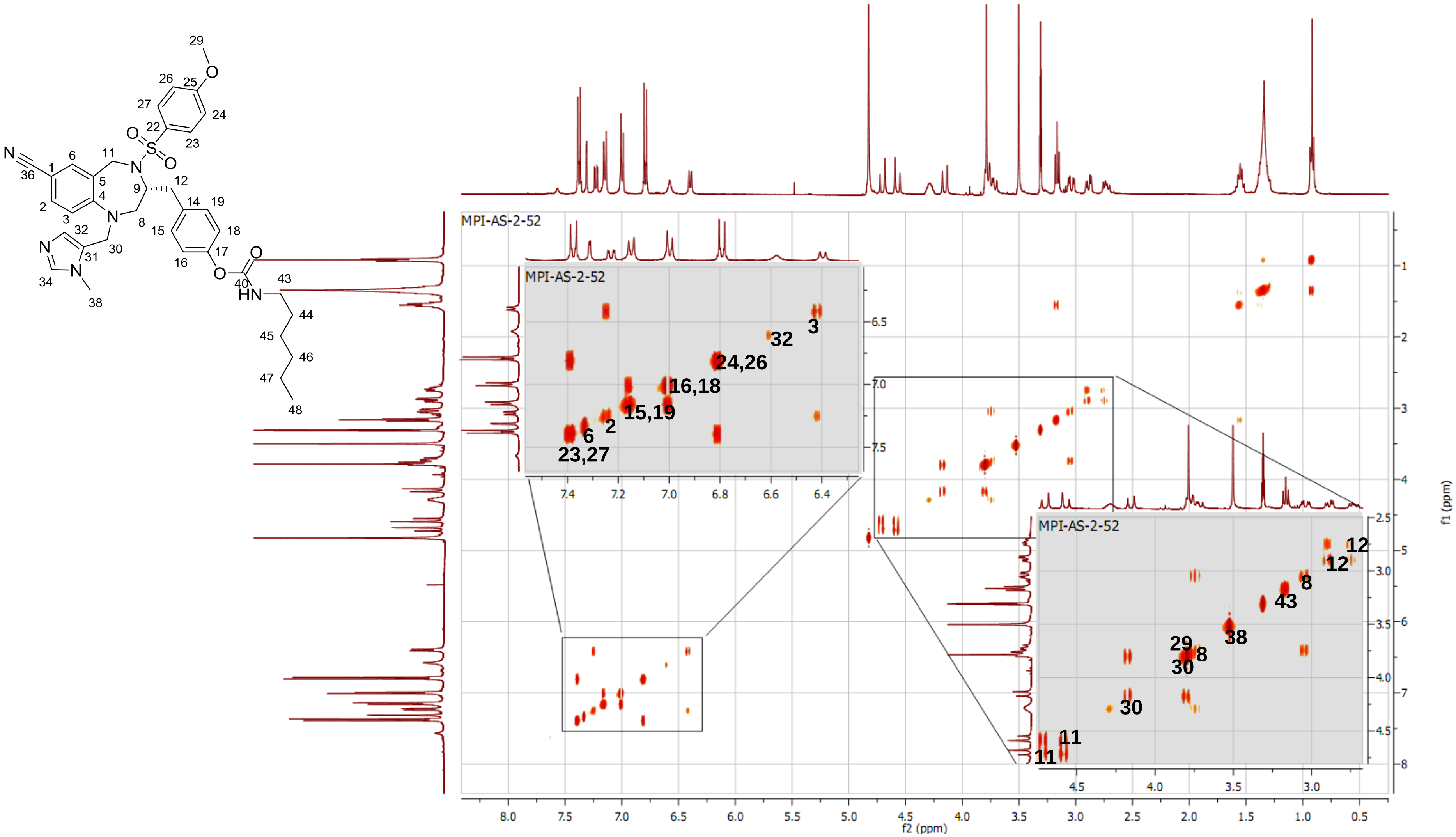

N
36
1
6
11
N
S
O
O
22
23
24
25
26
27
O
29
5
4
9
12
2
3
N
8
14
15
16
17
18
19
O
40
O
HN
43
44
45
46
47
48
32
N
31
30
34
N
38
MPI-AS-2-52
3
32
24,26
16,18
15,19
2
6
23,27
12
12
8
43
38
29
8
30
30
11
11
8.0
7.5
7.0
6.5
6.0
5.5
5.0
4.5
4.0
3.5
3.0
2.5
2.0
1.5
1.0
0.5
f2 (ppm)
f1 (ppm)
1
2
3
4
5
6
7
8
7.4
7.2
7.0
6.8
6.6
6.4
6.5
7.0
7.5
4.5
4.0
3.5
3.0
2.5

APT

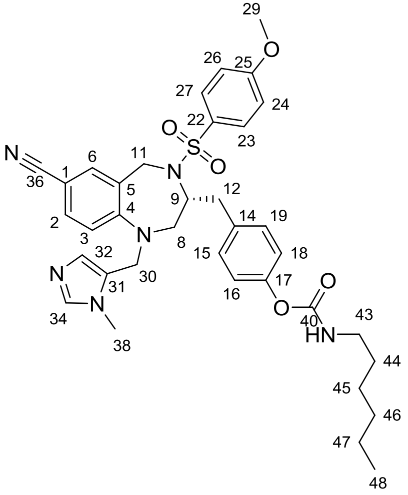

29
O
26
25
27
24
22
O
S
O
23
N
36
1
6
11
N
5
9
12
4
2
3
N
14
19
32
8
15
18
N
30
31
17
O
16
N
O
34
40
43
38
HN
44
45
46
47
48

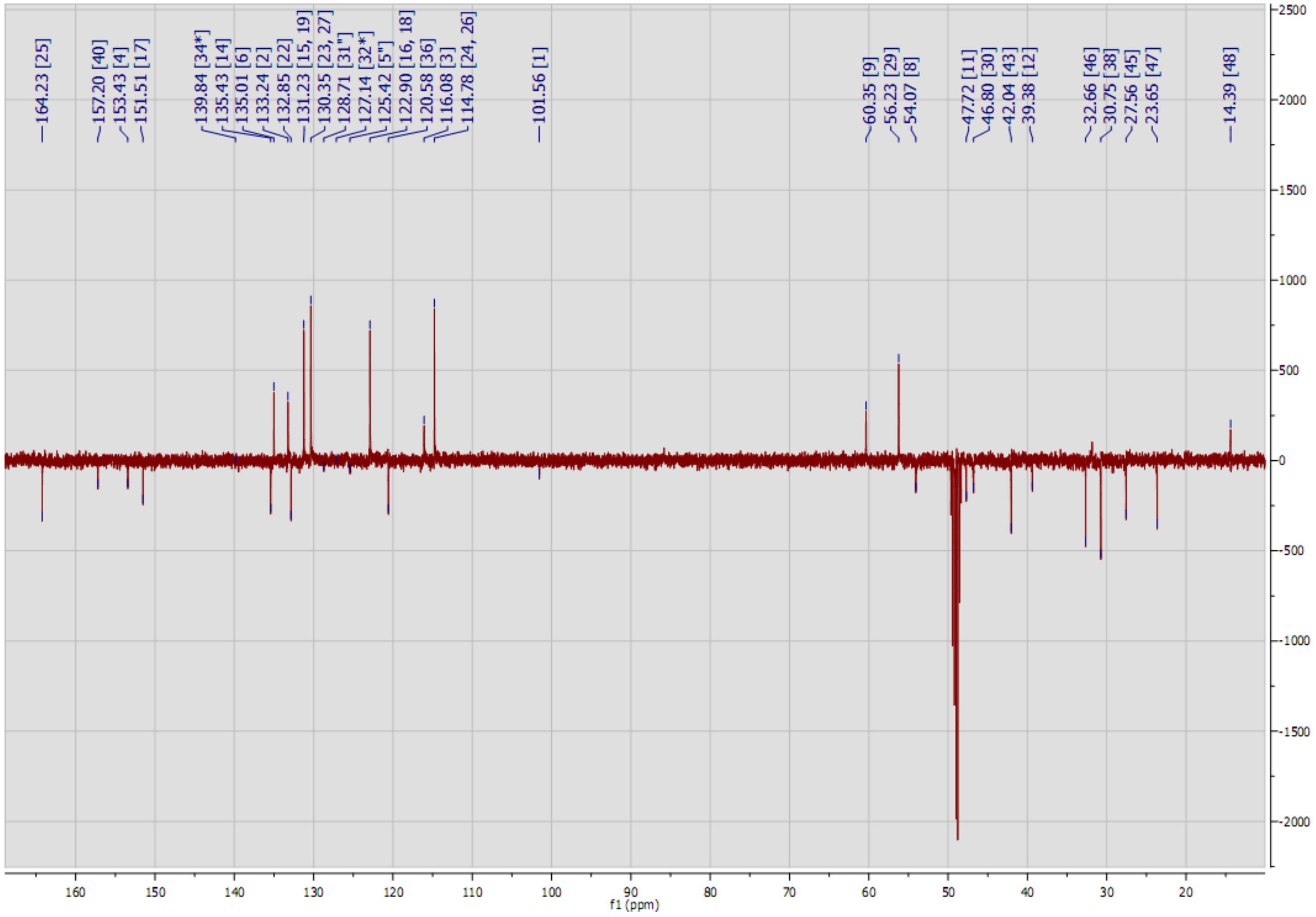

164.23 [25]
157.20 [40]
153.43 [4]
151.51 [17]
139.84 [34*]
135.43 [14]
135.01 [6]
133.24 [2]
132.85 [22]
131.23 [15, 19]
130.35 [23, 27]
128.71 [31"]
127.14 [32*]
125.42 [5"]
122.90 [16, 18]
120.58 [36]
116.08 [3]
114.78 [24, 26]
101.56 [1]
60.35 [9]
56.23 [29]
54.07 [8]
47.72 [11]
46.80 [30]
42.04 [43]
39.38 [12]
32.66 [46]
30.75 [38]
27.56 [45]
23.65 [47]
14.39 [48]
2500
2000
1500
1000
500
0
-500
-1000
-1500
-2000
160
150
140
130
120
110
100
90
80
70
60
50
40
30
20
f1 (ppm)

HSQC

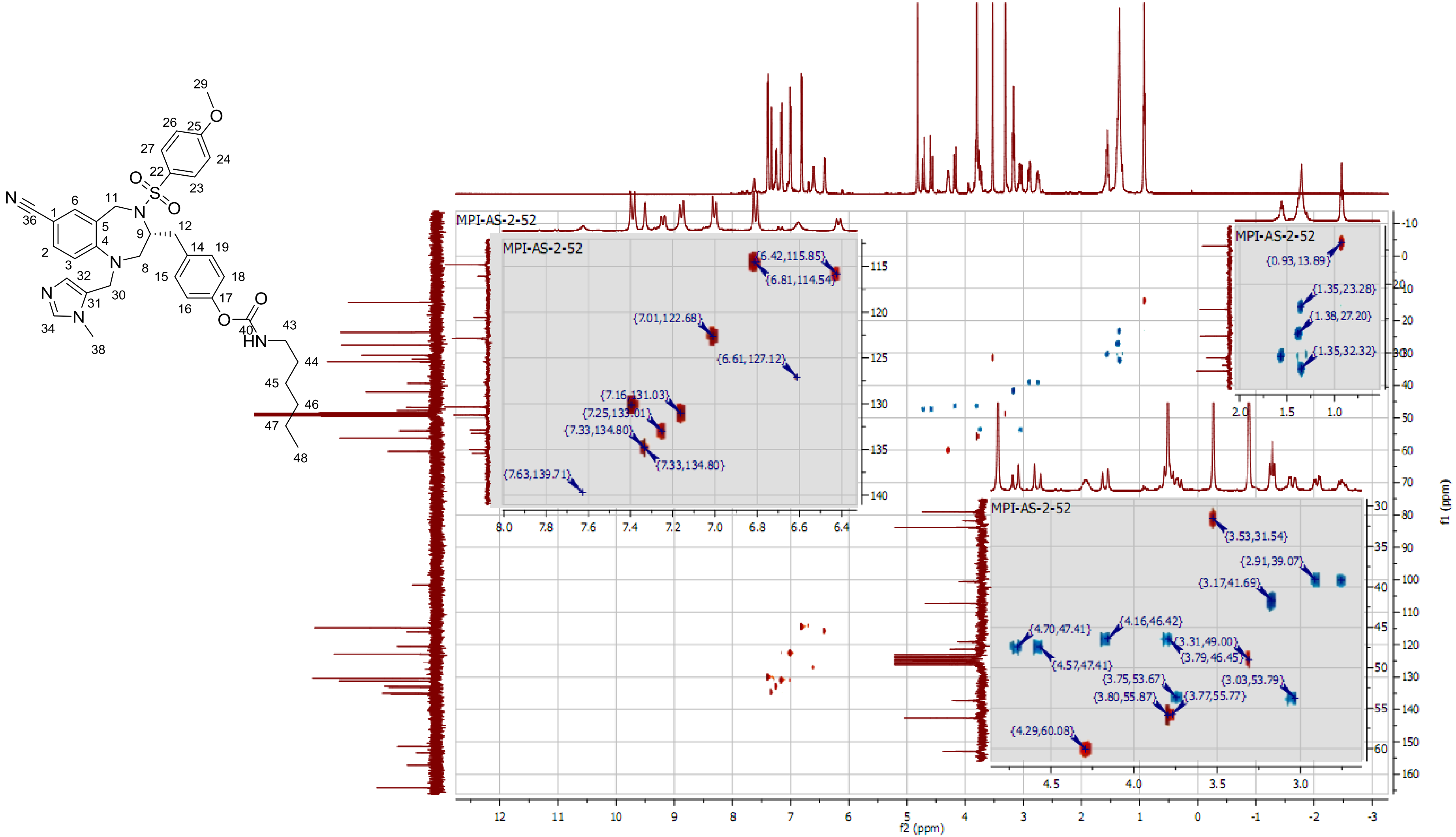
MPI-AS-2-52
{6.42,115.85}
{6.81,114.54}
{7.01,122.68}
{6.61,127.12}
{7.16,131.03}
{7.25,133.01}
{7.33,134.80}
{7.33,134.80}
{7.63,139.71}
{0.93,13.89}
{1.35,23.28}
{1.38,27.20}
{1.35,32.32}
{3.53,31.54}
{2.91,39.07}
{3.17,41.69}
{4.16,46.42}
{4.70,47.41}
{3.31,49.00}
{3.79,46.45}
{4.57,47.41}
{3.75,53.67}
{3.03,53.79}
{3.80,55.87}
{3.77,55.77}
{4.29,60.08}
f2 (ppm)
f1 (ppm)

HMBC

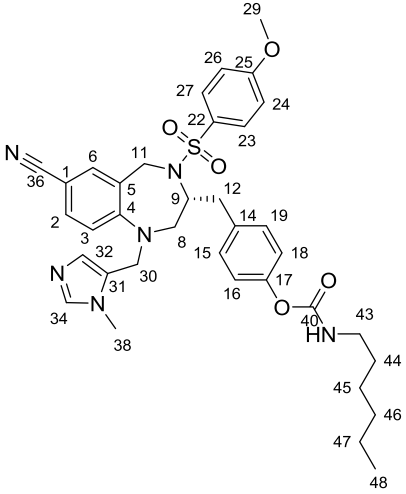
29
O
26
25
27
24
22
23
O
S
O
N
36
1
6
11
N
5
9
12
2
4
14
19
3
N
8
15
18
32
30
N
31
17
O
16
O
34
N
40
43
38
HN
44
45
46
47
48

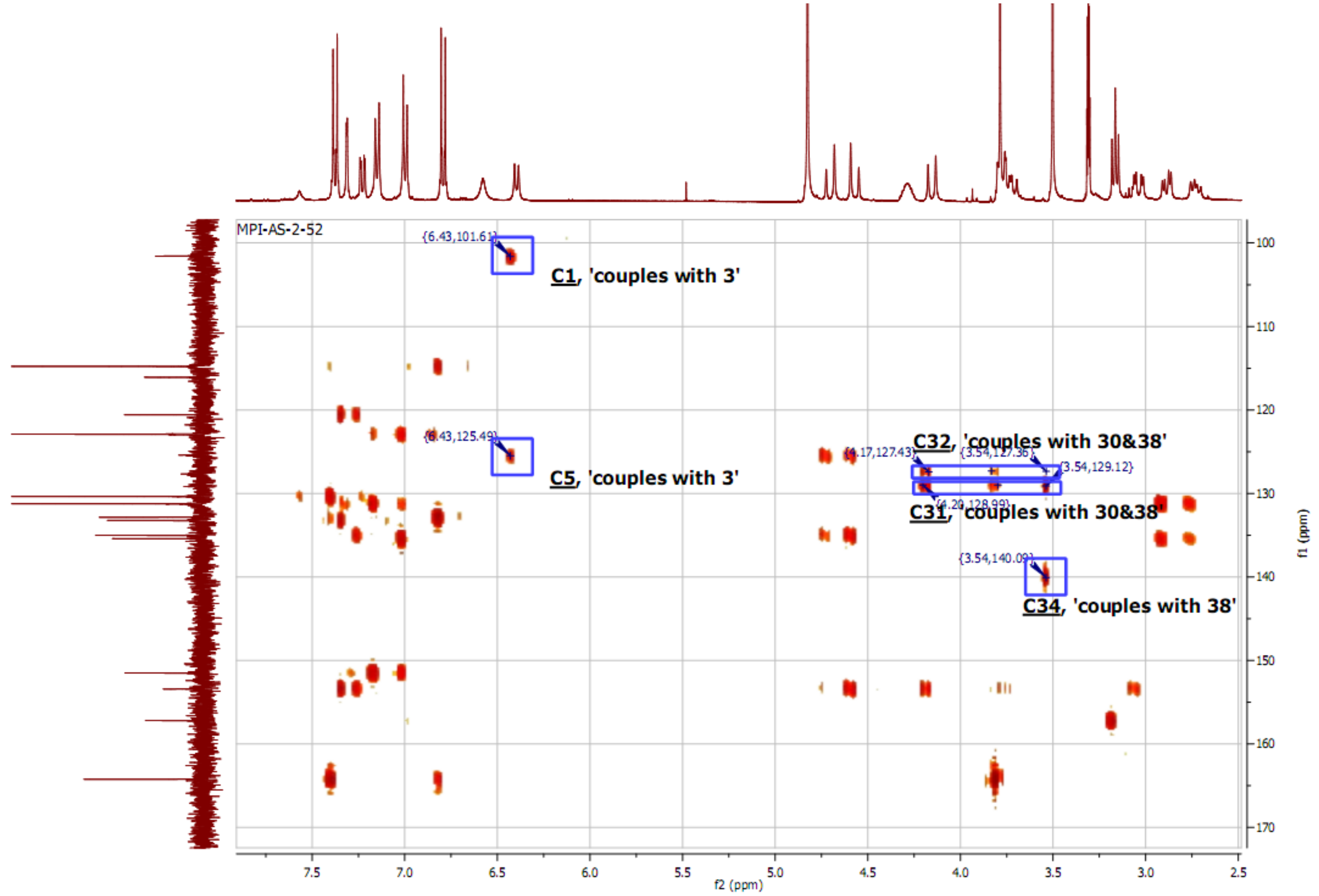
MPI-AS-2-52
{6.43,101.61}
C1, 'couples with 3'
{6.43,125.49}
C5, 'couples with 3'
C32, 'couples with 30&38'
{4.17,127.43}
{3.54,127.36}
{3.54,129.12}
{4.20,128.99}
C31, 'couples with 30&38'
{3.54,140.09}
C34, 'couples with 38'
100
110
120
130
140
150
160
170
f1 (ppm)
7.5
7.0
6.5
6.0
5.5
5.0
4.5
4.0
3.5
3.0
2.5
f2 (ppm)

---

j

Acknowledgement

Some of you have already been acknowledged in the PhD thesis due to contributions to the project. However, there are many others I'd like to mention here. Without the support of all of you, my PhD wouldn't have been the same

First of all, I would like to thank my supervisor, Prof. Dr. Herbert Waldmann. Thank you for giving me the opportunity to start my PhD under your supervision and for your continuous support during my PhD. I would also like to thank you for my PhD topic, which developed into a successful, finished project, under a balanced mix of supervision and independence. Additionally I would like to thank you for your support regarding my next career steps.

Secondly, I would like to thank Prof. Dr. Roger Goody. Not only because you were a part of my PhD committee, but also for your continuous support during the project. The collaboration between our two departments was essential for the project. I've always appreciated your input into difficult topics and your careful corrections of the paper drafts.

I would also like to thank Dr. Gabriele Troetscher-Kaus for being part of my PhD committee. Thanks for taking the time to read my thesis.

Robin, I would like to thank you for the great collaboration we had during the project. I learned a lot from you, and especially appreciated your continuous support, even after you continued your career Leeds. I would also like to thank you for your careful reading of my thesis. I think we did a great job together on the project and hope to go out for a drink again sometimes in the future. Super Bedankt!

I would also like to thank Yaowen and Zhong for their contributions on the project. Zhong, although I'm not familiar with crystallization techniques myself, I've always had the impression that you have a special crystallization talent. Without your crystal structures the project wouldn't have been the same. Yaowen, I would like to thank you for all your input regarding the binding mode studies.

Next, I would like to thank the LDC guys, Sascha, Axel, Alexander, Raffaella and Peter. It was a pleasure to work with you. I enjoyed our conversations and found it a privilege to work together with such experienced people this early in my career. Axel, I would like to thank you for your patience, your updates about the project and the streamlining of the data sets. Sascha and Alexander, I would like to thank you for all the assay data you generated. Sascha, thanks for all our fruitful discussions and for correcting parts of my thesis. Raffaella, I would also like to thank you for all our synthetic chemistry discussions.

I'll keep my fingers crossed for a RabGGTase Inhibitor in the clinic.

Thanks to Lena, Matthias, Tobias and Gemma for reviewing parts of my thesis. Special thanks for my Bart, who reviewed my whole thesis, even my experimental part.

I would also like to thank my trainees, Patrick, Timo and Charlotte. If you have a look in the thesis, you will probably recognize some of your work. You all made important contributions to this project! I enjoyed working with all of you and wish you all the best for the future.

Thanks to the analytic-team, Dr. Petra Janning, Andreas Brockmeyer, Evelyne Merten and Chantale Sevenich for all MS measurements.

I would also like to thank the IMPRS-team, Christa, Waltraud and Prof. Dr. Martin Engelhard. It has been great to be part of the IMPRS. I always enjoyed dropping by at the IMPRS office, for support or just for a coffee! Many thanks for the funding, for organizing the IMPRS retreats and for allowing us to organize a symposium.

Christian, I would like to thank you for offering a place to stay in the beginning of my PhD and for your inspiring enthusiasm and commitment to science.

I would like to thank all colleagues of the chemical biology department for providing a nice working atmosphere. In particular, I would like to thank my labmates of A3.12; Sureshan, Mandal, Bruno, Bart and Wei. You've been all a great support during my PhD, by discussing our projects, by exchanging practical tricks and techniques, and of course, by providing a great working atmosphere. I would also like to thank my office members, A3.32; Stefan, Stephan, Robin, Bahar, Domingo, Patrick, Nancy, Bjoern, Uschi and Martijn. It has been a pleasure sharing a few square meters with all of you!

A real working day is also incomplete without a lunch break, first with 'the Girls' and later on with 'the Germans'. Gemma, Bahar, Jacqui, Marta and Nancy, I enjoyed all our coffee breaks and lunches, as well as our trip to Lubeck and Hamburg. Uschi, Kristina, Hannah, Tobias, Bernhard, Kathrin, Claas, Peter, Gunther and Rebecca, thanks for the enjoyable lunch time and for trying to understand my German ;)

Special thanks go to my friends who were always there for me. Bart, Robin, Lena, Manuela, Euli, Uschi, Nancy, Bahar, Jacqui, Gemma, Domingo, Marta, Patrick, Claas, Kristina, Martijn, Bjoern, Valerie, Celine, Luc and Shen, thanks for all the great times we had outside the institute, having dinner or drinks or both ;).

I would also like to thank my "Dutch" friends for being there for me, even though I went abroad. Linde, Peter, Susanne, Tibert, Matthijs, Caroline, Geeske, Patrick, Ruben, Robin, Chris, Guido, Eveline, Irene and Katherine, thanks for visiting me in Dortmund and all the good times and support I've got from you during my studies, my PhD and hopefully for many years to come.

I would also like to thank my family for their unconditional support and love! Pap, Sven, Mirte en Wout, ik vond het geweldig dat jullie me zo vaak zijn komen opzoeken in Dortmund en het was altijd weer fijn om even thuis te zijn. Morien, Is, Rik, Leonie, Bink en Lisanne bedankt voor alle steun. Ik kijk uit naar ons weekendje weg om weer eens met zijn allen bij elkaar te zijn. Ik hou van jullie!

Bart, you've supported me in every possible way! Thanks for making my life complete. Ik ben zo blij dat je er bent, ik hou van je!

---

n

Declaration/Eidesstattliche Erklärung

Hiermit versichere ich an Eides statt, dass ich die vorliegende Arbeit selbständig und nur mit den angegeben Hifsmitteln angefertigt habe.

I hereby declare that I performed the work presented independently and did not use any other but indicated aids.

Dortmund, April 2011

Elisabeth Anouk Stigter